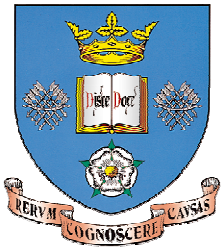

Constructed wetlands for the treatment of airport de-icer

Klaus M. Richter

This thesis is submitted in partial fulfilment of the requirements for the Degree of Doctor of Philosophy

University of Sheffield

Department of Civil and Structural Engineering

November 2003

DECLARATION

I declare that the work in this thesis has been composed by myself and no portion of the work has been submitted in support of an application for another degree or qualification of this or any other university or other institute of learning. The work has been my own except where indicated and all quotations have been distinguished by quotation marks and the sources of information have been acknowledged.

ABSTRACT

Airports are facing the dual challenge of maintaining public safety and protecting the environment. De-icer and anti-icer containing glycol based agents are used to ensure wintertime flight safety. These fluids have the potential to impose enormous oxygen demands on receiving waters, leading to degradation of the resources. Due to tighter discharge consent standards and an increase in the public awareness of environmental pollution, many airport operators are examining alternative methods for managing de-icing fluid wastewater.

This thesis deals with a novel way of treating the airport runoff. British Airport Authorities (BAA) commissioned a gravel type subsurface flow reed bed system to treat the glycol-laden runoff at Heathrow Airport. Constructed wetlands act as an efficient water purification system and nutrient sink and remove efficiently BOD, COD and other pollutants. Due to the movement towards sustainable, environmental engineering relying on natural ecologic processes, such artificial systems are being increasingly used rather than traditional energy and chemical intensive treatment processes.

In this thesis the performance of the subsurface reed beds at Heathrow Airport is assessed at the very beginning of operation and after one year of operation. Since no data of real scale applications of subsurface reed beds is reported up to now, the collected data and the subsequent assessment has a significant importance for further designs of constructed wetland based treatment applications.

In this thesis the hydraulics of the beds were examined by means of fluorescent tracer studies to gain insight in the residence time distribution of pollutants entering the constructed wetland. A framework for modelling pollutant transport in wetlands is developed and pollutant transport models based on multi-order Aggregated Dead Zone cells and the Advective Dispersive Equation are presented.

The treatment performance was studied in several tests. The overall removal of glycol as well as the removal of glycol within the constructed wetland was examined. Total removal of glycol was dependent on the influent concentration and measured up to a level of 45 mg COD/L. The removal of glycol within the wetland follows a first order reaction rate. The main removal of glycol was detected within the first half of the constructed wetlands. Short wetlands with a relatively high hydraulic load were found to have the most efficient layout in terms of removed glycol mass per area.

A pollutant removal model that incorporates the findings from the assessment of the hydraulics and the treatment performance is developed for the constructed wetland system and verified with real data.

CONTENTS

ABBREVIATIONS AND NOTATIONS

Abbreviations

BOD	biochemical oxygen demand
BOD_5, BOD_u	five day or ultimate biochemical oxygen demand
cBOD	carbonaceous BOD
COD	chemical oxygen demand
DEG	diethylene glycol
DOC	dissolved organic carbon
EG	ethylene glycol
PG	polyethylene glycol
ThOD	theoretical oxygen demand
ThTOC	theoretical total organic carbon
TOC	total organic carbon

ADE	advective diffusion equation
ADZ	aggregated dead zone
AIC	Akaike information criterion
EE	equation error
FWS	free water surface wetland
HF	horizontal flow
IV	instrumental variable
LS	least square
SRIV	simplified refined instrumental variable
SSF	subsurface flow wetland
VF	vertical flow
YIC	Young information criterion

Mathematical Notation

^	the "hat"-sign indicates an estimated value of a parameters
*	the "star"-sign indicate a pre-filtered parameter vector
-	the "overbar"-sign indicate a time averaged parameter
d, ∂	derivative of a parameter
dA	elemental cross-sectional area of the control element
dh/dx	hydraulic gradient
$\partial c/\partial t$	change of concentration with time
grad(c)	gradient of the concentration, (the gradient is pointing into the direction of the greatest increase of the concentration and its magnitude is the rate of increase in concentration per unit length into that direction)
$\frac{\beta}{s+\alpha}$	transfer function for the continuous time ADZ model
$\frac{bz^{-\delta}}{1-az^{-1}}$	transfer function for the discrete time ADZ model

Latin Letters

a	parameter or parameter vector
a_1, a_2, ...	1st, 2nd, ... parameter of vector a
A	cross-sectional area
A	wetland surface area
$A(z^{-1})$	transfer function polynom A
b	parameter or parameter vector
b_0, b_1,..	0st, 1st, ... parameter of vector b
$B(z^{-1})$	transfer function polynom B
c_i	concentration of pollutant at ith sample
C	concentration of the single reactant
C^*	background concentration
$C(x_i, t_i)$	concentration at location x_i at time t_i
d	average grain diameter
D	hydraulic radius
D_x	dispersion coefficient in x direction
D^*	coefficient of molecular diffusion
e_x	turbulent diffusion factor in x direction
$e(k)$	white noise
ET	evapotranspiration rate
h	water depth
i	index for the ith sample of observation

I	infiltration rate
k	the reaction rate constant
k_x	dispersion factor in x direction
K	hydraulic conductivity
L	length
m	number of parameters of the A polynom of a transfer function
n	number of parameters of the B polynom of a transfer function
n	effective porosity
n_M	MANNING'S n constant
n	reaction order in reaction kinetics
N	number of observations
P	precipitation rate
P	wetted perimeter of a channel
$P(k)$	inverse of the instrumental covariance matrix
q_A	area hydraulic loading rate
q_V	volumetric hydraulic loading rate
Q	flow rate
R_T^2	coefficient of determination
t	time
t_i	time of ith sample
$\bar{t}$	travel time, the difference in time between the centroids of the distributions
T_c	ADZ-cell residence time
u	fluid velocity
$u(k)$, u_k	kth element of vector u
U	mean velocity
v	fluid velocity
v	specific discharge
V	reactor volume, ADZ-cell volume
V	water storage in wetland
W	width
$x(k)$, x_k	kth element of vector x
X	data vector
$X_{i,k}$	sensitivity coefficient
$y(k)$, y_k	kth element of vector y

Greek Letters

τ	retention time
α_i	dispersivity as a characteristic property of the porous medium
γ	integration variable
δ	time step
Δ	indicates a small intervall
Δa	parameter perturbation of parameter *a*
Δt	sampling interval
ε_i	weighted residual error for the *i*th sample
μ	fluid viscosity
ξ	spatial variable of integration
$\xi(k)$	coloured noise at *k*th sample
ρ	fluid density
σ^2	sample variance of the model residuals
σ_s^2	spatial variance
σ_t^2	temporal variance
σ_y^2	sample variance of the measured output *y*
τ	advective time delay
ω_i	weighting factor for the *i*th sample

LIST OF TABLES

LIST OF FIGURES

Chapter 1

INTRODUCTION

In recent years the dealings of humans with natural resources has adapted steadily. More restrictive regulations by the water management bodies have already produced a positive effect on water resources in general.

The pollution of surface water has not only an impact on aquatic life forms in rivers and receiving streams, the ecosystem of the oceans as well as the groundwater, which represents an important part of our potable water resources, can be affected. The pollution of surface waters may lead to degeneration and extermination of known and even nowadays unknown aquatic resources. Impact on groundwater may lead to a quality, which may make it unsuitable for potable water uses or impose costly treatment activities. The protection of the environment, especially the protection of the water resources, is therefore very important.

Of environmental concerns are airport activities to ensure wintertime flight safety. Airports are facing the dual challenge of simultaneously maintaining the public safety and also protecting the environment. Ice formations on aircrafts as well as on runways and taxiways signify a dangerous threat to air traffic. Up to now the best way to remove ice formations in terms of safety and economical reasons is the use of de- and anti-icer. While the former are mainly glycol-based compounds, the latter consists of urea and a variety of acetate and formate based products (Switzenbaum *et al.*, 2001). The majority of these products are associated with a high BOD concentration that is detrimental to the quality of receiving waters and can also be directly toxic to aquatic life (Fisher *et al.*, 1995). Further, the quality of airport runoff is characteristically similar to that of urban and highway runoff, and therefore contains other contaminants such as heavy metals, nutrients, suspended solids, faecal coliforms and hydrocarbon based oils and lubricants (Chong *et al.*, 1999).

A novel way of treating the airport runoff was introduced with the implementation of a gravel type subsurface flow reed bed in a small experimental scale in 1994 at Heathrow Airport (Worrall, 1995).

The use of man made wetlands, known as constructed wetlands, have become relatively widespread and covers a large number of applications. Constructed wetlands act as an efficient water purification system and nutrient sink and remove efficiently BOD, COD, suspended solids, nitrogen, phosphorus, metals, hydrocarbons and pathogens. Due to the movement towards sustainable, environmental engineering relying on natural ecologic processes, such artificial systems are being increasingly used rather than traditional energy and chemical intensive treatment processes.

A whole host of chemical, biological and physical processes occur within these wetland environments, due to their unique hydrology, soils and vegetation, making them a dynamic and often complex system in terms of nutrient cycling. The hydrology of wetlands controls the formation of typical wetland vegetation and soils and acts therefore as an overriding factor.

The promising results of the experimental set-up of constructed wetlands (Revitt *et al.*, 1997) led to the construction of a full-scale treatment system at Mayfield Farm at Heathrow Airport, designed to receive and treat the runoff of the eastern and southern catchment of Heathrow Airport. Since very few airports have recovery or treatment systems for aircraft de-icer, there is a big interest in alternative methods for managing de-icing fluid wastewater (Bausmith and Neufeld, 1999).

Therefore the assessment of the performance of the subsurface reed beds at Heathrow Airport has a significant importance for further designs of treatment applications since no data of real scale applications of subsurface reed beds is reported up to now.

1.1 AIMS AND OBJECTIVES

The aim of this thesis is an assessment of the treatment performance in terms of removal of the glycol components of de-icer in airport runoff in the initial stage after completion of the building works.

The specific objectives for the research were as follows (Figure 1.1):

- Evaluation of the pollutant transport properties, that characterise the Heathrow Constructed Wetlands: Design and realisation of experiments of pollutant transport. Derivation of a mathematical framework for the stochastic evaluation of pollutant transport parameters.

- Evaluation of the treatment performance of subsurface reed beds with regard to the airport specific pollutant of glycol: Design and realisation of experiments to determine the removal of glycol components and evaluation of removal performance rates.

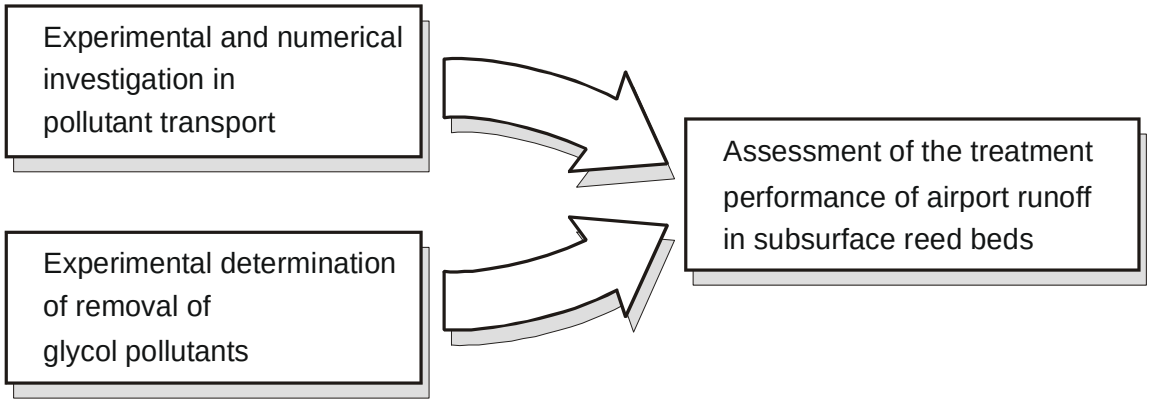

Figure 1.1. Aims and Objectives

1.2 STRUCTURE OF THE THESIS

In Chapter 2 a review of the relevant literature is presented. The characteristics of pollutant removal processes in constructed wetlands are highlighted in Section 2.1 and Section 2.2. In Section 2.3 the typical pollutants in airport runoff are presented. Section 2.4 covers the governing equations for the transport of pollutants in water and groundwater and focuses on the Advection Diffusion Equation (ADE) in Section 2.4.6 and the Aggregated Dead Zone model (ADZ) in Section 2.4.9. In Section 2.5 the computation of degradation rate kinetics is shown.

In Chapter 3 a framework for modelling pollutant transport is developed. Numerical techniques for modelling and parameter estimation with the ADE and ADZ model are highlighted in Section 3.2 and Section 3.3 respectively. Section 3.4 deals with the sensitivity and uncertainty of parameters while Section 3.5 covers aspects of the design of experiments.

The experimental investigations undertaken at the Heathrow Constructed Wetlands are presented in Chapter 4.

In Chapter 5 the experimental results are shown. Section 5.1 highlights the result of general tests, Section 5.2 shows the results of the test for hydraulic performance and Section 5.3 shows the test results of the treatment performance tests for glycol removal.

The discussion and evaluation of the experimental results is presented in Chapter 6. In Section 6.2 a pollutant transport model is developed. The performance of glycol removal is highlighted in Section 6.3. In Section 6.4 a pollutant removal model is developed.

The overall conclusions are summarised in Chapter 7 and suggestions for further work are made in Chapter 8.

Chapter 2

LITERATURE REVIEW

2.1 CONSTRUCTED WETLANDS

2.1.1 Introduction

Wetlands cover large areas of the world's surface. They can be found on every continent except Antarctica and subsequently in all climatic zones (Vymazal, 1998). Patten (1990) estimates, that wetlands cover some 7.7% of the Earth's landscape. Still there is considerable debate where those wetlands are estimated to exist. While some scientists state that up to 56% of the total wetland area is found in tropical and sub tropical regions, other estimate that a much higher percentage is found in boreal regions (Vymazal, 1998).

The term wetland is used to collectively describe areas of water saturated land which covers a diverse spectrum of ecological systems' (IWA, 2000). Spatially they are defined as transitional environments, found between dry land areas and deeply flooded lands (Kadlec and Knight, 1996). Thus areas which are not flooded but where the water is at or below the ground surface and the soil condition is saturated can be classified as wetlands. They provide a unique ecological habitat, which is in an ecological context an intermediate system between terrestrial and aquatic ecosystems (Raisin and Mitchell, 1995; Vymazal, 1998).

According to Vymazal (1998) the defining term "wetland" is a relatively new one. It is used to collectively describe areas of water-saturated land, originally known by different, often local, names. These would be used throughout the world to describe moorlands and fens, peat lands and swamp marshes, bogs and shallow freshwater and coastal zones. Despite this array of colloquialisms, these wetlands share common structural components typical for these ecosystems (IWA, 2000; Kadlec and Knight, 1996). The three major components that characterize wetlands are the hydrology, the vegetation and the soils.

- Hydrology: Standing water, which provides a habitat for aquatic organisms as living algae and populations of microbes, submerged and floating plant species and fish or other vertebrate animals.
- Vegetation: Hydrophytic plant species with the ability to grow, reproduce and persist in anaerobic soil conditions. Plants, with root systems, that emerge above the water surface.
- Hydric soils: Wetlands have unique soils, classified as water saturated hydric soil, which may develop anaerobic conditions and support chemical reducing processes.

The vegetation of wetland ecosystems are among the most productive plants in the world (Brix, 1993). The plants are highly adapted to their aquatic environment and are able to take advantage of the vast amount of light, water and nutrients available in it. The adaptations of the plants throughout the world are very similar, having evolved mechanisms to deal with the environmental stresses of free water supply and abnormal hostile chemical environment of the root zone (Etherington, 1983), rather than local climate factors. This highly adapted vegetation of wetland regimes enforces nutrient cycling, which leads to increased productivity of the vegetation and to accumulation of organic matter within the system (Vymazal, 1998). The annual organic productivity of temperate reed beds is between 30 and 60 t ha^{-1} $year^{-1}$, estimations of the annual productivity of tropical wetlands are up to 90 t ha^{-1} $year^{-1}$. Brix (1993) put this into context with fertile agricultural areas that have annual organic productivities between 20 and 25 t ha^{-1} $year^{-1}$.

Of equally high importance to the nutrient cycling processes of the plants are processes taking place in the wetland soils (IWA, 2000). Many physical and chemical transformations occur in this medium, while it is also a major source of available chemicals and nutrients for the plants. Settling or trapping effects of the medium may result in build-up of organic matter or mineral matter. A result from the flooding and water saturation of the medium is its isolation from atmospheric oxygen. The soil regimes are therefore dominated by anaerobic conditions and thus are often the major reducing element in the landscape (IWA, 2000). However, it still should be noted, that there might exist oxidised pockets in the soil and oxidised streaks corresponding to root channels allowing oxidisation processes to occur.

Nevertheless, the hydrology of the wetlands is the overriding factor, as this controls the formation of the typical soils and vegetation of the wetlands. The hydrological condition is the determinant of species composition and influences the soil and nutrients, which in turn influences the character of the biota (IWA, 2000). Disturbance in the biota or soil will produce a wetland in which the characteristic species or substrates will be, at least temporarily, absent. In contrast to this, the elimination of the characteristic hydrology of a wetland will result in the elimination of the wetland itself (Vymazal, 1998).

Wetlands have been used for wastewater treatment purposes for centuries. While in many cases the reasoning behind this was disposal rather than treatment, uncontrolled discharges of wastewaters lead to irreversible degradation of many wetland areas. Börner *et al.* (1998) note that wetlands were considered for long periods as "wastelands" and therefore were scientifically neglected. Increased knowledge and systematic research lead to a different attitude towards wetlands. The controlled use of wetlands for water treatment and purification developed, used in an increasing number of applications (Kadlec and Knight, 1996). Recognising the potential of wetlands for these purposes, scientists developed constructed wetlands.

Constructed wetlands are engineered systems, which are designed and constructed to utilize the natural processes involving typical wetland vegetation, soils and their associated microbiology within a more controlled environment. Scientific studies on constructed wetlands undertaken over the last four decades or so showed that these artificial systems, mimicking physical and chemical processes occurring in natural wetlands, are efficient in terms of water treatment and pollutant removal. The efficiency of these systems to remove suspended solids, organic compounds, nitrogen, phosphorus, heavy metals and pathogens from water had been shown in various applications (Kadlec and Knight, 1996).

Due to increased environmental awareness in the public, constructed wetlands are being progressively more used and accepted for the treatment of water. Relying on natural ecological processes, constructed wetlands are going further than traditional wastewater treatment methods in supporting the ideas of environmental and sustainable engineering. Compared to traditional methods, the use of constructed wetlands can be a cost-effective and technically feasible approach to the treatment of wastewater and runoff for the following reasons (IWA, 2000):

- constructed wetlands can be less expensive to build than other treatment options
- operation and maintenance expenses are low (labour, energy and supplies)
- operation and maintenance require only periodic, rather than continuous, on-site labour
- wetlands are able to tolerate fluctuations in flow
- wetlands are able to treat wastewaters with low organic load (too low for activated sludge)
- they facilitate water reuse and recycling

Further benefits are:

- they provide habitats for many wetland organisms
- they can be built to fit harmoniously into the landscape
- they are an environmentally sensitive approach that is viewed with favour by the general public

These advantages resulted in the involvement of many research groups, the water industry and the production industry into intensified studies for the optimisation of the wetland "technology" for the removal of specific pollutants or the design of specific applications. Although this technology is still somewhat innovative, long-term operational studies exist for some full-scale applications. This knowledge together with reports on pilot scale facilities and data of younger full-scale systems has led to an increased understanding of the physical, chemical and biological processes occurring in treatment wetlands and to the development of some design guidelines (e.g. IWA, 2000). Nevertheless, some studies also show the limitations of constructed wetlands. Therefore it is necessary to show the constraints of constructed wetlands for wastewater treatment and to highlight the problems arising from such (Gopal, 1999).

2.1.2 Types of constructed wetlands

Constructed wetlands are engineered systems designed to simulate the processes occurring in natural wetlands but having the advantage of a controlled environment. They are essentially recreations of natural wetlands, copying their topography and hydrology. They are designed to promote the growth of typical wetland vegetation and biota, allowing the complex chemical and biological interactions for the treatment of water to occur.

Due to their controlled environment, these designed systems are different in some specific topics compared to their natural counterparts. Constructed wetlands have typically a uniform hydrology, which does not vary over the year. Further they have a uniform substratum instead of a diverse soil system in the natural wetlands. The uniform hydrology and uniform substratum optimises the hydraulic movement of the water in the system and makes it unifom. Thus optimising the treatment performance (Gopal, 1999). As a result of this uniformity, constructed wetlands have typically a quite low diversity of plant species (IWA, 2000).

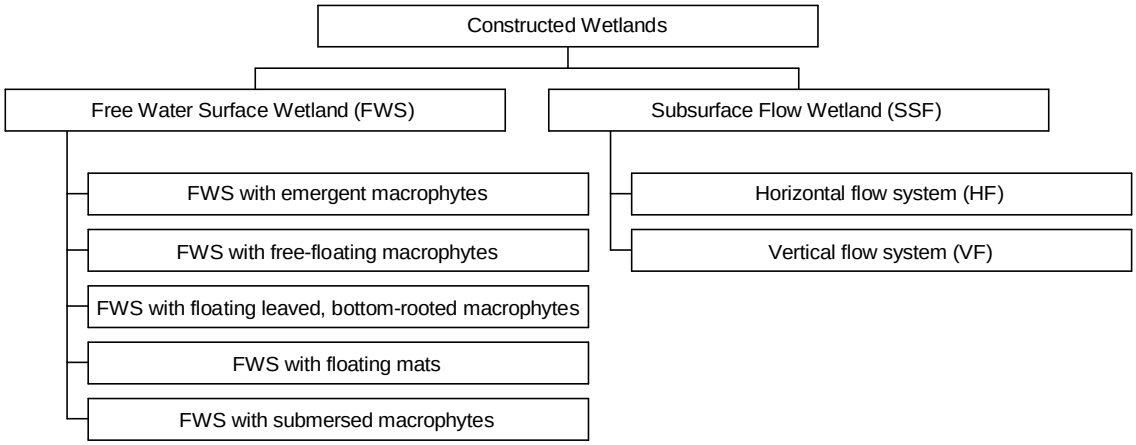

Figure 2.1. Classification of constructed wetlands

Generally, constructed wetlands can be ordered into two groups, the group of Free Water Surface treatment wetlands (FWS) and the group of Subsurface Flow treatment wetlands (SSF). The numerous types of wetlands can be classified accordingly to their property of having a free moving water body or the water moving through the soil (Figure 2.1).

Free water surface treatment wetlands. The technology of free water surface treatment wetlands is a direct mimic of the hydrological regime of natural wetlands. FWS are shallow ponds, containing 20 to 30 cm of rooting soil (Kadlec and Knight, 1996). Water flows over the soil surface from an inlet point to an outlet point. Anaerobic microbial processes dominate processes in the water column in deeper zones of FWS in the absence of light, similar to the processes occurring in facultative ponds. The net carbon production in the vegetated FWS tends to be higher than in ponds due to the high gross primary production in the form of structural carbon. In the process of elemental cycling, chemical free energy is extracted by the heterotrophic biota and fixed carbon and nitrogen are lost to the atmosphere. Further, phosphorus and other non-volatile elements may be lost from the element cycle, being accredited to the wetlands sediments. Wetlands themselves are autotrophic systems, where the pollutants from the receiving waters are simultaneously processed with the fixed carbon and nitrogen from the atmosphere. The net effect of these complex processes generally decreases the pollutant load in the water. Nevertheless, outflow concentrations are seldom zero and may even in some cases and for some parameters exceed inflow concentrations due to their internal autotrophic processes (IWA, 2000).

FWS wetlands with emergent macrophytes. FWS consists of shallow basins, where the base is a soil matrix to support the roots of the vegetation. The water is flowing above the soil with sediments and litter (Figure 2.2a). The live and dead plants extend above the wetland waters (emergent). Plants that are used are macrophytes such as common reed (*Phragmites australis*), bulrushes (*Scripus* spp.), sedges (*Cyperus* spp.) or cattails (*Typha* spp.). A water control structure maintains a shallow depth of the water. Typical water depths range from a few centimetres up to a metre.

The large cross-sectional areas result in low flow velocities, allowing incoming suspended solids (SS) to settle or be trapped. These particulates may contain particulate BOD, fixed forms of total nitrogen or total phosphorus or trace levels of metals and organics. They enter the element cycle within the water body or at the surface of the soil base. Microbial growth, the vegetation and the soil sorb parts of the dissolved fractions of these pollutants. Soluble BOD is removed by suspended or attached microbial growth. The reaeration at the water surface is the oxygen source for this reaction. While the deeper sections and the sediments are usually anaerobic, the near surface areas are aerobic. Therefore nitrification and denitrification in these

zones removes nitrogen. Nitrifying bacteria oxidise ammonia in aerobic zones, denitrifying bacteria convert nitrate to free nitrogen in the anoxic zones. Phosphorus is removed at the boundary layer between the water column to the soil. However, the removal rate is limited due to the small contact area (Brix, 1993).

While free water surface wetlands generally require less costs to build and to operate than other systems and are also relatively easy to construct, they require larger areas of land on which to be built (IWA, 2000).

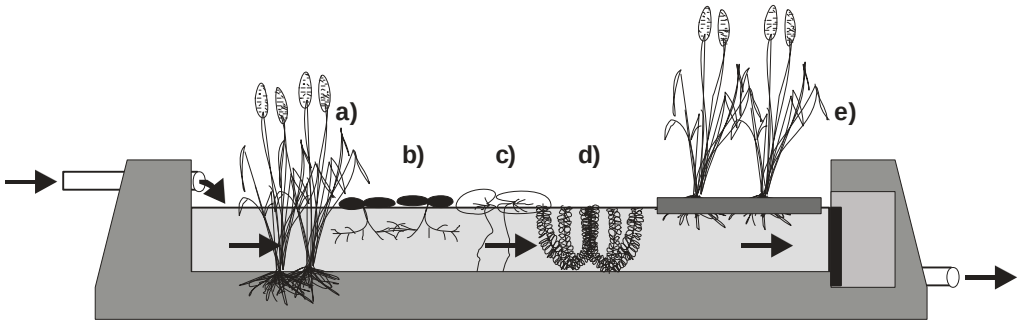

Figure 2.2. Free water surface wetland with different vegetation a) emergent macrophytes, b) free-floating macrophytes, c) floating-leaved, bottom-rooted macrophytes, d) submersed macrophytes and e) floating mats, rafted reed-beds

FWS with free-floating macrophytes. The structural difference of FWS with free-floating plants to FWS with emerged macrophytes is that they do not need soil as a support medium for the plants. This Floating Aquatic Plant (FAP) system utilizes species of floating vascular plants (Figure 2.2b). Plants used in these systems are water hyacinth (*Eichhornia crassipes*), duckweed (*Lemna* spp.) or water lettuce (*Pistia stratiotes*). These plants use photosynthesis in their parts at or above the water surface to convert atmospheric carbon dioxide into oxygen (Brix, 1993).

Like the FWS system mentioned before, suspended solids and particulate BOD are removed by sedimentation or filtration by the root of the plants. The plants themselves won't remove BOD or SS from the water, but provide support for it. The roots of the plants are supporting bacterial growth. Molecular oxygen from the process of photosynthesis is being translocated to the roots and is available to the root zone bacteria for aerobic metabolism. A further function of the roots is to take up nutrients from the water body (Vymazal *et al.*, 1998; Kadlec and Knight, 1996). The floating plants tend to cover the whole water surface, therefore gas transfer and light penetration into the water body is limited. Consequently, the water of FWS with floating macrophytes is anaerobic and nearly free of algae (IWA, 2000).

FWS with floating-leaved, bottom-rooted macrophytes. These FWS are a mix of both previously described systems (Figure 2.2c). While the plants themselves have roots, they utilise soil at the systems base as a support medium. However, their leaves are floating on top of the water surface. The plants used in this system are water lilies (*Nymphaea* spp.), lotus (*Nelumbo* spp.) and cowlily (*Nuphar* spp.) (IWA, 2000).

FWS with submersed macrophytes. Plants for the FWS with submersed macrophytes have their photosynthetic plant tissue below the water surface. The plant might or might not be rooted, being buoyant and suspended in the water column (Figure 2.2d). The submersed macrophytes used in FWS are waterweed (*Elodea* spp.), water milfoil (*Myriophyllum* spp.) and naiads (*Najas* spp.).

Since plants are being submersed, this type of system brings some drawbacks. The plants themselves are quite sensitive to anaerobic conditions. Further, their rate of ammonia removal is related to their photosynthetic rate. The process of photosynthesis allows nitrification by supplementing oxygen and also, the plants take carbon dioxide from the water up, raising the pH of the water. This allows the ammonia to convert into its unionized and volatile form that can diffuse into the atmosphere (IWA, 2000). However, with an increase in turbidity, the process of photosynthesis is reduced and with it some of the related treatment processes. Generally these systems are not widely used.

FWS with floating mats, rafted reed-beds. Some emergent macrophytes can form floating mats. Being buoyant through trapped air in roots and stems and becoming stable when roots and rhizomes of a large group of plants are woven together. Macrophytes are capable of forming these mats (Figure 2.2e). Plants used for this wetland type are common reed (*Phragmites australis*), cattail (*Typha* spp.), pennywort (*Hydrocotyle umbellata*) and giant sweetgrass (*Glyceria maxima*). Rafts with some penetrable mat, on which the macrophytes are planted, often give initial stability and buoyant support.

Removal of pollutants is similar to FWS with free-floating macrophytes, where the root system takes nutrient up and support microbial life (IWA, 2000).

SSF subsurface flow system with horizontal flow. SSF with horizontal flow (HF) consist of basins filled with a porous medium for the support of the vegetation (Figure 2.3). Water enters the wetland usually continuously in the in the inlet-zone, where it is distributed evenly over the cross-section. The wastewater then flows slowly through the porous medium on a horizontal flow path. The water is collected at the end of the porous medium at the outlet zone and finally discharged. The media used is usually sand or gravel, sometimes a less porous soil with clay particles (IWA, 2000).

During the passage through the medium, the wastewater is cleaned by physical and chemical processes and by biological degradation. The porous media is of particular importance for the treatment in such systems. It supports the vegetation and provides support and attachment surface for microorganisms. Further, there exist numerous aerobic, anaerobic and anoxic zones within the medium (Vymazal *et al*., 1998). Frequently used plants are common reed (*Phragmites australis*). Also reed canary grass (*Phalaris Arundinacea*), sweet mannagrass (*Glyceria maxima*), bulrushes (*Scripus* spp.), and cattail (*Typha* spp.) are used.

Suspended solids and settables are removed effectively by filtration. Aerobic and anaerobic processes, utilising microorganisms attached to the media or the roots and rhizomes of the plants, remove organic compounds. The re-oxygenation occurs by diffusion of oxygen leakage from the plants roots and rhizomes. Nevertheless both ways have quite a limited transfer rate (IWA, 2000). Nitrogen is removed in several ways, including nitrification and denitrification, volatilisation, adsorption and plant uptake. Phosphorus is removed by ion exchange with the media.

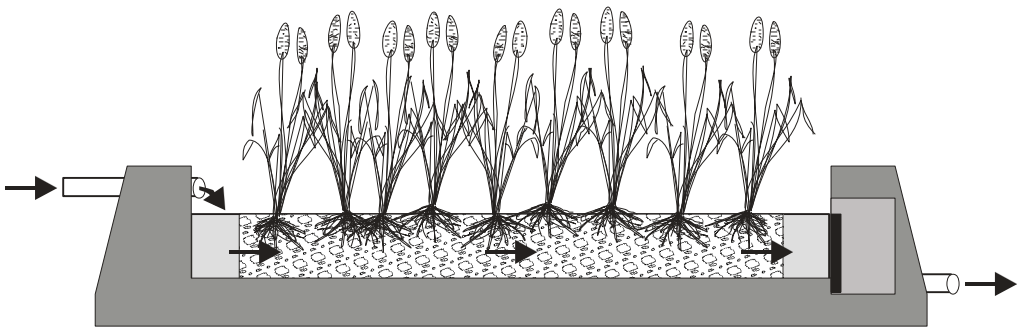

Figure 2.3. Subsurface flow wetland with horizontal flow

SSF subsurface flow system with vertical flow. Using support media similar to the horizontal flow SSF wetlands, the vertical flow (VF) SSF wetlands have a different hydraulic regime. Wastewater is fed intermittently in batches on top of the wetland, flooding its surface. The water then drains vertically through the porous medium, forced down by gravity. A drainage network at the base of the bed collects the water for discharge. The bed drains completely before the next batch of water is applied, causing the pore space to be filled with air. The rapidly applied next dose of water traps the air in the pore space. This process results in a good oxygen transfer. Vertical subsurface flow wetlands are very similar to rustic biological filters (Cooper *et al.*, 1996).

The ability of VF wetlands to hold back suspended solids and settables is obviously less good than those of the HF wetlands, but due to its good oxygen transfer, it has an increased ability to decompose BOD and to nitrify ammonia nitrogen.

Recent research has involved combined systems of HF and VF wetlands. These hybrid systems combine the advantages of the aerobic treatment of BOD and nitrification of ammonia in VF systems with the increase of denitrification in anaerobic HF systems (Cooper, 1999).

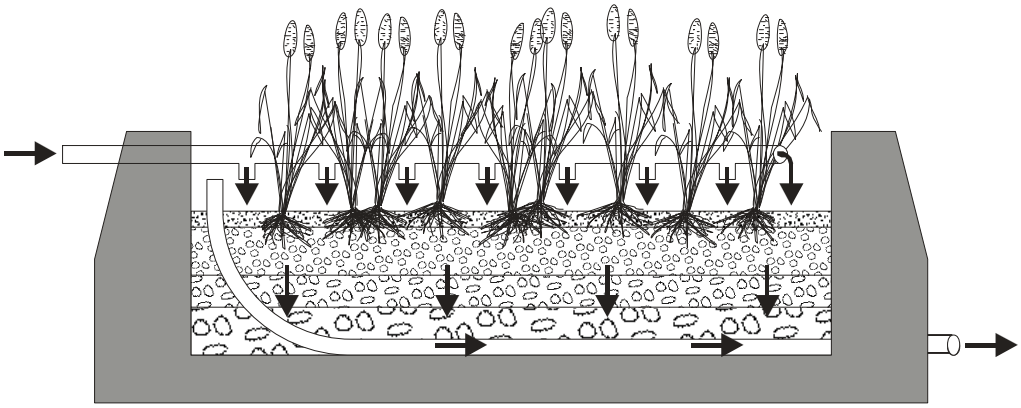

Figure 2.4. Subsurface flow wetland with vertical flow

2.2 POLLUTANT REMOVAL PROCESSES IN CONSTRUCTED SUBSURFACE FLOW WETLANDS

The research being covered in this thesis covers the treatment of glycol laden airport runoff in horizontal flow subsurface wetlands. Since the design of this treatment wetland has been given, this part of the literature review focuses, in the first hand, on treatment processes in subsurface flow wetlands as well as on the pollutants as such. Only little data are published on the use of these systems for this particular application. While there is some data available for a trial system (Revitt *et al.*, 1997), so far no data has been published on full-scale subsurface flow wetlands for the treatment of airport runoff. Nevertheless, it is still questionable, how far data from trial systems can be transferred to large-scale systems.

This chapter focuses therefore on a general review of removal pathways of pollutants in horizontal, subsurface flow treatment wetlands as well as on the different pathways utilised to treat glycol-laden airport runoff.

The knowledge of the different pathways and processes of pollutant removal is essential for the understanding of the removal of particulate pollutants from industrial processes and it allows conclusions to be drawn for further application of this technique.

While the pressure of dealing with airport runoff has increased within the last decade, this topic also became a focus for research in recent years. Therefore the second part of this review focuses on the treatment options for this specific pollutant and on treatment options being covered by recent research.

A common difficulty experienced by wetland treatment systems has been inadequate oxygen supply. When wetland systems are overloaded by oxygen demanding constituents, or

are operated with excessive water depth, highly reduced conditions occur in the sediments, resulting in plant stress and decreased removal efficiencies for biochemical oxygen demand and ammonia nitrogen (IWA, 2000, p10). A common problem encountered in SSF constructed wetlands is an inadequate hydraulic gradient, reducing flow through the bed and resulting in surface flow.

As highlighted before, a horizontal subsurface flow treatment wetland consists of the main three components of porous medium, vegetation and hydraulic regime. The interactions between these three components in the treatment process are quite complex. The general chemical and biochemical pollutant and nutrient cycling processes are well known, since they happen in treatment processes in wastewater treatment plants or in natural treatment processes, e.g. in rivers. The removal and cycling processes for main parameters, like BOD, COD, nitrogen and phosphorus is reviewed in this section. Plants undoubtedly play a major role in enhancing the wildlife habitat values, aesthetics and perceived naturalness. However, there is still much discussion on going, if plants make an actual difference to the treatment performance (Brix, 1997). Therefore first the general role of the macrophytes in that environment is highlighted, before discussing the different removal processes of pollutants, including the aspect of the plants in these processes.

The role of the Plants. The plants used in constructed wetlands are macrophytes. Macrophytes are organisms, which produce organic matter in a photoautotrophic process that uses solar energy to assimilate inorganic carbon from the atmosphere. Subsequently, this organic matter is the energy source for heterotrophic organisms like fungi, bacteria and animals.

Due to the water filled pore-space in the medium and a very low oxygen diffusion coefficient, the water-saturated medium consequently becomes anaerobic or anoxic except for a few millimetres at the surface of the medium. Anaerobic conditions in the water soil matrix can result in the release of reduced elements and compounds (Vymazal *et al.*, 1998). These reduced elements and compounds like Fe^{2+}, H_2S or Mn^{2+} can reach concentrations that are toxic to the roots. Similarly the reduced elements become soluble and mobile and therefore available for plant uptake. This may result in plant uptake that can also reach toxic levels. Oxygen cannot be taken up from roots and rhizomes but the macrophytes have the ability to transport oxygen internally within the plant, either through diffusion or convective flow (Brix, 1993a). This ability of the plants is vital to the plants, since they senescent rapidly and die within a few hours, if deprived of oxygen generated from photosynthesis or transported from the atmosphere to internal tissues (Wetzel, 2000). Some of this oxygen transported into the root leaks out and thus is detoxifying the reduced elements within the saturated soil matrix (Brix, 1993). While this effect is well documented and accepted (Vymazal *et al*., 1998), the quantitative oxygen release under in situ conditions remains a controversial topic of discussions (Sorrel and

Armstrong, 1994). Reported release rates estimated and measured are in the range of 0.02 g O_2 m^{-2} day^{-1} (Brix, 1990), 1 to 2 g O_2 m^{-2} day^{-1} (Gries *et al.*, 1990) and 5 to 12 g O_2 m^{-2} day^{-1} (Armstrong *et al.*, 1990). Sorrel and Armstrong (1994) showed the importance of providing an external oxygen sink during those oxygen release tests and concluded that earlier studies may have underestimated the oxygen release rate by roots. However, according to IWA (2000) the capacity of the reeds to transport and release oxygen to ensure aerobic decomposition in the rhizosphere is insufficient and Wetzel (2000) adds that any expectations that macrophytes can be adequately efficient to aerate saturated organic-rich sediments are not realistic.

Nevertheless, the predicted depth of plant root penetration, and thus the potential for oxygen release, has been proposed as a rational basis for determining the appropriate depth of SSF treatment wetlands (Reed *et al.*, 1995). Tanner (2000) highlights, that many studies report root penetration of less than 300 mm in gravel-type horizontal flow wetlands. That is considerably shallower than depths reported in commonly cited guidelines and reports of 300 to 760 mm, depending on the plant species. He goes on, that the primary environmental factor influencing the depth of root zone penetration was the increased concentration of BOD rather than nutrients. Since it is in the plant's interest to restrict oxygen losses from the roots as much as possible, this will be the limiting factor for the length and diameter of the roots. He highlights the consistency of his observations and conclusions with current theories and models of plant aeration (e.g. Sorrel *et al.*, 2000).

Wetlands form major sources of gaseous end products of fermentative metabolism of organic carbon. In particular they are releasing large amounts of CO_2 and CH_4 (Wetzel, 2000). Tanner (2000) states, that wetland plants may regulate the balance between gas production and consumption processes in the sediment. Lower methane emissions for planted than unplanted SSF wetlands are reported, concluding, that plant oxygen release is suppressing methanogenesis (a strictly anaerobic process) in the gravel media and/or enhancing root-zone methane oxidation.

A physical effect of the rooting system of the plants is, that they prevent clogging of the medium and increase or stabilize the hydraulic conductivity of the medium. As the roots and rhizomes grow, they disturb and loosen the soil. When roots and rhizomes die, they leave behind tubular pores and channel-type macropores (Brix, 1997). While this effect has been claimed to be of importance for soil-based subsurface flow beds, experiences in the U.K. showed that it is not valid for the many wetlands with gravel-type beds. Coombes (2000) highlights, that the hydraulic conductivity on these beds is more stable and does not rely on the effect of the roots to disturb and loosen the medium.

Quite important for the winter operation of wetlands in cold climates is the insulating effect of the vegetation of wetlands. Emergent plants reduce the wind speed and therefore the chill effect. The litter and the plants further help to protect the soil from freezing during the winter and, on the other hand, keep the soil cooler during summer (Vymazal *et al.*, 1998).

Suspended Solids. The removal of suspended solids can either happen by sedimentation/settling or filtration/trapping process. While sedimentation is not the dominant mode in subsurface flow wetland systems, it still can happen in some parts of subsurface flow systems due to its hydraulics. Open channels designed for water distribution and placed in front or between single wetland cells of a system, reduce the flow velocity and thus allow sedimentation. Deposits of sediments at these locations can result in operational problems, since it allows the plants to spread their territory and increases ground levels and thus may change the designed hydraulic characteristics of these channels (Kadlec and Knight, 1996).

Subsurface reed beds have a high potential to remove suspended solids due to their ability to filter (Cooper, 1999). Suspended solids will be filtered in the medium and deposited there (Börner *et al.*, 1998). The organic components will degrade biochemically (approximately 60% of the suspended solids). The remaining solids might then be rinsed out. High loads of suspended solids results in accretion and contributes to blocking or clogging of the medium especially near the inlet (Kadlec and Knight, 1996). This results in a reduced hydraulic conductivity and overland flow or ponding.

Reported removal rates for suspended solids in subsurface flow wetlands are high, ranging from values of 70% (Cooper and Green, 1998), over 75 to 85% (Brix, 1998) to 95% (Yang *et al*., 1995). It has to be noted, that the calculated performances largely depend on the inflow concentration, the types of wastewater and the hydraulic load. In nearly all cases the total effluent concentration is below 20 mg/L TSS. Compiled data for 37 Czech subsurface wetlands showed a decrease from a mean inflow concentration of 70 mg TSS/L to an outflow concentration of 11 mg TSS/L (IWA, 2000). A compilation of data of North American subsurface wetlands showed similar values, where the inflow concentration of 48 mg/L was reduced to 10 mg/L (IWA, 2000).

Organic Compounds (BOD and COD). In a wastewater of medium strength, typically 75 % of the suspended solids and 40% of the filterable solids are organic compounds (Metcalf & Eddy Inc., 1997). Organics are derived from nature (plant and animal tissues) or produced by synthesis reactions or fermentation processes in the chemical industries. Therefore industrial wastewater can contain high concentrations of soluble organics. Organic compounds are usually combustible, high in molecular weight, only sparingly soluble in water as molecules rather than ions, and a source of food for animal consumers and microbial decomposers (Hammer, 1986).

Organic compounds are composed of a combination of carbon, hydrogen and oxygen, together with nitrogen in some cases. Principal organic compounds found in domestic wastewater are proteins, carbohydrates and fats and oils. Glycols, used in de-icer, are carbon-

based compounds. Glycols are totally miscible with water and thus they are fully dissolved in the runoff of airports.

Settable organics are rapidly removed in subsurface wetlands by trapping and filtration. Soluble organic compounds are removed by suspended and attached microbial growth in the medium in terms of aerobic and anaerobic degradation. The oxygen for aerobic degradation is taken from the water. As stated before, re-aeration by diffusion is very slow and the oxygen supply by root leakage negligible. Uptake of organic matter by plants is also negligible compared with the biological degradation (Watson *et al.*, 1989; Cooper *et al.*, 1996).

Biological treatment of wastewater is based on microorganisms undertaking the treatment. To function properly and to continue to reproduce, these microorganisms must have an energy source. Carbon is used for the synthesis of new cellular material. Inorganic elements act as nutrient, such as nitrogen, phosphorus, sulphur potassium, calcium and magnesium. Organic nutrients may also be required. The two main carbon sources for the build up of cells are organic chemicals (organic matter) and carbon dioxide. Bacteria for biological degradation are classed into two groups and are called heterotroph, when using organic carbon for the formation of cell tissue (Hammer, 1986). They are called autotroph, when deriving cell carbon from carbon dioxide. Both groups of organisms use light or a chemical oxidation-reduction as an energy source for cell synthesis. The heterotrophic organisms are of special interest for the degradation of organic carbon in wastewater because of their requirement of organic matter as a carbon source and their higher rate of metabolism (IWA, 2000). The group of autotrophic bacteria which degrades organic compounds containing nitrogen under aerobic conditions are called nitrifying bacteria. This process is called ammonification and will be discussed in the section about nitrogen removal. These bacteria are further subdivided into three groups depending on their action towards free oxygen. Aerobes require free dissolved oxygen, anaerobes are able to oxidise organics in complete absence of dissolved oxygen by using oxygen bound in other compounds such as nitrate and sulphate. Facultative bacteria uses free dissolved oxygen if available but can also live in its absence by gaining energy from anaerobic reactions.

The following reactions describe the aerobic degradation of organic matter by the heterotrophic bacteria (e.g. Vymazal *et al.*, 1998; Hammer, 1986; Metcalf & Eddy Inc., 1997):

$$(CH_2O) + O_2 \rightarrow CO_2 + H_2O \qquad 2.1$$

With unlimited oxygen supply, the aerobic degradation will be governed by the amount of organic matter available for aerobic biological oxidation and an insufficient supply of oxygen will greatly reduce the rate of respiration and biological oxidation. Biological degradation can take place in the bulk of the wastewater, but will be low due to the limited number of bacteria in

suspension. The main biological degradation in wetlands takes place within the bacterial films present on the surfaces of the medium, sediments, roots and rhizomes and litter.

Anaerobic degradation is a multi-step process that takes place where oxygen supply is severely limiting. This may be the case for permanent saturated areas of wetlands or within the bed of horizontal subsurface-flow wetlands or in organically high loaded systems. The anaerobic degradation is performed by facultative bacteria or by obligate anaerobic heterotrophic bacteria. In the first step of the anaerobic degradation process, the organic matter is fermented to fatty acids, such as acetic acid (2.2), butyric acid and lactic acid (2.3), alcohols (2.4) and gases (Vymazal *et al.*, 1998).

$$C_6H_{12}O_6 \rightarrow 3CH_3COOH + H_2 \qquad 2.2$$

$$C_6H_{12}O_6 \rightarrow 2CH_3CHOHCOOH \text{ (lactic acid)} \qquad 2.3$$

$$C_6H_{12}O_6 \rightarrow 2CO_2 + 2CH_3CH_2OH \text{ (ethanol)} \qquad 2.4$$

The most predominant primary end product of the degradation of normal wastewater is acetic acid. The end product of the fermentation is then used by strictly anaerobic sulphate-reducing bacteria (2.5) and methane forming bacteria (2.6 and 2.7) to produce water, hydrogen sulphide and methane.

$$CH_3COOH + H_2SO_4 \rightarrow 2H_2O + H_2S \qquad 2.5$$

$$CH_3COOH + 4H_2 \rightarrow 2CH_4 + 2H_2O \qquad 2.6$$

$$4H_2 + CO_2 \rightarrow 2CH_4 + 2H_2O \qquad 2.7$$

The acid forming bacteria are fairly adaptable to the acidity of the water, but the methane-forming bacteria are more sensitive (Vymazal *et al.*, 1998). They will only work when the pH is in the range 6.5 to 7.5. Overproduction of acid by the acid formers can rapidly lower the pH. This will stop the operation of the methane-forming bacteria and results in the production of odorous compounds (rotten egg odour) within the wetland.

Biochemical Oxygen Demand. The Biochemical Oxygen Demand (BOD) and the Chemical Oxygen Demand (COD) are most commonly used to define the concentration of organics in wastewater and to define water qualities of water bodies. They also are used to evaluate waste loadings and efficiencies of wastewater treatment systems. The Biochemical Oxygen Demand (BOD) defines the quantity of oxygen, which is used by microorganisms to oxidise organic

matter in a sample under aerobic conditions. The BOD is usually quantified by measuring the amount of dissolved oxygen consumed over five days in a sample, resulting in a five day BOD measurement (BOD_5). In this reaction the bacteria metabolises organic matter by uptake of dissolved oxygen and release of carbon dioxide. Thus, a substantial increase in the bacterial population is gained (Hammer, 1986). In a second reaction the protozoa bacteria consumes oxygen while ingesting bacteria. Like Equation 2.1, Equation 2.8 shows the general biological reaction which takes place (Hammer, 1986). The biochemical oxygen demand for this reaction of degrading the organic matter is called carbonaceous BOD (cBOD).

$$\text{Organic matter} \xrightarrow[\text{bacteria}]{\text{dissolved oxygen}} CO_2 + \text{Bacterial cells} \xrightarrow[\text{protozoa}]{\text{dissolved oxygen}} CO_2 + \text{Protozoal cells} \qquad 2.8$$

Obviously the BOD is time dependent and not a single point value. The temporal development of the hypothetical biochemical oxygen demand of the carbonaceous reaction is shown in Figure 2.5. After a decent period of time, the biochemical breakdown of the pollutants reaches a threshold, the ultimate carbonaceous BOD ($cBOD_u$).

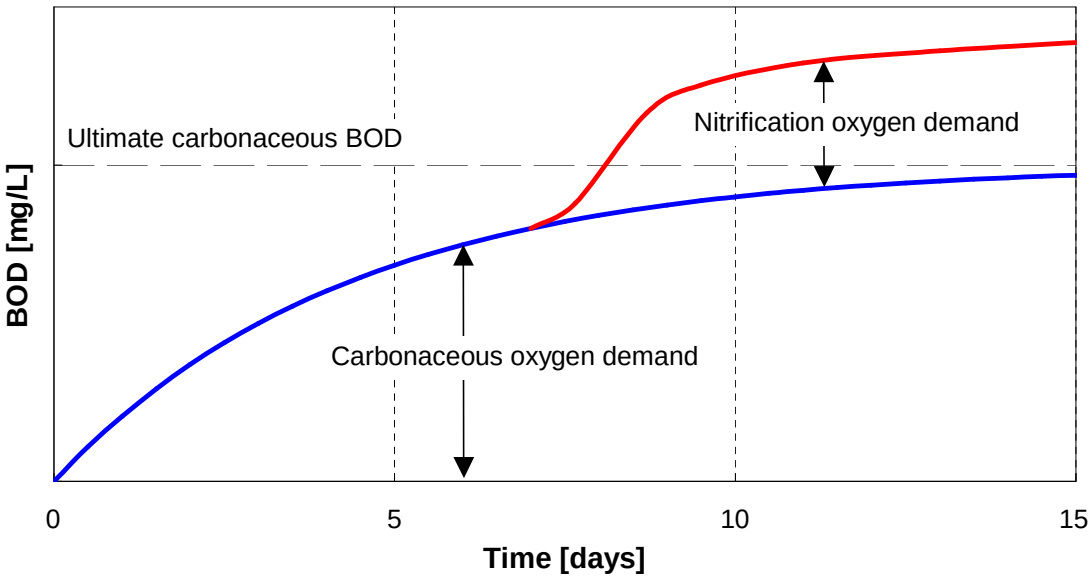

Figure 2.5. Hypothetical biochemical oxygen demand

The presence of ammonia nitrifying bacteria can also exert an oxygen demand. While the process of nitrification in untreated wastewater usually starts several days after the biochemical oxidation reaction process (see Figure 2.5), effluents of treatment systems and river water may show early nitrification and have therefore a nitrification oxygen demand. The process of

nitrification during the BOD tests can be inhibited with chemicals like Allylthiourea (ATU) which gives then cBOD or, as it is sometimes called, BOD (ATU).

A BOD test cannot reproduce the environment of treatment systems with its special physical, chemical and biological conditions accurately. Therefore this test is subject to some uncertainties and inaccuracies (Metcalf & Eddy Inc., 1997; Hammer, 1986). Firstly the bacteria in a sample have to be adapted to the pollutant. Otherwise the bacteria will just not recognise the pollutant as a source of energy and therefore the breakdown or oxidation process will start slowly or will not happen at all. Secondly, some other chemicals or by-products in the sample might inhibit the activity of the bacteria to break down the pollutants. Thirdly, the results of a BOD test depend largely on the actual concentration of bacteria in the sample, which is also not certain to be constant and may change due to the seasonal and temporal-load character of pollutants entering the treatment facility. Seeding the samples with microorganisms may be used to overcome this problem. But then again it is questionable whether the activity of the seeded bacteria is highly comparable with the bacteria of the treatment system. A fourth uncertainty is that only biodegradable organic matter is measured with this test, where easier degradable organics are obviously the first compounds to be degraded. Also, the test has no stoichiometric validity, after the soluble organic matter has been used. A further limitation is that the usual 5 day test-period may not match up to the time, where the soluble organic matter that is present has been used (Metcalf & Eddy Inc., 1997). Consequently for the reason of the variations in bacterial decomposition of organic material, the degree of reproducibility of the BOD test cannot be precisely defined. Tests have shown that the variations in observation vary in the range of 10 up to 20 percent on either side of the mean (Hammer, 1986).

Since this method of BOD determination cannot separate between different pollutants of a sample, it is indicating the organic load as a sum parameter. Nevertheless, since sometimes the pollutant is just a single substance and therefore known, these methods can than be interpreted in terms of an indirect method for the determination of mass of this specific pollutant in the water sample.

Chemical Oxygen Demand. The Chemical Oxygen Demand (COD) is also a parameter used to define the content of organic matter in wastewater. While the BOD test utilises bacteria to mediate the oxidisation of organic pollutants in a specific period of time, the COD test uses chromate to perform the oxidisation of the organic pollutants to carbon dioxide and water. The COD of the sample is then equivalent to the mass of oxygen consumed per volume of sample during this process of analysis. The general equation or this reaction using dichromate as the oxidising acid is given unbalanced in Equation 2.9. Since the Chemical Oxygen Demand test excludes the uncertainties of biological oxidisation of the sample, it has a much higher degree of

reproducibility. Test kits for the measurement of the COD in the range of 5 to 150 mg COD/L are accurate within 5 mg COD/L.

$$\underset{\text{matter}}{\text{Organic}} + Cr_2O_7^{--} + H^+ \xrightarrow[\text{catalyst}]{\text{heat}} CO_2 + H_2O + 2Cr^{+++} \qquad 2.9$$

The COD of wastewater is in general higher than its BOD, since more organics can be oxidised chemically than biochemically. For particular wastes a relationship between BOD and COD can be determined by comparison in several laboratory tests. Hammer (1986) states, that occasionally the COD of a soluble wastewater can be assumed to be numerically equivalent to its ultimate carbonaceous BOD value. Correlations among measures of BOD_5, COD, the Theoretical Oxygen Demand (ThOD), the amount Total Carbon (TOC) and the Theroetical Total Carbon (ThTOC) are given in Metcalf & Eddy Inc. (1997) and are shown in Figure 2.6. The ThOD and ThTOC can be computed from stoichiometric reactions, if the chemical formula of the organic matter is known. Of all the tests the BOD_5 is the most difficult parameter to correlate, as discussed before. For typical domestic wastewaters the BOD_5/COD ratio varies from 0.4 to 0.8 and the BOD_5/TOC ratio varies from 1.0 to 1.6 (Metcalf & Eddy Inc., 1997); Hammer, 1986).

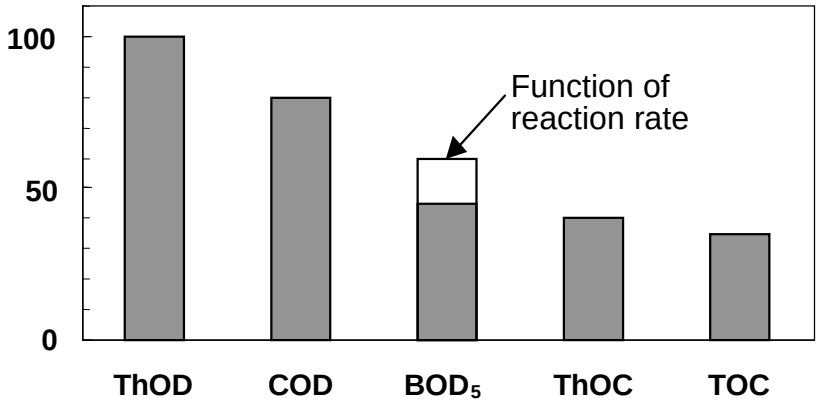

Figure 2.6. Approximate relationship among measures of the organic content of wastewaters (adopted from Metcalf & Eddy Inc.(1997))

The performance of horizontal subsurface flow reed beds in the U.K. is detailed by Cooper and Green (1998). The efficiencies of three beds used for secondary treatment gives performances of 85%, 85% and 95% correlating to inflow/outflow BOD_5-concentrations of 87/13 mg/L, 306/46 mg/L and 77/3.7 mg/L. A system for tertiary treatment showed an efficiency of 84% with inlet/outlet concentrations of around 9.1/1.5 mg/L. Data of 29 further

tertiary wetlands showed that effluent concentrations of less than 5 mg BOD_5/L were achieved. Similar observations from 107 wetlands are reported by Börner *et al.* (1998), where wastewaters of the inflow concentrations in the range between <20 and >1000mg BOD_5/L were treated to effluent concentrations of 3 to 166 mg BOD_5/L. Gravel type wetlands show efficiencies between 60% and 86%, resulting in effluent concentrations between 11 and 21 mg BOD_5/L. A similar observation is reported by Knight *et al.* (1993), where the performance of 69 surface flow and 15 subsurface flow systems showed an average effluent concentration of 10.5 mg BOD_5/L with the related average efficiency of 73%. Vymazal (2002) averages the removal efficiencies of 55 Czech horizontal subsurface flow wetlands with 88%, achieving a averaged effluent concentration of 10.5 mg BOD_5/L. Generally a poor relationship between inflow and outflow BOD_5 concentration was reported. The relationship of the observations for the Czech systems had a coefficient of regression of $R^2 = 0.32$ (Vymazal, 2002) and observations for the systems in Denmark have a coefficient of regression of $R^2 = 0.08$ (Brix, 1998). The wide spread of reported BOD_5 effluent concentrations shows its dependence on factors such as ratio of suspended/soluble BOD, chemical decomposition of BOD, hydraulic load and other hydraulic properties like retention time (Cooper and Green; Vymazal, 1998). The wide spread of reported efficiencies expressed as a percentage of removal could be misleading, since the percentage of efficiency will increase with increased inflow concentration (Vymazal, 2002).

The temperature of water and air also affects the removal rate of BOD. Winter efficiency in 5 Bavarian subsurface flow reed beds decrease between 5 and 15% (Börner *et al.*, 1998), which will result in a BOD increase in the effluent of 10 to 20 mg BOD_5/L. The same range of decrease is reported from a 7-year survey of a subsurface flow bed in the U.K. (Cooper *et al.*, 1996).

Reported effluent rates for COD are higher than those of BOD, observed efficiencies for COD are smaller than those of BOD. The reported effluent concentrations for the Bavarian subsurface flow wetlands are in the range of 34 to 73 mg COD/L and thus 2 to 3 times higher than the reported BOD. The removal rates of these wetlands are 4 to 13% lower than the equivalent rates for BOD_5 (Börner *et al.*, 1998). Yang *et al.* (1995) report similar rates for removal, 74% for COD compared to 91% for BOD_5. The same efficiencies had been observed for systems in the Czech Republic (Vymazal, 2002). The average efficiency was 74% with an effluent concentration of 53 mg COD/L. The general lower removal of COD compared to the BOD_5 is due to the presence of non- or low-biodegradable pollutants.

Nitrogen. Increased nitrogen and phosphorus concentrations in rivers and receiving water have quite a large impact on their quality. Nitrogen and phosphorus are nutrients to water plants and algae. Trace quantities of other elements, such as iron, are also needed for biological growth, but nitrogen and phosphorus are, in most cases, the major nutrients of importance. High

levels of nutrients may cause an increase in productivity of plants and algae (Metcalf & Eddy Inc., 1997). This process, called eutrophication, leads to increasing levels of respiration of oxygen by aquatic biota that will cause a decrease in oxygen concentration in water and may harm other aquatic life forms. Nitrogen compounds include ammonium (NH_4), nitrate (NO_3), nitrite (NO_2) and nitrous oxide (N_2O). The nitrogen present in wastewater is in particulate and dissolved form (proteins and nucleic acid) and inorganic form (ammonium and nitrate). Wetlands themselves contribute large amounts of organic nitrogen to the system as the plants die and the plant litter decompose. These different chemical and physical forms of nitrogen are interlinked and form the so-called nitrogen cycle. Thus, the process of nitrogen removal is quite complex and will happen in various ways (Kadlec and Knight, 1996).

The sequential processes of ammonification, nitrification and denitrification is the main mechanism for the removal of organic nitrogen. Organic nitrogen is mineralised to ammonia by hydrolysis and bacterial degradation. Ammonia is oxidised to nitrate by nitrifying bacteria under aerobic conditions. Denitrifying bacteria convert nitrates to nitric oxide (NO_2) and nitrous oxide (N_2O) under anoxic or anaerobic conditions. Other removal mechanisms of nitrogen in constructed wetlands are volatilisation, plant uptake and adsorption. These removal mechanisms are usually of less importance than the process of nitrification/denitrification (IWA, 2000).

Ammonia volatilisation. Un-ionised ammonia is relatively volatile and can be lost from the water to the atmosphere. Since un-ionised ammonia is only a small fraction of the total ammonia in the wastewaters and the rate of diffusion into the atmosphere is limited in subsurface flow constructed wetlands due to the medium, the process of volatilisation is believed to be insignificant for subsurface flow wetlands (Kadlec and Knight, 1996).

Ammonification (mineralisation). The biological process of ammonification (mineralisation) transforms organic nitrogen into inorganic nitrogen, especially NH_4^+-N. Ammonia may then be utilised from the water for the process of nitrification or is ready available for plant uptake. The highest rate of mineralisation can be found in oxygenated zones with aerobic bacteria. With lowering levels of dissolved oxygen the rate of mineralisation decreases, utilising facultative anaerobic and obligate anaerobic bacteria in anaerobic zones. The rate of ammonification is further dependent on temperature, available nutrients, the C/N ratio, soil conditions and the pH (Vymazal *et al.*, 1998).

Nitrification. The oxidation of ammonia to nitrate is called nitrification. This process is a two-step reaction sequence with nitrite as an intermediate. The nitrifying bacteria derive energy from the process of oxidising ammonia and/or nitrite for the synthesis of new cells. Nitrifying bacteria are strictly aerobic and the process of nitrification occurs in the aerobic zones of the

wetland (Equations 2.10 and 2.11). Approximately 4.3 mg of O_2 per mg of ammoniacal nitrogen oxidised to nitrate nitrogen is needed.

$$NH_4^+ + 1.5O_2 \rightarrow NO_2^- + 2H^+ + 2H_2O \qquad 2.10$$

$$NO_2^- + 0.5O_2 \rightarrow NO_3 \qquad 2.11$$

Nitrification is further influenced by temperature, pH value and alkalinity (Vymazal *et al.*, 1998). The minimum temperature for the nitrifying bacteria for the process of nitrification is 4°C and 5°C respectively. The optimum pH range is between 7.5 and 8.6. The process of nitrification also consumes a large amount of alkalinity. Approximately 8.64 mg of HCO_3^- per mg of ammoniacal nitrogen is needed.

Denitrification. Nitrogen in the form of nitrate can be removed by conversion to nitrogen gas by facultative heterotrophic bacteria in anoxic environment. This process is known as denitrification. The bacteria obtain energy for growth from the conversion process itself but require organic carbon source to act as a hydrogen donor and supply carbon for biological synthesis. The transformation of nitrate to molecular nitrogen via the intermediate nitrite can be seen in Equation 2.12 and Equation 2.13.

$$C_6H_{12}O_6 + 12NO_3^- \rightarrow 12NO_2^- + 6C0_2 + 6H_2O \qquad 2.12$$

$$C_6H_{12}O_6 + 8NO_2^- \rightarrow 4N_2 + 2CO_2 + 4CO_3^- + 6H_2O \qquad 2.13$$

The principle chemical pathways are not anaerobic but rather a modification of aerobic pathways. The facultative heterotrophs substitute oxidised N forms for O_2 as an electron acceptor in respiratory processes; therefore the term anoxic is used in place of the term anaerobic (Metcalf & Eddy Inc., 1997).

Due to the anaerobic conditions in subsurface flow wetlands, the denitrification rates are usually higher than the nitrification rates. It is generally acknowledged, that the lower nitrification rate results in a low nitrate production that will limit the rate of denitrification (Reddy and D'Angelo, 1997; Wittgren and Tobiason, 1995; Sikora *et al.*, 1995).

In addition to the presence of denitrifying bacteria, anoxic conditions and a carbon source, the pH value and the temperature will influence the rate of denitrification. The optimum pH range is between 7 and 8. Alkalinity produced during denitrification can increase the pH value. The rate of denitrification proceeds very slowly at temperatures below 5°C (IWA, 2000).

Plant uptake. Nitrogen is essential for plant growth and is taken up directly in the form of nitrates and ammoniacal nitrogen. Nevertheless, the rate of uptake is limited by the net productivity (growth rate) of the plant and the concentration of nutrients in the plant tissue (Vymazal, 1998). The uptake of nitrogen from emergent macrophytes is in the range of 1000 to 2500 kg N ha^{-1} yr^{-1} and could be removed by harvesting. If the wetland is not harvested, the majority of the nutrients will return in the wetlands nutrient cycle after decomposition of plant litter. Long-term storage just results from the undecomposed fraction of the litter. However, the amount of nutrients that can be removed by harvesting are insignificant in comparison with loadings into the systems from wastewaters (IWA, 2000).

Matrix adsorption. A further removal mechanism of nitrogen is adsorption. In a reduced state, NH_4-N is stable and can be adsorbed on active sites on the matrix of subsurface flow wetlands (Cooper *et al.*, 1996). Anyhow, adsorption is not being considered as a long-term storage, since the process is rapidly reversible. As the NH_4-N is lost from the system via nitrification, the adsorbed NH_4-N will redistribute itself to gain a stage of equilibrium.

The complex transformations and sequential series of reaction of nitrogen in wetlands must be considered when assessing performance rates. Influents where organic nitrogen is the dominant nitrogen parameter will first show an increase of ammonium concentration before nitrification can decrease it. If ammonia is the dominant parameter, nitrate might be observed as an increasing parameter before being decreased by denitrification. Vymazal (2002) highlights, that it has been generally agreed that the major removal mechanisms for nitrogen are ammonification and nitrification/denitrification. The author goes on, that higher rates of nitrogen removal are limited due to the anaerobic situation in subsurface flow treatment wetlands and thus a low rate of nitrification. As ammoniacal nitrogen is the prevailing form of nitrogen in wastewater, removal of nitrogen in horizontal flow constructed wetlands should be low. However, observations from existing systems show that nitrogen is removed in nearly all systems to some extent and in some systems even to a high level and that ammonification, nitrification and denitrification occur simultaneously in horizontal subsurface flow constructed wetlands (Vymazal, 2002).

The performance of a selection of subsurface reed beds for secondary and tertiary treatment is detailed in Cooper and Green (1998) for systems in the U.K.. In a five year operation period from 1990 to 1995 one secondary treatment system achieved an ammonia nitrogen removal performance of 86% on average with an outlet concentration of less than 2mg NH_4-N /L. This ammonia removal was attributed to high aeration and thus significant nitrification. Lower levels of ammonia reduction of 42% and 29% had been reported from two other secondary systems of subsurface flow reed beds. The lower levels were attributed to lower aeration and thus lower

nitrification. The authors note further, that a considerable amount of nitrogen was removed by denitrification. Observations by Börner *et al.* (1998) highlight the nitrogen efficiency for subsurface flow reed beds in Germany. Ammonia nitrogen and total nitrogen are both reduced on average by 55% to effluent concentrations of 36 mg NH_4-N/L and 52 mg N_{tot}/L, while the nitrate concentrations increased on average from 1.9 mg NO_3-N/L to 12 mg NO_3-N/L. These values suggest considerable levels of nitrification. The authors note further that in some subsurface flow beds no nitrification was observed. Vymazal (2002) presents observations of nitrogen removal efficiencies for Czech systems. Czech systems show a average removal efficiency for total nitrogen of 42% with an effluent concentration of 27.1 mg/L and a removal efficiency for organic nitrogen of 65% with a effluent concentration of less than 3 mg/L. Ammoniacal nitrogen is removed by 43% with a average effluent concentration of 16.1 mg/L. The Czech systems, similar to the observations of Börner *et al.* (1998), show an increase in nitrate nitrogen. These observations do not support the theory that the anaerobic conditions in subsurface flow systems are favourable for denitrification and nitrate nitrogen being the limiting factor in the denitrification processes. Vymazal (2002) highlights further that the removal efficiencies of Czech systems showed no significant change with a change of the temperature.

Phosphorus. Phosphorus is typically present in wastewaters as organic phosphorus, orthophosphate and dehydrated orthophosphate (polyphosphate). While oxidation results in the conversion of most phosphorus to orthophosphate, phosphorus removal in wetland systems is achieved by adsorption, plant uptake complexation and precipitation (Vymazal, 1998).

The major long term sink for phosphorus is the soil and most studies have shown that wetlands are not very effective as phosphorus sink (Richardson, 1985). The interaction of redox potential, pH value, and Fe, Al and Ca minerals control the adsorption and retention of phosphorus. Ligand exchange reactions are the most important retention mechanisms, where phosphorus replaces water or hydroxyl from the surface of Fe and Al hydrous oxides to form complexes. Precipitation as insoluble calcium phosphate is the dominant transform at pHs greater than 7.0. The adsorption of P is greater in mineral soil than in organic, related to higher amounts of Fe, Al and Ca minerals. Commonly used support media of the matrix does not contain adequate concentrations of these minerals (Vymazal, 1998). However, observations have shown an aging phenomenon for the removal of phosphorus, once adsorption and precipitation have become saturated (Kadlec and Knight, 1996).

Plants absorb phosphorus through the root system and build it into their tissue. However, the uptake of phosphorus from plants is even lower than the uptake of nitrogen and forms only a small fraction of the total phosphorus removed in the system. Similarly to nitrogen, the phosphorus is released back into the system after plant decay (Kadlec and Knight, 1996).

The reported performances of phosphorus removal of subsurface flow wetlands show highly variable rates. A summary of removal efficiencies of subsurface flow reed beds across Europe shows efficiency between 27% and 65% (Vymazal, 2002). Temporally varying removal rates had been reported, as many of the reed beds are now considered mature. Tanner *et al.* (1998) observed removal rates of 15 to 38% for a mature gravel bed system, which achieved up to 75% removal efficiency in the first two years of operation. Perfler *et al.* (1999) report initial phosphorus removal rates of 94%. This subsequently declined until P was added to the flow (by 3%) as it passed through the system. This decline in performance was attributed to the decrease in adsorption capacity of the bed substrate over time (Perfler *et al.*, 1999). Maehlum and Jenssen (1998) reported that the overall phosphorus removal efficiency could be higher than 90% when special media are used, e.g. lightweight ceramic particle aggregates. Temperature has little influence on P-removal because the most important pathways are chemical precipitation and adsorption.

Other Pollutants. The manifold removal mechanisms described in the sections before are also very effective for the removal of other pollutants such as metals, hydrocarbons and pathogens.

Metals are removed by sedimentation, filtration adsorption, complexation precipitation cation exchange plant uptake and also microbially mediated reactions, especially oxidation. Removal efficiencies of 71% Zn, 72% Cd, 69% Pb, 66% Cu, 34% Ni and 81% Cr were reported from a constructed wetland in the U.K. receiving urban storm runoff (Scholes *et al.*, 1999).

Many organic chemicals as phenol, benzene, tuolene and various oil componets can be biologically degraded in aerobic or anaerobic wetland environments. Litchfield (1993) reports how a wetland and lagoon complex at the Amoco refinery in Dakota is capable of removing hexavalent chromium, phenols, oil and grease to well within the consent limits. Studies in Canada have shown wetlands to remove over 96% of total extractable hydrocarbon in urban storm runoff (in Shutes *et al.*, 1997).

Kadlec and Knight (1996) show that constructed wetlands that receive untreated or partially treated municipal wastewater always show removal efficiencies for coliforms of greater then 90%. Laber *et al.* (1999) show an elimination rate of bacteria in wetlands treating hospital wastewater with a removal efficiency of at least 99.87%.

2.3 AIRPORT RUNOFF

To ensure wintertime flight safety large amounts of de- and anti-icer are used to remove and prevent ice formations on aircrafts as well as on runways and taxiways. Glycol based compounds and also urea and a variety of acetate and formate based products are used for de-

icing purposes (Switzenbaum *et al.*, 2001). The majority of these products, and here especially glycol, are associated with a high BOD concentration that is detrimental to the quality of receiving waters and also can be directly toxic to aquatic life (Fisher *et al.*, 1995).

2.3.1 Pollutants at the Mayfield Farm Constructed Wetland

The airport runoff at Heathrow airport contains significant amounts of glycol, since the de- and anti-icers used at Heathrow airport are mainly glycol-based compounds (Worrall, 2000). It was further shown, that the quality of airport runoff is characteristically similar to urban and highway runoff (Chong *et al.*, 1999). Thus the runoff may contain also contaminants such as heavy metals, suspended solids, nitrogen, phosphorus, faecal coliforms and hydrocarbon based oils and lubricants. It is anticipated that many of the suspended solids, metals and oils contained within the runoff will be removed in pre-treatment processes in storage reservoirs before entering the subsurface flow reed beds. However, the high levels of glycol associated with the runoff will remain in the wastewater and is for this reason the key parameter in terms of pollutant removal.

The glycol based compounds used for de-icing, also called aircraft de-icing fluid (ADF), at Heathrow airport are typically ethylene glycol, diethylene glycol and 1,2-propylene glycol (Worrall, 2000; Chong *et al.*, 1999). According to USEPA (1995) it takes 2 to 4 m³ of ADF to deice a larger commercial aircraft. A medium size airport may use over 1,000 m³ ADF over the entire winter season (Betts, 1999) or even more than 5,000 m^3 for the larger U.S. airports (Mericas and Wagoner, 2000). For aircraft de-icing typically a heated mixture of Type I aircraft de-icing fluid and water is used. Undiluted Type I ADF contains a minimum of 80% by weight of propylene glycol (PG) or ethylene glycol (EG) with the balance composed of water, buffers, wetting agents and corrosion inhibitors (Switzenbaum *et al.*, 2001). Type I ADF is applied to aircrafts at gate areas or at centralized de-icing facilities designed to collect ADF runoff. During intense snow or freezing-rain events, aircraft may be de-iced again at the end of a runway immediately prior to departure. Aircraft anti-icing prevents further accumulation of snow or ice while aircraft are waiting for take-off or during overnight parking. Type IV anti-icing fluid (AAF), applied for this purpose, consist of PG or EG along with thickeners (Switzenbaum *et al.*, 2001). The chemical components of typical de-icing-agents are (Nitschke *et al.*, 1996):

- 35% diethylene glycol (DEG), 20% PG, 3% inhibitor and thickener, 42% water
- 88% DEG, 2% PG, 1% inhibitor, 9% water
- 50% PG, 1% inhibitor, 49% water
- 75% PG, 5% urea, 1% inhibitor, 19% water

The concentrations of glycol and the associated BOD_5 in runoff can be highly variable, since it is mainly dependent on the dilution of the runoff caused either in large bodies of receiving waters or sewers or by the wash off effect through rainfall or snowmelt after a de-icing event. High levels of BOD_5 found in airport runoff are associated with aircraft de- and anti-icer as reported by Switzenbaum *et al.* (2001). Typical biochemical, chemical and theoretical oxygen demands of de-icer and their pure contents are shown in Table 2.1. Veltman *et al.* (1998) (in Switzenbaum *et al.*, 2001) measured a BOD_5 demand as high as 245,000 mg BOD_5/L on initial airport runoff. Kaul and Stewart (1986) even measured a value as high as 430,000 mg BOD_5/L. For an experimental reed bed at Heathrow airport relatively modest BOD_5 inlet concentrations were measured in a range of 0 to 18.4 mg BOD_5/L, with an average of 5.54 mg BOD_5/L (Revitt *et al.*, 1997). However, Worrall *et al.* (2001) highlights the significant loadings of glycol occurring in the surface runoff at Heathrow airport and states that these go directly into surface waters or into aerated balancing ponds. These loadings for Heathrow Airport are shown in Table 2.2.

Theoretical relations of BOD_5 to COD are reported with 0.73 for Type I PG-based de-icer and to 0.5 for Type IV PG-based de-icer (Cyrotech, 2002; Cyrotech, 2002a). Revitt *et al.* (1997) report related BOD_5 and COD levels in airport runoff with elevated COD levels (BOD5 in the range of 0.2 to 18.4 mg/L with a mean of 5.54 mg/L compared to COD in a range of 8.0 to 150.0 mg/L with a mean of 47.0 mg/L) and suggest that the elevated levels of COD are caused by presence of less biodegradable organics such as oil and grease in the airport runoff (Revitt *et al.*, 1997). Storm water samples collected from Baltimore-Washington International Airport have shown a similar but more extreme ratio of BOD_5/COD (Fisher *et al.*, 1995). BOD_5 has been measured in the range of 3 to 6,700 mg/L while COD has been observed in the range of 20 to 270,000 mg/L. Strong relationships between COD and polyethylene glycol (PEG) and COD and BOD_5 had been observed in runoff at a military airport in Massachusetts (Karrh *et al.*, 2002). Whilst correlation

Table 2.1. Summary of reported oxygen demands

Material	BOD_5 [mg/L]	COD [mg/L	ThOD [mg/L	Mol-weight
PG (pure)	0.8×10^6	1.6×10^6	1.7×10^6	76
EG (pure)	0.85×10^6	1.7×10^6	1.4×10^6	62
DEG (pure)	$0.4 \times 10^6 – 0.8 \times 10^6$		2.0×10^6	106
Type I ADF (PG based)	0.42×10^6	0.84×10^6		
Type I ADF (EG based)		0.87×10^6		
Type IV ADF (PG based)	$0.33 \times 10^6 – 0.38 \times 10^6$			
Type IV ADF (EG based)	0.37×10^6 - 0.46×10^6			

Table 2.2. Typical glycol applications and resulting contamination at Heathrow Airport (adapted from Worrall *et al.*, 2001)

Application	resulting contamination
Daytime de-icing of aircraft	189 kg
Nighttime de-icing of aircraft	291 kg
Over-spray onto aprons	10% to 25%
Potential daily pollution load from de-icing	51,000 kg glycol
Equivalent BOD load	41,000 kg
Daily BOD loadings from airfield pavement de-icing	17,600 kg
Peak BOD discharge	>500 mg/L

coefficients above 0.98 were observed for these parameters, TOC did not very well correlate with COD, BOD_5 or PG.

Kaplan *et al.* (1982) states that polyethylene glycol and diethylene glycol present minimal toxicologic problems and no carcinogenous hazards. Polyethylene glycol is the least toxic product and is commonly used in the pharmaceutical, cosmetic and food industries. They further state that diethylene glycol is slightly more toxic and that repeated large doses are needed for the appearance of toxic effects. Fisher *et al.* (1995) report, that samples taken from runoff in sewers leaving the de-icing areas of the airport showed a very high toxicity to *Daphnia Magna*, where the LC_{50} value was determined at concentrations as low as 1 to 2% of the effluent. While this was observed for samples taken in the peak of the storm event, the samples taken from the downstream outfall collection pond showed no toxicity. There is further evidence, that anti-icer used on aircraft is two orders of magnitude more toxic than de-icer used on runways (Hartwell *et al.*, 1995). Switzenbaum *et al.* (2001) highlights that the primary substances of concern are the additives in de- and anti-icer. Triazoles are commonly added as corrosion inhibitors. Cancilla *et al.* (1997) isolated those components from anti-icer and found them significant toxic. Pillard (1995) compared de-icing fluid with pure glycols and concluded that the additives in the de-icing fluids were the cause for an increased toxicity.

2.3.2 Biodegradation of glycol

The biodegradation of glycols from airport runoff and the biodegradation of glycol in general is covered by some literature. Many investigations were undertaken at bench scale size in the laboratory and some were undertaken at pilot scale size. Only few data is available from full-

scale applications for the treatment of glycol. Reported investigations cover pure microbial culture studies as well as aerobic and anaerobic degradation studies of glycols.

Initial studies in the 1950s used the 20-day biochemical oxygen demand test to study the biodegradability of glycol compounds (Cox, 1978). The glycol monomer EG was shown to be readily biodegradable in these tests, since 80% of the available dissolved oxygen was consumed and, thus, complete utilization of ethylene glycol was presumed. As only 10% of the available dissolved oxygen was used in these tests in the presence of diethylene glycol or triethylene glycol, the bioresistant nature of the higher molecular-weight glycols became evident. A series of activated sludge tests again revealed that ethylene glycol was degraded and DEG was not. The recalcitrant nature of DEG and other glycols to aerobic degradation led researchers to investigate the biodegradability of these glycols under anaerobic conditions. These investigations showed a reduction over 60% in COD. Similar observations of ethylene glycol and propylene glycol being readily degradable in the biochemical oxygen demand have been made by other researcher (Lamb and Jenkins, 1952; Price *et al.*, 1974; Briedie *et al.*, 1979). The reported degradation of diethylene glycol was shown to be somewhat variable and degradation has been proven to depend on the source and acclimatisation of the microorganisms.

The examination of biodegradability of mono- and diethylene glycols using river die-away tests are reported by Evans and David (1974). River water samples from a variety of sources were amended with the test compounds. Samples with ethylene glycol were incubated at 20°C, 8°C and 4°C, while diethylene glycol and triethylene glycol were incubated at 20°C and 8°C. Ethylene glycol biodegraded completely within 3 days at 20°C and within 14 days at 8°C. At 4°C the degradation of ethylene glycol was not greater than 20% of the rate at 8°C, indicating a reduction of bacterial activity as the temperature is lowered. Diethylene glycol was also readily degraded at the temperature of 20°C, while only minimal removal was observed at the lower temperatures.

Kaplan *et al.* (1982) reported the degradation of PG and DEG under aerobic and anaerobic conditions. PG was completely degraded within 2 to 4 days under aerobic conditions and 4 to 9 days under anaerobic conditions depending on the culture media used in the tests. The same initial concentration of DEG was degraded to 25% of the initial concentration after 32 days under both aerobic and anaerobic conditions. Since the DEG in a sterile control disappeared in a similar rate to DEG in cultures, the authors conclude that the decomposition appears to be nonbiological.

The biodegradation of aircraft deicing fluid has been also studied in wastewater and laboratory activated sludge systems (Jank *et al.*, 1974; Nitschke *et al.*, 1996). Jank *et al.* (1974) studied the biological treatment of different mixtures of sewage and glycol-based de-icing fluids. Bench scale reactors were operated at hydraulic residence times of 12 and 24 hours at temperatures of 2, 5 and 10°C. Treatment efficiencies in the range of 93% to 97% were

observed during 2 weeks of operation with influent concentrations of organic matter between 316 to 368 mg BOD/L and of de-icing fluid of approximately 230 mg BOD/L. Tests on the degradation of PG in laboratory activated sludge plants by Nitschke *et al.* (1996) showed treatment efficiencies of up to 99.9%. At temperatures of 18°C the influent concentrations of the basic substrate of 200mg COD/L and de-icer in concentrations up to 1,200 mg COD/L were degraded to concentrations in the range of 20 to 40 mg COD/L. The authors further observed increased sludge production with increased organic load of de-icer. They conclude that more nitrogen is incorporated in the biomass since no increase in ammonia concentration was measured. The degradation of DEG caused disturbance of the biodegradation. However, after adapting the sludge to DEG, shock load test showed DEG to be degraded 83%, 93% and 96% after periods of 2, 4 and 7 days respectively. Airport runoff was further discharged into a municipal sewage treatment works (STW). The sludge in the STW was adapted by a gradually increased load of the runoff entering the plant. Observations showed DEG in the effluent of the STW some days after the beginning of de-icing operations, indicating incomplete treatment of DEG.

Klecka *et al.* (1993) reported on the biodegradation of aircraft deicing fluids in soil. High degradation rates were shown for PG, EG and DEG of 19.7 to 27.0 mg kg^{-1} day^{-1} soil at a temperature of 8°C and 66.3 to 93.3 mg kg^{-1} day^{-1} soil at 25°C, while degradation rates dropped to 2.3 to 4.0 mg kg^{-1} day^{-1} soil at a temperature of -2°C.

High removal rates for EG were observed in a bench-scale batch loaded aerobic fluidized bed reactor (Saffermann *et al.*, 1998). Using a sand medium and adding oxygen and nutrients to the wastewater, observed removal rates were 4,200 g m^{-3} day^{-1} for EG and 5,100 g m^{-3} day^{-1} for BOD_u. Investigations on the biodegradation of PG in a saturated sand column showed removal rates of greater than 99% for different loading rates and conditions (Bielefeldt *et al.*, 2002). Tests with the absence of electron acceptors of oxygen, nitrate and sulphate showed similar high degradation rates. Bielefeldt *et al.* (2002) conclude that the degradation of PG is likely proceeded under a range of conditions, such as fermentation processes (methanogenic) and electron acceptor processes (oxygen reducing , nitrate reducing, sulfate reducing).

Near-complete degradation of de-icing fluid was observed under anaerobic conditions (Schoenberg *et al.*, 2001). First-order degradation rate constants of 3.5 d^{-1} for PG-based ADF and 5.2 d^{-1} for EG-based ADF were measured under mesophilic conditions (35°C)[1]. In batch tests first-order degradation rate constants were measured with 1.9 d^{-1} and 3.5 d^{-1} for PG-based

[1] Bacteria are classified according to their optimum temperature range for growth (Hammer, 1986). Mesophilic bacteria grow in a temperature range of 10 to 40°C, with an optimum of 37°C. Anaerobic digesters are normally heated near to the optimum level of 35°C. Above 40°C, mesophilic activity drops sharply and thermophilic growth starts. Thermophilic bacteria have a range of approximately 45 to 75°C, with an optimum near 55°C.

ADF and for EG-based ADF, respectively. Lower temperatures down to 25°C showed minimal affect on anaerobic degradability but substantial effects were observed below 25°C.

The vast number of literature about glycol degradation indicates that the pathways of glycol breakdown are manyfold. Schoenberg *et al.* (2001) observed metabolic intermediates of the process of anaerobic breakdown of PG and EG. The degradation process of PG formed immediately and simultaneously propanol and propionate and thereafter acetate. Metabolic intermediates formed simultaneously after the start of the tests on degradation of EG were ethanol and acetate and small amounts of propionate. The authors conclude that the first-order degradation rate obtained from COD measurements therefore characterize the overall metabolic and thermodynamic complexities of anaerobic degradation of these glycols. Aerobic degradation forms similar intermediates (Cox, 1978; Klecka *et al.*, 1993). The sequential oxidation degrades via an aldehyde to a carboxylic acid; the stepwise oxidation showed to be catalyzed by microbial dehydrogenases. Lactic acid was observed as an intermediate of the breakdown of PG, glycolic acid was found in the breakdown process of EG. DEG has been determined to be degraded to a carbolxylic acid. These intermediates are then assimilated and used in cell metabolism (Klecka *et al.*, 1993).

Similar aerobic and anaerobic degradation processes of airport de-icer take place in wetlands. However, only a few systems are in operation and published data is limited. Seven other airport are using or investigating the use of wetlands to manage their de-icing wastes. A full-scale vertical flow system is installed at Toronto airport, Canada and is reported to be in operation since 2001. A full-scale horizontal subsurface flow system is installed in Edmonton, Canada and was due to be started in 2000. In Wilmington, Ohio, U.S. a full-scale subsurface wetland is installed and in operation. A pilot horizontal subsurface-flow system with soil as a substratum was installed at Berlin Schöneberg airport. This system was later abandoned and the effluent is now discharged into a nearby new build sewage treatment works. Further, a horizontal subsurface flow system is in design or builds stage at Westover Air Reserve Base in Massachusetts, U.S. From all these systems no treatment data is published up to date. Design data is published for the system at the Westover Air Reserve Base.

A pilot constructed wetland system was installed at Zürich airport, Switzerland. Treatment data of this system is published from the airport authority in the form of a nonscientific press publication (Flughafen Direktion Zürich, 1999). In a first treatment stage the wastewater enters a vertical system (area 1,800 m^2) and is then passed through three horizontal subsurface flow systems in parallel (area each 1,500 m^2). For the support media, a mixture of humus and gravel from bricks was used and the plants used were reeds. During the pilot study the hydraulic load was in the range of 4.5 to 17 m^3/d and the pollutant load was measured in the range of 18 to 100 kg COD/d. The author highlights that in the second year of operation loads of 1,710 mg DOC/L in wintertime and 3,140 mg DOC/L in the summertime were treated to below the discharge

consent (10 mg BOD_5/L, 20 mg COD/L) during several month of operation. The average removal rate was calculated to be 32 g COD m^{-2} d^{-1}. Further information is shown in a graph, from which the following values were taken. During summertime operation continuous loads of approximately 1,200 mg CSB/L resulted in effluent concentrations of approximately 70 mg COD/L in the first month of operation and approximately 40 mg COD/L in the second month of continuous operation. Continuous loads in the wintertime in the range of 600 to 900 mg COD/L resulted in similar effluent concentrations of 40 mg COD/L. The author highlights further, that during a 4-week frost-period the efficiency of the system was around 99%.

Table 2.3. Glycol removal on wetland pilot system at Heathrow Airport (from Revitt *et al.*, 1997)

Parameter	PG [%]	EG [%]	DEG [%]
Subsurface Bed			
January 1996	99.6	99.4	90.0
June 1996	59.2	71.6	69.1
October 1996	95.3	76.6	44.5
Surface Bed			
June 1996	48.6	60.2	61.3
October 1996	59.7	50.1	45.8

A pilot constructed wetland system is reported at Heathrow airport, consisting of two rafted system, one surface flow system and one subsurface flow system (Revitt *et al.*, 1997; Chong *et al.*, 1999). The two rafted systems have each a surface area of 15 m^2 and are planted with common reed (*Phragmites australis*) and cattails (*Typhia latifolia*). The surface and the subsurface systems have identical dimensions of 30m x 5m and are mainly planted with common reed. Glycol shock dosing experiments were undertaken during the second year of operation on the surface and subsurface systems (Revitt *et al.*, 1997). A mixture of PG, EG and DEG was introduced into the beds. Observed parameters were PG, EG and DEG, where the analysis was performed by gas chromatography/mass spectrography. Glycol traces had been observed in the effluent after 5 to 10 hours for the surface bed and after 10 to 17 hours for the subsurface beds, the flow rates were measured at 52.7 L/min and 45.4 L/min respectively. Removal efficiencies were calculated from the observed parameters and are lower for the surface flow bed. The dosing tests in January, June and October 1996 showed the removal efficiencies listed in Table 2.3. The authors remark that the high removal rates from the test in January 1996 are not verified and must be taken with some caution. The authors conclude that

removal rates are higher in winter and autumn month than in the summer. Clearly, with or without taking the test from January 1996 into account, this only holds true for PG, the efficiency for EG is similar and the efficiency for DEG is smaller. Unfortunately these efficiencies are not verified with BOD or COD measurements. It is unclear if the reported efficiencies are only based on the determination of the pure glycol contents. Schoenberg *et al.* (2001) conclude, that gas chromatographic analysis might not measure the overall metabolic and thermodynamic complexities of degradation of glycols. It is therefore unclear if these reported efficiencies from the pilot system at Heathrow Airport (Revitt *et al.*, 1997) are valid for the total degradation of the glycols in constructed wetlands or if they only indicate the rate of forming intermediates from the pure glycols.

2.4 HYDROLOGY AND POLLUTANT TRANSPORT

The preceding expositions have shown that constructed wetlands are complex and dynamic ecosystems, existing in different form with different soils, vegetation and fauna and different abilities to treat pollutants. IWA (2000) stated, that the main driving or overriding parameter is the hydrology (Chapter 2.1.1). When considering constructed wetlands for treatment purposes, the prediction of the degree of treatment performance becomes quite important. To achieve this, it is essential to describe the flow of pollutant in the system, the interior chemical mass balance and the reaction rate expressions.

Fundamental for the description of the flow of pollutants in the system are the knowledge of the hydrology and the temporal conveyance of pollutants. Typically models are used to describe the hydraulics and the temporal flow patterns. Various mathematical models have been developed to describe pollutant transport in open channel flow and saturated media, like groundwater flow. Since wetland systems have similar flow conditions, the same principles for open channel flow and flow in saturated media can be applied and, thus, flow models can be developed that incorporate the hydrology.

2.4.1 Hydraulic properties of subsurface flow wetlands

Contrary to the simplicity of the mathematical formulation of the mass balance for a control element, it is one of the most important physical properties in water resources engineering. From the mass balance formulation, more complex models are derived, as will be shown later. The mass balance for the continuous time is

$$\Delta M = \overline{M_{in}}\,\Delta t - \overline{M_{out}}\,\Delta t \qquad 2.14$$

It states simply that the change in mass ΔM is equivalent to the difference of the mass entering a system ΔM_{in} within a period of time Δt and the mass leaving the system ΔM_{out}. In hydrology, the mass balance is extended to the dynamic overall water budget of the transfer of water within a catchment or wetland as (IWA, 2000)

$$Q_i - Q_o + Q_c - Q_b + Q_{sm} + (P - ET - I)A = \frac{dV}{dt} \qquad 2.15$$

where

Q_i	water inflow rate ($L^3 T^{-1}$)
Q_o	water outflow rate ($L^3 T^{-1}$)
Q_c	catchment runoff rate ($L^3 T^{1}$)
Q_b	bank loss rate ($L^3 T^{-1}$)
Q_{sm}	snow melt rate ($L^3 T^{-1}$)
P	precipitation rate ($L T^{-1}$)
ET	evapotranspiration rate ($L T^{-1}$)
I	infiltration rate ($L T^{-1}$)
A	wetland area (L^2)
V	water storage in wetland (L^3)
t	time (T)

For steady conditions not all terms make a significant contribution and so the water budget reduces to:

$$Q_o = Q_i + (P - ET)A \qquad 2.16$$

If the precipitation and the evapotranspiration are negligible, than the mass balance is simply $Q_o = Q_i = Q$. Then the hydraulic retention time or, as sometimes stated the nominal detention time, gives a theoretical time for the water to travel through the wetland. It is calculated by the quotient of the volume of free water in the wetland over the flow rate:

$$\tau = nLWh / Q \qquad 2.17$$

where

τ	retention time (T)
n	effective porosity ($L^3 L^{-3}$)
L	length (L)
W	width (L)

h water depth (L)

Q flow rate ($L^3 T^{-1}$)

Since the premise that the whole water in the system is involved in the flow is not true, the nominal retention time is not necessarily the actual retention time. Furthermore, there are uncertainties in estimating the depth of water and the porosity of the matrix of the saturated media. Thus the measured retention times are usually smaller than the calculated nominal values (IWA, 2000).

A popular design criterion is based on a maximal level of pollution load a treatment plant, or in this case a wetland, can deal with. It is called hydraulic loading rate and can be calculated by means of an area loading rate, using the relation of the flow rate and the wetland plan area (Kadlec and Knight, 1996) (Equation 2.18) or by means of a volumetric loading rate by the relation of the flow rate and the rector volume (Equation 2.19).

$$q_A = \frac{Q_i}{A} \qquad 2.18$$

$$q_V = \frac{Q_i}{V} \qquad 2.19$$

where

q_A area hydraulic loading rate ($L T^{-1}$)

q_V volumetric hydraulic loading rate (T^{-1})

V reactor volume (L^3)

2.4.2 Flow through saturated media

The flow of water through open channels, pipes and saturated media has been a topic of intensive research for a long time in various fields of science. An equation describing flow through saturated media was presented in 1856 by HENRY DARCY (Freeze and Cherry, 1979). Observing the flow through sand filled pipes, DARCY defined the specific discharge through a porous medium, also known as Darcy velocity or filter velocity, as:

$$v = \frac{Q}{A} \qquad 2.20$$

where

v specific discharge ($L T^{-1}$)

Q flow rate ($L^3 T^{-1}$)

A cross-sectional area (L^2)

The experiments DARCY carried out showed a linear relationship between the average linear fluid velocity v and the hydraulic gradient dh/dx. Introducing a parameter K as a constant of proportionality Darcy's law can be written as:

$$v = -K \frac{dh}{dx} \qquad 2.21$$

where

K hydraulic conductivity ($L\ T^{-1}$)

dh/dx hydraulic gradient ($L\ L^{-1}$)

Substituting Equation 2.20 in Equation 2.21 yields an alternative form of Darcy's law as

$$Q = -K \frac{dh}{dx} A \qquad 2.22$$

2.4.3 Open channel flow

A similar resistance DARCY discovered in his flow experiments governs also the flow in a uniform open channel. In open channel flow friction is caused by the roughness of the channel boundaries. ROBERT MANNING has generally identified the relation between discharge and boundary friction in 1889. Since other research workers in the field derived similar formulas independently, including GAUCKLER in 1868 and STRICKLER in 1923, this equation is known as the GAUCKLER-MANNING-STRICKLER formula for discharge and can be written as (Chadwick and Morfett, 1993):

$$Q = \frac{1}{n_M} \frac{A^{5/3}}{P^{2/3}} \left(-\frac{dh}{dx} \right)^{1/2} \qquad 2.23$$

where

n_M MANNING'S n, a constant ($T\ L^{-1/3}$)

A cross-sectional area of the channel (L^2)

P wetted perimeter of the channel (L)

dh/dx hydraulic gradient ($L\ L^{-1}$)

2.4.4 Laminar and turbulent flow

The pattern of the flow, regardless of in an open channel, pipes or through saturated media is described by its state. The flow can be laminar, turbulent or in transition. The criterion for determining state of the flow is the dimensionless Reynolds number, *Re* (Charbeneau, 2000).

For flow through saturated media the Reynolds number is

$$R_e = \frac{\rho v d}{\mu} \qquad 2.24$$

where

ρ fluid density ($M\,L^{-3}$)

μ fluid viscosity ($M\,L^{-1}\,T^{-1}$)

v specific discharge ($L\,T^{-1}$)

d average grain diameter (L)

Bear (1972) states that "DARCY'S law is valid as long as the Reynolds number based on average grain diameter does not exceed some value between 1 and 10". The flow through granular medium is laminar for Reynolds numbers below value of 1. Between the values of 1 and 10 the transition section starts, where the flow is still laminar, but the hydraulic gradient is not linear (Freeze and Cherry, 1979).

For open channel flow the Reynolds number may be written as (Chadwick and Morfett, 1993)

$$R_e = \frac{\rho u D}{\mu} \qquad 2.25$$

where

u fluid velocity ($L\,T^{-1}$)

D hydraulic radius (L)

The hydraulic radius is defined by the ratio of the cross-sectional area A over the wetted perimeter P as

$$D = \frac{A}{P} \qquad 2.26$$

where

A cross-sectional area (L^2)

P wetted perimeter (L)

For laminar channel flow $Re < 500$ and for turbulent channel flow $Re > 1000$.

2.4.5 Advective transport

The advective transport is the movement of a solute as it is carried along with the bulk fluid movement (Charbeneau, 2000). For steady flow without sources and sinks the advective transport is stated as

$$\frac{\partial c}{\partial t} + v \bullet \text{grad}(c) = 0 \qquad 2.27$$

where

$\partial c/\partial t$ change of concentration with time

v fluid velocity

grad(c) gradient of the concentration, (the gradient is pointing into the direction of the greatest increase of the concentration and its magnitude is the rate of increase in concentration per unit length into that direction)

2.4.6 Advective dispersive transport in a saturated medium

The advection dispersion equation is based on the law of conservation of mass. The assumptions are a fully saturated homogenous and isotropic medium, a steady-state flow and the application of Darcy's law. Thus the flow has an average linear velocity and carries the solutes by advection, which would imply a plug flow. In a plug flow a slug of solute in the water would not spread out while conveyed within the flow. However, this is not observed in reality, instead the solute spreads out caused by a mixing process, named hydrodynamic dispersion. The term hydrodynamic dispersion incorporates the effect of mechanical mixing during fluid advection and the effect of molecular diffusion. Since diffusion is only a factor of importance at low velocities, the dispersion in most applications is caused entirely by the motion of the fluid. This is known as mechanical dispersion. The spreading of solute in direction of the bulk flow is named longitudinal dispersion; the spreading in direction perpendicular to the flow is named transverse dispersion.

The solute flux through a small control volume in the porous medium will be considered. The specific discharge v has the components (v_x, v_y , v_z), where the average linear velocity $\bar{v} = v / n$ is described with its components $(\bar{v}_x, \bar{v}_y, \bar{v}_z)$. The mass of solute in this control volume is defined as the concentration C times the porosity n and is therefore nC. So for a homogenous medium it can be stated that

$$\frac{\partial(nC)}{\partial x} = \frac{n\partial C}{\partial x} \qquad 2.28$$

The mass of solute transported in the x direction of the flow J_x can then be presented for the transport by advection as

$$J_{x,1} = \bar{v}_x nC dA \qquad 2.29$$

and for the transport by dispersion as

$$J_{x,2} = nD_x \frac{\partial C}{\partial x} dA \qquad 2.30$$

which is analogous to Fick's first law (Charbeneau, 2000), where

D_x dispersion coefficient in x direction ($L^2\ T^{-1}$)
dA elemental cross-sectional area of the control element (L^2)

As stated before the hydrodynamic dispersion can be expressed in terms of two components

$$D_i = \alpha_i \bar{v} + D^* \qquad 2.31$$

where

α_i dispersivity as a characteristic property of the porous medium (L)
D^* coefficient of molecular diffusion ($L^2\ T^{-1}$)

Therefore the total mass of solute transported in the x direction through the control element per unit time can be written as

$$F_x = \bar{v}_x nC - nD_x \frac{\partial C}{\partial x} \qquad 2.32$$

and similarly for the y and z directions. The total mass of solute entering the control volume is then

$$F_x dzdy + F_y dzdx + F_z dxdy \qquad 2.33$$

and the mass leaving the control element can be written as

$$\left(F_x + \frac{\partial F_x}{\partial x}dx\right)dzdy + \left(F_y + \frac{\partial F_y}{\partial y}dx\right)dzdx + \left(F_z + \frac{\partial F_z}{\partial z}dx\right)dxdy \qquad 2.34$$

The partial terms are indicating the change of the solute mass in the specified direction. The difference of mass entering and leaving the control element is then

$$\left(\frac{\partial F_x}{\partial x} + \frac{\partial F_y}{\partial y} + \frac{\partial F_z}{\partial z}\right)dxdydz \qquad 2.35$$

The change of mass within the control element can be stated as

$$-n\frac{\partial C}{\partial t}dxdydz \qquad 2.36$$

The law of conservation of mass may be expressed as

$$\frac{\partial F_x}{\partial x} + \frac{\partial F_y}{\partial y} + \frac{\partial F_z}{\partial z} = -n\frac{\partial C}{\partial t} \qquad 2.37$$

Substituting the Equations 2.32 in 2.37 yields, after cancellation of n

$$\left[\frac{\partial}{\partial x}\left(D_x\frac{\partial C}{\partial x}\right) + \frac{\partial}{\partial y}\left(D_x\frac{\partial C}{\partial y}\right) + \frac{\partial}{\partial z}\left(D_x\frac{\partial C}{\partial z}\right)\right] - \left[\frac{\partial}{\partial x}\left(\bar{v}_x C\right) + \frac{\partial}{\partial y}\left(\bar{v}_y C\right) + \frac{\partial}{\partial z}\left(\bar{v}_z C\right)\right] = \frac{\partial C}{\partial t} \qquad 2.38$$

Under the assumption that the linear velocity $\bar{v}$ is steady and uniform and the porous medium is homogenous, the dispersion coefficients do not vary through space so Equation 2.38 becomes

$$\left[D_x\frac{\partial^2 C}{\partial x^2} + D_y\frac{\partial^2 C}{\partial y^2} + D_z\frac{\partial^2 C}{\partial z^2}\right] - \left[\bar{v}_x\frac{\partial C}{\partial x} + \bar{v}_y\frac{\partial C}{\partial y} + \bar{v}_z\frac{\partial C}{\partial z}\right] = \frac{\partial C}{\partial t} \qquad 2.39$$

This equation is known as the advection dispersion equation (ADE) for solute transport in saturated media. The solution of this equation will provide the solute concentration C as a function of space and time and will take the form $C(x, y, z, t)$.

2.4.7 Advective dispersive transport in open channel flow

The derivation of the advection dispersion equation for laminar flow in open channels is equivalent to the procedure described before for flow in a saturated medium. The solute flux through a small control volume is again considered. The flux of water has the velocity v with its components (v_x, v_y, v_z).

Since the open channel flow is a single phase, the effects causing mixing are named as molecular and turbulent diffusion as well as velocity shear caused by some kind of friction. In the near field, the turbulent diffusion describes the transport process for solutes. Thus using Fick's first law it can be stated that the mass of solute transported in x direction is

$$J = e_x \frac{\partial C}{\partial x} dA \qquad 2.40$$

where

e_x turbulent diffusion factor in x direction ($L^2\ T^{-1}$)

In the mid field, the mixing effect of shear friction has more importance hence Fick's first law yields

$$J = k_x \frac{\partial C}{\partial x} dA \qquad 2.41$$

where

k_x dispersion factor in x direction ($L^2\ T^{-1}$)

Now the advection dispersion equation can be derived in a manner similar to the equation for the transport of solutes in a saturated medium as

$$\left[e_x \frac{\partial^2 C}{\partial x^2} + e_y \frac{\partial^2 C}{\partial y^2} + e_z \frac{\partial^2 C}{\partial z^2} \right] - \left[v_x \frac{\partial C}{\partial x} + v_y \frac{\partial C}{\partial y} + v_z \frac{\partial C}{\partial z} \right] = \frac{\partial C}{\partial t} \qquad 2.42$$

Again we assume that e_x, e_y, e_z and v_x, v_y, v_z, do not vary with x, y, z, t.

2.4.8 Solutions for the mixing equations

Analytical solutions for the mixing equations are presented by Rutherford (1994). For their approach in a saturated medium, the following substitutions may be used

open channel		saturated medium
v_x, v_y, v_z,	with	$\bar{v}_x, \bar{v}_y, \bar{v}_z$

e_x, e_y, e_z with D_x, D_y, D_z

Instantaneous Point Source. If an instantaneous release of solute with its mass M is made at the location x = 0, y = 0, z = 0 and time t = 0 then the concentrations in an unbounded water profile are given by

$$c(x,y,z,t) = M \frac{\exp\left[-\frac{(x-v_x t)^2}{4e_x t}\right]}{\sqrt{4\pi e_x t}} \frac{\exp\left[-\frac{(x-v_y t)^2}{4e_y t}\right]}{\sqrt{4\pi e_y t}} \frac{\exp\left[-\frac{(x-v_z t)^2}{4e_z t}\right]}{\sqrt{4\pi e_z t}} \qquad 2.43$$

Constant Point Source. Downstream from a steady point source the effects of longitudinal diffusion or dispersion are negligible. Thus the vertical and transverse spreading of the plume can be described by

$$c(x,y,z) = m \frac{\exp\left(-\frac{y^2 v_x}{4e_y x}\right)}{\sqrt{4\pi e_y x}} \frac{\exp\left(-\frac{z^2 v_x}{4e_z x}\right)}{\sqrt{4\pi e_z x}} \qquad 2.44$$

Of course this equation is again only valid in infinitely wide location.

Solution for Bounded Conditions. The solutions for the mixing equations presented in the latter are restricted to infinitely wide conditions. Thus considering the method of images (Rutherford, 1994) allows the use of those analytical solutions in bounded conditions.

With the idea of reflections, the media boundaries are considered to be perfect mirrors and to reflect the plume with an imaginary source. Therefore the equations are solved for infinitely boundary conditions and then the solution is mirrored at the boundaries and summed up within the confines. This is illustrated in Figure 2.7.

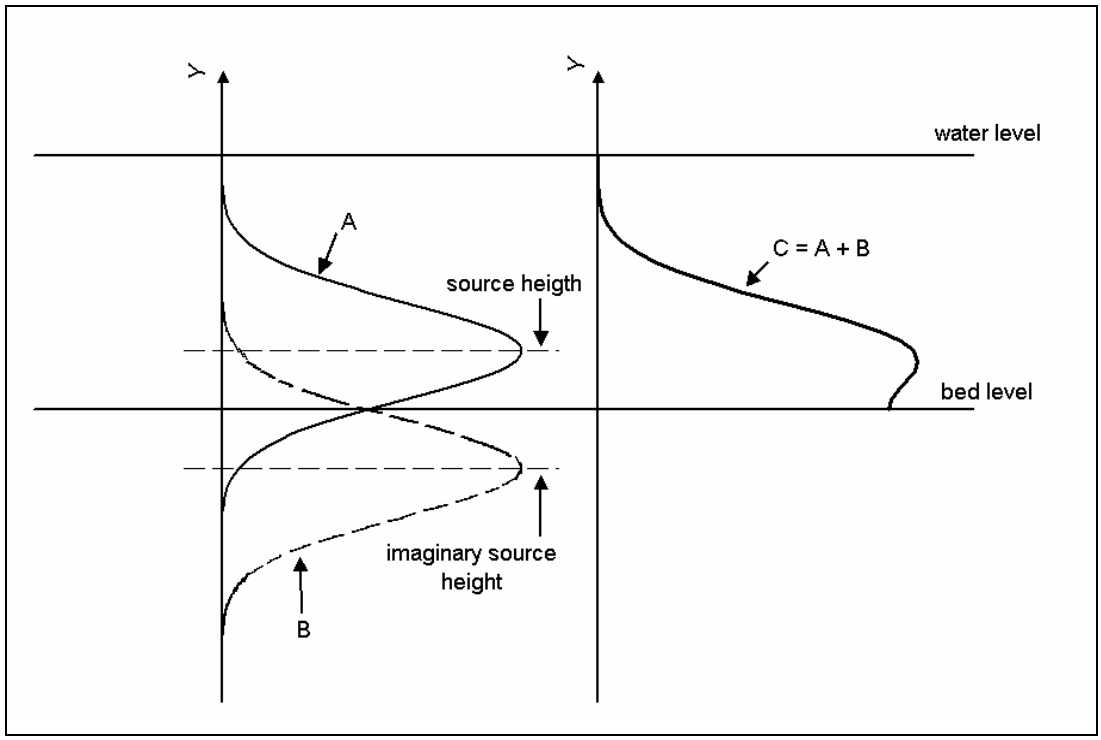

Figure 2.7. Method of images

Solution for One-Dimensional Observations. Assuming that the tracer is dispersed through the entire depth of the continuum, the three-dimensional transport equation can be averaged over the cross-section to yield a one-dimensional transport equation. The average linear velocity v_i in the control volumes of Equation 2.42 can be expressed as a cross-sectional averaged value $\bar{\bar{v}}_i$ plus a fluctuation about the average v_i'' (where *i* is a index for the individual direction *x*, *y* or *z*) as shown in Equation 2.45. A similar procedure for the concentration *C* is given in Equation 2.46.

$$v_i = \bar{\bar{v}}_i + v_i'' \qquad 2.45$$

$$C = \bar{\bar{C}} + C'' \qquad 2.46$$

Substituting the averages into Equation 2.42 gives:

$$\left[e_x \frac{\partial^2 (\bar{\bar{C}} + C'')}{\partial x^2} + e_y \frac{\partial^2 (\bar{\bar{C}} + C'')}{\partial y^2} + e_z \frac{\partial^2 (\bar{\bar{C}} + C'')}{\partial z^2} \right] - \left[(\bar{\bar{v}}_x + v_x'') \frac{\partial (\bar{\bar{C}} + C'')}{\partial x} + (\bar{\bar{v}}_y + v_y'') \frac{\partial (\bar{\bar{C}} + C'')}{\partial y} + (\bar{\bar{v}}_z + v_z'') \frac{\partial (\bar{\bar{C}} + C'')}{\partial z} \right] = \frac{\partial (\bar{\bar{C}} + C'')}{\partial t} \qquad 2.47$$

However, if the pollutant is fully mixed over the cross-section, the variations in y- and z-directions become negligible. Furthermore all terms containing a solitary fluctuation component of concentration or velocity reduce to zero since these fluctuations will have a zero mean over the cross-section. Thus Equation 2.47 becomes:

$$e_x \frac{\partial^2 \overline{\overline{C}}}{\partial x^2} - \overline{\overline{v_x}} \frac{\partial \overline{\overline{C}}}{\partial x} - \frac{\partial \overline{\overline{(C'' v_x'')}}}{\partial x} = \frac{\partial \overline{\overline{C}}}{\partial t} \qquad 2.48$$

The third term of Equation 2.48 states the effect of the change of concentration due to fluctuation in velocity and in analogy to Fick's first law (Equation 2.40) a diffusion coefficient for shear flow can be introduced as:

$$-\overline{\overline{C'' v_x''}} = e_k \frac{\partial C}{\partial x} \qquad 2.49$$

Substituting Equation 2.49 into Equation 2.48 yields the one dimensional longitudinal dispersion equation under the condition of a fully cross-sectionally mixed pollutant which is advecting into the x-direction with the mean velocity *U*:

$$\frac{\partial C}{\partial t} + U \frac{\partial C}{\partial x} = (e_x + e_k) \frac{\partial^2 C}{\partial x^2} \qquad 2.50$$

Introducing a bulk dispersion coefficient K simplifies to Equation 2.51 which is commonly referred to as the "Taylor advective dispersion equation". However, it should be noted that for open channel flow the shear dispersion is governing the process of spreading the pollutant in the flow field and therefore $e_k \approx K$.

$$\frac{\partial C}{\partial t} + U \frac{\partial C}{\partial x} = K \frac{\partial^2 C}{\partial x^2} \qquad 2.51$$

A solution for this differential equation can be derived with the initial conditions of the pollutant occurring as a direc-delta function where $C(x, t = 0) = 0$ for $x > 0$ and $C(x, t = 0) = C_0$ for $x = 0$ (Rutherford, 1994). This equation describes the spatial evolution of this initial spike of pollutant with time, as it is advected within the flow field and spread out by dispersion:

$$C(x,t) = \frac{C_0}{2\sqrt{\pi K t}} \exp\left[-\frac{(x - Ut)^2}{4Kt} \right] \qquad 2.52$$

A general form of this equation applicable for any kind of spatially distributed input can be derived using the principles of convolution. Splitting the upstream distribution into a series of individual direc-delta functions with each spatial concentration $C(\xi, t_1)$ at the time $t = t_1$ and routing them to a downstream location, the overall downstream concentration profile is given by the spatial integration of the individual routed concentrations as (Rutherford, 1994):

$$C(x_2, t_2) = \int_{\xi=-\infty}^{\infty} \frac{C(\xi, t_1)}{2\sqrt{\pi K (t_2 - t_1)}} \exp\left[\frac{[x_2 - \xi - U(t_2 - t_1)]^2}{4K(t_2 - t_1)}\right] d\xi \qquad 2.53$$

where

$C(x_i, t_i)$ Concentration at location x_i at time t_i (i = 1, 2), corresponding to upstream or downstream location respectively ($L^3 L^{-3}$)

K dispersion coefficient ($L^2 T^{-1}$)

ξ spatial variable of integration

The similarity of Equation 2.53 to the Gaussian normal distribution (Equation 2.54) indicated, that the spatial propagation of pollutant with an initial distribution of a direc-delta function tends towards a Gaussian distribution while advecting downstream.

$$\Phi(z) = \frac{1}{\sqrt{2\pi}} \int_{-\infty}^{z} \exp\left(\frac{-z^2}{2}\right) dz \qquad 2.54$$

However, since in practice most observations of pollutants travelling within a flow field are being observed at a fixed location with time rather than at over space at a fixed time, Equation 2.53 can not be used in these circumstances. Nevertheless, this problem can be approached under the assumption that the process of advection is dominating the mixing (Fischer, 1979; Rutherford, 1994):

$$\frac{x}{U} >> \frac{D}{U^2} \qquad 2.55$$

In the "frozen cloud" approximation this result is adopted to make the assumption that in the time it takes the plume to pass a given point there is no significant mixing. This is not strictly valid as a discernible degree of mixing does occur in the time taken to pass a given point. However, the "frozen cloud" approximation is a useful result. Under the "frozen cloud" approximation $x_1 = U\, t_1$. Then a spatial profile can be obtained from a spatial observation with its centroid at the upstream location x_1:

$$C(x,t_1)=C\left(x_1,t_1+\frac{x_1-x}{U}\right) \qquad 2.56$$

Once the temporal observation is converted to a spatial format, Equation 2.53 can be applied to route the profile downstream. The resulting spatial downstream profile can than be transformed into a temporal profile by reversing Equation 2.56:

$$C(x_1,t)=C\left(x_1+U(t_1-t),t_1\right) \qquad 2.57$$

The incorporation of the conversion actions into the routing procedure gains a directly applicable equation for routing temporal observation data (Rutherford, 1994):

$$C(x_2,t)=\int_{\xi=-\infty}^{\infty}\frac{C(x_1,\gamma)U}{2\sqrt{\pi K\bar{t}}}\exp\left[\frac{-U^2\left(\bar{t}-t+\gamma\right)^2}{4K\bar{t}}\right]d\gamma \qquad 2.58$$

where

$\bar{t}$ travel time, the difference in time between the centroids of the distributions (T)

γ integration variable (T)

2.4.9 Non-Fickian dispersion models

The Fickian theory of dispersion is used by application of the advection dispersion model quite successfully for predicting mixing phenomena. However, while the ADE can predict reliably travel times, it has been often noticed that there are discrepancies in its ability to describe observed dispersion behaviour. Observations of dispersing pollutant clouds showed persistent deviations from the predicted behaviour of the ADE and rarely attain a Gaussian distribution in space (Young and Wallis, 1986). One reason for this is that observations are rarely made at long enough times after the injection for Gaussian distributions to evolve. A other reason is the nonuniformity of real stream channels which leads to different patterns and mechanisms of mixing than those predicted by the ADE (Young and Lees, 1993).

Various studies investigated alternative dispersion models, which describe the observed "non-Fickian" behaviour with much greater accuracy. Some of these models include "storage zones" in which pollutants are trapped or held back for a while and cause a temporal spread in the flow regime when being released.

Continuously Stirred Tank Reactor. A simple approach to modelling a storage zone is a continuously stirred tank reactor (CSTR). This completely mixed system can be used to

model flow and concentration in a sub-reach of a natural water body (see Figure 2.8). For a finite time period the mass balance for a conservative pollutant can be expressed in terms of the change of concentration in the volume as

$$\frac{dV(t)C_{out}(t)}{dt} = Q_{in}(t)C_{in}(t) - Q_{out}(t)C_{out}(t) \qquad 2.59$$

If there are steady flow conditions (V, Q const.) then we can simplify and rearrange

$$\frac{dC_{out}(t)}{dt} = \frac{Q}{V}\left(C_{in}(t) - C_{out}(t)\right) \qquad 2.60$$

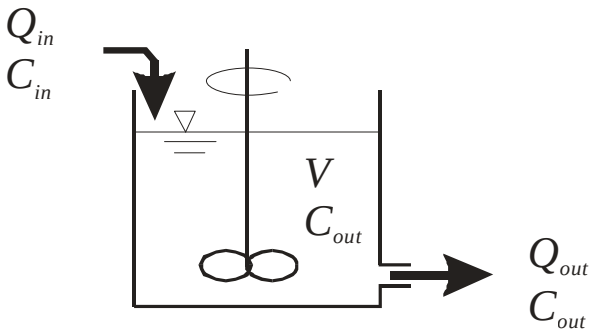

Figure 2.8. Continuously stirred tank reactor model

This equation is a 1st order differential equation that can be solved using analytical or numerical methods. To solve this differential equation, we introduce the differential operator for continuous time

$$sx(t) = \frac{dx(t)}{dt} \quad \text{or for this case} \quad sC(t) = \frac{dC(t)}{dt} \qquad 2.61$$

Substituting the differential operator into Equation 2.60 and introducing the hydraulic residence time T gives

$$TsC_{out}(t) = C_{in}(t) - C_{out}(t) \qquad 2.62$$

where

T hydraulic residence time, calculated as $T = V/Q$ (T)

or in a rearranged form

$$C_{out}(t) = \frac{1}{1+Ts} C_{in}(t) \qquad 2.63$$

The term $1/(1 + Ts)$ is called transfer function since it describes how the input has to be transferred to gain the output of the function. Analytical solutions of this continuous time model can be computed with Laplace transforms for simple inputs. If C_{in} is a direc-delta impulse of pollutant, rearranging the transfer function and multiplying it with the Laplace transform of a unit impulse can solve the model. The Laplace transform of a unit impulse is 1, hence:

$$\frac{1}{1+Ts} \times 1 = \frac{\frac{1}{T}}{\frac{1}{T}+s} \times 1 = \frac{1}{T} \frac{1}{\frac{1}{T}+s} \qquad 2.64$$

The inverse Laplace transform of a transfer function $1/(a + s)$ is e^{-at}. Taking the inverse Laplace transform of Equation 2.64 gives

$$C_{out}(t) = \frac{1}{T} e^{-\frac{1}{T}t} \qquad 2.65$$

With the continuous time model for a CSTR given with Equation 2.65, the concentration of pollutant C_{out} leaving the reactor can be calculated at time t after an instantaneous release of the pollutant with a concentration C_{in}. Obviously, this equation computes an exponential decaying concentration leaving the reactor.

Aggregated Dead Zone Model. Investigations of Beer and Young (1983) and Young and Wallis (1986) lead to the conceptualisation that an aggregated dead zone is primarily responsible for observed dispersion. Applying this theory to mixing in rivers it is considered that the potential effects of dead zones or storage zones is caused by factors such as holes in the bed and banks, large turbulent eddies, or pool-riffle sequences. These effects, not covered by the classical Fickian theory, can be introduced into the ADE by adding a fully mixed zone, which then allows for these effects of interchange between the main flow and the dead zones to take place.

However, for many applications it can be assumed that most of the observed dispersion arises because of the effect of the dead zones. While Fickian type dispersion from shear flow and diffusion takes place to some extent, the whole mixing process is dominated by dispersion caused by dead zones.

The conceptualisation of an aggregated dead zone model (ADZ) considers the aggregative effect of the many individual dead zone regions in a given reach of a river or part of a hydraulic

system as being equivalent to a single dead zone, with a defined volume and an associated residence time. This aggregated dead zone can than be seen as a CSTR. Apparently, the translational effects of the flow regime dominate hydraulic systems like rivers. While the CSTR provides a mechanism for the mixing processes in such systems, a mechanism in terms of a plug flow time delay is also incorporated in the ADZ model to allow for the translational effect. This conceptualisation can be seen in Figure 2.9.

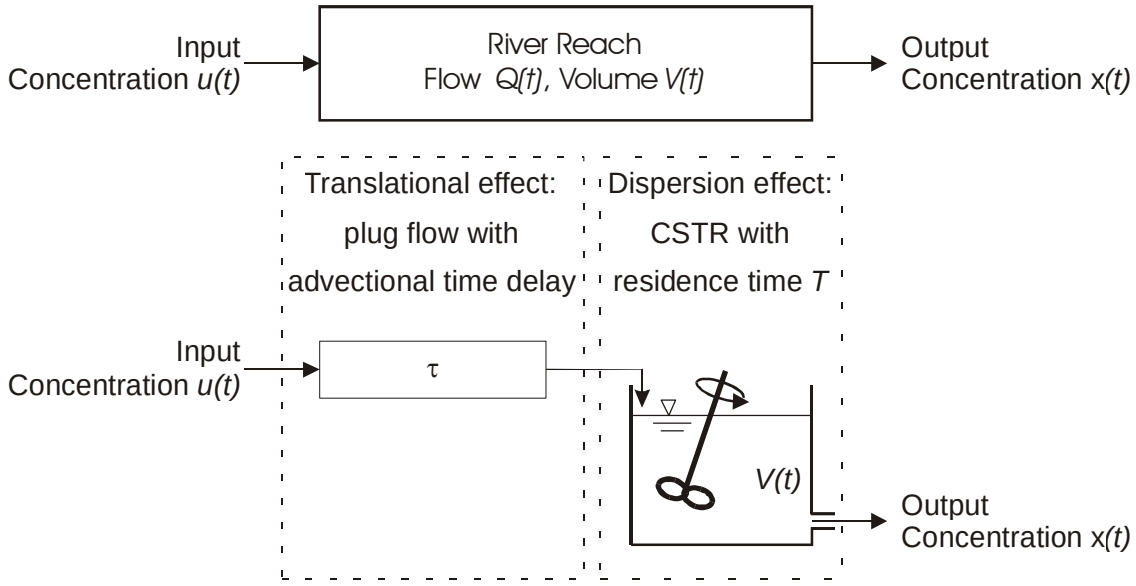

Figure 2.9. Conceptualisation of the ADZ model for a river reach

Allowing for the advectional time delay and including the CSTR, in which a simple proportional decay process of the pollutant in the reach can also take place, the mass balance of this model concept can be stated as:

$$\frac{dV(t)x(t)}{dt} = Q(t)u(t-\tau) - Q(t)x(t) - k\left[V(t)x(t)\right] \qquad 2.66$$

Under the assumptions of steady state condition ($V(t)$ and $Q(t)$ are constant) this equation simplifies to:

$$\frac{dx(t)}{dt} = \frac{Q}{V}u(t-\tau) - \left(\frac{Q}{V} + k\right)x(t) \qquad 2.67$$

where

V ADZ volume (L^3)

T ADZ residence time, $T = V/Q$ (T)

τ advective time delay (T)

k degradation rate constant (T^{-1})

$u(t)$ input/upstream concentration

$x(t)$ output/downstream concentration

It has to be noted, that the ADZ volume V representing the reach is not necessarily equivalent to the physical volume of water V_t within the reach. While this holds true for the completely CSTR, it cannot be considered an imperfectly mixed hydraulic system like a river, where the fully mixed volume V is only a fraction of the total volume V_t. The ratio of V to V_t defines the mixing characteristics within the system and is called Dispersive Fraction (DF). It can also be expressed at the ratio of the travel times as $DF = T/(\tau + T)$. The travel time $\bar{t}$ within the reach can be calculated as $\bar{t} = T + \tau$.

A solution for the first order differential equation in form of a continuous time transfer function can be calculated as follows. Substituting

$$\alpha = \frac{Q}{V} + k\ ,\ \beta = \frac{Q}{V} \quad \text{into Equation 2.67 yields}$$

$$\frac{dx(t)}{dt} = -\alpha\, x(t) + \beta\, u(t-\tau) \qquad 2.68$$

Using the differential operator of Equation 2.61 and substituting in Equation 2.68 gives

$$\begin{aligned} sx(t) &= -\alpha\, x(t) + \beta\, u(t-\tau) \\ (s+\alpha)\, x(t) &= \beta\, u(t-\tau) \\ x(t) &= \frac{\beta}{s+\alpha} u(t-\tau) \end{aligned} \qquad 2.69$$

where

$\frac{\beta}{s+\alpha}$ transfer function for the continuous time ADZ model

In practice data is often collected in discrete time rather than in continuous time. For a discrete solution for Equation 2.68 a simple finite difference approximation for the derivative is

$$\frac{dx(t)}{dt} = \frac{x_k - x_{k-1}}{\Delta t} \qquad 2.70$$

where

Δt sampling interval (T)

x_k sampled concentration value at time step k ($L^3\ L^{-3}$)

Thus Equation 2.68 becomes

$$\frac{x_k - x_{k-1}}{\Delta t} = -\alpha\, x_{k-1} + \beta\, u_{k-\delta}$$

$$x_k - x_{k-1} = -\alpha\, \Delta t\, x_{k-1} + \beta\, \Delta t\, u_{k-\delta}$$

$$x_k = (1 - \alpha\, \Delta t)\, x_{k-1} + \beta\, \Delta t u_{k-\delta} \qquad 2.71$$

where

δ nearest integer value to $\frac{\tau}{\Delta t}$ (-)

A continuous time transfer function is an exact representation of the differential equation for the model. While there is only one single ADZ model in continuous time for a specific reach of a hydraulic system, there is a whole set of discrete time ADZ models. Each of these ADZ models for discrete time is defined for the selected value of sampling interval Δt.

For the transfer function expression of this discrete time model it is first necessary to introduce the mathematical definition of the backward shift operator z^{-n}, where

$$z^{-n} x_k = x_{k-n} \qquad 2.72$$

Substituting $a = (1 - \alpha\, \Delta t)$ and $b = \beta\, \Delta t$ into Equation 2.71 gives

$$x_k = -a\, x_{k-1} + b u_{k-\delta} \qquad 2.73$$

and applying the backward shift operator yields

$$x_k = -a z^{-1} x_k + b z^{-\delta} u_k$$

$$(1 - a z^{-1})\, x_k = b z^{-\delta} u_k$$

$$x_k = \frac{b z^{-\delta}}{1 - a z^{-1}}\, u_k \qquad 2.74$$

where

$\frac{b z^{-\delta}}{1 - a z^{-1}}$ transfer function for the discrete time ADZ model

It is quite obvious from Equation 2.73 that the ADZ model is a linear equation. Linear models like these are used within the research field of System Engineering to describe general

engineering applications. Deterministic models are developed from physical principles and conceptualisations of the real structure of the system. Thus, these models can get very complex when incorporating all physical factors or might even be incorrect when not covering the important physical factors driving the systems dynamic. Some modelling techniques in System Engineering uses data-based approaches based on stochastic principles (Young, 2001). This does mean, that the information of the system structure is contained in the data that is collected from system observations rather than implying a deterministic structure to that system. Based on the general transfer functions, a number of different transfer functions are calibrated to the data to get a model that explains the observed data best. Generally is this approach called "black-box" modelling, since the engineer is not interested in what drives the system dynamics. More or less in these circumstances the efficiency and quality of the model describing observed data is the main interest. In contrast to this, the ADZ model has meaningful parameters that can be related to physical properties of the system. These parameters are the dispersive fraction *DF* and the travel times τ and *T*. The approach of modelling hydraulic systems with the ADZ model is therefore called a "grey-box" modelling approach.

However, this grey-box approach of modelling with transfer functions is useful. The linearity of the models allows connecting up a number of component models, e.g. a river may be split into several reaches or a wetland may be split into slow flow and fast flow mechanisms. The transfer functions can be combined and manipulated for this purposes in a similar way to standard algebraic equations. The powerful method of system identification, developed for the purposes of System Engineering, may be utilised for formulating and solving the models. These methods are explored further in Chapter 3.

2.5 DEGRADATION RATE KINETICS

The degradation of a pollutant with time follows usually a pattern. The pattern of the depletion of pollutant with time is called degradation rate kinetics. The kinetics or the rate of degradation processes can be expressed quantitatively by the law of mass action, where the rate is proportional to the concentration of the reactants (Hammer, 1896; Chapra, 1997). Degradation rate kinetics can be estimated from measurements in laboratory tests, either in a closed system in the form of a batch test or in an open system with steady state conditions of flow rates, pollutant loads and pollutants leaving the system.

Batch tests. Assuming a constant volume of a medium that contains a pollutant of a initial concentration $C_A = C_0$, than the change in concentration C_A of a substance with time t in this volume can be expressed as:

$$\frac{dC_A}{dt} = -kf(C_A, C_B, ...) \qquad 2.75$$

This relationship specifies that the rate of reaction is dependent on the product of a temperature-dependent constant k and a function of the concentrations of the reactants $f(C_A, C_B, ...)$. The functional relationship can be determined experimentally. Equation 2.75 can be rewritten as:

$$\frac{dC_A}{dt} = -k\, C_A{}^{\alpha} C_B{}^{\beta} \qquad 2.76$$

The concentrations are raised to a power to respect the influence of the reactant. This power is called the reaction order. If we focus on one single reactant, then the equation can be simplified to

$$\frac{dC}{dt} = -k\, Cc^{n} \qquad 2.77$$

where

C concentration of the single reactant (M L^{-3})

n the reaction order (-)

k the reaction rate (M L^{-3} T^{-1})

For the orders of 0 and 1, which are quite commonly used in water research, the reaction rates can be calculated as follows.

Zero-order. With $n = 0$ and the inital conditions of $C = C_0$ at $t = 0$, Equation 2.77 can be integrated to yield

$$C(t) = C_0 - k\, t \qquad 2.78$$

This model specifies a constant rate of degradation per time unit and the plot of concentration versus time is a straight declining line (Figure 2.10).

First-order. With $n = 1$ and the inital conditions of $C = C_0$ at $t = 0$, Equation 2.77 can be integrated to yields Equation 2.79. Taking the exponentials of both sides of this equation gives Equation 2.80.

$$\ln C - \ln C_0 = -k\, t \qquad 2.79$$

$$C(t) = C_0 \exp^{-kt} \qquad 2.80$$

This model specifies an exponential degradation rate per time unit and the plot of concentration versus time asymptotically approaches zero with time (Figure 2.10). For some parameters a non-zero background concentration necessitate the introduction of a further parameter, C^*, in addition to the first order rate constant k to describe field observations. The Equation 2.80 becomes

$$C(t) - C^* = (C_0 - C^*) \exp^{-kt} \qquad 2.81$$

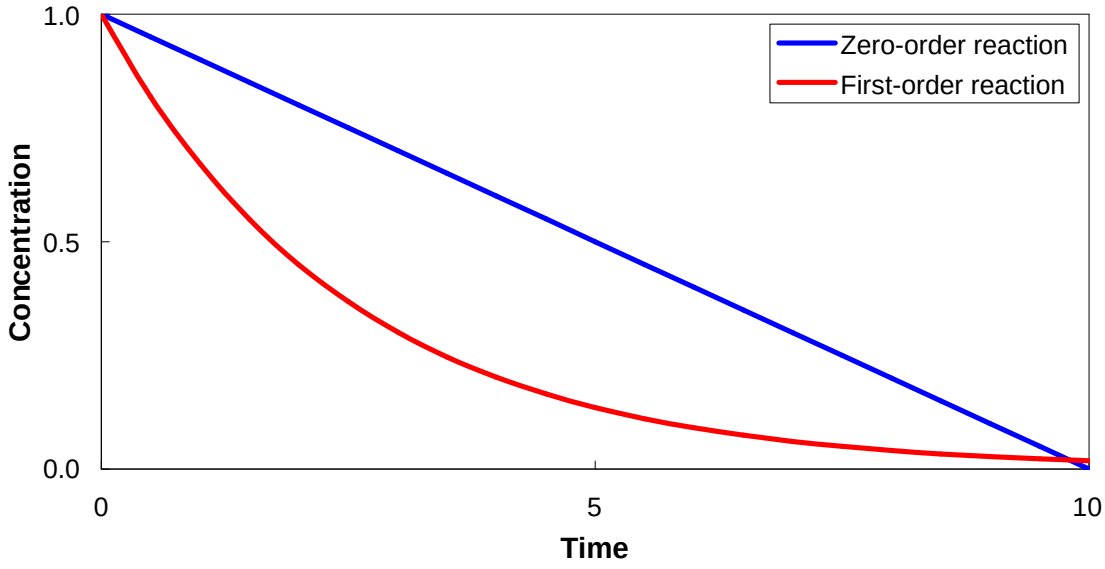

Figure 2.10. Pollutant depletion with a zero-order and first-order reaction

Open system. A commonly used simple model in water quality, the continuously stirred tank reactor (CSTR) can be used to develop degradation kinetics for continuously loaded reactors. Assuming a completely mixed tank with a fixed volume V, a inflow flow rate Q_{in}, a outflow flow rate Q_{out} and influent and effluent concentrations C_{in} and C_{out} the change of concentration in the reactor can be expressed as:

$$V\frac{dC}{dt} = Q_{in}C_{in} - Q_{out}C_{out} - kVC_{out} \qquad 2.82$$

Under steady-state conditions $dC/dt = 0$ and $Q_{in} = Q_{out} = Q$, thus Equation 2.82 gives:

$$0 = C_{in} - C_{out} - k\frac{V}{Q}C_{out} \qquad 2.83$$

or

$$C_{out} = \frac{C_{in}}{1 + k\frac{V}{Q}} \qquad 2.84$$

The term V/Q is the hydraulic residence time of this reactor. A plot of the ratio C_{in}/C_{out} versus the residence time would therefore give a line whose slope is k.

Chapter 3

MODELLING OF SOLUTE TRANSPORT

3.1 INTRODUCTION

In Chapter 2 the fundamental concepts underlying the transport of solute pollutants in water were discussed. This chapter covers the numerical techniques for the application of the concepts and highlights the issues that may be encountered when they are applied. Each application of a solute transport model is unique and therefore not directly transferable from one application to the other. However, a framework of a systematic and iterative approach to the problem of solute modelling may be used for various other applications in a similar manner. This is outlined in Figure 3.1.

The first question that has to be answered at the beginning stage of building a pollutant transport model is the question about the purpose of the model. A general goal, in a scientific sense, is to gain a better understanding of the transport regime. This is to quantify the dominant processes controlling the transport of solutes and to test that the conceptual model defined by hypotheses will match the observations made. Further of importance is the ability of the model to predict future pollutant transport, either under existing conditions or under altered flow regimes.

The next step is to bring together all important and relevant information about the site to be modelled, e.g. cross-sectional data or slope data of river sections or information about the support-matrix of subsurface reed beds in which the flow takes place. This may then help to build a conceptual model of the observed structures and to design tests to gain data, which is needed to verify the model. This "a priori knowledge" may also help in the decision about the complexity of a model. A model of a "real world system" should not be too complicated or too simple. In fact, an under-simplified conceptual model will lead to a model that may be too complex and computationally demanding to be a useful tool (Zheng and Bennett, 2002). On the

other hand an over-simplified model will fail to capture essential features of the "real world system"[2] and thus lead to a model that is not capable to describe observed field data.

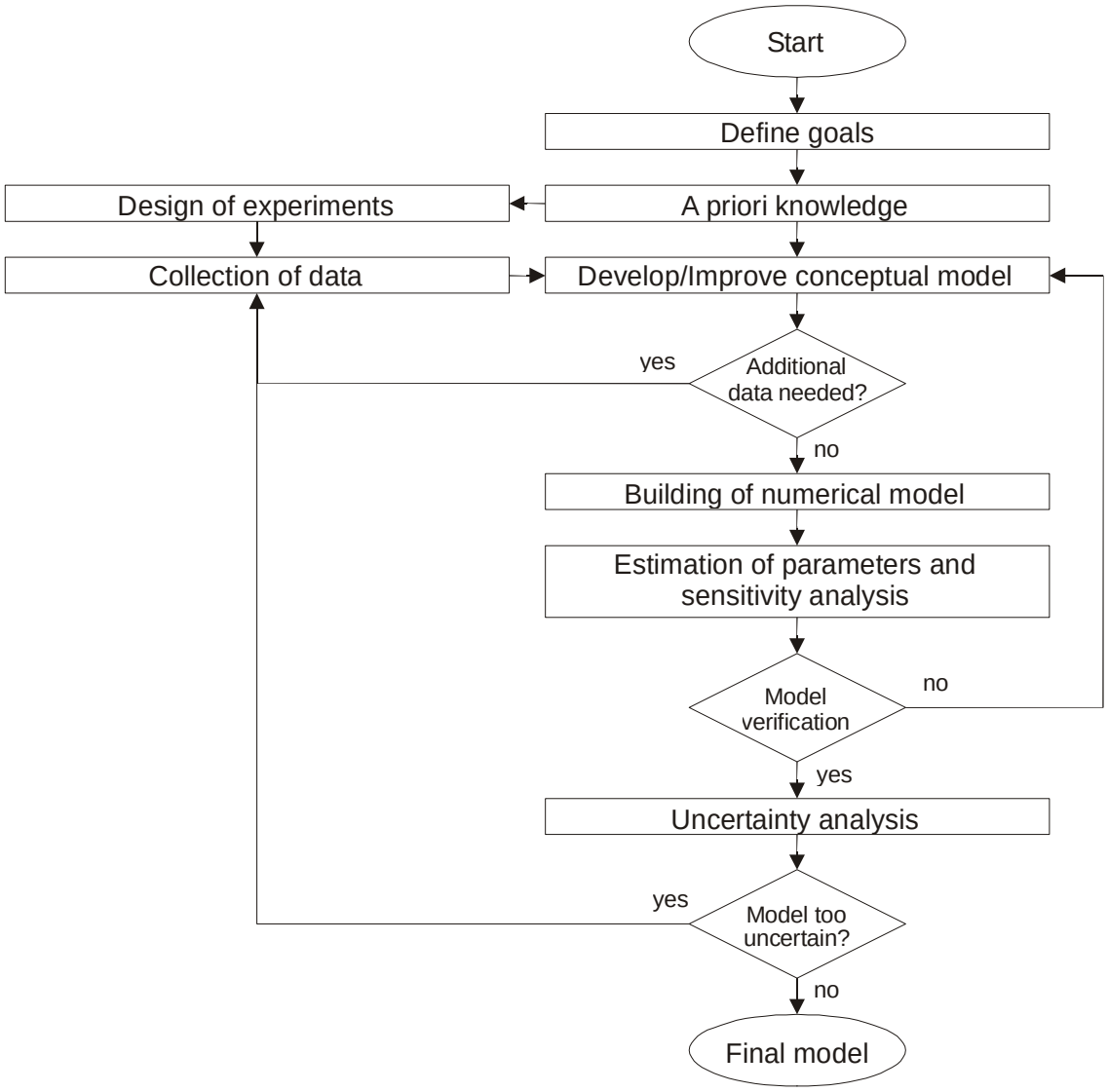

Figure 3.1. A framework for model applications

[2] The term "system" used is a quite loose definition. Ljung states, "... a system is an object in which variables of different kinds interact and produce observable signals. The observable signals that are of interest to us are usually called *outputs*. The system is also affected by external stimuli. External signals that can be manipulated by the observer are called *inputs*. Others are called *disturbances* and can be divided in those that are directly measured and those that are only observed through their influences on the output.". In this context the term *system* describes observable reactions on man-made or natural events in hydrology or hydraulics. This may be the effect of rainfall (input) to rising water levels in streams (output) or the spread of a pollutant (output) caused by a spill (input) in a river reach when travelling downstream.

Since environmental scientists have different academic backgrounds, it is quite obvious that they will consider the conceptual model from rather different standpoints and subjective interpretations (Young and Lees, 1993). Therefore the appropriateness of an conceptual model cannot be tested until a numerical model is built and comparisons between field observations and model simulations are made (Zheng and Bennett, 2002). Thus a numerical model is not only useful since it will simulate observed data but also that it is a tool to test and iteratively improve the conceptual model of the "real world system".

The next step is to set up the numerical model. The model will be selected upon the goals defined in a previous step and the a priori knowledge. It has to be taken into account whether just a simulation of advective transport is sufficient or whether an advective-dispersive or advective-dispersive-reactive transport model is needed. Further considerations have to be made whether a one-, two- or three-dimensional model is needed. However, these considerations have to take account of spatial and temporal discretisation and have to answer the question, if the "real world system" can then be modelled in one section or has to be divided into several sub-sections. In any case, the decision has to be made if the model has to match steady state conditions or transient conditions. The a priori knowledge should further help to determine the parameters that are known sufficiently, and are therefore treated as predetermined model inputs, and to determine those parameters which are targets of the process of model calibration or parameter estimation. The process of parameter estimation then proceeds iteratively until the unknown parameters result in a model output that "best" matches the observed data. If the evaluation of data turns out to be not sufficient, additional data has to be collected.

When the "best" model has been found, it is necessary to analyse the sensitivity of the parameters. The sensitivity is the measure of the effect of change in one parameter on another parameter and may show the important parameters and the less important or less dependent parameters.

The model may be used for predictive simulations, based on postulated future stresses. The problems associated with future predictions are the uncertainties in the model estimated for the current conditions itself, in the nonuniqueness of the estimated parameters and the uncertainties in the forecast of future stresses. If predictive simulations are necessary, these uncertainties should be considered and their consequences should be addressed in some way.

3.2 PARAMETER ESTIMATION FOR THE ADE-MODEL

As derived in Chapter 2, the numerical model used for one dimensional solute transport, considering the processes of advection-dispersion, is the routing procedure of the ADE-equation, stated as

$$C(x_2,t)=\int_{\xi=-\infty}^{\infty}\frac{C(x_1,\gamma)U}{2\sqrt{\pi K\bar{t}}}\exp\left[\frac{-U^2\left(\bar{t}-t+\gamma\right)^2}{4K\bar{t}}\right]d\gamma \qquad 2.58$$

where all the symbols were defined previously. In applications that uses this transport equation to model observed data, the unknown parameters are the velocity *U*, the time of travel $\bar{t}$ and the dispersion coefficient *K*. The parameters for the process of estimation are usually the travel time $\bar{t}$ and the dispersion coefficient *K*, while the velocity *U* can be calculated from the relation of the travel time with the measurable or predetermined parameters of the discharge, cross-sectional area and porosity.

Most processes of parameter estimation are indirect approaches, that involve the task of minimizing an error or objective function of a relation of the observed data and the predicted data from the model. This involves an iterative process of updating the estimated parameters depending on calculated errors in previous steps and the calculation of the new-modelled data from the updated estimated parameters to gain minimised errors or to minimise the objective function. The process of calculating the new model predictions is called an "en-bloc" process, since estimated parameters are updated after each calculation of the new model predictions rather than continuously.

The objective function, sometimes called cost function, is usually defined as the weighted sum of squares *S* of the residual errors between the observed data and the modelled data

$$S=\sum_{i=1}^{N}\varepsilon_i=\sum_{i=1}^{N}\omega_i(y_i-\hat{y}_i)^2 \qquad 3.1$$

where

i	index for the *i*th sample of observation
N	number of observations
ε_i	weighted residual error for the *i*th sample
ω_i	weighting factor for the *i* th sample
$y_i,\hat{y}_i$	measured and calculated dependent values at the *i*th sample

Since a weighting factor is not generally necessary, it may be omitted. Sometimes it may be also useful to use a simpler cost function that just minimises the sum of absolute residual errors instead of the squared term shown in Equation 3.1. For a linear model with two parameters, a and b, the response surface for the sum of squared errors *S* is well defined and has a unique minimum point (Figure 3.2a). For nonlinear models, the response surface is less well defined (Figure 3.2b) or even has a global minimum and several local minima and maxima (Figure 3.2c), leading to numerical difficulties in the iterative process of computing the "best"

parameters for the model. The ADE-equation is a nonlinear model and has a response surface for the objective function of the sum of the squared error similar to Figure 3.2b.

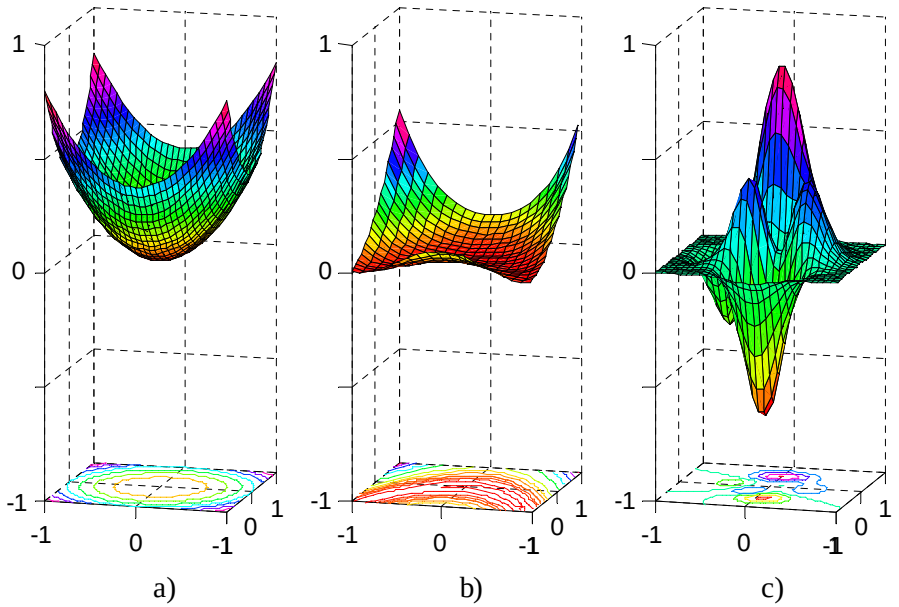

Figure 3.2. Response surfaces of sum of squared error function for a a) linear model, b) nonlinear model and c) highly nonlinear model

Nonlinear models generally require numerical solutions. A reliable and relatively fast algorithm is the Downhill Simplex Method developed by Nelder and Mead (Lagarias *et al.*, 1998). This is a direct search method that does not use numerical or analytic gradients and is therefore also quick to encode. A simplex in n-dimensional space is characterized by n+1 distinct vectors, also called vertices. For a two-parameter problem, a simplex is a triangle; for a three-parameter problem it is a pyramid. At each step of the search, a new point in or near the current simplex is generated after evaluating the model for this parameter combination and computing the objective function for this combination. The value of the objective function at the new point is compared with the function values at the vertices of the simplex and, if the error is smaller, the new point replaces one of the vertices. This gives a new simplex and moves the simplex towards the (local) minimum. This step is repeated until the diameter of the simplex is less than the specified tolerance in the vertices. An initial simplex for the routine is calculated from the initial starting guess by computing the other n points as

$$P_i = P_0 + \lambda e_i \qquad 3.2$$

where

i index for the ith dimension

P_i vertices in the ith dimension

P_0 starting guess

λ constant for the computing of vertices in each dimension

e_i unit vector in each dimension

A good initial starting guess and a narrow range of the parameters is essential for the routine to converge fast within the specified tolerances of the vertices. Therefore the a priori knowledge should be used to specify the initial guess and to restrict the parameter range with constraints. The flow chart for a computer program for the parameter estimation of the ADE routing equation is shown in Figure 3.3. The program was written in the MATLAB® programming language.

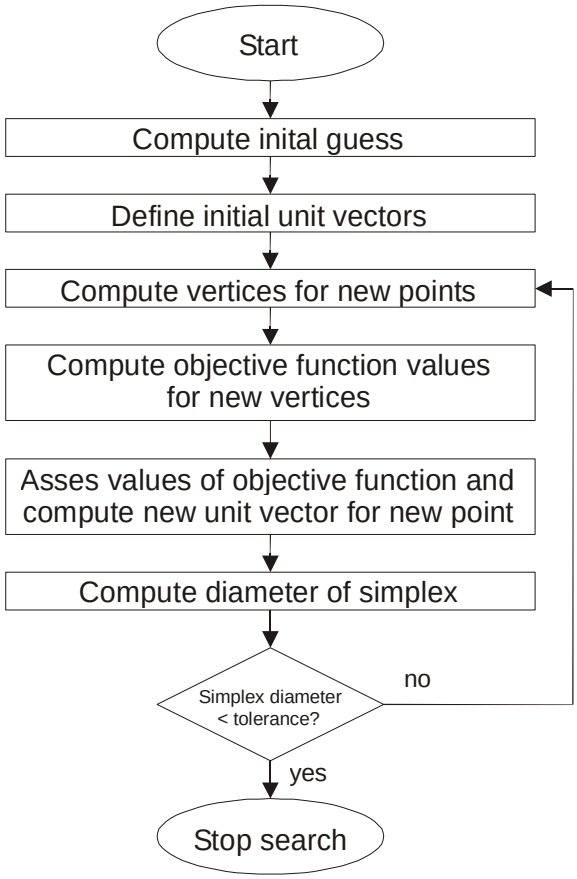

Figure 3.3. Flow chart of computer program for parameter estimation of the ADE routing equation

The initial starting guess in this implementation of the simplex-algorithm is gained by the method of moment evaluation for the travel times and the dispersion coefficient. Research undertaken by Aris (1956) showed that the spread of a solute pollutant could be calculated in terms of the spatial variance of the distribution about its centre of mass. Further findings

showed that the increase of the variance rapidly tends towards a constant, thus Aris (1956) concluded

$$\lim_{t\to\infty}\frac{1}{2}\frac{d\sigma_s^{\,2}}{dt}=K \qquad 3.3$$

where

σ_s^2 spatial variance (L^2)

t time (T)

Fischer (1966) goes on, that the spatial variance was found to be directly proportional to the temporal variance, thus

$$\partial\sigma_s^{\,2}=U^2\partial\sigma_t^{\,2} \qquad 3.4$$

where

σ_t^2 temporal variance (T^2)

U mean velocity (LT^{-1})

Substituting Equation 3.4 into Equation 3.3 and discretisation of the resulting equation leads to Equation 3.5 from which the dispersion coefficient can be calculated from two temporal solute distributions as

$$K=\frac{1}{2}U^2\,\frac{\sigma_{t_1}^{\,2}-\sigma_{t_2}^{\,2}}{\bar{t}_2-\bar{t}_1} \qquad 3.5$$

where

$\sigma_{t_1}^{\,2}$ temporal variance of pollutant distribution at observation location 1 or 2 (T^2)

$\bar{t}$ temporal centroid of pollutant distribution at observation location 1 or 2 (T)

However, it has to be noted that this equation only works sufficiently when the distributions are not too skewed, thus are Gaussian. The temporal centroid and temporal variance of a distribution can be calculated from its temporal moments as follows

*R*th moment

$$M_R(f)=\int_{-\infty}^{\infty}f(t)\,t^R\,dt \qquad 3.6$$

Area under distribution

$$A = M_0 = \int_{-\infty}^{\infty} f(t)\,dt \approx \sum_{i=-\infty}^{\infty} c_i \Delta t \qquad 3.7$$

Temporal centroid

$$\bar{t} = \frac{M_1}{M_0} = \frac{\int_{-\infty}^{\infty} f(t)\,t\,dt}{\int_{-\infty}^{\infty} f(t)\,dt} \cong \frac{\sum_{i=-\infty}^{\infty} c_i t_i \Delta t}{\sum_{i=-\infty}^{\infty} c_i \Delta t} \qquad 3.8$$

Temporal variance

$$\sigma_t^{\,2} = \frac{M_2}{M_0} - \bar{t}^{\,2} = \frac{\int_{-\infty}^{\infty} f(t)\,t^2\,dt}{\int_{-\infty}^{\infty} f(t)\,dt} - \bar{t}^{\,2} \cong \frac{\sum_{i=-\infty}^{\infty} c_i (t_i - \bar{t})^2 \Delta t}{\sum_{i=-\infty}^{\infty} c_i \Delta t} \qquad 3.9$$

where

c_i concentration of pollutant at ith sample (-)

t_i time of ith sample (T)

Δt sampling time step (T)

3.3 PARAMTER ESTIMATION FOR THE ADZ-MODEL

3.3.1 Higher order ADZ-models

In Chapter 2 the ADZ model was derived in the form of a simple equation (Equation 2.71) and in transfer function form (Equation 2.74). It is quite obvious, that both equations are linear in their parameters. Further on, in this form of a single ADZ-cell, there are three unknown parameters in the equation, which are α, β and δ or a, b and δ respectively. If the pollutant is conservative, the number of parameters is reduced to two, since then $\alpha = \beta = Q/V$.

$$x(k) = (1 - \alpha\,\Delta t)\,x(k-1) + \beta\,\Delta t\,u(k-\delta) \qquad 2.71$$

$$x(k) = \frac{bz^{-\delta}}{1 - az^{-1}}\,u(k) \qquad 2.74$$

In this simple case, the model can be solved with a simple search algorithm that varies the parameter of α and evaluates the model in an *en-bloc* approach, while keeping the time delay δ constant. Due to the linearity of the model, there is only one best parameter of α for each time

delay δ, thus a repeated search for different time delays gives the best solutions for both parameters.

As already stated in Chapter 2, the linearity of the ADZ-model allows to connect up a number of component models. A real physical system can be divided into sub-systems, where a single ADZ-model represents each sub-system with a different flow and mixing mechanism. While the transfer function of Equation 2.74 represents a first order system, higher order systems can be linked together by combining multiple single order systems and manipulating them in a similar way to standard algebraic equations. Some examples for transfer function arithmetic follows below, where the terms G1, G2, ... each represent a first order transfer function.

Single transfer function

$$x = G_1 u$$

Transfer functions in serial connection

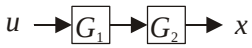

$$x = G_1 G_2 u$$

Transfer functions in parallel connection

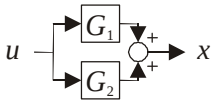

$$x_1 = G_1 u_1 \qquad x_2 = G_2 u_2$$

$$x = (G_1 + G_2) u$$

Transfer functions in combination

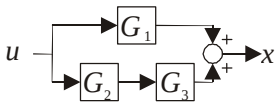

$$x = (G_1 + G_2 G_3) u$$

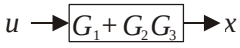

A set of parallel and serial combined transfer functions is represented through the following general transfer function for the discrete time

$$x(k) = \frac{B(z^{-1})}{A(z^{-1})} u(k-\delta) \qquad 3.10$$

where the backward shift operator is $z^{-n} x_k = x_{k-n}$, as defined before and the polynomials $A(z^{-1})$ and $B(z^{-1})$ are defined as

$$A(z^{-1}) = 1 + a_1 z^{-1} + a_2 z^{-2} + ... + a_n z^{-n} \qquad 3.11$$

$$B(z^{-1}) = b_0 + b_1 z^{-1} + b_2 z^{-2} + ... + b_m z^{-m} \qquad 3.12$$

In the difference equation form the general transfer function then becomes the following linear equation:

$$x_k = -a_1 x_{k-1} - a_2 x_{k-2} - ..... - a_n x_{k-n} + b_0 u_{k-\delta} + b_1 u_{k-1-\delta} + ... + b_m u_{k-m-\delta} \qquad 3.13$$

3.3.2 Numerical algorithms for the parameter estimation of ADZ-models

Transfer function models such as 3.13 are "input-output" models that describe the overall behaviour of the system. They are used in many scientific areas to represent time series data, such as the temporal change of shares in the stock market, temporal development of sales in relation to advertisement, temporal changes in telephone calls, roll and pitch of aircrafts in relation to the steering or river water levels in relation to rainfall. Thus transfer functions provide a parametrically efficient representation of time-series data (Young, 1992). In general, no prior assumptions are made about the order of the polynomial of $A(z^{-1})$ and $B(z^{-1})$ since the process of the parameter estimation is used to find a combination of the orders of *n, m* and the delay δ that forms the "best" model to describe the observed data. Subsequently, we refer to a model using the triad [*n*, *m*, δ]. The modelling procedure then incorporates the definition of ranges or values for [*n*, *m*, δ] and estimating the parameters from the collected field data enabling a range of solution algorithms. The most well-known and widely used method is that of the Least Squares (LS). Among other different methods for the parameter estimation of transfer functions developed in the scientific field of System Engineering are the well known and popular method of the Equation Error (EE) and the Instrumental Variable (IV) (Ljung, 1999). From the IV method, derived techniques are the Refined Instrumental Variables (RIV) and the Simplified Refined Instrumental Variables (SRIV) (e.g. Söderström and Stoica, 1989; Young, 1984). Finally, once each of the models of the defined ranges for [*n*, *m*, δ] has been

parameterised, an objective criterion is used to identify the "best" model. Different criteria for this process are the coefficient of determination, the Aikake Identification Criterion (AIC) or the Young Identification Criterion (YIC), which will be explained later in this section.

Observations of times-series data in real-world applications, as the collection of tracer data of hydrological processes, are often disturbed with noise. The general transfer function may then be expanded with a noise term that summarises all noise influences, such as measurement noise or instrumental noise, as:

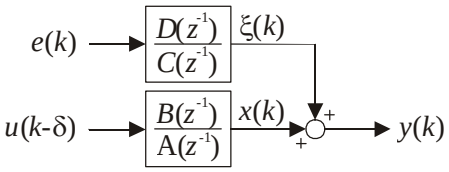

$$y(k) = \frac{B(z^{-1})}{A(z^{-1})}u(k-\delta) + \frac{D(z^{-1})}{C(z^{-1})}e(k) \qquad 3.14$$

$$y(k) = \frac{B(z^{-1})}{A(z^{-1})}u(k-\delta) + \xi(k) \qquad 3.15$$

where

$e(k)$ white noise

$\xi(k)$ coloured noise, $\xi(k) = \frac{D(z^{-1})}{C(z^{-1})}e(k)$

White noise is a zero mean and serially uncorrelated sequence of random variables with a variance σ^2. Coloured noise is a non-zero mean and serially correlated sequence of random variables. Usually noise of data collected from hydrological processes is random and uncorrelated white noise. Nevertheless, instruments that are faulty or influenced by the 50 Hz AC power signal may produce coloured noise patterns while recording data.

The process of estimating the parameters for a model as defined by Equation 3.15 generally involves the definition of a cost function that, when minimised, will provide the best parameterisation of this model. Thus the cost function provides a measure of the goodness of the model explaining the observed data. Introducing $\hat{A}(z^{-1})$ and $\hat{B}(z^{-1})$ as the model estimates[3] of the system polynomials $A(z^{-1})$ and $B(z^{-1})$, then a simple formulation is the response error $\hat{e}(k)$ that defines the difference between observed data and model output as

$$\hat{e}(k) = y(k) - \frac{\hat{B}(z^{-1})}{\hat{A}(z^{-1})}u(k-\delta) \qquad 3.16$$

[3] Please note that the "hat" symbol always indicates an estimate of a variable, thus $\hat{a}$ is the estimate of the variable a.

Minimising this response error is usually approached by the "least squares" cost function *J*, defined as

$$J = \sum_{k=1}^{N} \hat{e}(k)^2 \qquad 3.17$$

Since Equation 3.16 is not linear in the parameters, this model must be solved using numerical optimisation techniques. To obviate the problem of the non-linearity of the parameters, the cost function can be transformed to a linear form and regression techniques can then be utilised for process of parameterisation. Assuming that the observed data is disturbed by measurement noise, hence $\xi(k) = e(k)$, Equation 3.15 becomes

$$y(k) = \frac{\hat{B}(z^{-1})}{\hat{A}(z^{-1})} u(k-\delta) + e(k) \qquad 3.18$$

$$\hat{A}(z^{-1})\, y(k) = \hat{B}(z^{-1}) u(k-\delta) + \hat{A}(z^{-1}) e(k) \qquad 3.19$$

$$e_E(k) = \hat{B}(z^{-1})\, u(k-\delta) - \hat{A}(z^{-1})\, y(k) \qquad 3.20$$

where

$$\hat{e}_E(k) = -\hat{A}(z^{-1})\, e(k) \qquad 3.21$$

The model estimates $\hat{A}(z^{-1})$ and $\hat{B}(z^{-1})$ can simply be calculated by utilising values of the observed input and output data. This method can be readily implemented when using the vector form. Thus Equation 3.18 becomes

$$y(k) = X(k-\delta)\hat{a} + e_E(k) \qquad 3.22$$

where $X(k-\delta)$ is the vector for the observed input and output data and $\hat{a}$ is the vector for the parameter estimates, these are defined as

$$X(k-\delta) = \left[-y(k-1) \quad \ldots \quad -y(k-n) \quad u(k-\delta) \quad \ldots \quad u(k-\delta-m)\right] \qquad 3.23$$

and

$$\hat{a} = \left[a_1 \quad \ldots \quad a_n \quad b_0 \quad \ldots \quad b_m\right]^{\mathrm{T}} \qquad 3.24$$

From the Normal Equations $\hat{a}$ can be calculated as

$$\hat{a} = \left[X^{\mathrm{T}} X\right]^{-1} X^{\mathrm{T}} y \qquad 3.25$$

These simple calculations can be used in a spreadsheet to immediately obtain the parameters estimates $\hat{a}$ from observed data using the simple matrix operation of Equation 3.25. However, the parameters $\hat{a}$ will only be estimated correctly if there is no noise present in the data, thus if $e(k) = 0$. With increasing noise the parameter estimates $\hat{a}$ will be biased away from their true value a, because this procedure minimises $e_E(k)$. It can be shown, that the parameter bias is caused by the squared output terms in the normal equations (Young, 1984).

This parameter bias can be eliminated, if simply replacing some instances of the output and past data values by values of the model output. This is the method of the Instrumental Variables (IV) (e.g. Young, 1985; Ljung, 1999), since then we are using values obtained by the model as instruments to eliminate the parameter bias, so that

$$\hat{a} = \left[\hat{X}^{\mathrm{T}} X\right]^{-1} \hat{X}^{\mathrm{T}} y \qquad 3.26$$

The estimated values in the vector $\hat{X}$ can be calculated with the parameter estimates $\hat{a}$ and Equation 3.18. Including the past values, the vector $\hat{X}$ is defined as

$$\hat{X}(k)^{\mathrm{T}} = \left[-\hat{y}(k-1) \quad \ldots \quad -\hat{y}(k-n) \quad u(k-\delta) \quad \ldots \quad u(k-\delta-m)\right] \qquad 3.27$$

Since this method replaces data values with values calculated from model estimates, the computation of the estimates is an iterative process. The initial guess for the parameter estimates is calculated with the Equation Error method. The method of Instrumental Variables always gives unbiased estimates, no matter how big the noise is (Young, 1985). Nevertheless, the parameter estimates are not minimum variance estimates.

To get optimal estimates the method of Refined Instrumental Variables (RIV) is used (Young, 1984). Equation 3.14 is transformed into a linear form with the following steps

$$\hat{e}(k) = \frac{\hat{C}(z^{-1})}{\hat{D}(z^{-1})}\left(y(k) + \frac{\hat{B}(z^{-1})}{\hat{A}(z^{-1})} u(k-\delta) \right) \qquad 3.28$$

$$\hat{e}(k) = \frac{\hat{C}(z^{-1})}{\hat{D}(z^{-1})\hat{A}(z^{-1})}\left(\hat{A}(z^{-1}) y(k) + \hat{B}(z^{-1}) u(k-\delta)\right) \qquad 3.29$$

$$\hat{e}(k) = \hat{A}(z^{-1}) y^{*}(k) + \hat{B}(z^{-1}) u^{*}(k-\delta) \qquad 3.30$$

where the data values $y(k)$ and u(k) are pre-filtered to gain $y^{*}(k)$ and $u^{*}(k)$ as

$$y^*(k) = \frac{\hat{C}(z^{-1})}{\hat{D}(z^{-1})\hat{A}(z^{-1})} y(k)\,; \quad u^*(k) = \frac{\hat{C}(z^{-1})}{\hat{D}(z^{-1})\hat{A}(z^{-1})} u(k) \qquad 3.31$$

The filtering by $\hat{C}/\hat{D}$ in the Equation 3.31 removes the biasing effects of the coloured noise, because it is the inverse of the noise model (Young, 1984, p.173). Since we are transforming coloured noise into white noise, this filtering is called pre-whitening. The filtering with $1/\hat{A}$ has two effects. First the filter $1/\hat{A}$ will pass the data within the frequency band defined by the transfer function $1/\hat{A}$. In other words, the filter $1/\hat{A}$ is filtering at the band-pass of the system, which is reducing the noise outside the frequency of the signal we are interested in (Young, 1984, p.173). The second effect of the pre-filter is, that it converts a single unit impulse of the input to a decaying exponential sequence. Young states, that "the information in the signal is effectively 'spread out' by the pre-filter and this helps to increase the statistical efficiency of the estimates, with a clear improvement in the estimated values." (Young, 1984, p.197). Young (1985) further highlights, that this effect is extremely useful and important in practice, particularly in situations where the input signal *u*(*k*) does not "excite" the system sufficiently. That means the pre-filter helps to provide good parameter estimates where the input signal was defined poor due to practical experimental restrictions. This method is computationally quite intensive, since the noise model $\hat{C}/\hat{D}$ has to be estimated simultaneously with the parameter estimates.

If we assume again that the noise $\hat{e}(k)$ is white noise, then no simultaneous estimation of a noise model is required and the pre-filters $\hat{C}$ and $\hat{D}$ can be set to $\hat{C} = \hat{D} = 1$. The pre-filtering with $1/\hat{A}$ is still required to gain minimum variance estimates, thus the model from Equation 3.29 and 3.30 becomes

$$\hat{e}(k) = \hat{A}(z^{-1})y^*(k) + \hat{B}(z^{-1})u^*(k-\delta) \qquad 3.32$$

where the data vectors *y*(*k*) and u(*k*) are pre-filtered to gain $y^*(k)$ and $u^*(k)$ as

$$y^*(k) = \frac{1}{\hat{A}(z^{-1})} y(k)\,; \quad u^*(k) = \frac{1}{\hat{A}(z^{-1})} u(k) \qquad 3.33$$

This method is called the Simple Refined Instrumental Variable (SRIV) method (Young, 1985). The SRIV method is an iterative algorithm since it requires simultaneously the estimation system parameters and using them for the pre-filtering of the data. Implementations of the general IV method in *en-bloc* or recursive form can be found in literature (e.g. Söderström and Stoica, 1989; Ljung, 1999; Young, 1984), in which the pre-filtering of the data for the SRIV method has to be added in the iterative process of updating the estimates. Young (1985) states,

that the recursive-iterative SRIV method is a very reliable implementation of the SRIV algorithm.

The recursive-iterative form of the algorithm can then be expressed as follows, where the variable *j* is the index for the steps of the iterations and the variable *k* is the index for the *k*th data sample for the recursion through the data. The model estimate $\hat{a}(k)$ of the system parameter vector *a* at the *k*th recursion step is defined as

$$\hat{a}(k) = \hat{a}(k-1) + \hat{P}(k-1)\hat{x}^*(k)\varepsilon(k \mid k-1) \tag{3.34}$$

where

$$\varepsilon(k \mid k-1) = \frac{y^*(k) - z^*(k)^{\mathrm{T}}\hat{a}(k-1)}{1 + z^*(k)^{\mathrm{T}}P(k-1)\hat{x}^*(k)} \tag{3.35}$$

and

$$P(k) = P(k-1) + \frac{P(k-1)\hat{x}^*(k)z^*(k)^{\mathrm{T}}P(k-1)}{1 + z^*(k)^{\mathrm{T}}P(k-1)\hat{x}^*(k)} \tag{3.36}$$

where the values for $z^*(k)$ and $\hat{x}^*(k)$ are computed as

$$z^*(k)^{\mathrm{T}} = \left[-y^*(k-1) \quad \ldots \quad -y^*(k-n) \quad u^*(k-\delta) \quad \ldots \quad u^*(k-\delta-m)\right] \tag{3.37}$$

$$\hat{x}^*(k)^{\mathrm{T}} = \left[-\hat{x}^*(k-1) \quad \ldots \quad -\hat{x}^*(k-n) \quad u^*(k-\delta) \quad \ldots \quad u^*(k-\delta-m)\right] \tag{3.38}$$

The star superscript denotes the pre-filtered data variables of the input $u^*(k)$ and output $y^*(k)$. For the *j*th step of the iteration these variables are generated by filtering with $1/\hat{A}_{j-1}(k)$, where the polynom $\hat{A}_{j-1}(k)$ is generated from the parameter estimates $\hat{a}(k)$ of the current completed iterative step $j-1$. The values of $\hat{x}^*(k)$ are the similarly pre-filtered version of the values of the instrumental variable signal $\hat{x}(k)$ and are also generated after completion of the recursion in the iteration-step $j-1$ as

$$\hat{x}(k) = \frac{\hat{B}_{j-1}(z^{-1})}{\hat{A}_{j-1}(z^{-1})}u(k) \tag{3.39}$$

$$\hat{x}^*(k) = \frac{1}{\hat{A}_{j-1}(z^{-1})}\hat{x}(k) \tag{3.40}$$

The polynomial $\hat{A}$ and $\hat{B}$ of the recursive-iterative SRIV algorithm are initiated with parameter estimates from the Equation Error method (Equation 3.25). The recursive-iterative SRIV algorithm usually converges after five iterations (Young, 1985).

Conveniently, the standard errors of the estimates of the unknown model parameters can be calculated from the outlined SRIV algorithm. The matrix $P(k)$ is the inverse of the instrumental covariance matrix,

$$P(k) = \left[\sum_{i=1}^{k} \hat{x}^*(i)\, z^*(i)^{\mathrm{T}} \right]^{-1} \qquad 3.41$$

Young (1984) highlights that this is a good estimate of the error covariance matrix $P^*(k)$ associated with the estimated parameter vector $\hat{a}(k)$ by equation

$$P^*(k) = \sigma^2 P(k) \qquad 3.42$$

where $P^*(k)$ is the expected value *E* of the product of the parameter estimation error $\tilde{a}(k)$ with its transpose, defined as

$$P^*(k) = E\left\{ \tilde{a}(k)\, \tilde{a}(k)^{\mathrm{T}} \right\} \qquad 3.43$$

and the parameter estimation error at the *k*th data sample is defined as the difference between the estimated parameter vector and the true parameter vector as defined in Equation 3.24 as,

$$\tilde{a}(k) = \hat{a}(k) - a \qquad 3.44$$

An estimate, $\hat{\sigma}^2$, of the noise variance σ^2 can be computed from the model residuals if the algorithm is implemented for offline use, that means if it is only used for previously collected data.

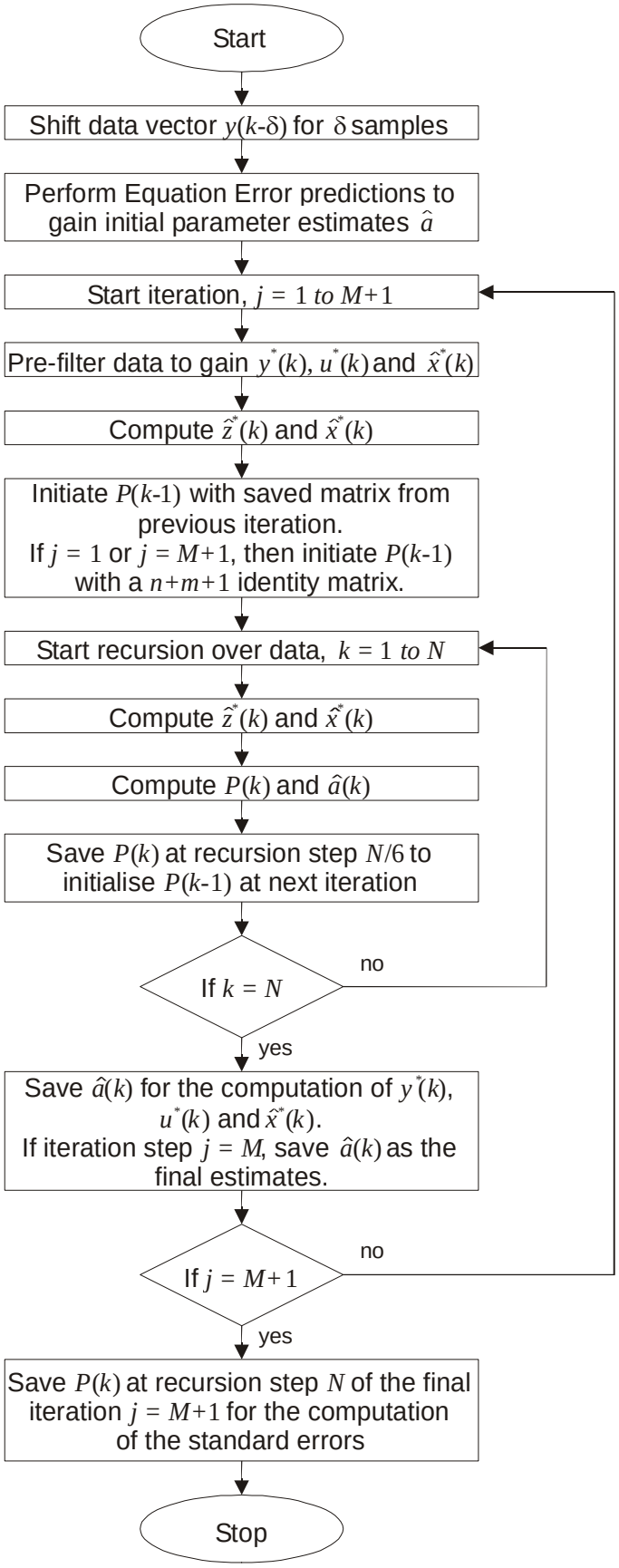

Figure 3.4. Flow chart of algorithm for parameter estimation with the SRIV method

The recursive-iterative algorithm for the SRIV estimation method was implemented in the MATLAB© environment. A flow chart of the implementation of this algorithm for offline use is shown in Figure 3.4.

As highlighted previously, the estimation process involves the computation of a whole range of models with varying numbers of parameters in their *A* and *B* polynomial as well as time delay steps δ. Therefore an objective criterion is needed to compare the different models and select the "best" or most appropriate one among these models. A widely used and well known measure is the coefficient of determination (e.g. Young, 1985) that is defined as

$$R_T^{\,2} = 1 - \frac{\sigma^2}{\sigma_y^{\,2}} \tag{3.45}$$

where σ^2 is the sample variance of the model residuals and $\sigma_y^{\,2}$ is the sample variance of the measured output *y*(*k*) about its mean value $\bar{y}$. With improving model fit the variance of the residuals tends to zero, thus the value of $R_T^{\,2}$ tends toward unity. However, the straightforward approach of the coefficient of determination takes no account of the complexity of the model in terms of the number of parameters in the polynomial *A* and *B* as well as the standard errors associated with them. These factors are being taken into account by the Akaike Information Theoretic Criterion (AIC) (Ljung, 1999) and the Young Information Criterion (YIC) (Young, 1992).

The AIC is defined as

$$\mathrm{AIC} = \log\left\{\det\left(P^*(k)\right)\right\} + \frac{2(n+m)}{N} \tag{3.46}$$

where $P^*(k)$ is the error covariance matrix as defined before, *n* and *m* are the numbers of parameters of the polynomial *A* and *B* and *N* is the number of data samples. The first term of the AIC is a measure of the uncertainty of the parameter estimates, thus less error in the estimates leads to a lower value. The second term is a penalty for over-parameterisation of the model, clearly more elements in the parameter polynomial leads to a higher value. Thus a compromise between the two terms of the error in the estimates and a low number of parameters to avoid over-parameterisation leads to a "better" model with the lowest (usually negative) AIC.

The YIC is defined as

$$\mathrm{YIC} = \ln\left\{\frac{\sigma^2}{\sigma_y^{\,2}}\right\} + \ln\left\{\frac{1}{n+m+1}\sum_{i=1}^{n+m+1}\frac{\hat{\sigma}^2 p_{ii}}{\hat{a}_i^{\,2}}\right\} \tag{3.47}$$

where the variables of the first term are as defined in Equation 3.45 and n and m as defined before; p_{ii} is the ith element of the $P(N)$ matrix, so that $\hat{\sigma}^2 p_{ii}$ is an estimate of the error variance associated with the ith parameter estimate after N samples; $\hat{a}_i^2$ is the ith element of the final estimated parameter vector $\hat{a}$. In comparison to the AIC, the YIC also incorporates a parameter for the goodness of fit of the model. The first term computes the goodness of fit, where a better fit leads to a lower value. The second term is a measure of the parameter uncertainty with a penalty to avoid over-parameterisation. It measures the error variance associated with each parameter normalised with respect to that parameter, leading to a model with little uncertainties in the parameter estimates and avoiding over-parameterisation. The YIC criterion identifies a model that compromises a good fit and parameter efficiency. Again, the best model has the lowest, usually negative, YIC.

In practice the minimisation of the YIC or AIC will not always result in the "best" identified model. Noisy or inadequate data may lead to a YIC or AIC identified model structure that may not be acceptable for some physical reasons (Young and Lees, 1993). Therefore, these criteria should be used together with the R_T^2 and a priori knowledge, such as physical considerations, to select an appropriate model; e.g. if physical processes occur in parallel in the system, such as parallel flow paths of water, then this would obviously lead to the description of such behaviour by the selection of a model of at least second order.

Example 3.1: Parameter estimation of ADZ model. In this example a first order ADZ model will be estimated by the Equation Error method, the Instrumental Variable method and the Simple Refined Instrumental Variable method. In this example an artificially computed set of data is used. Considering a first order ADZ model as

$$x(k) = -a_1 x(k-1) + b_0 u(k-\delta) \qquad 3.48$$

with the parameters of a_1 = -0.8 and b_0 = 0.2 and a delay δ = 0, the output of the model as a result of a unit impulse is shown in Figure 3.5. To gain a disturbed signal, a random white-noise sequence was added to the output signal of the transfer function.

The results of the parameter estimation process are shown in Table 3.1. The estimated standard errors of the IV and SRIV method are also shown. The results show clearly, that the parameters estimated with the SRIV method are clearly closer to the true parameter values. Further it is obvious, that that all methods identify the parameter b_0 with a greater accuracy than the parameter a_1. This is also highlighted by the estimated values of the standard errors from the IV and SRIV method. While the standard error of the parameter b_0 is approximately three times smaller than the error of parameter a_1 when estimated with the IV method, it is one order of magnitude smaller when using the SRIV method.

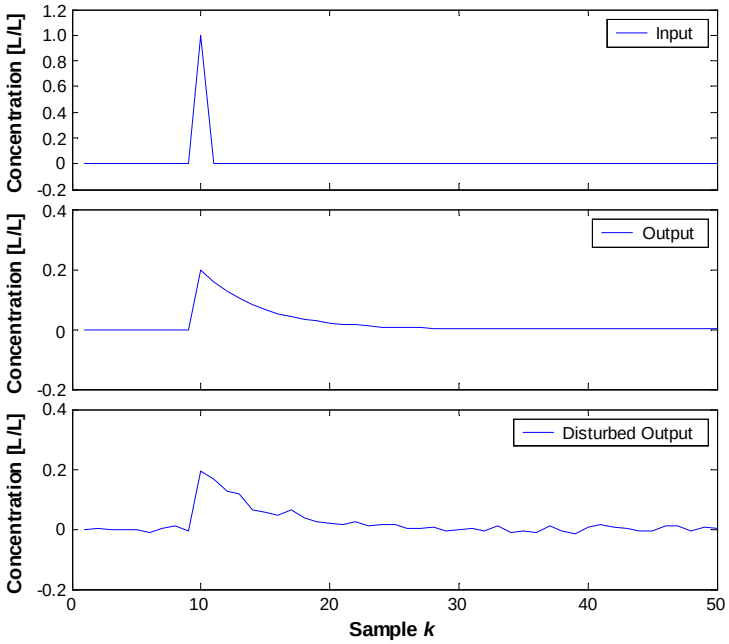

Figure 3.5. Synthetic input and output for Example 3.1

Table 3.1. Parameter estimation results (where the estimated standard errors are shown in brackets)

Parameter	true value	EE method	IV method	SRIV method
a_1	-0.8	-0.78561	-0.80599	-0.80178
			(0.033425)	(0.011972)
b_0	0.2	0.19953	0.19965	0.19993
			(0.011239)	(0.0085901)

3.3.3 Decomposition of higher order ADZ-models

After the estimation and identification of a "best" higher order transfer function model there is naturally an interest in decomposing it into first order sub-systems, which then can be interpreted as physical sub-systems, e.g. sections of reaches in rivers.

This process is quite straightforward, if the denominator polynomials $A(z^{-1})$ have real eigenvalues. In this case the decomposition into a series and/or parallel connection of first- and second-order sub-systems can be made unambiguously. Simple examples of this process have been highlighted by Young (1992) and are shown in Figure 3.6. Here a second order system can be decomposed into a parallel or series connection of sub-systems, depending on the polynomial of the numerator $B(z^{-1})$ of the transfer function.

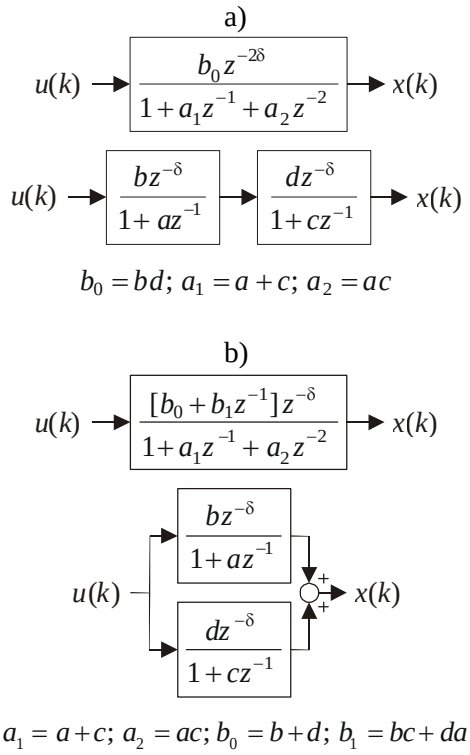

Figure 3.6. Serial (a) and parallel (b) decomposition of second order transfer function with real eigenvalues (adopted from Young, 1992)

The decomposition of higher order transfer functions by partial fractions expansion is not as straightforward if some, or all, of the eigenvalues are complex numbers. In this case the model will be re-estimated by a non-linear optimisation procedure where the eigenvalues are constrained to be real. Young (2001) showed for a hydrology model, that an estimated model of the order [4 2 22] with eigenvalues of {0.988, 0.964, 0.860±0.132*j*} could be decomposed with such a procedure to a model with real eigenvalues of {0.980, 0.855, 0.855, 0.855}. Interestingly the coefficient of determination R_T^2 for the constrained model is the same as for the unconstrained model. However, the model structure obtained from the estimation process of the transfer function parameters is used as a priori knowledge. Thus the model structure used for the constrained optimisation procedure is based on a physical interpretation of the model structure gained in the previous parameter estimation process by the modeller.

3.4 SENSITIVITY ANALYSIS AND UNCERTAINTY OF PARAMETERS

3.4.1 Sensitivity analysis

Sensitivity is a measure of the effect of change in one factor on another factor (e.g. Saltelli *et al.*, 2000; Zheng and Bennett, 2002). The sensitivity is the partial derivative of a model

dependent parameter with respect to a change in the value of a model input parameter (Wagner and Harvey, 1997)

$$X_{i,k} = \frac{\partial \hat{y}_i}{\partial a_k} \tag{3.49}$$

where $X_{i,k}$ is the sensitivity coefficient of the model dependent variable $\hat{y}$ with respect to the *k*th parameter at the *i*th observation point. The sensitivity is especially useful when calibrating a model with parameter estimation techniques, since they display importantly the dependence of different parameters on dependent parameters values.

Since the differentiation of some equations with regard to the dependent parameters is not always straightforward, e.g. the routing procedure in Equation 2.58, the sensitivity coefficient can be approximated by making a small perturbation in the parameter while keeping all other values constant and then dividing the change in the dependent variable by the change in the parameter, as

$$X_{i,k} = \frac{\partial \hat{y}_i}{\partial a_k} \approx \frac{\hat{y}_i(a_k + \Delta a_k) - \hat{y}_i(a_k)}{\Delta a_k} \tag{3.50}$$

This equation can be normalised for comparing the sensitivity coefficients among different parameters, as

$$X_{i,k} = \frac{\partial \hat{y}_i}{\partial a_k / a_k} \approx \frac{\hat{y}_i(a_k + \Delta a_k) - \hat{y}_i(a_k)}{\Delta a_k / a_k} \tag{3.51}$$

where a_k is the parameter and Δa_k is the perturbation of the parameter; $\hat{y}_i(a_k)$ and $\hat{y}_i(a_k + \Delta a_k)$ are the values of the model for the parameter and its perturbed parameter. In practice a sensitivity analysis in respect to *M* parameters consists of one calculation with the base parameters a_k and additional *M* calculations for each perturbation of the parameters $a_k + \Delta a_k$. The sensitivity coefficient is then a response of the model at a particular time and/or distance to a give parameter. Higher magnitudes of $X_{i,k}$ represents a higher sensitivity to a change in that parameter. Choosing a perturbation too small can result in negligible differences that are obscured by round-off errors, while to large perturbations can yield inaccurate sensitivities. As a rule of thumb, the perturbation size should be between 1 and 5% (Zheng and Bennett, 2002).

3.4.2 Uncertainty of parameters

As highlighted before, the model for the transport of solute may also be used as a predictive tool for future loads and conditions. Hence, all these future studies are subject to uncertainty, since apart from uncertain future conditions, also the estimated model parameters are uncertain to some extent. Uncertain parameters in terms of solute transport models are mainly physical model input parameters, such as dispersion coefficients, discharge rates, cross-sectional areas, porosities or dispersive fractions. Similarly, future stresses are uncertain, e.g. temporal concentration distributions. Therefore it seems to be quite useful to be able to quantify levels of uncertainty associated with the solute transport models that have been derived in the modelling exercise.

The most commonly used method to assess uncertainty is the Monte Carlo (MC) analysis. The Monte Carlo analysis is based on performing multiple evaluations with randomly selected model input, and then using the results of these evaluations to determine both uncertainty in model prediction and apportioning to the input factors their contribution to this uncertainty (Saltelli *et al.*, 2000). The Monte Carlo analysis is quite straightforward, involving in general the following steps.

After selection of the range for each parameter and distribution for those parameters, a large number of samples (or realisations) are generated through a computer-based random-number generator. In the MC analysis it is assumed that the distribution of each parameter follows a certain probability. These parameter distributions are called probability density function (PDF) and commonly uniform, normal or log-normal distributions are used. The selection of a PDF for the input may have an impact on the estimated distributions of the output variables, so assumptions should be made on physical reasons. The model will then be evaluated for each of the realisations. After completion of the model evaluations, each parameter realisation is plotted against the value of the objective function in a scatter plot. A well-defined minimum of the surface of the scatter plot indicates the parameter to be well identified. Realisations with a poor response of the objective function are an indication for parameters resulting in model behaviour that deviate far from the observed system. Thus these parameter realisations can be considered to be non-behavioural for the characterisation of the system. These realisations are not considered for further calculation, e.g. by selecting only the best performing 5% of the parameters in terms of the objective function for these further calculations. For the remaining parameters the likelihood is computed[4]. The likelihood can be

[4] The likelihood is a performance measure that is zero for non-behavioural models and increases as the performance of the model to fit the observations increases (Beven, 2000). When adding up, the likelihood must be monotonically increasing and add up to one. The realisations of the objective function (OBJFUN) of $(1 - R_T^2)$ can simply be converted into the likelihood (LIKELIHOOD) by the following calculations on the parameter vectors:

$$\text{LIKELIHOOD} = 1 - \text{OBJFUN} = 1 - (1 - R_T^2)$$

plotted in histograms (frequency plot) to get their probability density function. Further the Cumulative Density Function (CDF) is computed from the PDF of the likelihood. From the PDF of the likelihood the mean, median, variance and the confidence limits can be calculated. A more sensitive parameter has its PDF in a more confined value range. This is also indicated by a steeper gradient of the CDF.

However, the Monte Carlo analysis is computationally demanding in terms of the number of realisations needed to gain statistically meaningful results. The theoretical number of possible combinations of realisations is infinite and since the evaluation of the model can only be done for a finite number of realisations, the required number of realisations may get large. The number of sufficient realisations for the MC analysis to converge has to be tested with a repeated test with a larger number of realisations. Significantly different results of the MC analysis indicate that analysis has not yet converged (Zheng and Bennett, 2002).

Example 3.2: MC analysis of the system of Example 3.1. In this example the first order ADZ model of Example 3.1 will be used to demonstrate the Monte Carlo analysis. Using a uniform PDF for both parameters, on three data sets with 5,000, 8,000 and 10,000 random realisations were calculated in the parameter range of $-1.0 < a_1 < -0.65$ and $0.0 < b_0 < 0.35$. For each of the realisations the model was evaluated and the coefficient of determination ($1 - R_T^2$) was computed as the objective function. The results are given in Table 3.2. The calculated values for the mean and the standard deviation of the parameters a_1 and b_0 for the 5,000 and 8,000 realisations show some change, but there is much less change in the parameters between the sets of 8,000 and 10,000 realisations, suggesting sufficient realisations for the analysis to be converged. The results for the set of 10,000 realisations are shown in Figure 3.7 to Figure 3.9. In Figure 3.7 the realisations are shown as scatter plots, the "best" realisation is indicated as the best parameter value. It is clear from this plot, that the realisations cover a whole range of behavioural and non-behavioural sets of parameters. The surface of the scatter plots further show a clear minimum for both parameters, also indicating a better identifiable parameter b_0 with a steeper surface slope. The best two hundred realisations were selected to compute the probability density function and the cumulative probability function, as shown in Figure 3.8. The better identifiability of parameter b_0 is indicated through the smaller base of the PDF for this parameter compared to the PDF of parameter a_1 and further through the steeper slope of the CDF. The mean and standard deviation are calculated from the PDF, the median and the confidence limits, as the 5th and 95th percentile, are calculated from the CDF and the values are

---

IF MIN(LIKELIHOOD) < 0 THEN LIKELIHOOD = LIKELIHOOD - MIN(LIKELIHOOD)

LIKELIHOOD = LIKELIHOOD / SUM(LIKELIHOOD)

summarised in Table 3.2. In Figure 3.9 the response surface of the likelihood is plotted as a 3-dimensional surface plot over the parameters a_1 and b_0.

At this point it should be mentioned, that objective functions based on variance measures are not ideal measures of the goodness of fit or the likelihood for hydrologic models (Beven, 2000, p.225). Beven quotes three reasons for this:

- Large residual will tend to be found near peaks. Since the errors are squared this can result in the predictions of the concentration peaks being given greater weight than predictions of lower concentrations.
- The measure may be sensitive to timing errors in the prediction. Models predicting well in shape and magnitude but with slight time differences may result in significant residuals in rising and falling limbs.
- The measures of variance do not take into account that the residuals at successive time steps may not be independent but may be autocorrelated with time.

These problems have led to the use of different likelihood measures, borrowed from the theory of maximum likelihood in statistics. However, bringing this further is beyond the scope of this work. Nevertheless is it of importance to realise the problems associated with measures of the goodness of fit or likelihood based on the error variance.

Table 3.2. Result of the Monte Carlo analysis of Example 3.2

	5,000 realisations	8,000 realisations	10,000 realisations
Mean a_1	-0.79368	-0.79928	-0.80085
StDev a_1	0.029928	0.023986	0.019293
Mean b_0	0.20317	0.20002	0.19985
StDev b_0	0.019308	0.014163	0.013368
Best parameter value a_1	-0.80421	-0.80394	-0.80224
Best parameter value b_0	0.19963	0.19936	0.19955
Best parameter value R_T^2	0.96115	0.96116	0.96114
5th Percentile a_1	-0.84142	-0.83605	-0.83377
50th Percentile a_1	-0.79261	-0.7978	-0.80026
95th Percentile a_1	-0.74906	-0.76328	-0.77098
5th Percentile b_0	0.17225	0.17934	0.17972
50th Percentile b_0	0.20432	0.19975	0.20004
95th Percentile b_0	0.23196	0.22248	0.21939

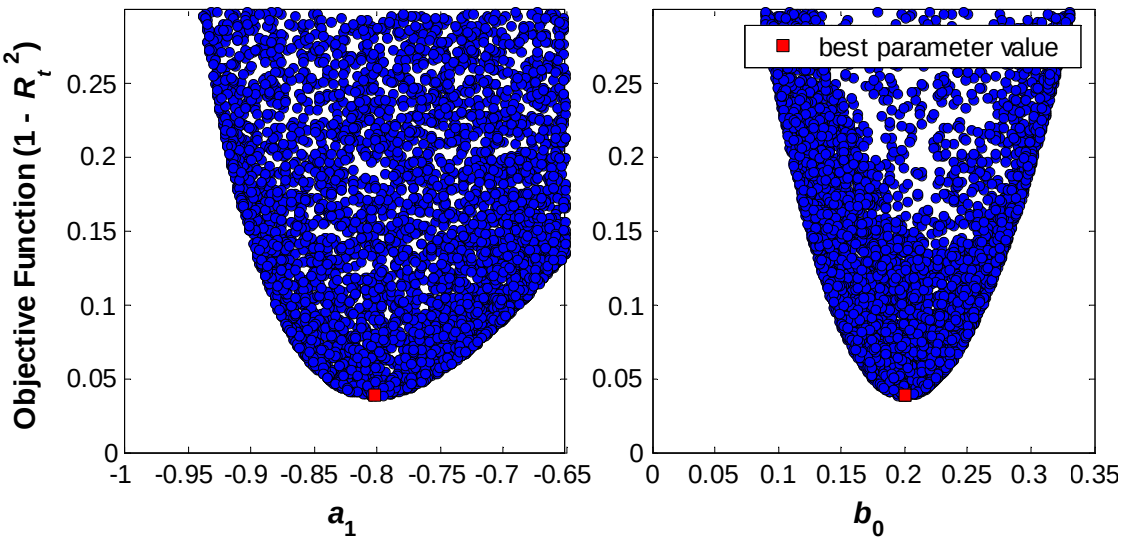

Figure 3.7. Scatter plot of the 10,000 realisations for the objective function (1 - R_T^2)

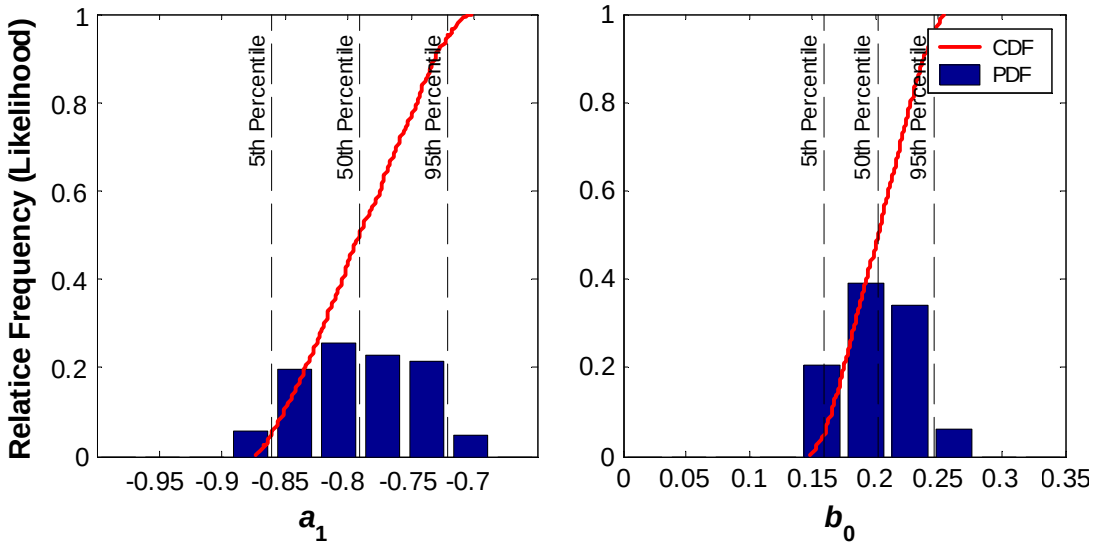

Figure 3.8. Probability density function (PDF), cumulative density function (CDF) and levels of uncertainty for the likelihood of the parameters, calculated from the best 200 realisations

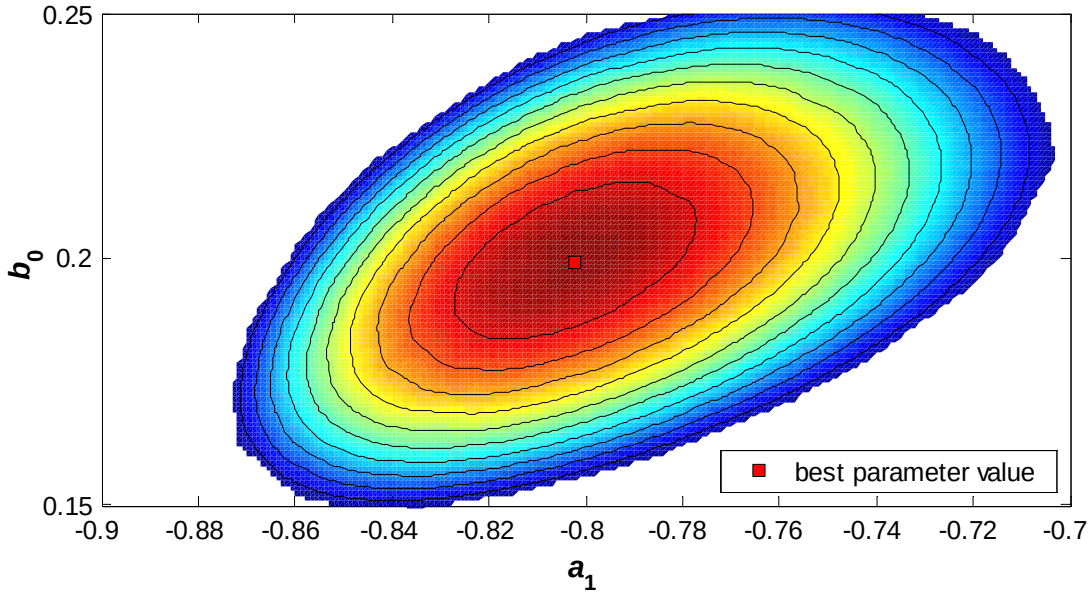

Figure 3.9. Response surface of the likelihood, calculated from the best 200 realisations and best parameter value

3.5 DESIGN OF EXPERIMENTS

When performing tracer studies for hydrological investigations the three main parameters that can be influenced are the concentration, the duration and the shape of the injection. While it is quite straightforward to alter the first two parameters, it is much more difficult to influence or define the third. For many experiments these parameter will need to be chosen due to practical reasons. Nevertheless, this chapter will investigate some effects of all these parameters on hydrological models.

The second section of this chapter covers aspects on how to obtain data from experiments and how to manipulate it for analysis.

3.5.1 Aspects of tracer injection

In one-dimensional dispersion studies the immediate distribution of the injected tracer cannot be generally taken as an upstream distribution for analysis. In most applications, the tracer must be cross-sectional fully mixed at the observations locations, e.g. the "input"-location and the "output"-location of the model. In practice this is achieved by injecting the dye upstream of the first observation point of interest, giving the tracer time to experience all cross-sectional parts of the flow. This will eventually result in skewed rising and falling limbs of the tracer distribution profile at the first point of observation, independent of the length of the observation. Short or instantaneous injections will result in bell shaped curves. Much longer injections will result in "Table Mountain" shaped distributions, where the maximum concentration of the distribution equals the maximum concentration of the injection, if the tracer is considered to be conservative

and no tracer is lost in the system. These distributions will be called "constant injections" in the further text.

In systems where no cross-sectional mixing of the dye is needed or immediately achieved and where the duration of the injection is short compared with the residence time, the injection of dye can be considered to have a direc-delta distribution. The main advantage of using a direc-delta signal as a systems input is that this signal has not to be measured, thus can be taken as granted without any measurement errors. The disadvantage from the practical point of view is, that the injected dye may be not distributed evenly in the whole system due to some preferential flow path. Thus the flow patterns with lower flow rates and lower velocity may be underrepresented in the observed output. In terms of System Engineering this problem is addressed in literature as a case, where the input signal u_k might not 'excite' the all modes of the system sufficiently (e.g. Söderström and Stoica, 1989; Young, 1985). However, when for practical reasons, injections that can be considered as "long" compared to the systems residence time, cannot be made, the direc-delta input of tracer is the only option.

Anyway, it might be of interest for the design of experiments, if the equations used for hydrological models have regions of special sensitivity for each parameter. This problem was addressed for the analytical solution of the ADE-equation by van Genuchten and Alves (1982) (in Knopman and Voss, 1987), where bell shaped distributions were considered. A study for the Transient-Storage model solution of the ADE by Wagner and Harvey (1997) considered pulse injections and constant injections. The equation sensitivities of the routing-procedure solution of the ADE and also of the ADZ-model are not reported up to date, while it can be assumed that equation-sensitivities for the routing procedure may be similar to the results reported by Knopman and Voss (1987).

For this study theoretical model inputs were generated in the form of bell shaped distributions and also in the form of plateaus with rising- and falling limb from constant injections. The sensitivities of the routing-procedure equation and the single cell ADZ-model were calculated analogue to the procedure described in Chapter 3.4.1. The parameter considered in the analysis were:

- ADE equation: the dispersion coefficient D, the distance x and the travel time $\bar{t}$
- ADZ-equation: the residence time T (or the parameter a_1 of the A-polynom) and the time delay δ.

The results of this analysis are plotted in Figure 3.10 and Figure 3.11 for the analysis of the ADE routing-procedure and in Figure 3.12 and Figure 3.13 for the ADZ-equation.

The sensitivity of the ADE-equation to the travel time shown in Figure 3.10 indicated that it its maximum value is related to the middle part of the rising limb and the middle part of the

falling limb. With increasing time the level of the maximum sensitivity does not change significantly. The plot of the sensitivity of change in distance indicates that the maximum sensitivity is related to the peak of the tracer distribution. Smaller sensitivities are also related to the first third and last third of the rising limb and falling limb respectively. With increased time the maximum sensitivity is decreasing. The sensitivities for the change in dispersion coefficient show a similar pattern with the maximum value associated with the peak of the distribution and a decreased sensitivity with increased time.

The sensitivity of the ADE-equation to a change in travel time for the constant injection distribution is shown in Figure 3.11. The sensitivities are clearly related to the point of change in slope at either the rising limb or the falling limb. With increasing time the sensitivities are also increasing. The maximum sensitivity of the equation against the change in distance indicates to be related to the first third and last third part of either the rising or falling limb. The sensitivity does not change significantly with distance. The sensitivity against a change in dispersion coefficient is related to the parts of the distribution with the larges change in slope. Again, the sensitivity against change in dispersion coefficient does not change significantly with increased time. For all three parameters the maximum plateau of the distribution is never associated with the sensitivity of any parameter.

From this observations the following conclusions may be drawn. The estimates for the travel time become more accurate with increased time, since the sensitivity is increasing as well. The change in distance and the dispersion coefficient have their greatest sensitivity at the peak of the short injection distribution. Therefore their estimates are mainly dependent on the accuracy of the observation of this peak. This confirms the observation of Beven (2000), stated earlier, that squared errors of the residuals found near peaks may become large and can result in the predictions of the concentration peaks being given greater weight than predictions of lower concentrations. A further negative point is, that also mass balance errors tend naturally to influence the peak more than the parts of the distribution with lower concentration. This will eventually be the case, if the duration of observations is not long enough or if the accuracy of the observations is not good enough to record the concentrations and thus tend to bringing to much weight into the peak when performing a mass balance. These issues will eventually result in biased estimates of the dispersion coefficient and the distance, if then predicted.

Interestingly this does not hold true for the long injection distributions, since the sensitivities are all related to the rising and falling limbs of the distributions. Also the mass balance is not an issue, since it can easily be achieved by comparing the concentrations of the maximum plateau. Further, it can be stated, that the sensitivities of the dispersion coefficient and the distance are at least one order of magnitude lower than the sensitivity of the travel time. If it is assumed that the peak concentrations are measured with less confidence due to

measurement errors, then a weighted objective function might be used that gives less weight to the observed data points at the peak.

Figure 3.12 and Figure 3.13 show the sensitivities of the change in time delay and residence time to the ADZ-model. Interestingly, the parameters are all related to the rising and falling limb. The parameters tend all to be more sensitive to the rising limb. Further, the sensitivities are decreasing with distance.

Since the sensitivities are not related to the peak of the distribution, the issue of mass balance on the ADZ-model might not exist to that extent as seen previous with the ADE-equation. It is not an issue at all, when estimating all the parameters of the *A*- and *B*-polynom, since the mass balance factor can be calculated from their relation.

For the sampling of the distributions the conclusions may be drawn, that is it of high importance to sample the distribution at a frequency that is sufficiently high enough to reproduce the rising and falling limbs sufficiently. For the ADE-equation more sampling effort is required to estimate the dispersion coefficient and the distance with the same confidence as the travel time, since their sensitivity is much lower.

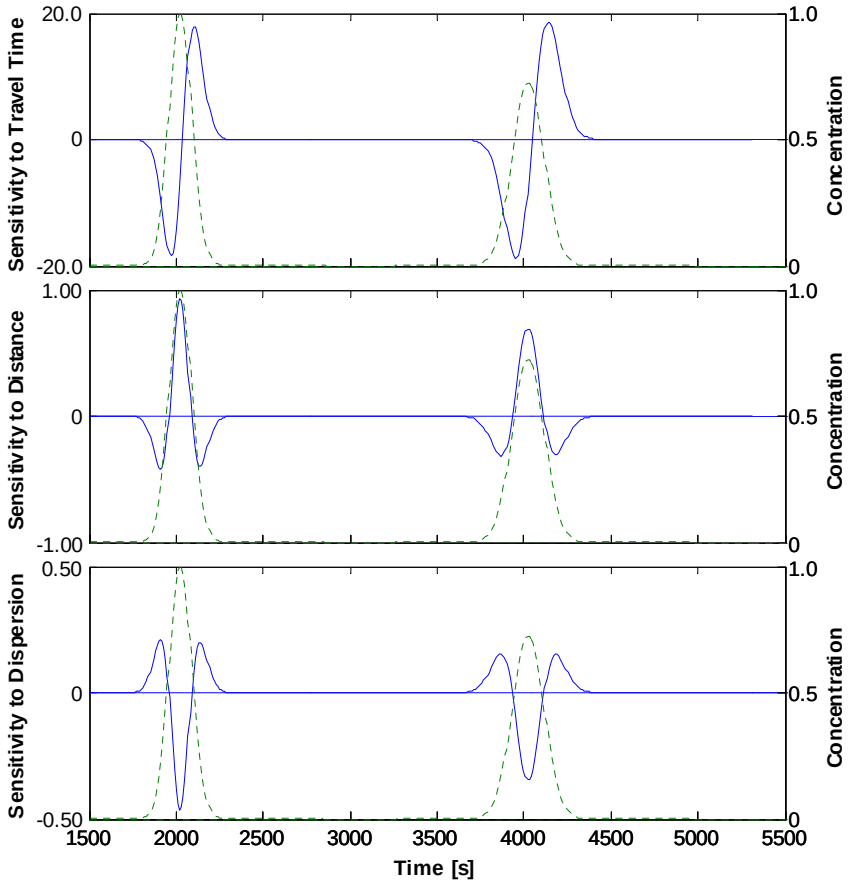

Figure 3.10. Sensitivity of ADE routing-procedure to travel time, distance and dispersion coefficient for a bell-shaped distribution

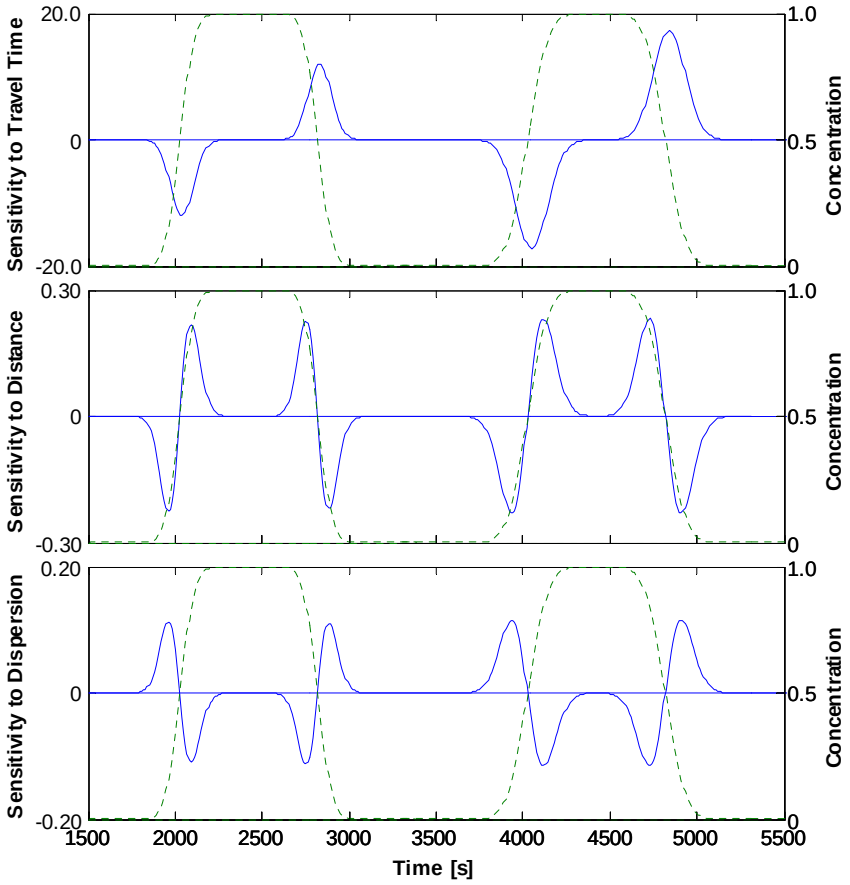

Figure 3.11. Sensitivity of ADE routing-procedure to travel time, distance and dispersion coefficient for a constant-injection distribution

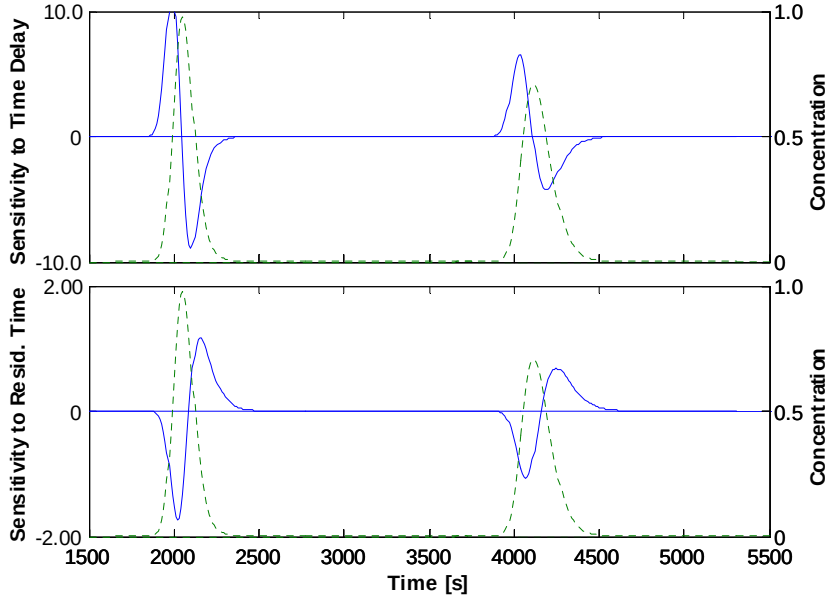

Figure 3.12. Sensitivity of ADZ-equation to travel time, distance and dispersion coefficient for a bell-shaped distribution

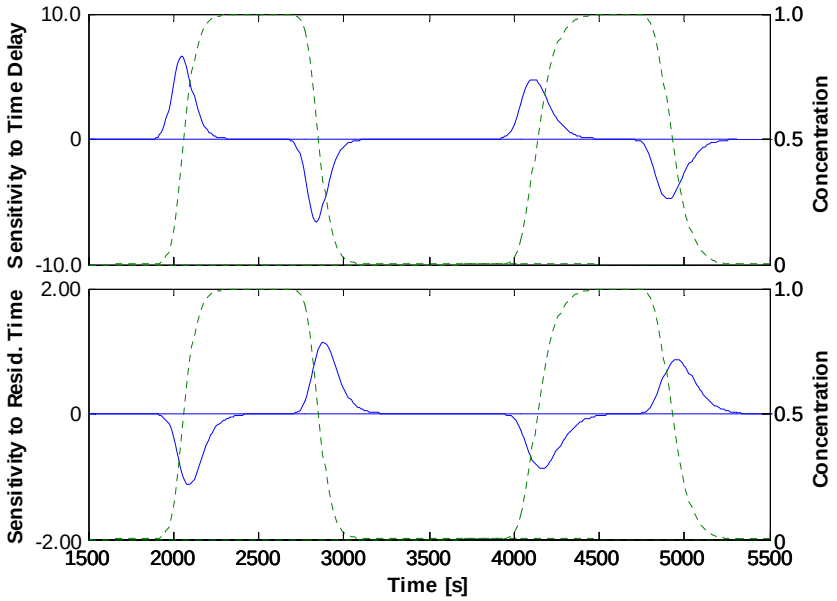

Figure 3.13. Sensitivity of ADE routing-procedure to travel time, distance and dispersion coefficient for a constant-injection distribution

3.5.2 Sampling rate and filtering of data

The sampling rate of data in hydrological applications is important for several reasons. On one hand, the sampling frequency has to be above a certain threshold to ensure all required information is contained in the observation. On the other hand, the sampling frequency may have an upper limit due to data storage limitations of the instrument. Also, a huge amount of data may not be easy to evaluate when applying to a numerical model, i.e. the computing time may restrict the amount of data for simulation, which then again affects the sampling frequency. Therefore, the sampling interval has to be chosen due to practical requirements in the field or in the laboratory and due to the computational requirements.

Theoretical considerations about the sampling frequency are based on the sampling theorem (Ljung, 1999). A sinusoidal signal may be considered that is sampled at a frequency of $\omega_s = 2\pi / T$. Then the sampling theorem states that any sinusoid of a frequency higher than the Nyquist frequency $\omega_N = \omega_s / 2$ cannot be distinguished from one in the interval $[-\omega_N, \omega_N]$. This means, that parts of the signal spectrum corresponding to higher frequencies than the Nyquist frequency will be interpreted as contributions from lower frequencies and the spectrum of the sampled signal is a superposition of different parts of the spectrum below the Nyquist frequency. That means, that sampling loses all information about frequencies higher than the Nyquist frequency, that is half the sampling frequency for a sinusoidal signal. Obviously, it is therefore necessary to sample at least twice the frequency of interest.

A second reason for high sampling rates is due to the fact that most data sampled in environmental field or laboratory studies consists of a useful part (the signal we are interested in) and a disturbance part (from the noise). This may lead to problems when using system identification techniques on higher order ADZ-models. Since the disturbance part of the signal is more broadband than the useful part of the signal, these techniques tend to identify the noise rather than the signal (Ljung, 1999). Therefore a filter is needed to remove the disturbance part. The problem is here again, that the frequency of the useful signal is in most cases not known in advance.

Generally it is accepted, that a convenient way of reducing the noise in a signal is simply by averaging several signals, if the noise is white noise. When averaging several repeated tests, white noise will average itself out and thus will reduce the variance in parameter estimates. If it is not possible or inconvenient to repeat tests, then a filter may be used on the signal to achieve a similar effect. It has to be noted, that the frequency the filter is working on must be higher or equal to the Nyquist frequency of the part of the signal we are interested in. Since such filters cut off the high frequencies above the cut-off frequency, these filters are called low-pass filters. A simple filter that might be used for this is a moving average filter (that means that each data point of the filtered signal is an average of the following N points of the original signal) such as

$$x_{F,i} = \frac{1}{N}\sum_{j=0}^{N-1} x_{O,i+j} \qquad 3.52$$

where

$x_{F,i}$	ith sample of filtered data
$x_{O,i+j}$	$(i+j)$th sample of the original data
N	number of samples

Again it is not obvious, how to define the frequencies of the useful part of the signal and of the filter.

Ljung (1999) states that the optimal frequency of the signal used for further parameter estimation techniques in the science of system identification is in the range of the time constant of the system. For practical purposes a suitable estimate of the sampling frequency can be evaluated, when applying a step impulse (a constant injection with a steep front) to the system and then selecting the sampling interval so that it gives 4 to 6 samples during the rise time (Ljung, 1999). Unbehauen and Rao (1987) state similarly, that the number of sample to reach 63% of the steady state value of a step impulse is in the range of 6 to 10 data points.

However, it might be not possible to produce such a defined input due to practical reasons. Guymer (1999) argues, that in many cases Gaussian distributions are being observed. He argues

from a statistical point of view that approximately forty data points are needed to describe a Gaussian distribution with an error in the estimated area of less than one percent. Considering the assessment of Ljung's (1999) or Unbehauen and Rao (1987) and taking into account that the sharp rising front of an constant injection will eventually become a Gaussian shape when the tracer spreads out, then this might lead to a multiple number of four or five times of the initial number of data points describing the leading part of the distribution. This then seems to be comparable to the number of twenty points from Guymer's statistical point of view.

Anyhow, both approaches will be considered in a study. The estimated parameters for the dispersion coefficient and the travel time of a real experiment on a straight pipe were taken and synthetic, noise free data was produced, as shown in Figure 3.14a. The ADE routing-procedure was used to estimate the parameters, involving down sampling of the original data set in steps of 5 samples in the range of 1 in 10 samples to 1 in 100 samples. The estimated parameters are plotted against the down-sampling factor in Figure 3.14c. It can be seen that the parameters are estimated correctly up to a down-sampling step of 1 in 55 samples, where the correct parameters are shown as the dotted line in those plots. With down-sampling ratios higher than 1 in 55 the estimated parameters are no longer estimated correctly and are tending to either side of the correct parameters.

To study this observation under noisy conditions, white noise with a standard deviation of 0.03 was added to the synthetic signal, as it can be seen in Figure 3.14b. The parameters were again estimated with the ADE routing procedure. In one case the data were pre-filtered with a moving average filter, where the cut-off frequency was defined from the frequency obtained from each individual down-sampling frequency. The results of these computations are shown in Figure 3.14d. It can be seen that the parameter estimates are again constant up to a down-sampling factor in the range of 1 in 50 to 1 in 60 samples. After that the estimates deviate from the correct values. Further it has to be noted, that the residence time is biased away from the original value, even at down-sampling rates lower than 1 in 50. Obviously a filter can never totally restore the original signal. Thus this bias-effect is due to the effect of the squared errors in the objective function, as highlighted in Chapter 3.3.2.

The same procedure was repeated on the noisy data, but without using a filter on the data. The results of these computations are shown in Figure 3.14e. It can be seen, that the noise causes a great variance in the parameter estimates, independent of the chosen down-sampling factor. It further shows the importance of eliminating the noise. Where repeated tests are not suitable, high sampling frequencies and the application of an averaging filter can be utilised to achieve this effect (Söderström and Stoica, 1989).

The smallest best performing down-sampling rate found in this example was approximately the rate of 1 in 50 samples. The temporal spread of the original down-stream distribution in Figure 3.14a is roughly in the time range between 200 seconds and 1000 seconds. Hence the

total number of samples for the original distribution is 800, from which a minimum sample number of 800/50 = 16 samples can be calculated. Clearly, this number is much lower than the number of 40 samples proposed by Guymer (1999). Thus with the previous findings it can be assumed that the number of 40 samples should be in most times sufficient to describe a dispersed tracer cloud. Obviously this might not hold true for distributions with very long falling limbs. The total number of samples might than be chosen from the sampling rate obtained, where 40/2 = 20 samples describe the rising limb of the distribution.

To prove the suggestion of Ljung (1999) that approximately six samples are needed to describe the rise time of a response to a step impulse, a step impulse was applied to the ADE routing-equation using the parameters of dispersion coefficient and travel time of the example of Figure 3.14. The equation was evaluated for sampling rates of 1 in 1 sample and 1 in 50 samples. The obtained response to this step impulse is shown in Figure 3.15. The numbers of samples for the evaluation of the sampling rate of 1 in 50 samples show, that six to seven samples describe the rising limb of the step impulse response. Taking the previous findings into account, this result shows clearly the applicability of the suggestion of Ljung (1999) that a sample rate is sufficient to reproduce a distribution, where six samples describe the rising limb of a step impulse response.

Although several approaches have been investigated for the evaluation of a suitable sampling interval, for practical considerations and where computing time is a limiting factor, it might be useful to do a repeated evaluation of sampling rates to find a proper sampling rate in an approach similar to the one shown before. If computing time is no limiting factor than the approach of Guymer (1999) may be chosen, where the sampling interval is chosen such that twenty samples describe the rising limb of a distribution. However, the effect of noise to parameter estimates was also shown, hence it is recommend to sample a signal at a high frequency and then applying a low-pass filter with a cut-off frequency chosen according to the down-sampling ratio.

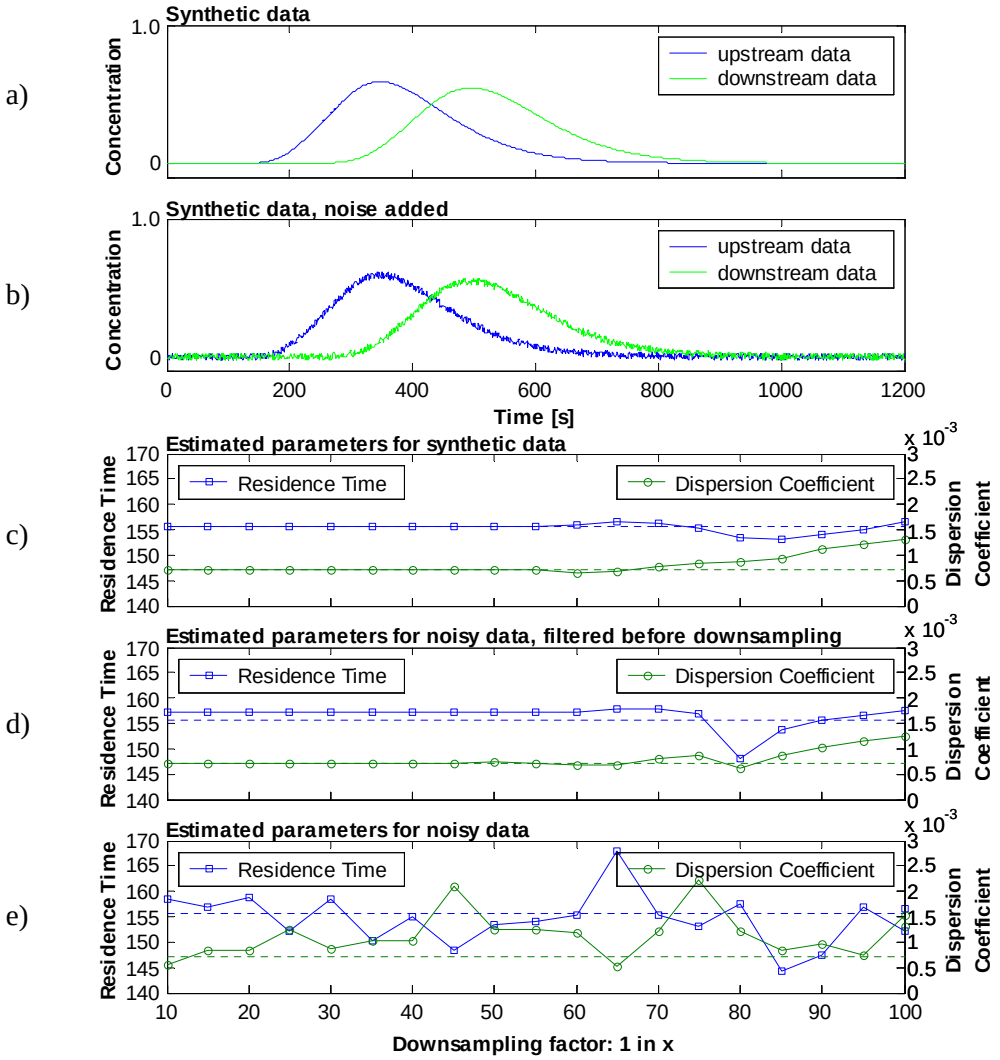

Figure 3.14. Effect of down-sampling factor and data filtering on parameter estimates of pipe experiment

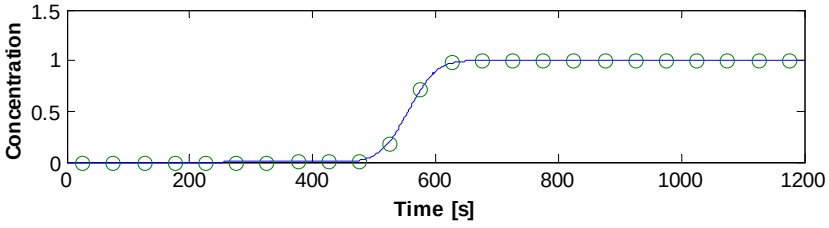

Figure 3.15. Output to a step impulse input on system with parameters of pipe experiment

Chapter 4

THE HEATHROW CONSTRUCTED WETLANDS

4.1 RUNOFF TREATMENT DESIGN CONCEPT

The design of the Heathrow Constructed Wetlands is based on the management of two of the largest catchments of the airport (Figure 4.1). The Southern Catchment has an area of 290 ha of which 78% is impermeable and includes terminals, runway areas and cargo areas. The Eastern Catchment has a size of 309 ha of which 80% is impermeable has supports terminals, runways and maintenance areas build on it.

The most contaminated runoff derives from the Eastern Catchment (Worrall *et al.*, 2001). The catchment discharges into the Eastern Reservoir. Here the runoff will be diverted to either the "dirty" side or to the "clean" side of a floating and flexible butyl curtain, depending on the BOD_5 concentration of the runoff. The threshold for runoff to be diverted to the "dirty" side is 100 mg BOD_5/L in winter and 50 mg BOD_5/L in summer. The BOD_5 measurement points are equipped with continuously operating instruments that are deriving the BOD-level from oxygen depletion within a conditioned microbial culture within 15-minutes (BiOX meter, manufactured by ISCO-STIP). The installation of a flexible and floating butyl curtain provides storage capacity for runoff that has to be treated. The curtain is fixed to the bottom of the pond and increases or reduces the volume for dirty water storage by its movement in response to differential water heads between both sides. The runoff on the "clean side will be aerated while it passes through the reservoir before being discharged into the River Crane. Within the "dirty" side of the curtain up to 43,000 m^3 of runoff is retained and aerated until its BOD_5 level is below 170 mg/L. It is then transferred to the Mayfield Farm Constructed Wetlands for treatment. The water from the Eastern Reservoir is pumped into Rafted Reedbeds on the Heathrow Constructed Wetlands (HCW) site, where biodegradation and filtration occurs over a 28-hour retention period before being discharged into an aerated Balancing Pond.

The water from the Southern Catchment enters a diversion chamber on HCW where its BOD_5 level is monitored. Water with a BOD_5 level of more than 40 mg/L is diverted into the Main Reservoir, which has a capacity of 45,000 m^3. Water below that threshold is transferred into the Southern Reservoir at Clockhouse Lane Pit, from where it is discharged into the River Thames. The runoff in the Main Reservoir is aerated to reduce its BOD_5 level from an estimated level of 128 mg/L to a threshold below 115 mg/L before being pumped into the Balancing Pond (Worrall *et al.*, 2001).

In the Balancing Pond the water from the Eastern and Southern Catchments will be aerated, and thus mixed, and pumped into a gravel-filled subsurface flow wetland for treatment. The size of the subsurface flow reedbed of 2.08 ha was designed to treat water with an estimated removal efficiency of 63%, based on an estimated inflow concentration of 108.1 mg BOD_5/L and a target level of 40 mg BOD_5/L, a estimated retention time of 25 hours and a flow rate of 40 L/s (Worrall *et al.*, 2001).

The water leaving the reedbeds is discharged through into a series of small ponds, where public access is possible through a public footpath, a cycle way and a boarded platform. The BOD_5 level of the water is measured again at the outlet of the ponds. Water with a BOD_5 level below 40 mg/L is discharged to the diversion chamber from where it is transferred to the Southern Reservoir a Clockhouse Lane Pit and finally the River Thames. Water with a level above the threshold is diverted back into the system for further treatment.

4.2 THE SUBSURFACE FLOW REED BED SYSTEM

The 2.08 ha subsurface flow reedbed consist of three distinct areas or terraces that have differing sizes, aspects, and input flow rates. Each bed comprises of a number of individual cells that have the dimensions of approximately 20 m x 20 m. As can be seen in Figure 4.2 the system consists of two discrete beds of six cells in series (Bed 1 and 2), further of seven discrete sets of four cells in series (Bed 3 to 9) and three discrete sets of two cells in series (Bed 10 to 12). The configuration of the surface flow beds can be seen in Figure 4.2, the dimensions can be obtained from Table 4.1.

Each bed is hydraulically isolated from the adjacent bed in the terrace by concrete dividing walls. An open water channel of the dimensions 20 m x 2 m is situated at the front and at the end of the beds and between the cells of a bed. While the front and end channels distribute and collect the water flowing through the beds, the intermediate channels reduce the incidence of channelisation and short-circuiting along the whole length of the bed. Each cell consists of gravel of 10 mm sub-angular flint/chert with a varying degree of limestone and have the dimensions of 20 m x 20 m x 0.6 m. The upstream and downstream front of each cell is made from a gabion, filled with reject brick and has the dimensions of 20 m x 0.6 m x 0.6 m. An

impermeable bentonite liner underlies each bed to prevent loss from or ingress to the system. In cell 2, 3 and 4 of Bed 2 pipes are fitted just below the gravel surface to allow a short circuit of each these cells. Butterfly valves are fitted at each end of the pipes to control the flow. The valves had been fully opened during all tests.

The beds were planted with *Phragmites* reeds in summer 2001. Figure 4.3 shows a gravel bed before the planting of the reeds took place. Figure 4.4 shows the reedbeds in autumn 2001 after planting of the reeds took place. Figure 4.5 shows the reedbeds in autumn 2002.

The design hydraulic loading rates for the whole system is 20 L s^{-1} ha^{-1}, based on a design flow rate of 40 L/s. Due to the different surface areas of each bed, the design inflow rates for each bed vary to maintain a constant hydraulic loading rate across the system.

Construction of the subsurface reed beds was completed in autumn 2001, the commissioning of the system ended in the winter period 2002/2003.

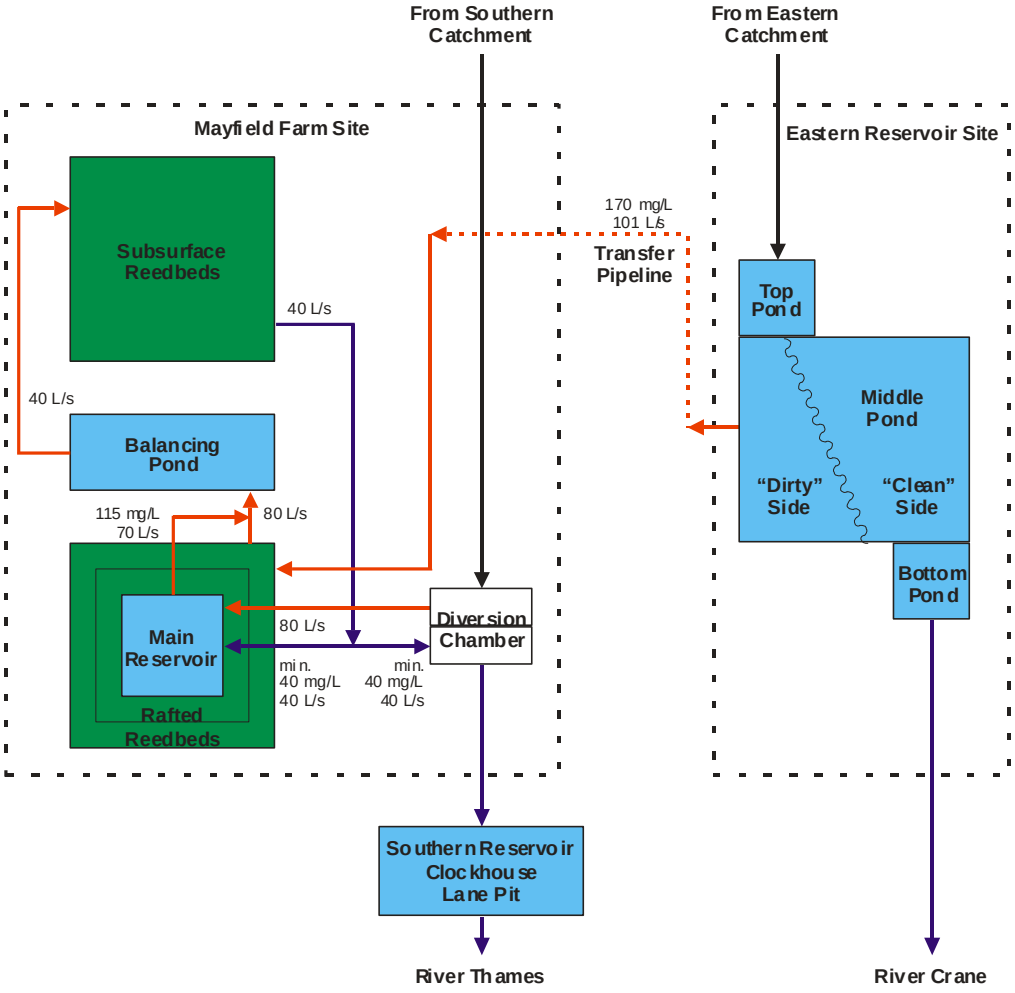

Figure 4.1. General plan of complete integrated system at Heathrow Airport

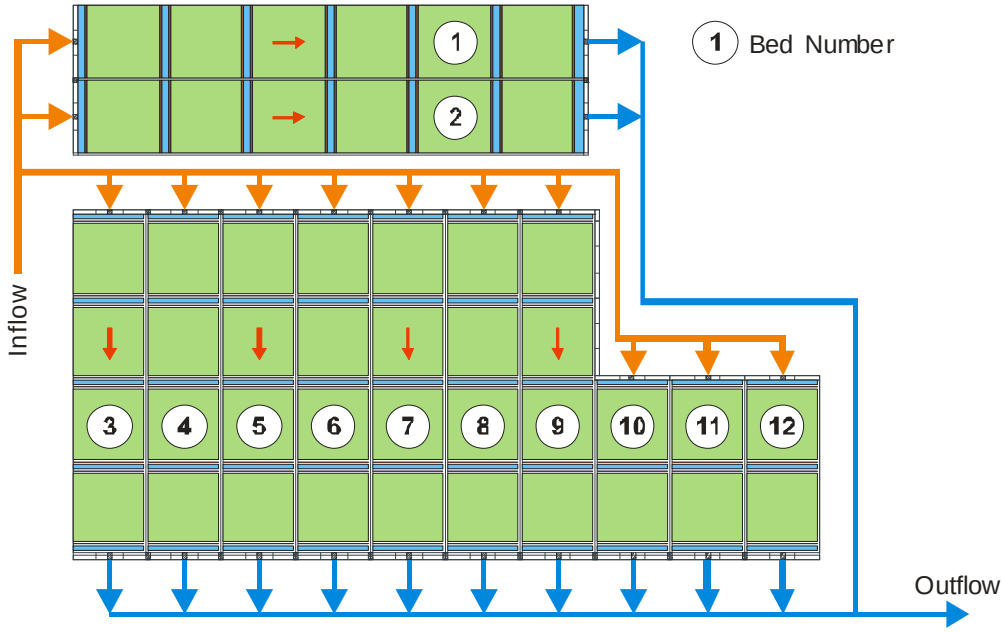

Figure 4.2. Subsurface bed configuration

Figure 4.3. Unplanted subsurface gravel bed

Figure 4.4. View over the planted subsurface reed beds, Autumn 2001

Figure 4.5. View over the planted subsurface reed beds, Autumn 2002

Table 4.1. Design dimensions

Bed no	Units	Bed 1, 2	Bed 3	Bed 4 - 9	Bed 10, 11	Bed 12	Total
No of cells		6	4	4	2	2	
Dimensions							
Bed width	m	19.75	19.75	19.70	19.70	19.75	
Cell length	m	19.333	19.363	19.363	19.425	19.425	
Gabion length	m	0.60	0.60	0.60	0.60	0.60	
Open water section length	m	2.00	2.00	2.00	2.00	2.00	
Total bed length	m	137.20	92.25	92.25	47.25	47.25	
Areas							
Single cell area	m^2	381.83	382.42	381.45	382.67	383.64	
Gravel cells, total	m^2	2,290.96	1,529.68	1,525.80	765.35	767.29	17,564.40
Gabions, total	m^2	142.20	94.80	94.56	47.28	47.40	1,088.52
Open water sections, total	m^2	276.50	197.50	197.00	118.20	118.50	2,287.40
Total area	m^2	2,709.66	1,821.98	1,817.36	930.83	933.19	20,940.32
Volume of Water storage (assuming non flow, water depth z = 600 mm)							
Porosity of gravel	-	0.45	0.45	0.45	0.45	0.45	
Porosity of gabion	-	0.45	0.45	0.45	0.45	0.45	
Gravel cells	m^3	618.559	413.013	411.967	206.643	207.168	4,742.39
	Vol-%	75.2%	74.1%	74.1%	71.2%	71.2%	
Gabions	m^3	38.394	25.596	25.531	12.766	12.798	293.90
	Vol-%	4.7%	4.6%	4.6%	4.4%	4.4%	
Open water sections	m^3	165.900	118.500	118.200	70.920	71.100	1,372.44
	Vol-%	20.2%	21.3%	21.3%	24.4%	24.4%	
Total water volume	m^3	822.85	557.11	555.70	290.33	291.07	6,408.73
Theoretical detention times							
Design discharge	l/s	5.26	3.61	3.61	1.39	1.39	
Detention time	h	43.5	42.9	42.8	58.0	58.2	

Chapter 5

EXPERIMENTAL RESULTS

This chapter shows the results of the field tests undertaken in the period between April 2001 and November 2002 on the subsurface reed beds of the Heathrow Constructed Wetlands. The tests include general investigations for the determination of some material properties, retention time studies for the assessment of the wetlands hydraulic properties and treatment efficiency tests.

The naming of the tests follows the general development of the subsurface reed bed, in terms of advance in time and in terms of advances in the development of this bio-system. The first set of tests was conducted on the unplanted gravel beds during the hydraulic commissioning of the system. Therefore tests performed in this time are named as "Series 0". The second set of tests was performed within the first de-icing season on the planted gravel beds in February 2002 and is called "Series 1". The third set of tests took place in November 2002 as part of wetland conditioning before the de-icing season. This series is termed "Series 2".

5.1 GENERAL TESTS

5.1.1 Discharge tests

Floating arm inlet structures regulate the inflow of water into each bed of the subsurface reed bed system according to a design value of hydraulic load. The actual discharge rates were measured volumetrically and are shown in Table 5.1. Each given single value of the discharge rate is an average of at least three measurements. A total theoretical error for the measurements can be calculated. The errors for the calibration of the volumetric containers used for the measurements are around 2 % for the tests in 2001 and less than 1% for the test in 2002. The absolute error for taking the reading on site is approximately 0.5 cm, which correspondents to an error of around 1.5%. The error in timing the actual discharge measurement is around 1 second. The total errors for the measured discharge rates for the tests in 2001 can then be

calculated with approximately 7 % for the measurements on Beds 1 to 2, approximately 5% for the measurements on Beds 3 to 9 and approximately 3% for the measurements on Beds 10 to 12. The errors calculated for the test in 2002 are 5.5 %, 3.5% and 2%, respectively. All these theoretical errors are larger than the actual observed standard deviations of the measurements around each average value.

It should be noted that the orifices of the floating arm structures of Beds 5 and 11 were swapped during the tests in 2002 to investigate into the effect of different hydraulic loading rates.

Table 5.1. Discharge of wastewater into subsurface reed beds

(* Orifices swapped between Bed 5 and Bed 11 in 2002 test)

Bed No.	Discharge Rate [L/s]			
	Design Rate	Series 0, March 2001	Series 0, April 2001	Series 2, November 2002
1	5.26	5.47 ±7%		
2	5.26	5.32 ±7%	5.55 ±7%	5.16 ±5.5%
4	3.61		4.23 ±5%	3.87 ±3.5%
8	3.61	3.82 ±5%		
9	3.61	3.96 ±5%	4.24 ±5%	
11*	3.61			4.21 ±3.5%
5*	1.39			1.99 ±3.5%
10	1.39			0.98 ±2%
11	1.39			
12	1.39	2.05 ±3%	2.10 ±3%	2.33 ±2%

The measured discharges have clearly a wide spread around their design value. The measurement of discharges in 2001 for the Beds1 and 2 are, with values between 5.32 L/s and 5.55L/s, above the design value of 5.26 L/s, while the measured discharge rate for the test in 2002 is below it. The discharges of Beds 3 to 9 are in the range between 3.82 L/s and 4.24 L/s and thus are above the design value of 3.61 L/s. There is no significant difference in the measured values between the tests in 2001 and 2002. The measured discharge rates for Bed 10 to 12 are with values around 2 L/s again clearly larger than the design value of 1.30 L/s. The restricted movement of the floating arm caused the extremely low value observed during the tests in 2002 on Bed 10. The floating arm was not in its normal position relative to the water

surface. This was caused by a high stiffness in the joint of the arm. The observed discharges of the floating arm structures tend in general to be higher than their design value.

5.1.2 Test for determination of the porosity

The volume of water filling the pore space of the gravel measures the porosity *n.* The porosity was determined for the fresh gravel in a laboratory test and was measured at 0.45.

5.1.3 Test for determination of the hydraulic conductivity

The hydraulic conductivity of the fresh gravel was estimated in a laboratory experiment. The gravel was placed in a laboratory rig to form a gravel bed of the dimensions L x W x H 1.20m x 1.10m x 0.60m. A horizontal flow was set up and the difference in hydraulic head was measured at different flow rates. Using Darcy's equation the hydraulic conductivity was computed from tests at 10 different flow rates with 2.4×10^{-1} m/s.

Similar measurements were undertaken at the Heathrow Constructed Wetlands. Hydraulic conductivities were computed from observations of water levels of the open channel sections and are shown in Table 5.2.

The results from the laboratory experiment match with the results from the field test undertaken in May 2001 on the new and unplanted gravel beds. The results from the tests in November 2002 show a decrease in conductivity of around half an order of magnitude.

Table 5.2. Hydraulic conductivities obtained from field measurements

Bed No.	Hydraulic Conductivities [m/s]	
	Series 0	Series 2
1	$1.0 – 2.1 \times 10^{-1}$	
2	$1.0 – 1.6 \times 10^{-1}$	$0.9 - 1.1 \times 10^{-1}$
4	$1.4 – 2.8 \times 10^{-1}$	$0.9 - 1.0 \times 10^{-1}$
6	$1.0 – 2.1 \times 10^{-1}$	
7	$1.1 – 2.3 \times 10^{-1}$	
10	$1.6 – 2.4 \times 10^{-1}$	$0.4 – 1.0 \times 10^{-1}$
11	$1.6 – 2.4 \times 10^{-1}$	$0.9 – 1.0 \times 10^{-1}$
12	$1.5 – 2.4 \times 10^{-1}$	$0.7 – 0.8 \times 10^{-1}$

5.1.4 Determination of organic matter

Organic matter content was determined throughout the beds in May 2001 and November 2002. Visual observations in May 2001 could not detect significant and observable organic matter accumulation, confirming that little organic matter was expected in this early stage prior to the

planting of the reeds and development of a bio-film. Gravel samples were collected for testing from unused gravel, bagged at the time of construction, and from a number of locations throughout Bed 2, Bed 4 and Bed 11 of the subsurface reed bed system at different depth. These samples were analysed according to the method of "determination of mass loss on ignition" (BS1377). The observed values of organic matter were in the range of 0.18 to 1.33 g/L. A variation of organic matter was observed over the depth of the beds, were the highest value were measured at the surface, a smaller value at the depth of 100 mm and then a slightly higher value at the base of the bed. In comparison, a control sample from a matured 5-year-old experimental bed gave an organic matter content of 19.26 g/L (Richter *et al*., 2002).

Organic matter was also visually inspected during the test in November 2002. High concentrations of organic matter were found in front of each first cell of the beds up to a distance of approximately 10 to 20 cm downstream throughout the cross-section. It can be assumed that this accumulation of organic matter in the front is mainly due to the effect of filtering of particulate organics and suspended solids being transferred with the water from the Balancing Pond. Further on, organic matter was found in the form of plant litter on top of the gravel beds. This plant litter, originated from the dead leaves, started to decompose. Small particles with a size up to 3 to 4 mm were found up to depth of 3 to 4 cm, probably transferred there by precipitation. At greater depths no visual increase in organic matter was observed.

Samples were collected within the gravel matrix throughout Bed 2 and Bed 11 to assess a change in organic matter that is not caused by the accumulation of particulate organics and suspended solids. The obtained organic matter content of those samples is in the range of approximately 1g/L and did not show a significant increase in organic matter within the gravel matrix compared to the results of the test in May 2001.

5.2 FIELD TEST FOR HYDRAULIC PERFORMANCE

Tracer studies were performed for the assessment of the hydraulic performances of the different subsurface reed beds of the Heathrow Constructed Wetlands.

The tracer dye used in all tests was "Rhodamine WT" in liquid form. The instruments used for the observation of the dye leaving the subsurface reed beds were "SCUFA" fluorometers. These submersible fluorometers are manufactured by "TURNER DESIGNS", Sunnyvale California. The fluorometers are equipped with probes for fluorescence and turbidity, temperature correction and an internal data logger.

5.2.1 Dye adsorption

A lab study was performed to assess the adsorption of dye on the gravel matrix of the subsurface reed beds. The test set-up consisted of a column with a length of ca. 500 mm and a diameter of 200 mm. A dye solution of known concentration of the tracer dye Rhodamine WT was circulated over a period of 40 hours through this column using a peristaltic pump. During this time the dye concentration and the turbidity was measured in a reservoir tank. Within this time the measured concentration of dye decreased by an amount of approximately 5 percent of the starting value (see Figure 5.1). It can further be seen, that the readings of fluorescent concentration and turbidity first drop, then rise and then finally drops again. Since the change in concentration reading and turbidity happens simultaneously, the detection and reading of concentration is obviously interfered by the change in turbidity of the fluid.

The influence of turbidity on the reading of concentration cannot be accurately quantified. Nevertheless it can be assumed, that the influence of the turbidity on the reading of fluorescence is mainly due to two reasons. First, different types of particles causing the turbidity will have different impacts, e.g. a milky fluid filtering the light compared to small solid particles that might reflect the light. Second, the quality of the fluorescent probe will have an impact to it, e.g. the bandwidth of the filters and of the detector should be designed to filter out all light not caused and emitted by excited dye.

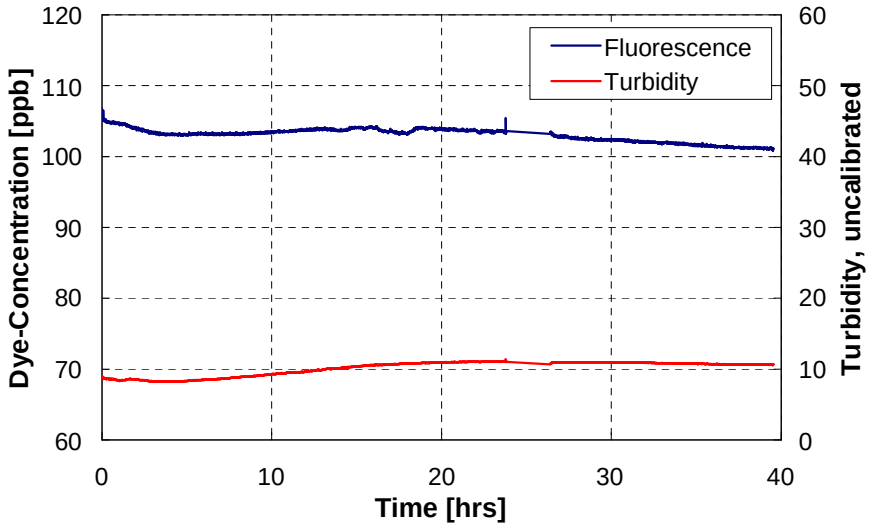

Figure 5.1. Dye adsorption test

In general a small increase in turbidity will result in an increase in fluorescent reading, mainly due to additional light reaching the optics due to scattering effects (Turner-Designs, 2003). A further increase in turbidity will then have the opposite effect. The turbidity will result in less light exiting the dye, causing less emitting light, which will be further decreased before reaching the optics of the instrument.

After a time period of 20 hours the turbidity remains approximately constant, while the fluorescence reading start to drop again. Therefore it can be assumed, that the observed decrease in fluorescent reading coincides with a loss of dye due to an adsorption process. The loss of dye can be estimated as approximately 3 % within 40 hours.

5.2.2 Determination of dispersivities

The spread of solutes in the gravel matrix in each cell of the subsurface reed beds can be observed with fluorescent dye studies. These observations allow the estimation of longitudinal and transverse dispersivity parameters. For this purpose laboratory test and field tests were conducted.

For the observations of the transverse spread of solutes, the tracer Rhodamine WT was injected as a constant point source in the centre of an upstream cross-section and was observed across a downstream cross-section by measuring the spatial variation of dye concentrations. The locations of injection and observations are shown in Figure 5.2. In Figure 5.3 the spatial locations of observation points in a cross-section are given. The observed spatial concentrations are shown in Figure 5.4 to Figure 5.7.

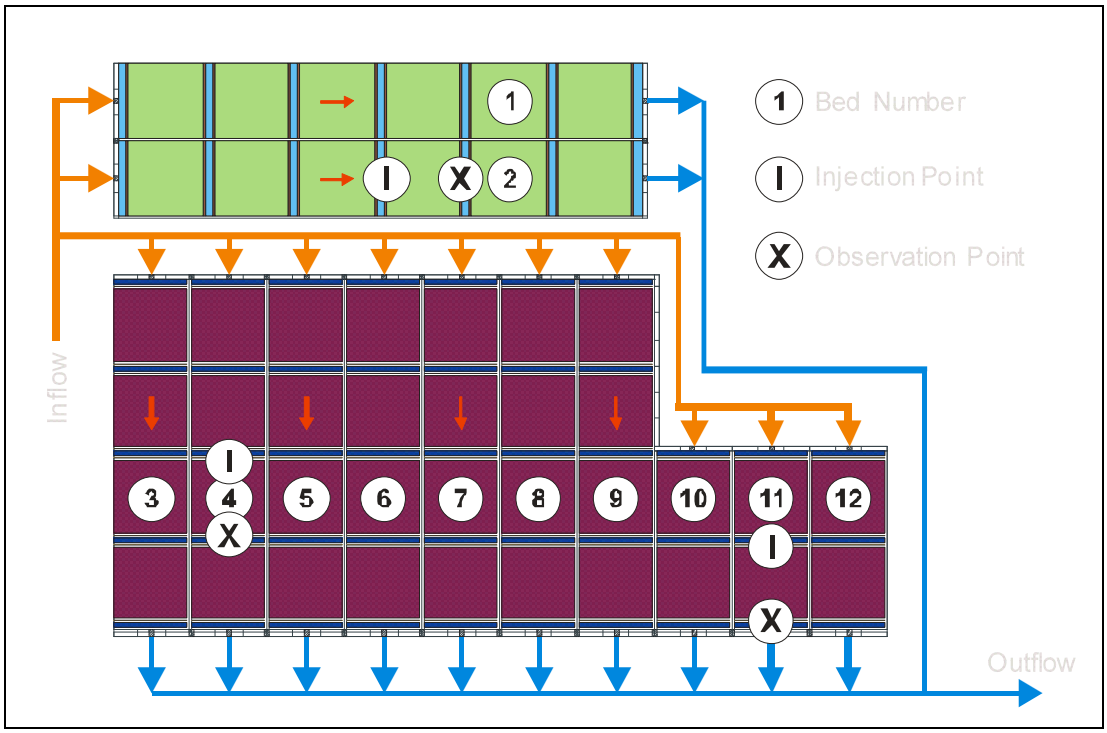

Figure 5.2. Locations of injection and observations for constant injection tests

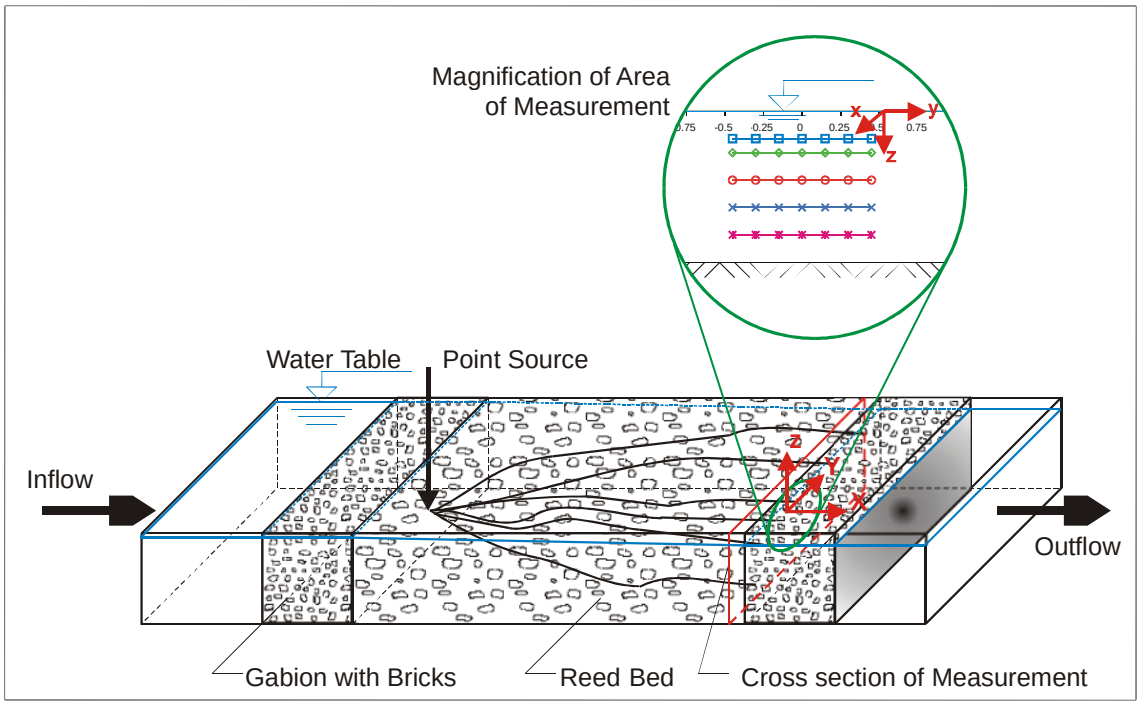

Figure 5.3. Locations of spatial observation for constant injection tests

The concentration distributions of Figure 5.4 and Figure 5.5 for the tests on Bed 2 and Bed 5 respectively show clearly higher concentrations of dye in the centre of the observed area in both horizontal or vertical direction. The observed concentration distribution of this single point constant injection at the downstream side of the gravel bed is quite confined, stretching just across an area of around 0.35 to 0.40 m radius, where the radius for Bed 5 seems to be smaller. The spread of dye for this flow pattern shows further a kind of Gaussian- or bell shaped concentration distribution over the cross-section. The peak of the bell shaped distribution is approximately at the same cross-sectional location as the point of injection, the centroid of the cross-section, just shifted down stream. Since the test had been performed on cell 4 on Bed 2 and cell 3 on Bed 5 respectively, it is unlikely that the flows through these cells are interfered by turbulent or directed flow conditions of the inlet- or outlet channel of the beds. Therefore a mainly horizontal and straight downstream flow pattern can be assumed for these tests.

The observed concentration distributions of Bed 11 in Figure 5.6 show a significant deviation of the higher concentrations towards the water surface. The test had been performed on the cell 2, placed directly upstream of the overflow weir outlet of Bed 11 in approximately 2.8 m distance. Due to the low hydraulic conductivity of the gravel it can be assumed that the flow pattern within the gravel is influenced by the flow condition caused by the overflow weir outlet and therefore it can be assumed that the stream path lines are deviated from the ideal path of a horizontal and down stream directed straight line. Without further investigations the influence affecting the flow field within the gravel bed is unknown and therefore the data from Bed 11 will be not taken into account for further analysis.

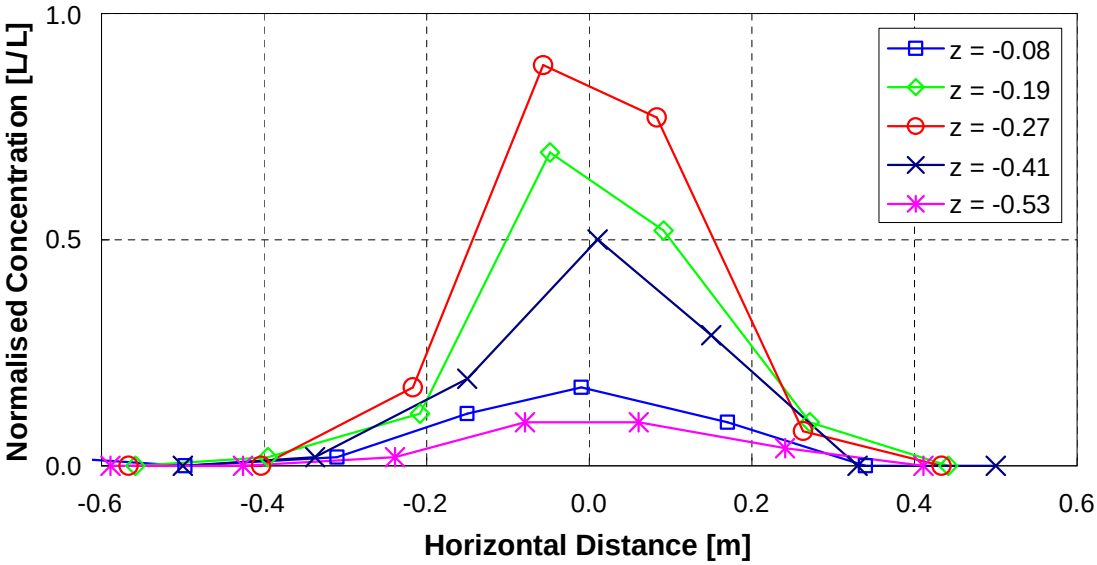

Figure 5.4. Constant injection test on Bed 2, Series 0

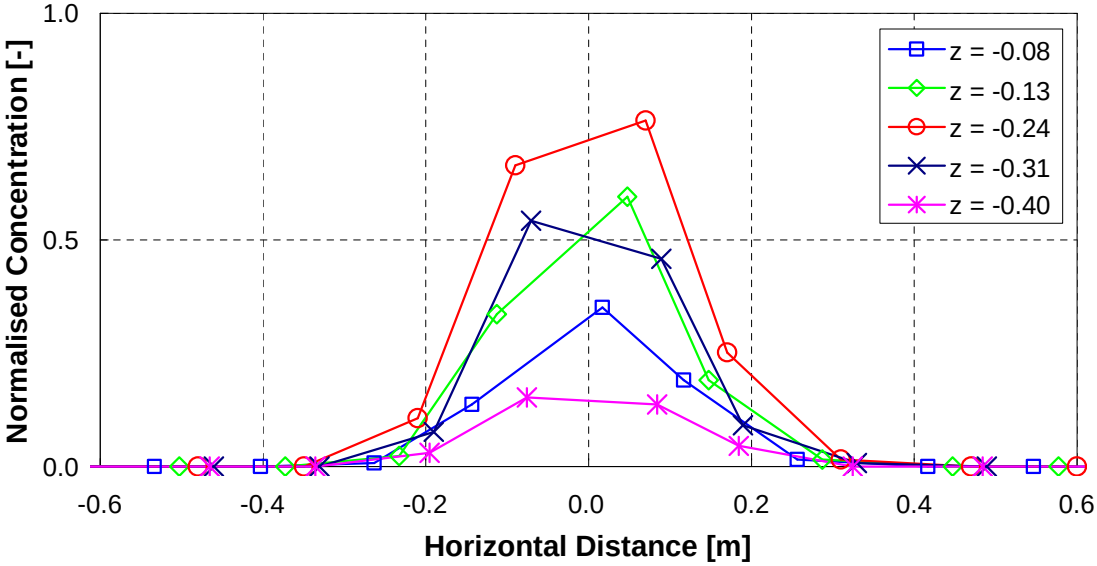

Figure 5.5. Constant injection test on Bed 5, Series 0

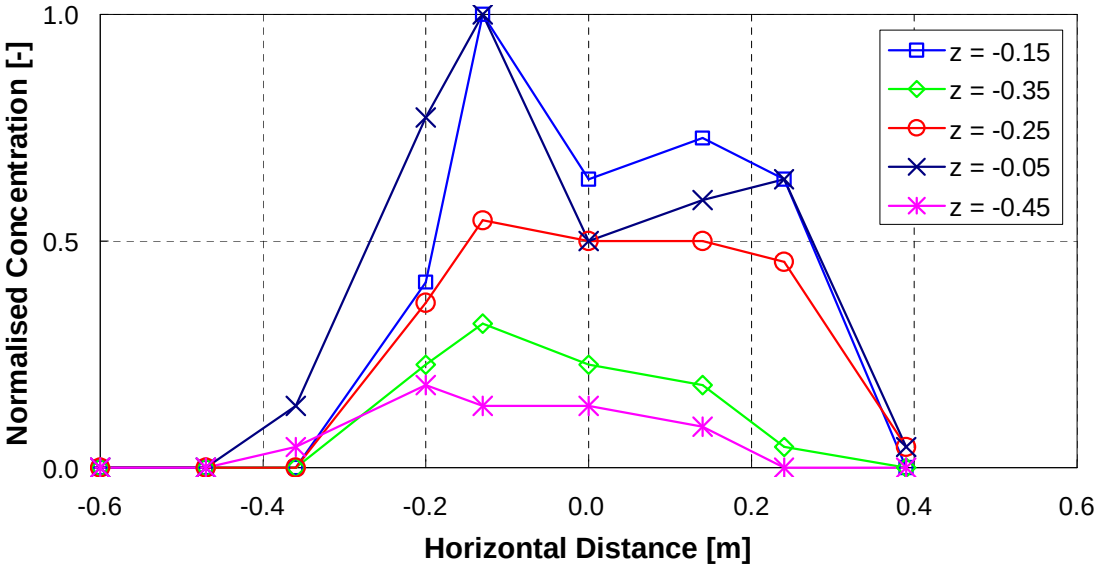

Figure 5.6. Constant injection test on Bed 11, Series 0

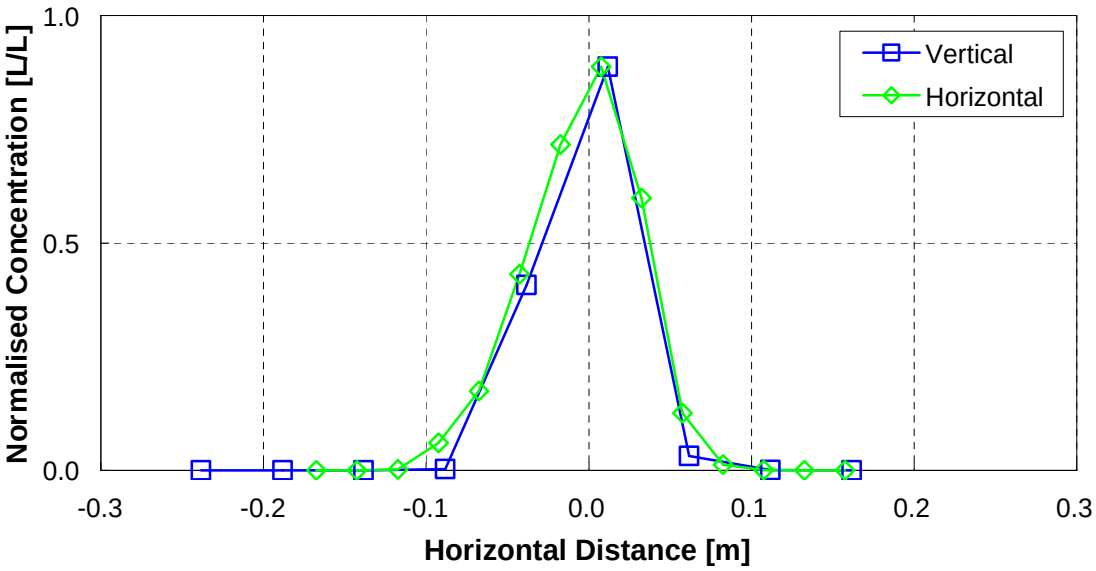

Figure 5.7. Constant injection test on laboratory rig

The observations on the laboratory rig shows a dye distribution similar to the observations made in the field tests.

The dispersivities or combined transverse mixing coefficients can be estimated from these observations by substituting the observed concentrations and parameters into the analytical solution of the Advection-Diffusion-Equation for a constant point source (Equation 2.44). The transverse mixing parameters were estimated by fitting observed concentrations to calculated values with a least square optimisation technique. The boundary condition of a unconfined vertical direction is not true for this case. The matrix is confined in vertical direction with the upper limit of the water table and the lower limit of the base of the bed. This was taken into account by application of the solution for bounded conditions (Figure 2.7).

The calculated transverse mixing coefficients are summarised in Table 5.1. The theoretical distributions of the dye concentrations calculated from the estimated dispersivities are shown in Figure 5.8, Figure 5.9 and Figure 5.10.

The longitudinal dispersion coefficient of the gravel was estimated from a tracer test within cell 4 of bed 2. The tracer was injected as an instantaneous injection at the vertical and horizontal centre at the start of the cell and was observed in the middle and at the end of the cell in downstream direction, also in the horizontal and vertical centre of the cell. Using an optimisation procedure based on the ADE-Routing Algorithm (Equation 2.53 and Chapter 3.2), the longitudinal mixing coefficient was estimated from the observed data. The results of the estimation are shown in Table 5.4. The observed concentration distributions and the theoretical distribution calculated from the estimated longitudinal dispersivity with the ADE-Routing algorithm are shown in Figure 5.11.

Table 5.3. Transverse dispersion coefficients, Series 0

	Bed 2	Bed 5	Lab Rig
Velocity u [m/s]	1.06×10^{-03}	8.04×10^{-04}	6.75×10^{-04}
Transverse Dispersion Coefficient D_T [m^2/s]	3.76×10^{-07}	2.57×10^{-07}	3.04×10^{-07}
Dispersivity ($A_T = D_T/u$) [m]	3.55×10^{-04}	3.20×10^{-04}	4.50×10^{-04}

Table 5.4. Longitudinal dispersion coefficient, Series 0

	Bed 2
Velocity u [m/s]	1.06×10^{-03}
Longitudinal Dispersion Coefficient D_L [m^2/s]	1.29×10^{-04}
Dispersivity ($A_L = D_L/u$) [m]	1.22×10^{-01}

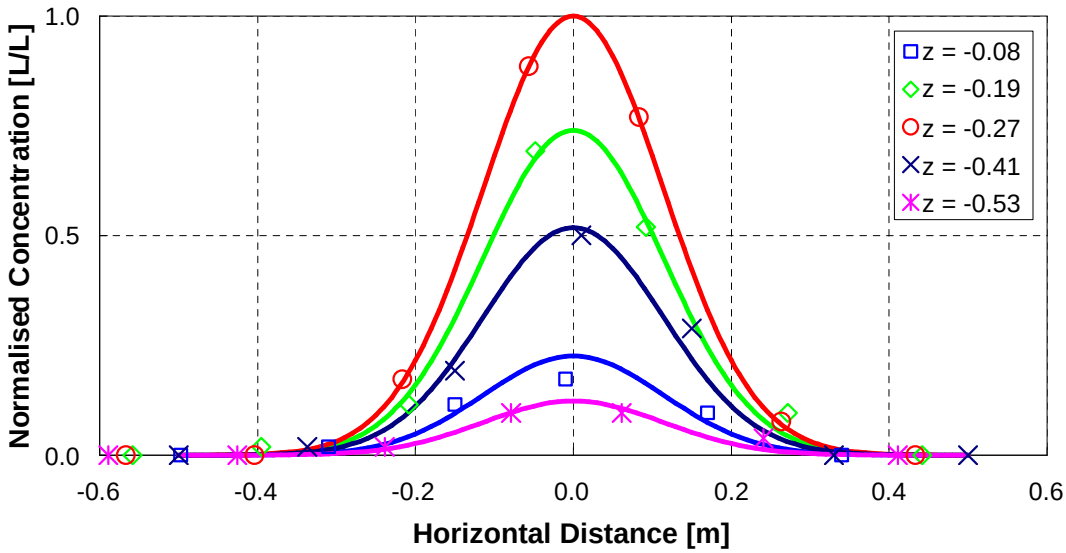

Figure 5.8. Theoretical against observed dye distribution, Bed 2, Series 0

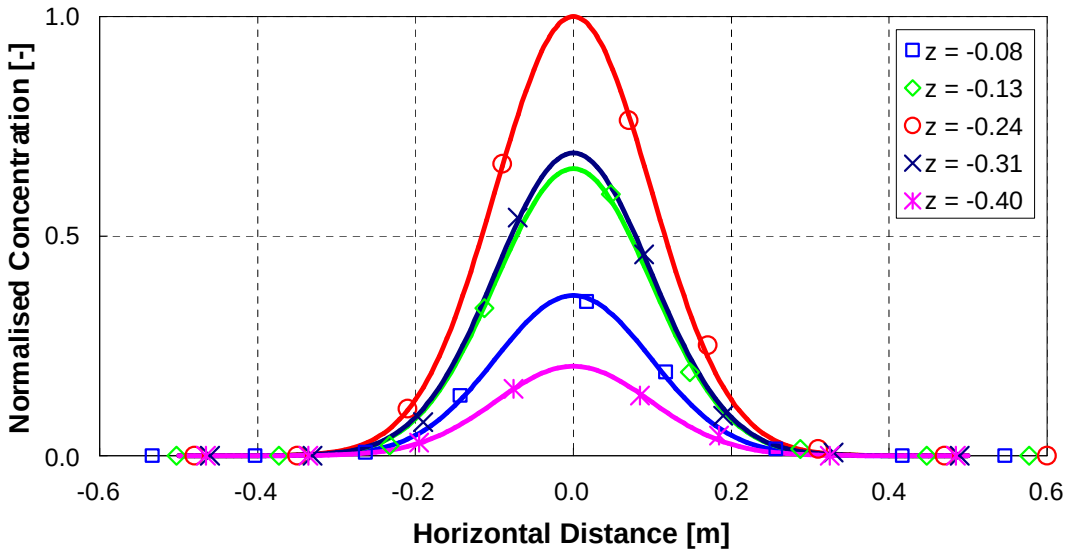

Figure 5.9. Theoretical against observed dye distribution, Bed 5, Series 0

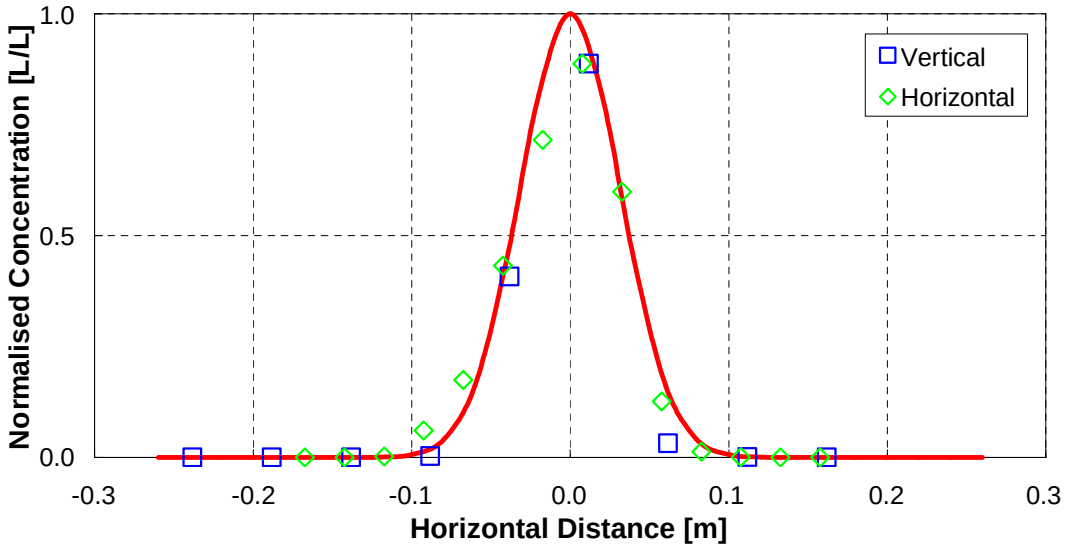

Figure 5.10. Theoretical against observed dye distribution of a horizontal and vertical cross section, Laboratory test, Series 0

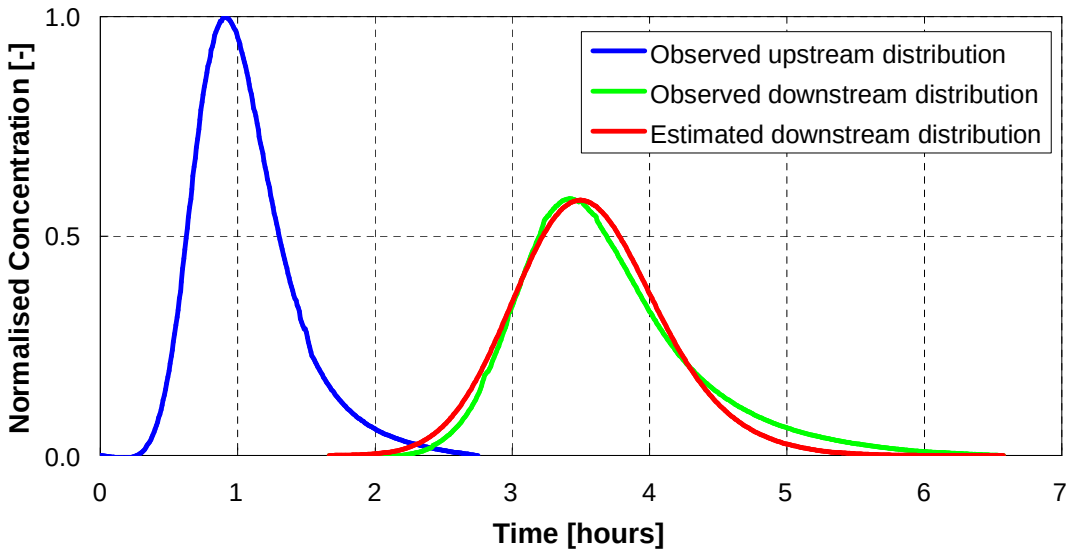

Figure 5.11. Slug injection test on Bed 2, Cell 4, Series 0

5.2.3 Temporal observations

Residence Time Distributions were measured using the fluorescence dye technique. The dye-tracer Rhodamine WT was injected with a constant rate over a period of 10 minutes into the floating arm inlet structures of each bed to allow for mixing (Figure 5.12). For each injection 10 ml of neat dye was mixed with 10 L of water. Temporal concentration distributions of the dye were observed at the outlet structures of the beds using submersible fluorometers with a temporal resolution of one sample per minute over time periods between 4 and 7 days. The fluorometers were installed in the pipes of the outlet structures of Bed 2 and 4. At the outlets of Bed 10 and 11 a wooden board with a pipe attached was fitted. The temporary fitted board blocked the direct flow over the weir of those beds and diverted the water into the pipe, allowing the fluorometer to observe the whole outflow of the bed (see Figure 5.13). The positions of dye injection and dye observation are shown in Figure 5.14.

The observed residence time distributions (RTD) and their cumulative plots are shown in Figure 5.15 to Figure 5.23. The distributions are in normalised form to allow easier comparison. Table 5.5 contains a summary of the calculated mean retention times, times of first and last observed concentrations and time of observed peak of the distributions. The times of first and last observed concentration were estimated at the time where the concentrations of each distribution are above and below respectively a value of 1% of the peak concentration.

Figure 5.12. Injection of dye for instantaneous injection tests

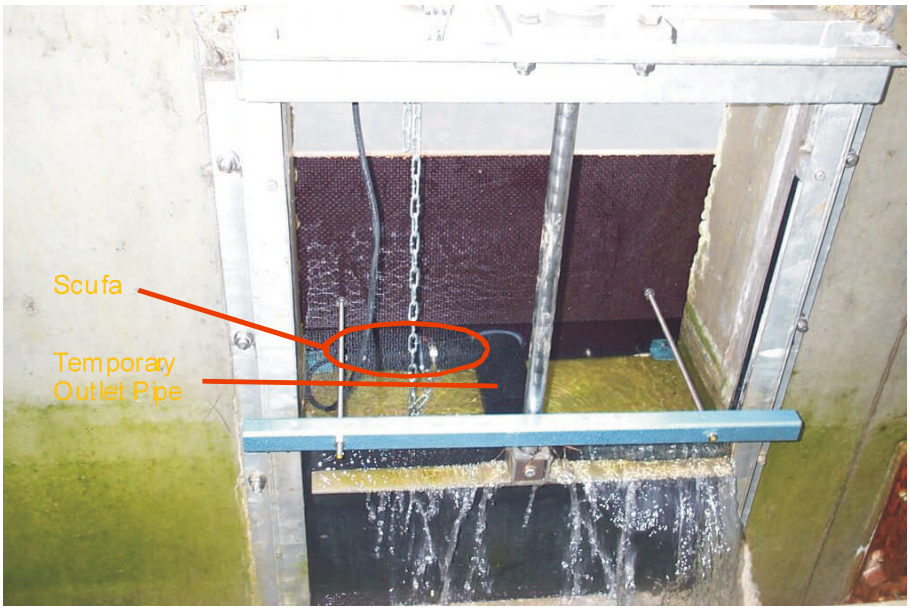

Figure 5.13. Scufa fluorometer installed at outlet of Bed 10

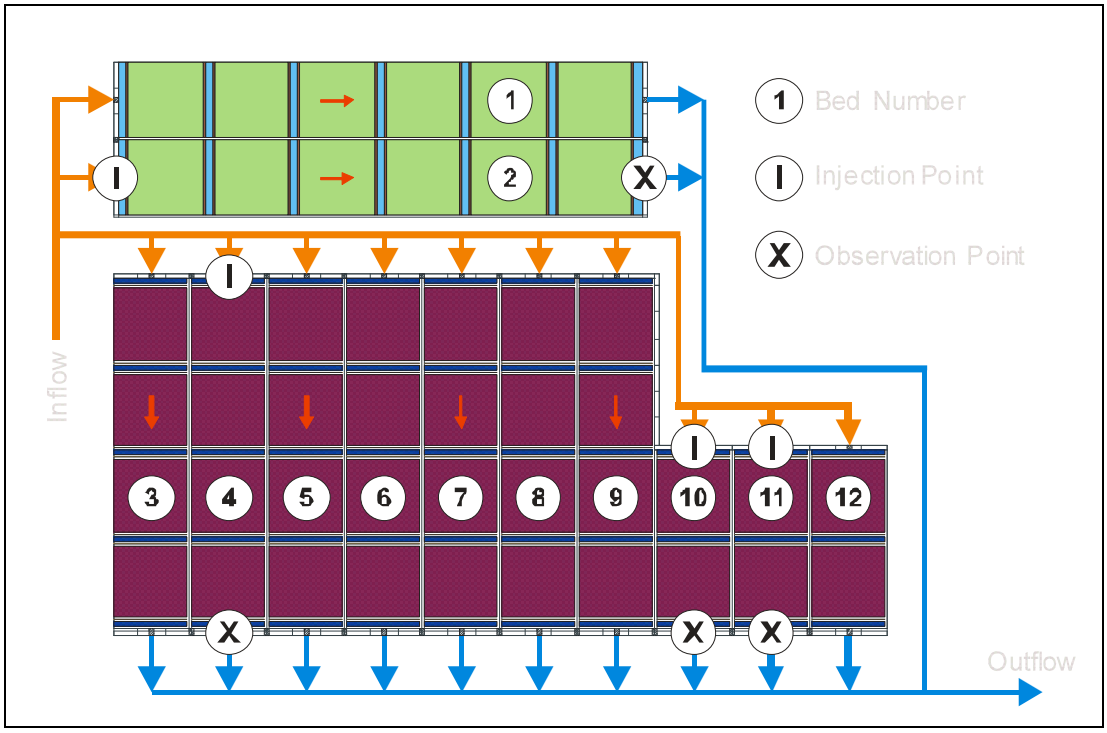

Figure 5.14. Locations of injection and observations for instantaneous injection tests

Table 5.5. Summary of residence time parameters of the observed residence time distributions

	Mean Retention Time [days]	First observed concentration [days]	Observed Peak arrival time [days]	Last observed concentration [days]
Series 0, Bed 2	-	0.69	1.53	-
Series 0, Bed 4	1.85	0.97	1.35	3.65
Series 0, Bed 11	2.07	0.97	1.49	4.41
Series 1, Bed 2	1.89	0.42	0.90	6.15
Series 1, Bed 4	1.91	0.35	1.08	6.22
Series 1, Bed 11	1.65	0.66	1.15	4.65
Series 2, Bed 2	2.09	0.21	0.90	6.28
Series 2, Bed 4	1.78	1.01	1.46	3.61
Series 2, Bed 10	2.19	0.87	1.46	5.73

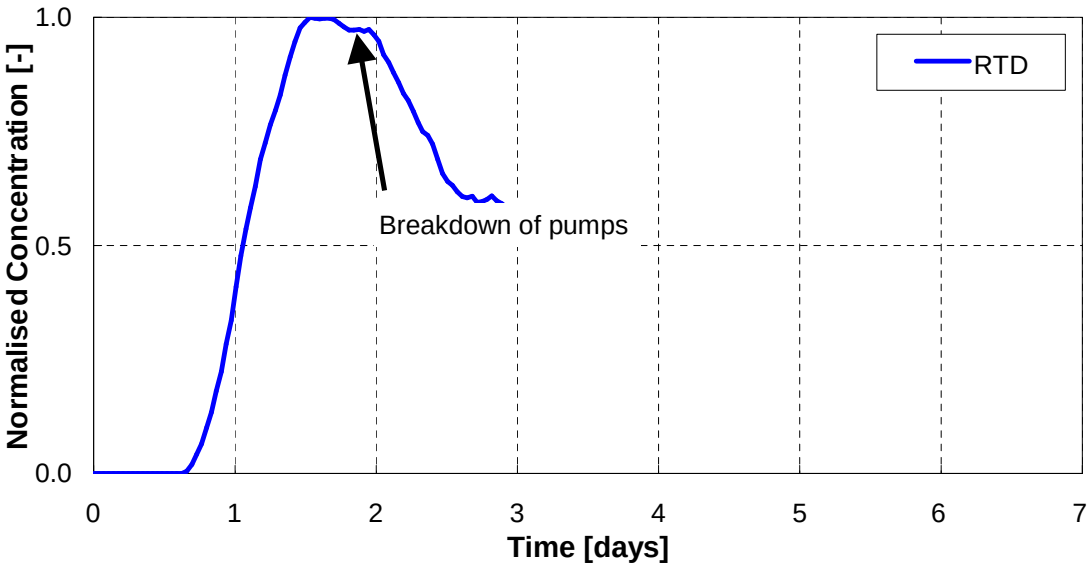

Figure 5.15. Residence Time Distribution (RTD), Series 0, Bed 2

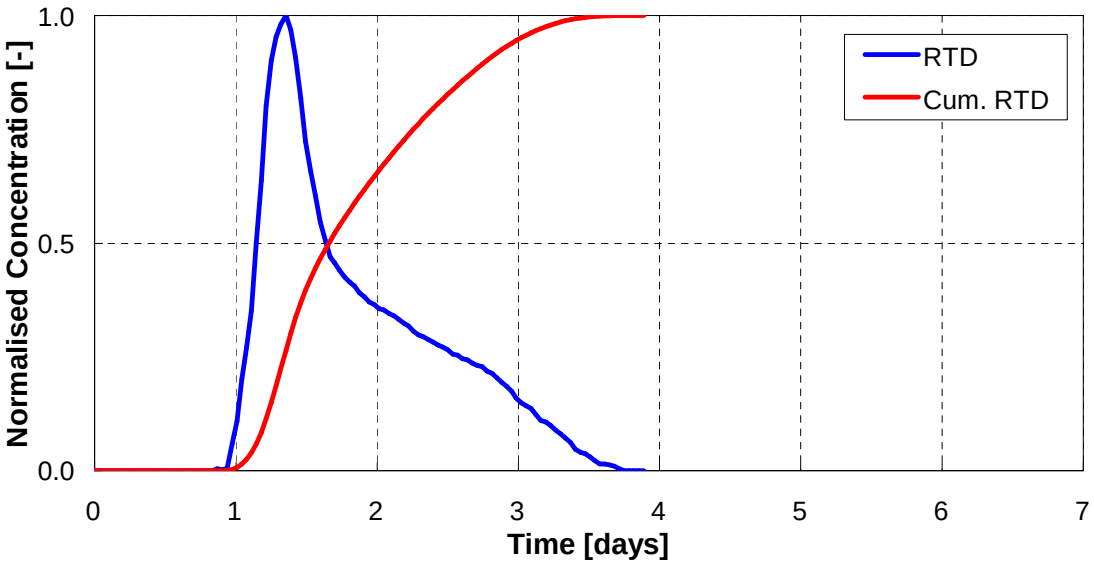

Figure 5.16. Residence Time Distribution (RTD), Series 0, Bed 4

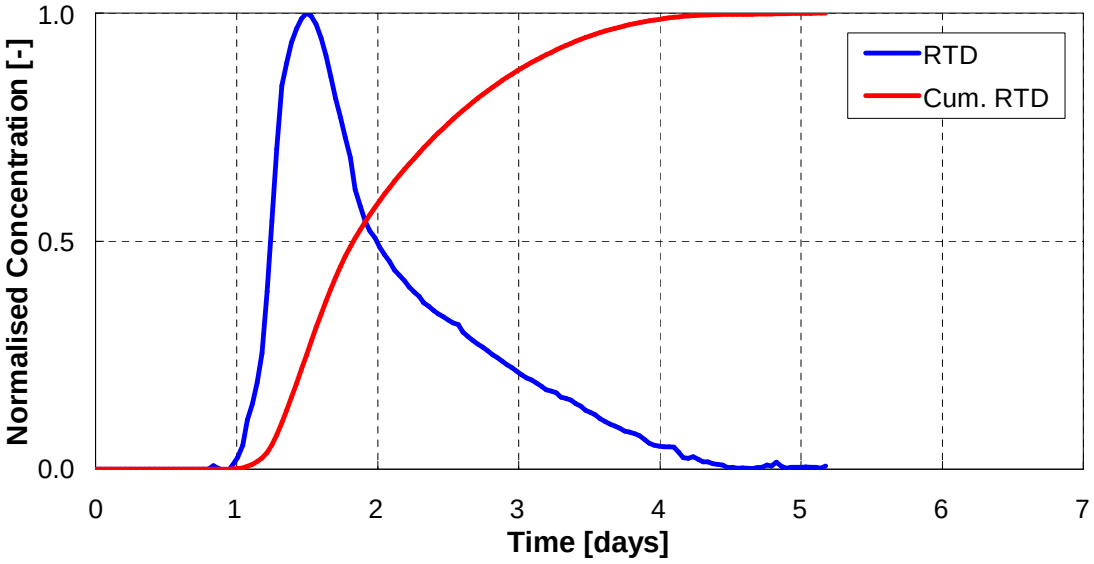

Figure 5.17. Residence Time Distribution (RTD), Series 0, Bed 11

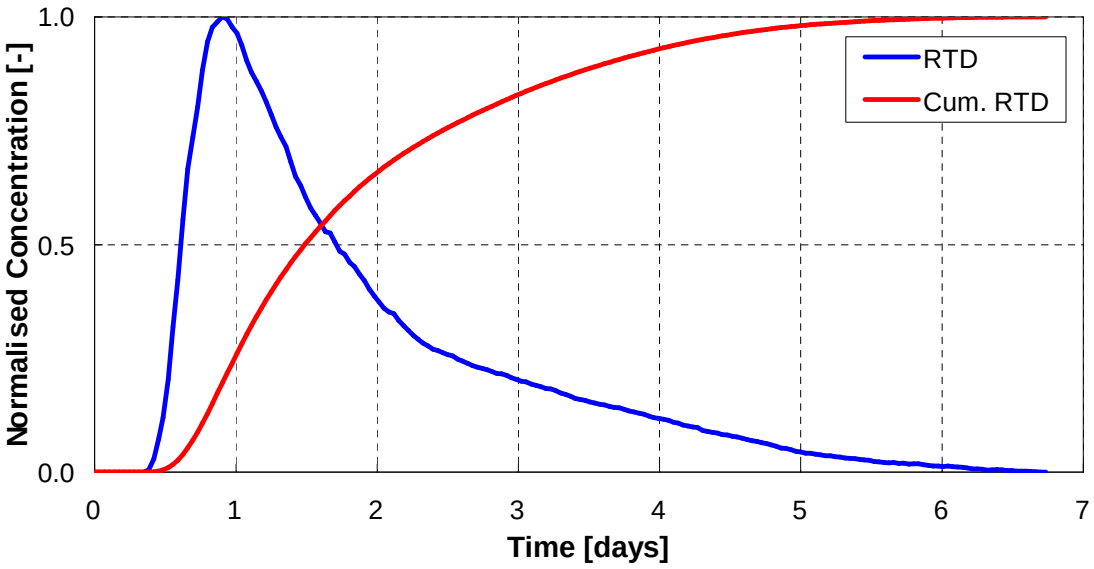

Figure 5.18. Residence Time Distribution (RTD), Series 1, Bed 2

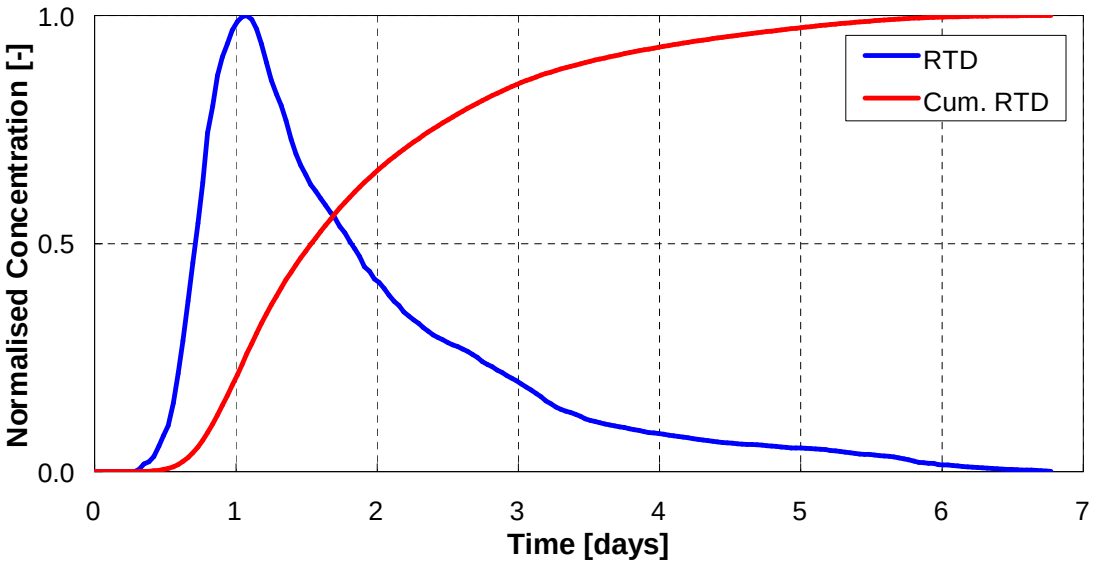

Figure 5.19. Residence Time Distribution (RTD), Series 1, Bed 4

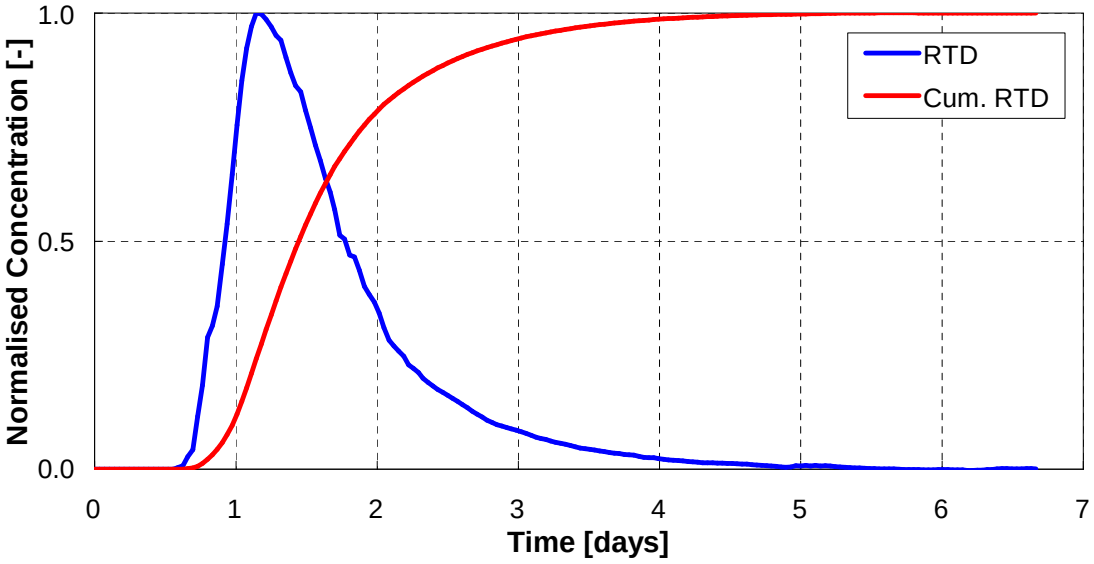

Figure 5.20. Residence Time Distribution (RTD), Series 1, Bed 11

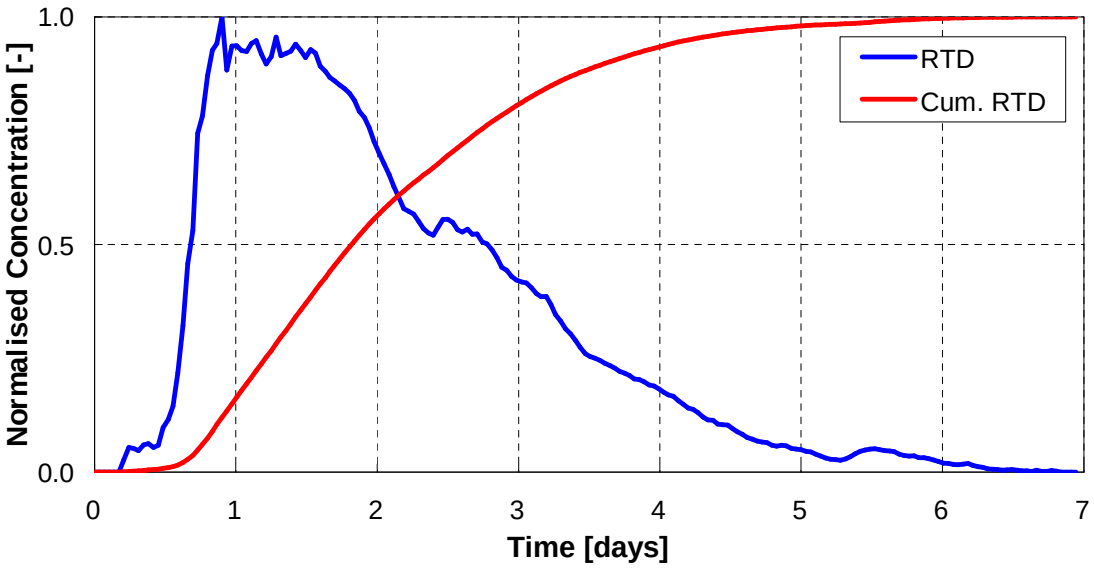

Figure 5.21. Residence Time Distribution (RTD), Series 2, Bed 2

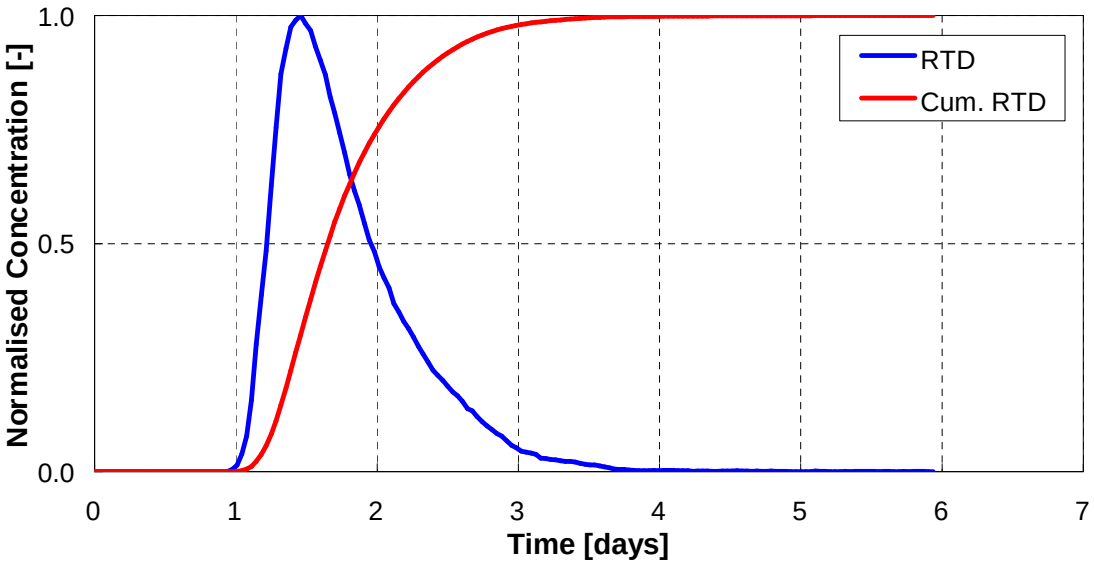

Figure 5.22. Residence Time Distribution (RTD), Series 2, Bed 4

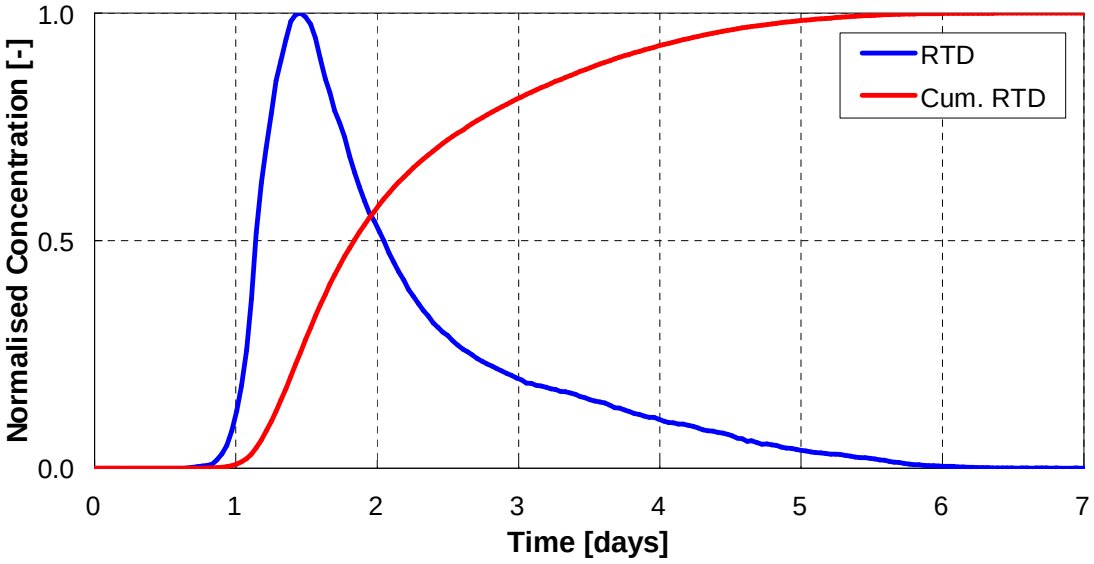

Figure 5.23. Residence Time Distribution (RTD), Series 2, Bed 10

While the dye was fully mixed with the water entering the subsurface reed bed, this is not true for the first distribution channel at the inlet of each bed. Transverse mixing in the inlet channel was only created by water pouring vertically into the channel. The water entering the channel caused a turbulent flow field in the immediate surrounding water body and encouraged re-circulating flow patterns (see Figure 5.24). Naturally, the velocity of the water particles of this re-circulating flow decreased with distance. Therefore it took quite a long time for dye particles to reach the outer parts of the inlet channel. As a matter of fact, by the time of the dye reaching the outer parts of the inlet channel, the injection of dye was already long over and clear water started to move from the centre outwards. This temporal development can be seen in Figure 5.25 and is shown schematically in Figure 5.26.

Figure 5.24. Turbulent mixing in the centre of the inlet channel

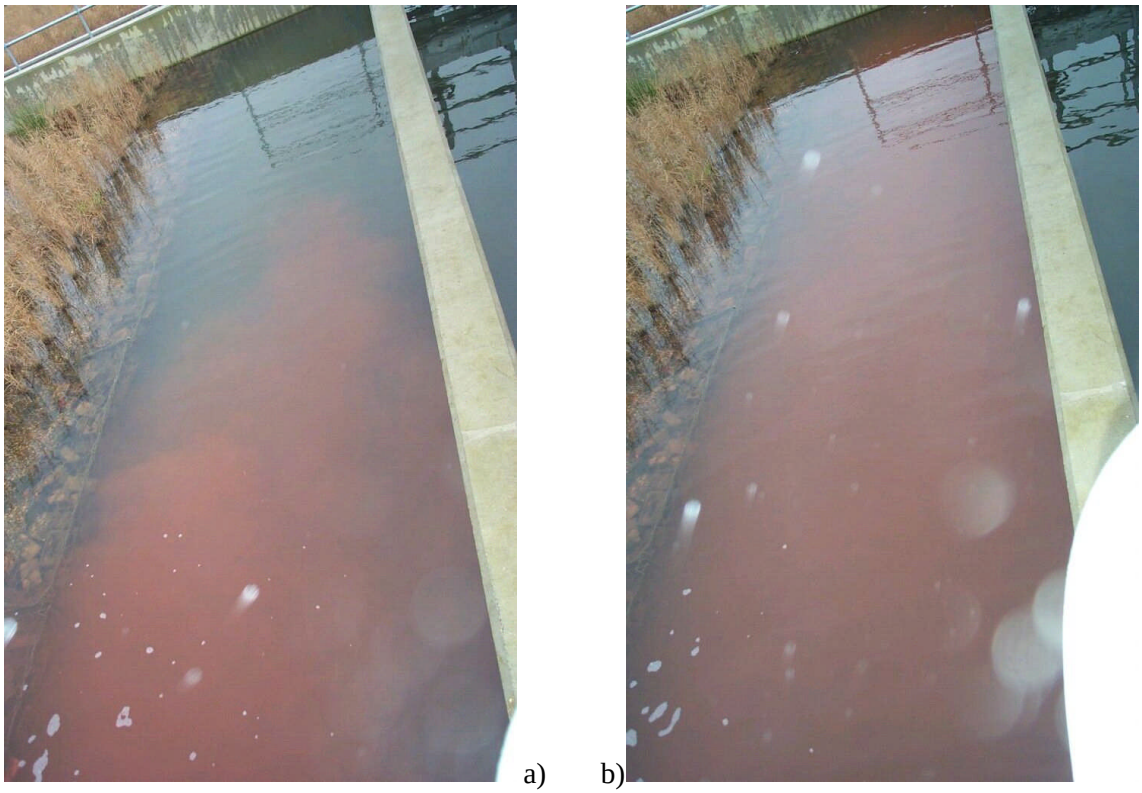

a) b)

Figure 5.25. Distribution of dye in the inlet channel at ca.0.5 hours (a) and at ca. 1.5 hours (b) after injection

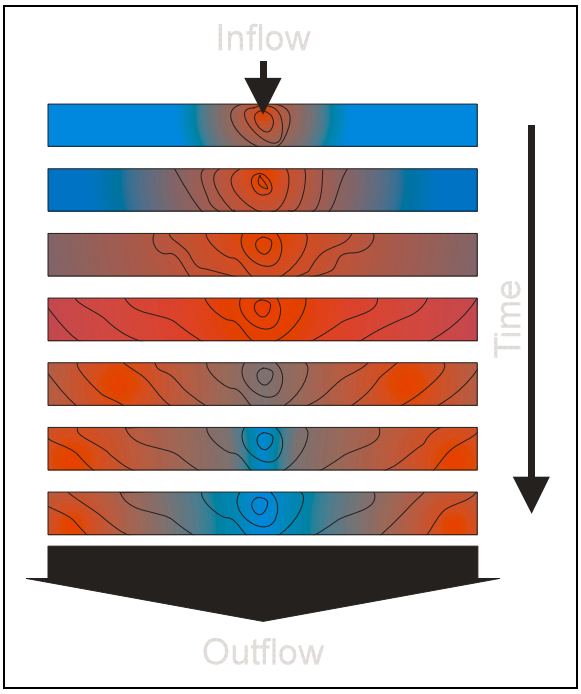

Figure 5.26. Temporal development of concentrations in inlet channel

5.3 TREATMENT PERFORMANCE TESTS FOR GLYCOL REMOVAL

Since the Heathrow Constructed Wetlands is a novel system designed to treat airport runoff, a major target of this thesis is the assessment of the treatment efficiency. For this reason two sets of field tests were performed. The first set of tests, Series 1, took place within the first operational season in February 2002, approximately three months after beginning of the de-icing season. The second test, Series 2, took place in November 2002 as part of a wetland conditioning, thus before the actual start of the de-icing season.

To compliment the field tests, a series of lab tests were performed on a bench scale substratum reactor.

5.3.1 Parameters, methods of analysis and sample preparation

In test Series 1 the samples were analysed for COD and DO-measurements were taken. In the second test series the parameters of BOD, glycol and nutrient parameters were analysed additionally. A summary of the parameters is shown in Table 5.6 for each test. The analysis of the samples for the parameters were performed according to the procedures listed as follows.

The biochemical oxygen demand was determined on site as the 5-day BOD according to BS-EN 1899-1. Dissolved Oxygen levels in the BOD bottles were measured with an YSI-58 DO-meter with BOD-bottle stirrer. The chemical oxygen demand was measured on site using the method of dichromate digestion and colorimetric determination. Hach (21258-25) and

Chemetrics (K-7355) manufactured the COD digestion vials. A Hach DR/2000 Spectrophotometer was used for the colorimetric analysis. Glycol was determined with the Chemetrics Glycol Test Kit- K-4423. A Hach DR/2000 Spectrophotometer was used for the colorimetric analysis. Nutrient parameters were analyzed with Ion Chromatography. Dissolved Oxygen levels in the field samples were measured with an YSI-58 DO-meter with BOD-bottle stirrer.

BOD was determined on raw samples. For all other tests samples were prepared by removing suspended solids from the samples using a 6µm filter. Sample preparation took place immediately before analysis. Samples for later laboratory analysis were stored in PE containers and frozen shortly after field collection.

Table 5.6. Observed Parameters in the field tests

Observed Parameter	Series 1, February 2002	Series 2, November 2002
BOD_5	×	✓
COD	✓	✓
Dissolved Oxygen	✓	✓
Glycol	×	✓
Nutrients	×	✓

5.3.2 Field tests, Series1, February 2002

Tests were performed under steady state flow conditions. Glycol was injected with a constant mass flux into the wetland. The pollutant used for the injections was an aircraft de-icer with the brand name "Kilfrost ABC-S" (Cyrotech, 2002a). This de-icer is a mono-glycol based fluid which contains at least 50 Vol-% of propylene glycol.

The glycol was injected into the floating arm inlet structure of the wetland to enhance mixing of the pollutant with the water. The pollutant was injected over a period of 3 days to allow for replacement of water within the gravel matrix of the wetland. This time is based on theoretical calculations and practical considerations. On the practical side the length of the test period was restricted through the constant weather conditions and thus for the time delay of the runoff reaching the system after a rain event of approximately 2 to 3 days. On the theoretical side the time period of the injection of pollutant can be estimated from temporal residence time distributions. The mean travel time calculated from temporal residence time distributions is approximately 1.5 days. Thus the injection time of 3 days would allow an exchange of water of approximately 2 times for the flow in the macro pores. The cumulative retention time

distributions of Figure 5.16 and Figure 5.17 indicates, that only 80 to 90 % of the total available water in the pore space would have been exchanged.

Therefore the fluorescent dye "Rhodamine WT" was simultaneously injected at a constant rate. The additional measurements of dye concentrations in the samples allow a correction of the measured glycol concentrations, depending on the observed dye variations within the wetland. The test set-up for the injection with the injection pump and containers for dye and pollutant is shown in Figure 5.27.

The water leaving the system was discharged into the main reservoir. Due to the mixing and dilution processes in the large water body of the main reservoir, an increase in background concentration of pollutant or dye in the receiving water of the wetlands could be excluded.

Figure 5.27. Test set-up for pollutant and dye injection

A well system was constructed, to allow the extraction of pore water from the matrix at different levels of depth (Figure 5.28). These wells were placed in three longitudinal rows along the cells of Bed 4 and 11 of the constructed wetland system (Figure 5.29). The water was extracted from the wells using a small pump. The actual sample was taken after pumping the well clear for a short period. The wells reached into the matrix to depth below the surface of -5 cm, -15 cm, -25 cm, -35 cm, and -55 cm.

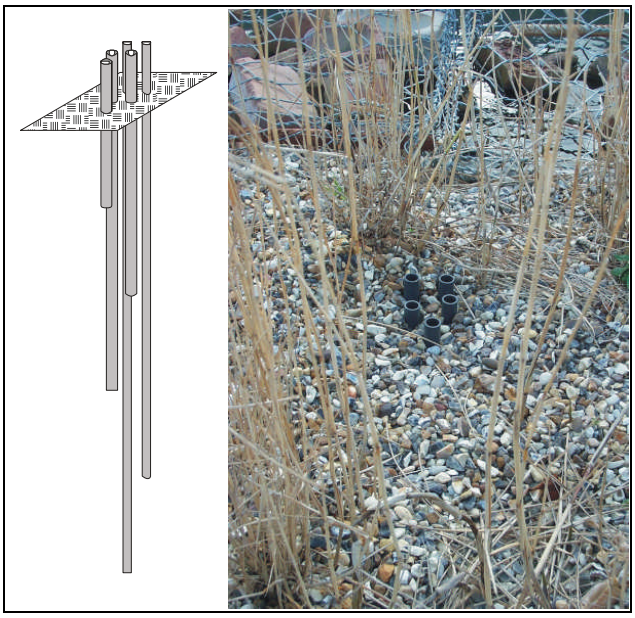

Figure 5.28. Extraction Wells

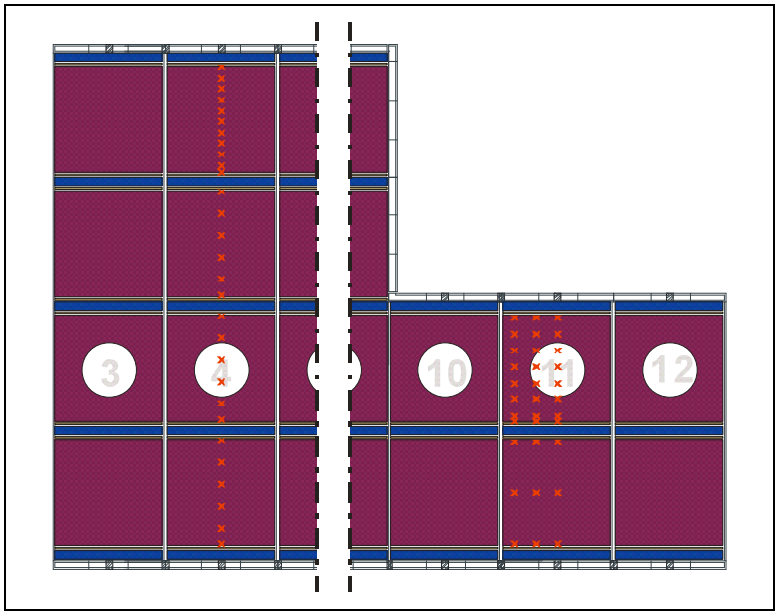

Figure 5.29. Spatial distribution of the extraction wells for test Series 1

Dissolved oxygen was measured in water samples taken along the centre line of the wells in middle depth on Bed 4. On Bed 11 dissolved oxygen concentrations were measured in water samples taken in the open channel sections of the wetland. The results, including the fluorescence corrected COD concentrations, are shown in Figure 5.30 for Bed 4 and in Figure 5.31 for Bed 11 respectively.

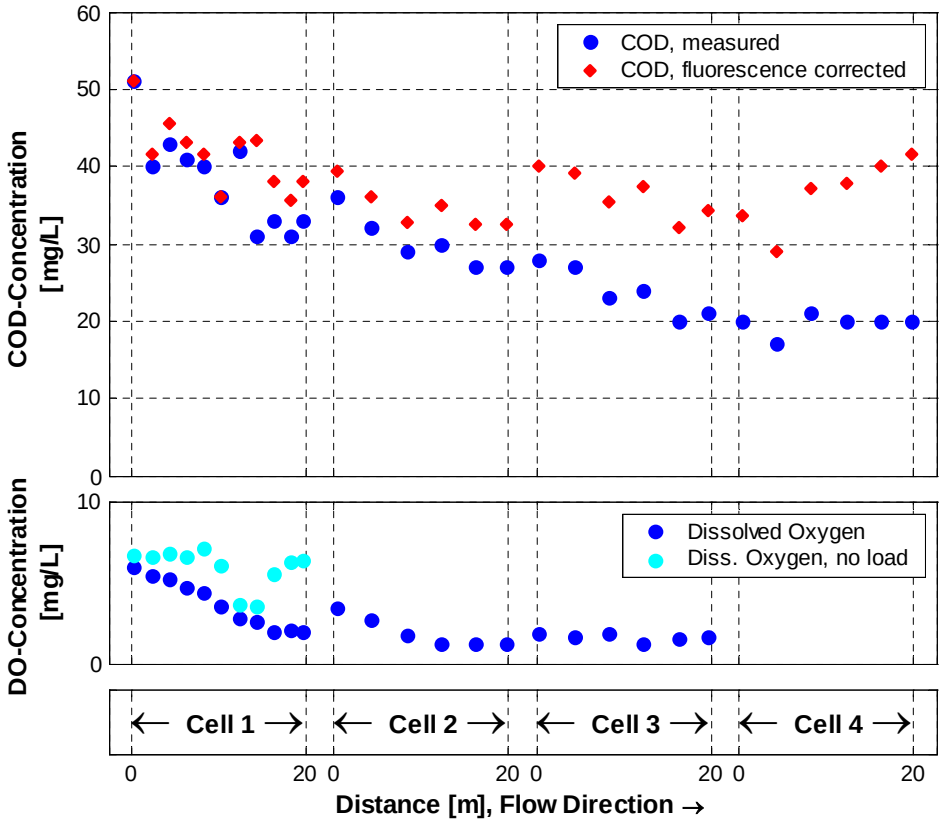

Figure 5.30. Longitudinal measured COD and dissolved oxygen concentrations on Bed 4, Test Series 1

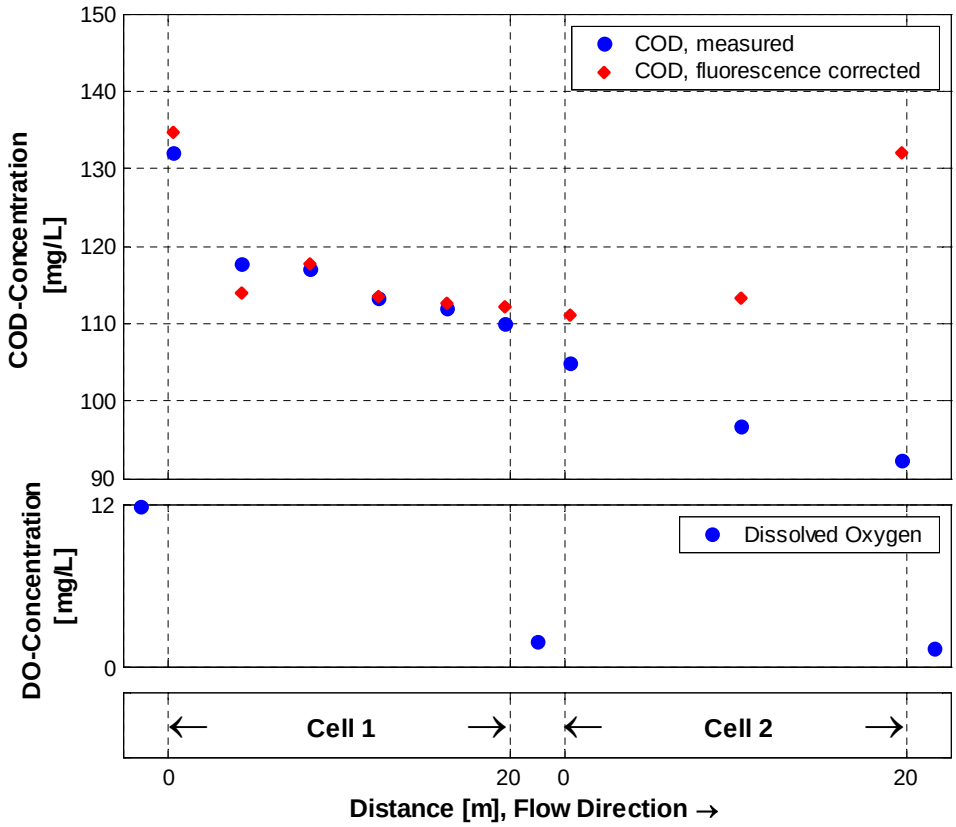

Figure 5.31. Longitudinal measured COD and dissolved oxygen concentrations on Bed 11, Test Series 1

5.3.3 Field tests, Series 2, November 2002

In November 2002 the subsurface reed beds of the Heathrow Constructed Wetlands were conditioned prior to the de-icing season. A volume of 28 m³ of mono-propylene glycol was used for this purpose. The glycol used for this purpose was coolant from an industrial cooling application that contained approximately 50 Vol-% mono-propylene glycol. It was transferred into the Main Reservoir, where it was mixed and diluted with runoff water before transfer into the reed beds started. The system was run in closed loop, thus the water leaving the subsurface reed beds was pumped into the Main Reservoir. Therefore a steady dilution took place in the Main Reservoir. Aeration systems in the Main Reservoir and Balancing Pond were used to oxygenate the water. Within the framework of the conditioning of the Beds, field tests were undertaken for the assessment of the treatment performance of the reed beds.

The delivery of the pollutant took place on 02/11/2002. The pollutant was mixed and aerated in the Main Reservoir and Balancing Pond up to 13/11/2002. The transfer pumps were switched on at 15:15 hrs on 13/11/2002. Tests started on 14/11/2002 and ended on 27/11/2002.

To study the impact of nutrients on the treatment, Bed 12 was fertilized during the test period. A water-soluble commercial fertilizer was used for this purpose. The fertilizer was mixed with water and then evenly distributed in the inlet channel and the middle channel. This procedure of fertilization took place three times a day, at around 8.30 a.m., 12.00 a.m. and 6.00 p.m..

Orifices of Bed 5 and Bed 11 were swapped during the observation time. This allowed the simulation of the impact of different hydraulic loads to the treatment efficiency of the beds. The ranges of hydraulic loads are shown in Table 5.7.

Table 5.7. Hydraulic loads of different beds

Bed no	Units	Bed 2	Bed 4	Bed 10	Bed 12	Bed 5	Bed 11
Area of Gravel	m^2	2291.0	1525.8	765.3	767.3	1525.8	765.3
Design discharge	$L\ s^{-1}$	5.26	3.61	1.39	1.39	1.39	3.61
Hydraulic Load	$L\ s^{-1}\ ha^{-1}$	2.30	2.37	1.82	1.81	0.91	4.72
Measured Discharge	$L\ s^{-1}$	5.16	3.87	1.99	2.33	1.99	4.21
Hydraulic Load	$L\ s^{-1}\ ha^{-1}$	2.25	2.54	1.28	3.04	1.30	5.50

Similar to the test in February 2002, samples were taken spatially along longitudinal sections of the subsurface reed beds (transect data). In addition to these spatial observations, temporal data was also collected. Here water samples were taken at the inlets and outlets of the subsurface reed beds throughout the test period.

The samples from the temporal observation were analysed for their chemical oxygen demand. Additionally, some samples were analysed for their biochemical oxygen demand content and their glycol content and some nutrient parameters. The samples from the spatial observation were analysed for their chemical oxygen demand, while nutrient parameters and dissolved oxygen were analysed additionally in some samples (see Table 5.8). Additionally the data from the online BiOX-BOD-meters were collected.

The spatial tests were performed on Beds 4 and 10. The locations of transects on Beds 4 and 10 are shown in Figure 5.32. Samples were extracted from wells installed in the beds, as described before. Two lines of wells were installed in downstream direction, one line in the centre of the bed and one line in the quarter-line of the bed. Only one well was used at each point of observation, reaching half way down to the bottom of the bed. Wells and extraction pump are shown in Figure 5.33. The results of the COD analysis and dissolved oxygen observations are shown in Figure 5.34 and Figure 5.35.

Table 5.8. Observed Parameters in the field tests, Series 2

Observed Parameter	Spatial Observations	Temporal Observations
BOD_5	×	✓
COD	✓	✓
Dissolved Oxygen	✓	×
Glycol	×	✓
Nutrients	✓	✓

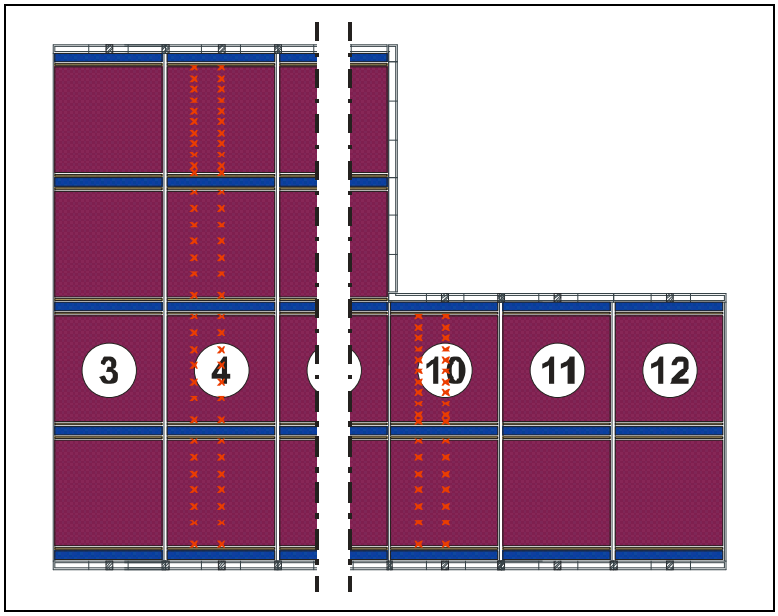

Figure 5.32. Spatial distribution of the extraction wells for Test Series 2

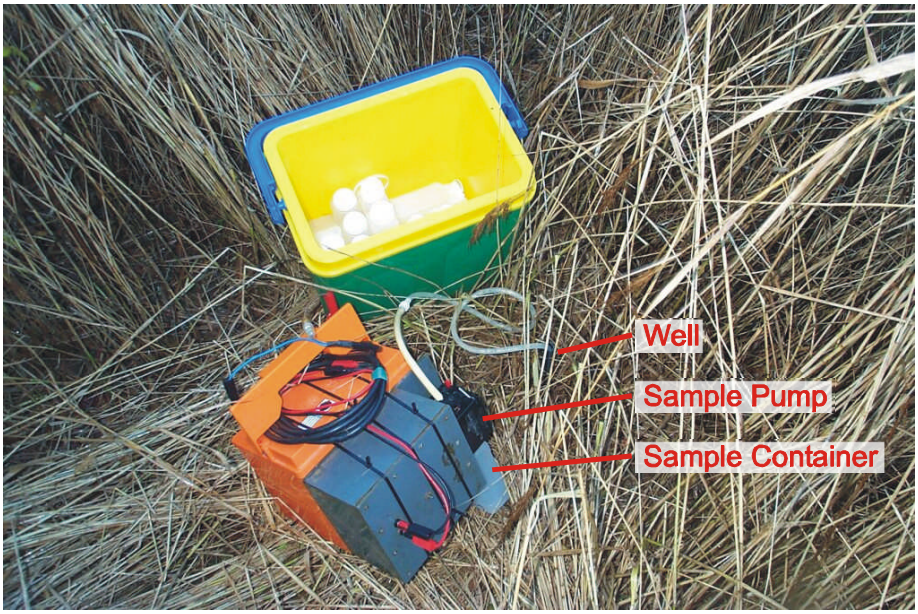

Figure 5.33. Extraction well and sample pump

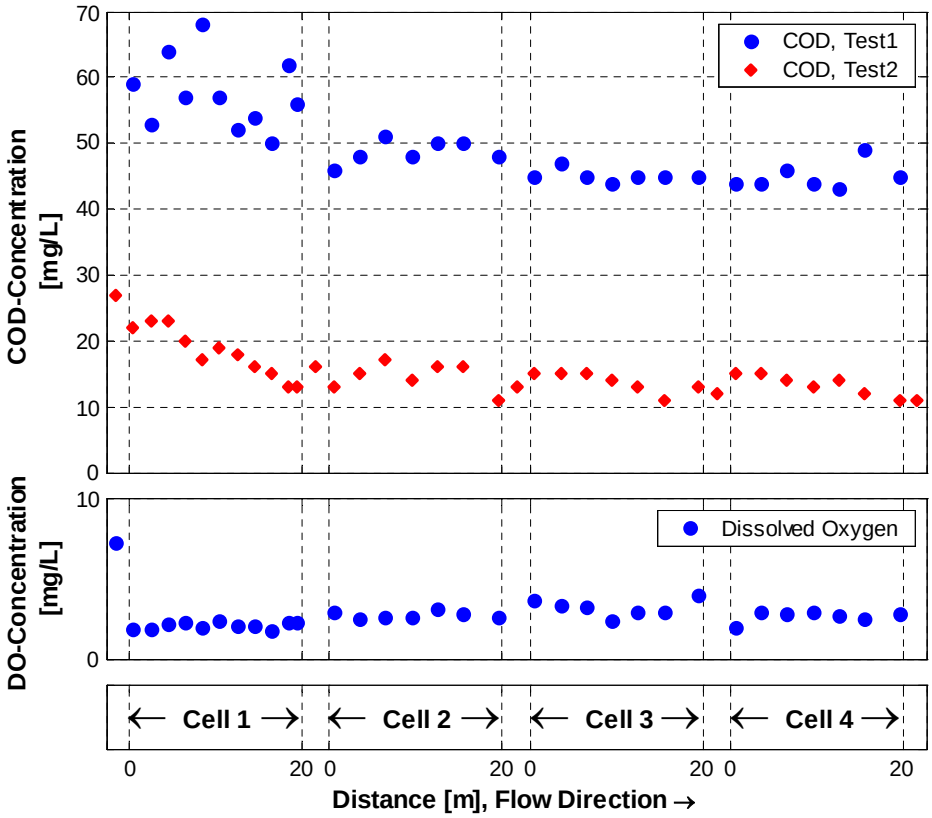

Figure 5.34. Longitudinal measured COD and dissolved oxygen concentrations on Bed 4, Test Series 2

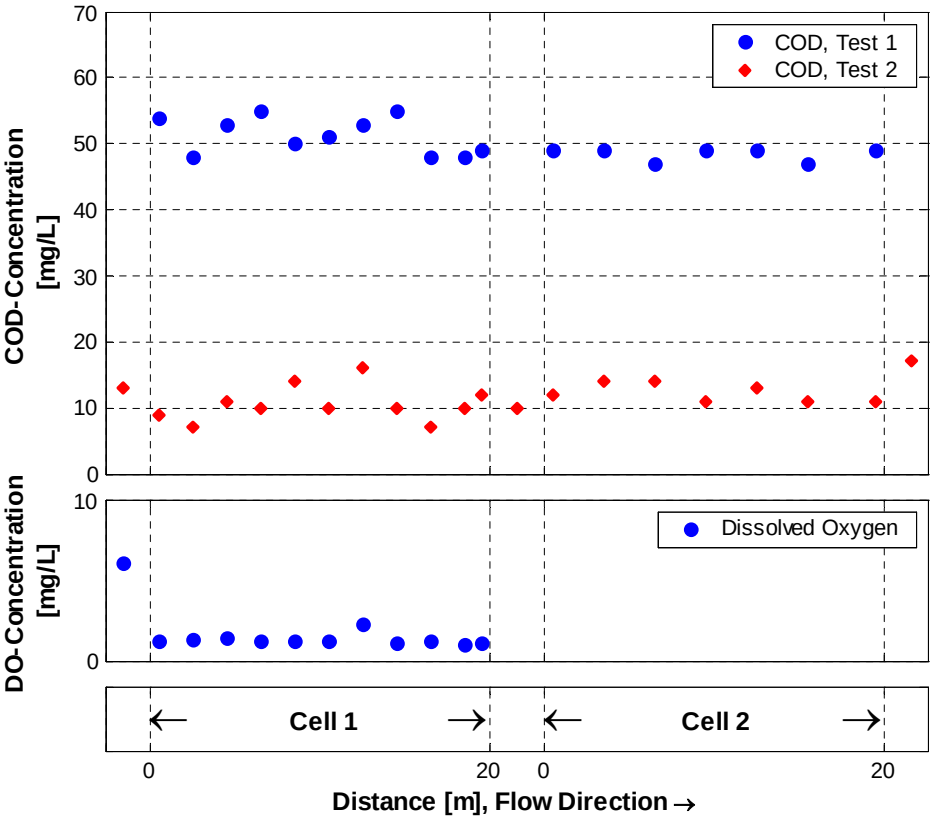

Figure 5.35. Longitudinal measured COD and dissolved oxygen concentrations on Bed 10, Test Series 2

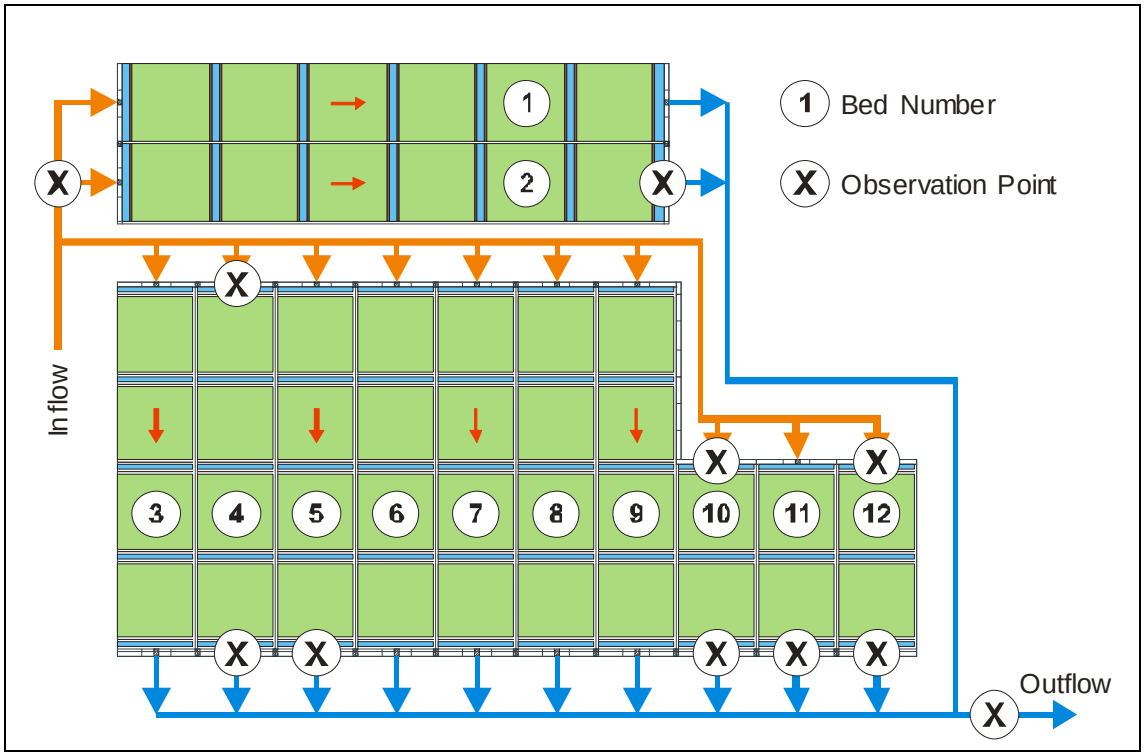

Figure 5.36. Observation locations for temporal observation

Temporal observations at the subsurface reed beds were performed at Bed 2, Bed 4 Bed 10 and Bed 12. The samples were taken at inlet and outlet of each bed. Further samples were taken at the total outlet, the outlet of Bed 5 and the outlet of Bed 11. The sampling was performed twice a day, in the morning and in the afternoon. The locations of observation are shown in Figure 5.36.

The measured COD and BOD concentrations of the temporal observation are shown in Figure 5.37 and Figure 5.38 respectively. The observed concentrations of the inlet show a steady decrease with time. The observed concentrations at the outlet are increasing for about 2 days and start to decrease after having reached the maximum value. The observations did start at the 14/11/2002. While COD was observed up to the 27/11/2002, BOD was observed up to the 21/11/2002. BOD was analysed after 5 days as carbonaceous BOD_5. ($cBOD_5$). These BOD tests were conducted with the use of the nitrification inhibitor ATU.

The results of the online BiOX-meter for the Main Reservoir, the Balancing Pond and the Outlet of the subsurface reed beds are given in Figure 5.39. The output of the BiOX-meters was recorded at intervals of 2 minutes. No data was recorded during periods with gaps.

The non-carbonaceous BOD_5 was measured to assess the impact of nitrification on the BOD. The comparison of these non-carbonaceous BOD test results with the carbonaceous BOD test results are shown in Figure 5.40.

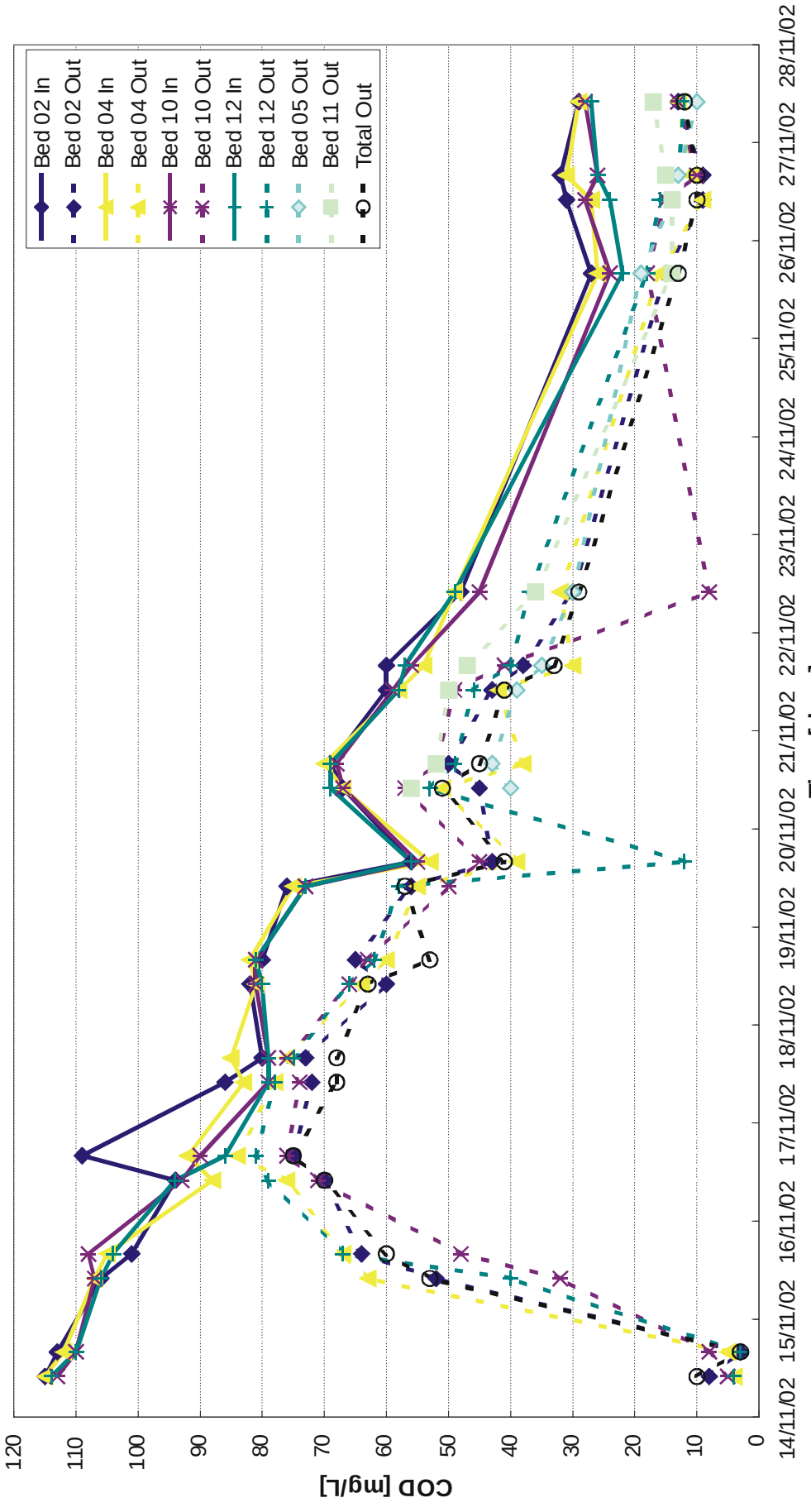

Figure 5.37. Temporal COD observations

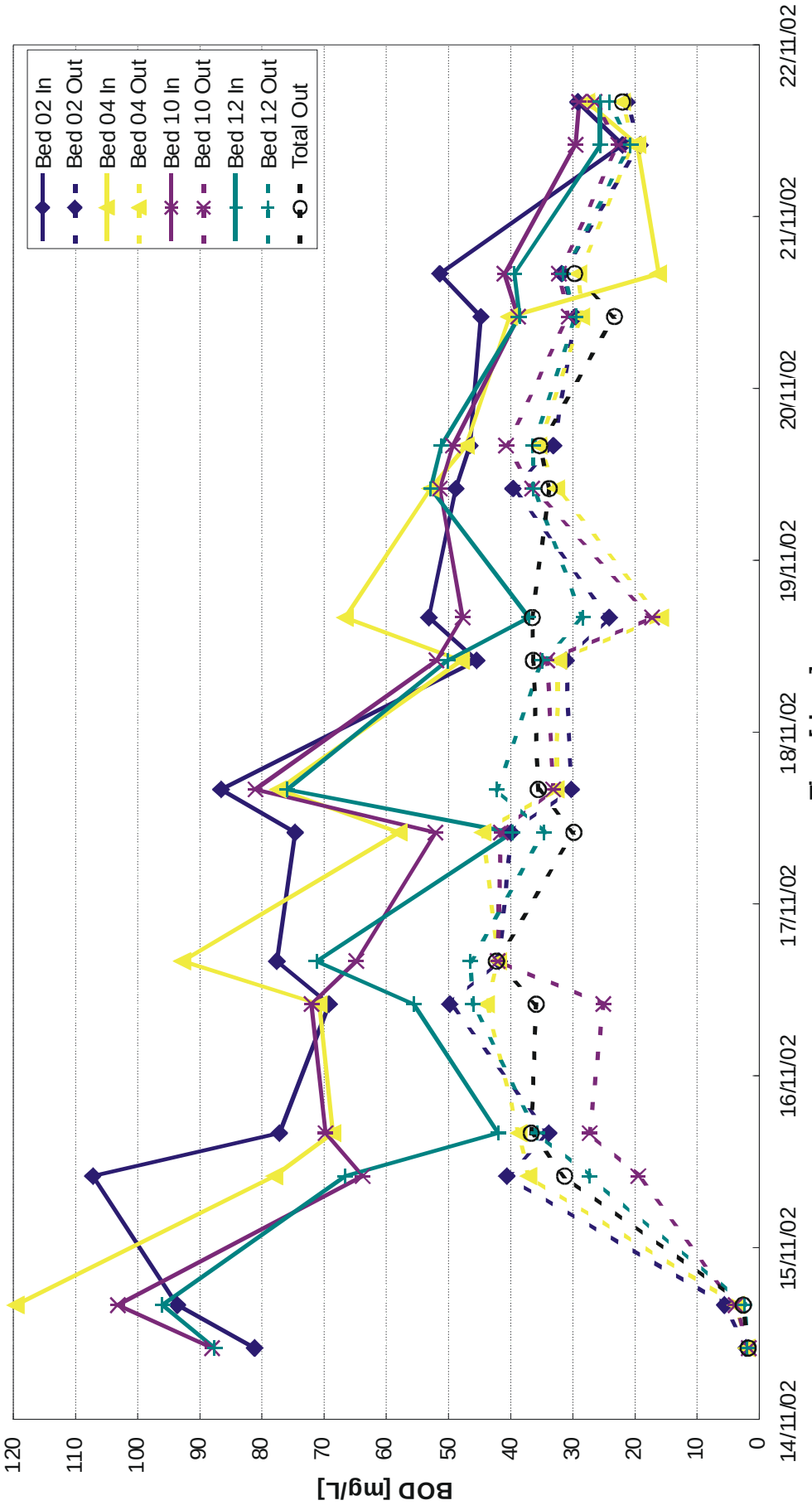

Figure 5.38. Temporal BOD observations

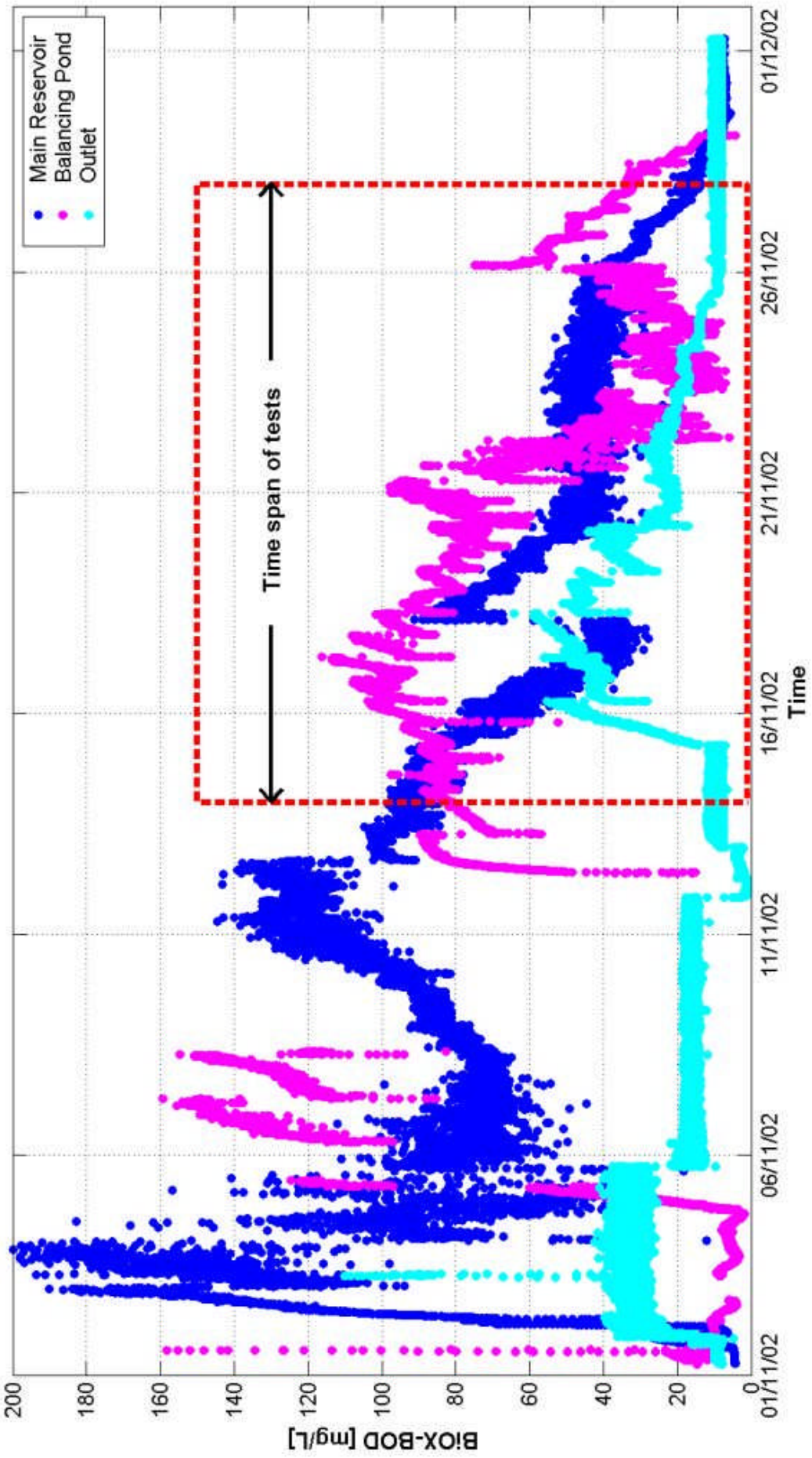

Figure 5.39. Temporal BiOX-BOD observations

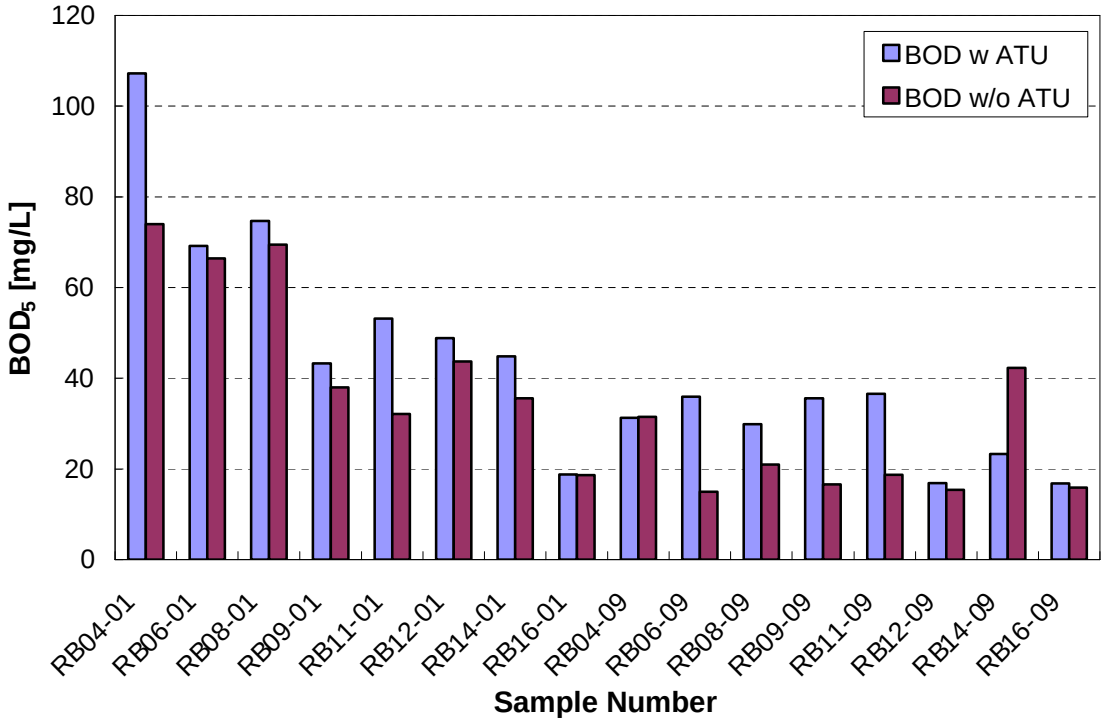

Figure 5.40. Comparison of BOD_5 test data, obtained with and without inhibiter of nitrification (ATU)

Propylene glycol was measured at the inlet and Outlet of Bed 4. The results of the tests are given in Figure 5.41. The general trend shows a steady decrease of the concentration at the inlet of the bed, similar to the COD observations. In contrast to the observed COD concentrations show the observed propylene glycol concentrations at the outlet an initial peak that decreases to zero after less than half the time of observation.

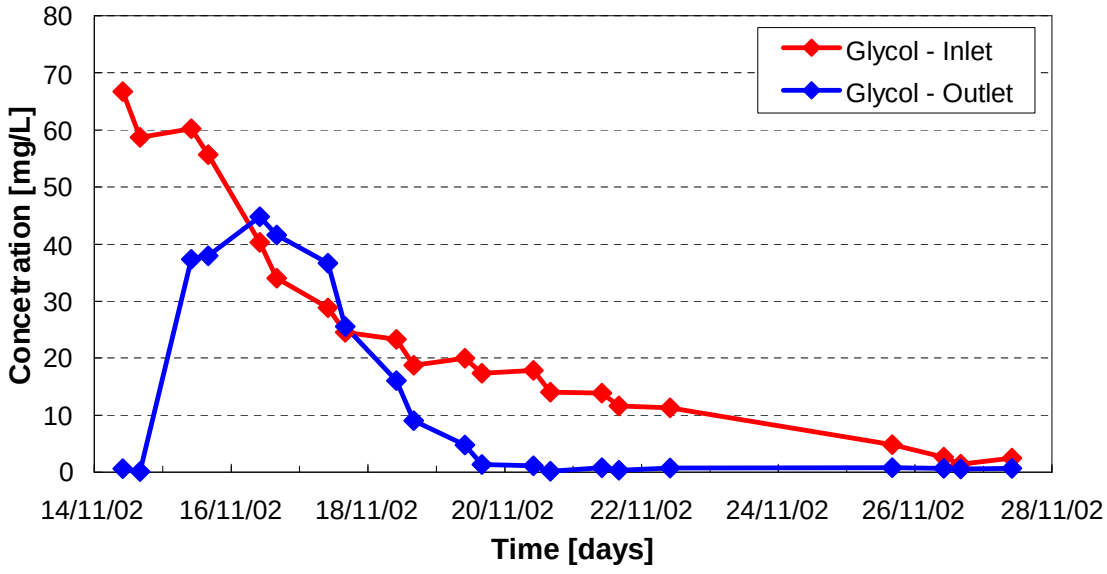

Figure 5.41. Observed propylene glycol concentrations at inlet and outlet of Bed 4

The collected samples of the temporal observations and the spatial observations were analysed for the following nutrients and compounds:

Fluoride, Cloride, Nitrite, Bromide, Nitrate, Phosphate, Sulphate, Acetate, Sodium, Ammonium, Potassium, Magnesium and Calcium

The chemical analysis could not detect any of the nutrients phosphate, ammonium, nitrate and nitrite in the samples. This was most likely through defrosting of the samples when the freezer was accidentally switched of for one week. Unfortunately, the nutrient analysis cannot contribute to the assessment of the treatment performance.

5.3.4 Laboratory tests

To support the field tests, laboratory tests were performed to simulate the aerobic and anaerobic treatment of glycol-laden water within a gravel matrix. Four bench-scale reactors were constructed from pipes (Figure 5.42). Each reactor has an internal diameter of 100 mm and a length of 800 mm. Gravel was filled to a length of 750mm, supported at the bottom with a holed plate for an optimised distribution of the water flowing into the reactor. The flow direction was from bottom to the top. Glycol was mixed with the water in a tank and then pumped into the reactor.

The system was filled with gravel taken from the Heathrow Constructed Wetlands. Further, water from within the pore space was used for the initial conditioning of the bench scale reactors. Later, water from a canal was added to fill the tank. The system was therafter conditioned during a period of three weeks, where glycol was added regularly to the water in the tank.

During the aerobic tests, pipes were fitted to the overflow of the reactor, allowing the re-circulation of the water. The water in the tank was aerated. For the anaerobic tests the reactors were sealed against external air. Pipes from the outlet were directly conected with the water body within the tank, prohibiting air to stream back into the reactor. The water was not aerated during the anaerobic tests.

Samples were taken at the inlet in the tank and at the outlet of each reactor. Samples were analysed on their COD-content during both tests. Dissolved oxygen was measured during the aerobic test on all samples. During the anaerobic tests the dissolved oxygen level was measured in the tank for control. Dissolved oxygen levels in the tank were between 8.9 and 9.7 mg/L during the aerobic tests, indicating fully saturation of the water and DO-levels depending on the actual air pressure. The control measurements during the anaerobic tests indicated a level of dissolved oxygen in the tank of approximately 0.5 to 1.0 mg/L.

Flow rates were altered during both tests. The test results for the aerobic tests are shown in Figure 5.43. In this plot the difference of the DO-level and COD-level between inlet and outlet of the reactors are plotted against the specific velocity, depending on the flow rate. Figure 5.44 shows the result for the anaerobic test for the difference of the COD-level between inlet and outlet of the reactors. Further shown are the calculated values of the anaerobic treatment from the aerobic tests. These levels are obtained by subtracting the difference in measured DO-level from the difference of the measured COD-levels between inlet and outlet.

Figure 5.42. Laboratory bench scale reactor

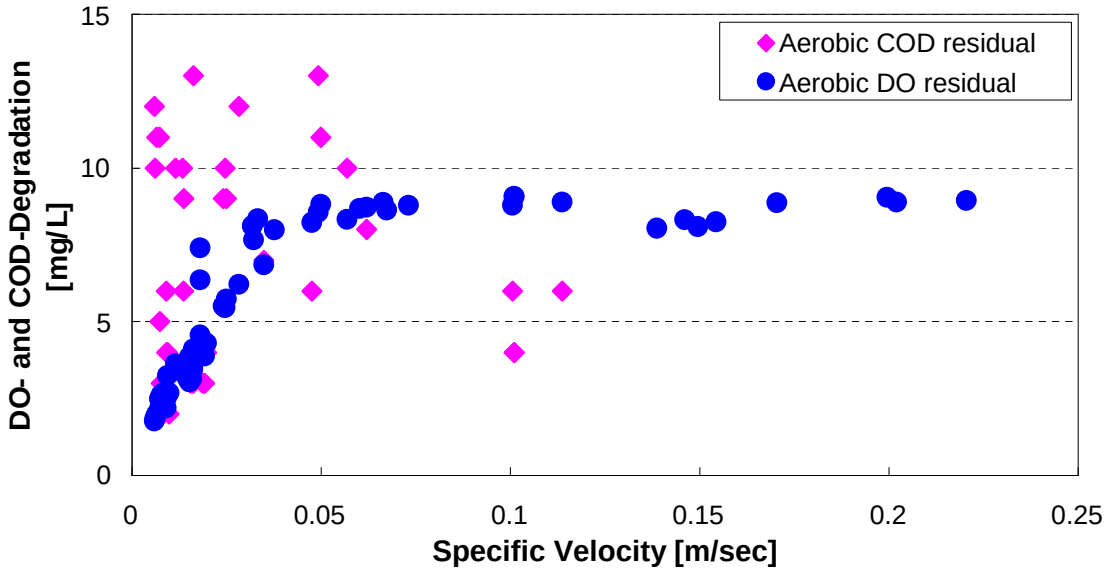

Figure 5.43. Laboratory tests, aerobic degradation of glycol

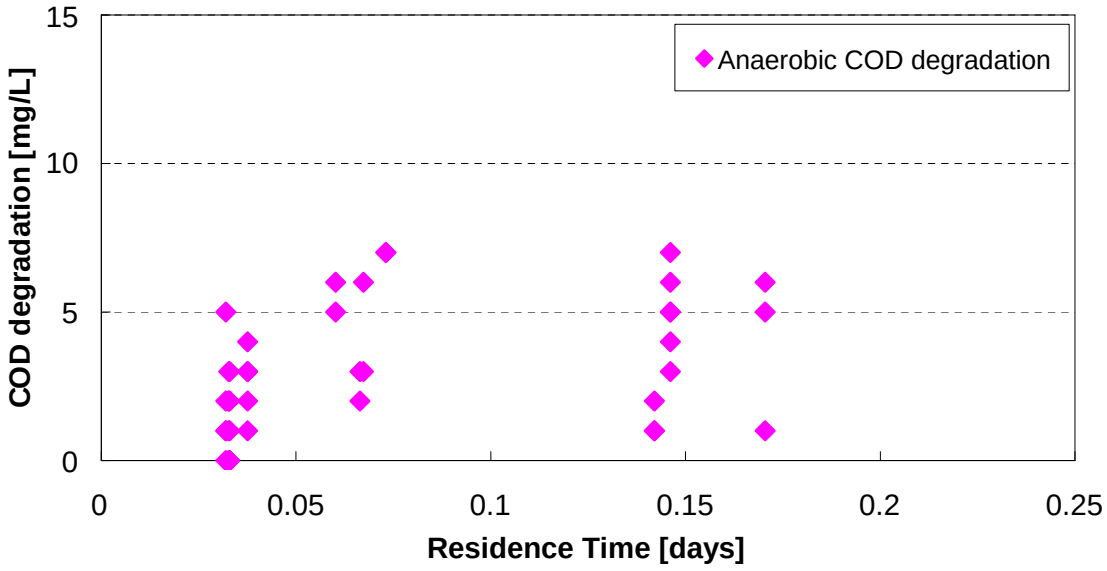

Figure 5.44. Laboratory tests, anaerobic degradation of glycol

Chapter 6

DISCUSSION

6.1 INTRODUCTION

The ultimate goal of this thesis is the assessment of the treatment performance of glycol components in airport runoff in a large-scale subsurface reedbeds, as shown in Figure 1.1. Two main primary objectives can be identified to meet this goal. The first and most obvious objective is an investigation into the pollutant degradation rates for glycol components. These investigations will show the temporal degradation of these glycol components in the aquatic environment of a constructed wetland. These investigations cannot be seen in isolation. Furthermore, it has to be assessed in the context of their movement within and through this environment. Investigations into the pollutant transport are therefore necessary to highlight the effects and influences that the flow processes may have on the degradation of the pollutant within the wetland.

6.2 PART A: POLLUTANT TRANSPORT IN CONSTRUCTED WETLANDS

6.2.1 Assessment of the collected data

6.2.1.1 General test

Discharge rates. The observed discharge rates of water into the reedbeds were presented in Table 5.1 and showed varying values. Albeit a general inaccuracy in discharge is caused by the floating arm structure itself, varying discharges may further be caused by the delivery pumps. During the test Series 0 temporary pumps were used prior the completion of the pipe works. Prior to the test Series 1 the normal delivery pump was damaged due to silting. As later learned, the damaged normal operation pump and the standby pump were operated in parallel.

Therefore much more water was delivered to the subsurface reed beds. Due to the inaccuracy of the floating arm structures it is likely that more water was discharged into each bed, instead of being disposed through the overspill. Being unaware of this problem, unfortunately no discharge measurements were undertaken. The measurements of the test Series 1 have to be assessed under these uncertain circumstances.

During test Series 2 the normal operating pump was in use. The observed discharge rates of this test show similar varying values compared with the values of test Series 0. Further, volumetric discharge measurements were performed with a calibrated container. Since the time to fill the container is a reciprocal relationship to the discharge rate, the measurements of the lower discharge rates are more accurate than those of the higher discharge rates. This error was minimised by averaging several repeat measurements.

However, these measurements do not take into account, that a change in water head in the Balancing Pond would also cause varying discharge rates. Since up to now the delivery of water from the Main reservoir is manually controlled, the delivery pumps from the Main Reservoir are usually switched off during the night and at the weekends, allowing the water level in the Balancing Pond to drop and therefore reduce the delivery rate into the Subsurface Reedbeds.

Information about the change of the delivery rate in regard to the change in water head can be taken from the pump manufacturers data sheet (Flygt, 2003). Assuming the delivery rate of 40 L/s to be in the middle of a change of the water head of 2 m, then the delivery rate will change between 45 L/s and 35 L/s when water level of the Balancing Pond is full or 2 m down. If the delivery rate of 40 L/s was calculated from a topped up Balancing Pond, then a water level drop of 2 m will decrease the pump delivery rate to 32 L/s. This change in delivery rate will not affect Beds 1 and 2, since their supply is hydraulically separated from the supply of the other Beds. Therefore a change in delivery rate in the order of 5 L/s will change the discharge rate of Beds 3 to 12 in the order of 17%, while a change of 8 L/s will change it in the order of 27%. Obviously, a change in delivery rate has a much higher impact on the discharge rate in any flow model than the uncertainties from the measurement of the actual discharge rate into each individual bed.

Gravel porosity and organic matter. The porosity of the gravel was measured on a fresh gravel sample (Chapter 5.1.2). In wetland applications, a change in porosity of the matrix is caused by blockage of the pore space through biological growth on the gravel, accumulation of organic matter and suspended solids and the growth of roots of the planted reeds (Chapter 2.2; e.g. Kadlec and Knight, 1996). Clearly, not all of these factors cause a smaller value of porosity in the same location throughout the bed. On gravel samples taken throughout the beds at different locations and depths (Chapter 5.1.4), a thick bio film was not visible, indicating that either only a thin bio film coated the gravel pebbles or that the organics were only suspended within the pore space. In test Series 0 the only observable matter within the pore space were

small amounts of mineral particles such as dust of crushed gravel that was attached to the sieved gravel as it was delivered. An increase in organic matter and suspended solids with time was observed at the front of each first cell of the beds (Chapter 5.1.4). At test Series 2 this accumulation of the suspended particles was observed only to take place in the front of the first cell of each bed within a distance of 1 to 2 m. No accumulation of suspended solids or organics was visible further downstream. These observations were proved by measurements of the organic matter content in the gravel matrix. The results did not show any significant change in organic matter content between May 2001 and November 2002. The measured organic matter content was for both tests in the range of 1 g/L (Chapter 5.1.4).

Further, accumulation of organic matter took place on the surface of the gravel beds. Organic litter from the planted reeds was found up to a depth of around 5 cm below the gravel surface during the tests of Series 2. Another influential factor in the change of porosity is the development of the root system of the reeds. Since the wetlands are dynamic systems, the state of the roots is constantly changing. At this early stage, the root system was mainly growing and developing. While at the time of test Series 1 it was still possible to pull a reed out of the gravel bed, this was not any longer possible at the time of the test Series 2. This indicates that the growing root system will mainly decrease the porosity and since the roots are growing downwards, the porosity at the upper regions or the gravel bed are more influenced than the lower regions (Chapter 2.2; e.g. Kadlec and Knight, 1996). Dying roots may have an opposite effect (e.g. Brix, 1997). Before their structural decomposition the dead roots may act as a pipe, thus causing an increase in porosity. The porosity is, unlike other parameters such as the discharge or the water head, not easily and readily observable in the field. Thus any value obtained in a field measurement is spatially influenced by various other parameters and therefore attached with a high uncertainty that will limit its general use in a numerical model of flow or transport processes.

Hydraulic conductivity. The hydraulic conductivities were measured in the tests of Series 0 and Series 2 (Table 5.2). The observed individual values of each test series showed scatter throughout each bed. Interestingly, they did not show any significant trend of rising or falling values from the upstream cells towards the downstream cells. The observed values of the test of Series 2 are approximately half an order of magnitude lower than the values of Series 0. Obviously, the decrease in hydraulic conductivity is somehow related to the development of the system in terms of biological growth or accumulation of suspended solids and organic matter. Since the accumulation of suspended solids and organic matter is mainly restricted to the first few metres of the first cells in each bed, the development of the root system is most likely to have caused the decrease in hydraulic conductivity.

During the tests of Series 0 it became obvious, that the hydraulic conductivity caused an unacceptable water head at the downstream end of Bed 1 and Bed 2 when the control weir at the

outlet of those bed was set to allow no surface flooding on the first cells. The water head was just around 0.2 m, thus approximately the top 0.4 m of the gravel matrix was dry. Since this low water level is unacceptable in terms of the encouragement for the growth of the plants, such "dry land" also encourages the, unwanted, growth of weeds. Sloping the base of the wetland usually compensates the obvious head loss of water flowing through wetlands (e.g. IWA, 2000). However, the designers deliberately chose a horizontal base for the wetlands to prevent the gravel matrix becoming dry when stagnant water was produced with pumps switched off during the summer period of no operation. This problem, caused by the high discharge rate and the greater length of Beds 1 and 2, was solved when the designers decided to utilise pipes in the first four cells of Bed 1 and Bed 2. This allowed some of the flow to bypass those cells and thus a reduced effective discharge minimised the effect of the draw down.

Figure 6.1. Draw down at the end of Bed 1 without short-circuiting of the flow

While the tests on Bed 2 of Series 0 and Series 1 were undertaken before the pipes were placed in the gravel or with blocked pipes, respectively, the test of Series 2 was undertaken with open pipes partially bypassing the flow. In the other beds, the initially observed difference between the front and rear water levels during the tests of Series 0 were approximately -0.2m for the Beds 3 to 9 and approximately -0.05 m for Beds 10 to 12, much smaller than the observed -0.4 m on Beds 1 and 2. For the computation of the hydraulic conductivities DARCY'S law (Equation 2.21) was used. The measured discharge rates of Table 5.1 were taken. Since the measurement of the discharge rates and the measurements of the water levels were performed at the same time, the uncertainties in the pump delivery rate due to a temporal change in water head in the Balancing Pond are not applicable. Uncertainties associated with the computation of the hydraulic conductivities were: the measurement errors of the water head and the errors associated with the measurement of the discharge rates into each bed. The error in the

measurements of the water level between the locations is approximately 0.005 m, that produces a maximum error in the computation of the hydraulic conductivity of approximately 10%. Combined with the error in the measurements of the discharge, that is less than 5%, the computation of the hydraulic conductivities have a maximum associated error of 15%.

However, in Chapter 2 it was shown that DARCY'S law for the computation of hydraulic conductivities for the gravel matrix is only valid as long as the Reynolds number *Re* does not exceed some value between 1 and 10. Reynolds numbers, calculated for the lowest observed water level of approximately 0.4 m, are presented in Table 6.1 for the flow in the gravel matrix and the flow in the open channel. The calculated numbers show that both the flow in the gravel matrix and the flow in the open channel sections, are laminar, since the threshold values of 10 and 500, respectively, are not exceeded.

Table 6.1. Reynolds numbers for the flow in the gravel matrix and for open channel flow

Bed No.	Reynolds Number *Re* water level of 0.3 m for flow in	
	Gravel Matrix	Open Channel
Bed 2	5.8	222
Bed 4	4.4	169
Bed 11	2.2	86

6.2.1.2 Assessment of the residence time distributions and the observed dispersivities

From recorded residence time distributions for all experiments of Series 0, Series 1 and Series 2 (Figure 5.15 to Figure 5.23) it can be shown, that the mixing in all beds follows a similar pattern. Evaluating all the recorded retention time distributions, all distributions show a non-gaussian mixing behaviour, having a quick, sharp rising limb and a long, slow falling limb. Interestingly, the duration of the rise of the concentration from the time of the first detected arrival up to the time of the detected peak is in all cases around 0.5 days. Furthermore, the shape of this rising limb has, in all cases, the shape of a gaussian "bell-shape" distribution.

This is clearly not true for the falling limbs of the distributions, which show for all observed cases considerably long tails. Generally, it has to be stated that the concentration readings increased with time through a build up of organic matter on the optics of the instruments during the test. While the build-up of organic matter was considerably lower in the tests of Series 0, it was much higher during the other tests. Due to the high travel costs in

attending site, it was not possible to clean the optics regularly during the tests. This increase in organic matter was recorded as well as turbidity on the instruments second channel. These turbidity readings were then used to correct the concentration readings. However, there is a degree of uncertainty associated with this correction. This uncertainty is increasing with time, since the build up of organic matter causes more noise in the sensor and in the meantime the real concentration of the tracer in the water is getting smaller.

To compensate for the effect of the decreasing tracer concentration, a second test series with a constant injection was performed. Unfortunately, the treatment plant operators switched off the pumping system during this test series for internal testing purposes and it was not possible to repeat these tests.

The observed times of first arrival and peak of the distributions are at approximately 1 day and 1.5 days for the tests of Series 0 and 2 and approximately at 0.5 days and 1.0 day for the tests of Series 1. The significant shorter arrival times observed at the tests of Series 1 are obviously caused by the higher discharge rate due to the operation of both delivery pumps.

The sharp rising front of the observed residence time distributions (Figure 5.15 to Figure 5.23) suggest that the process of advection is dominating the process of dispersion within the subsurface reed beds (Chapter 2.4.8; Fischer, 1979). For all three discharge rates the magnitudes of the process of advection and dispersion were calculated according to Equation 2.55 and are summarised in Table 6.2. Clearly, from the last two columns of that table it can be taken that within the gravel beds for all discharges the process of advection is governing the process of dispersion. A similar statement cannot be made for the open channel sections between the gravel cells, since no information exists about the dispersion coefficient in the open channel sections.

Table 6.2. Comparison of the magnitude of advection and dispersion

Discharge Q [L/s]	Water depth h [m]	Porosity n [-]	Velocity U [m/s]	Dispersivity α_L [m]	Dispersion coefficient D [m^2/s]	x/U [s]	D/U^2 [s]
2.33	0.4	0.45	6.47E-04	1.22E-01	7.90E-05	31	188
3.87	0.4	0.45	1.08E-03	1.22E-01	1.31E-04	19	113
5.16	0.4	0.45	1.43E-03	1.22E-01	1.75E-04	14	85

From the test for the transverse dispersivities in the field, as well as in the laboratory, a small transverse dispersion coefficient was obtained (Table 5.3). The observed distributions show that the dye from a injected point source can be found directly downstream at the end of a cell only within a radius of less than approximately 0.3 m (Figure 5.8, Figure 5.9). This indicate

that the transverse exchange of dissolved pollutants is quite small. The pollutants will therefore leave a bed at the same cross-sectional location where they did enter the cell at the downstream end of the cell. The low transverse dispersion may be interpreted as a set of stream-tubes (Carleton, 2002) where each tube represents longitudinal sections within a cell. A hypothetical layout for such a stream tube model is shown in Figure 6.2, where the middle section of a cell, the left and right outer parts of the cell the regions in between are each represented by a stream-tube. Since the head loss in all stream-tubes is the same, so is the velocity of the flow in each stream-tube as well as the total time of travel within a tube. It was shown in Figure 5.26 that water entering the beds needs more time to reach the outer sections of the bed. Further on, the distance of the outer sections to the outlet structure of each bed is longer than the distance from the inner sections. Thus the fraction of a solute pollutant that takes its way through the bed in an outer stream-tube will need longer than that fraction that takes the stream-tube in the centre of the bed. The resulting residence time distributions have therefore different absolute travel times. This is indicated by the time-staggered distributions shown in Figure 6.2 for an instantaneous injection of pollutant. The travel times for the pollutant in the in the last open channel section and the distribution of mass for the stream tubes was selected hypothetically from the visual observations (see Figure 5.26). The residence time distributions for each stream-tube were calculated for the layout of Bed 11 with Equation 2.52, where the velocity was calculated from the measured discharge rate and the dispersion coefficient was calculated from the computed dispersivity as shown in Table 5.4. For simplicity, the water head in each stream-tube was assumed to be constant.

Obviously, the degree of lateral mixing of the water in the open channel sections between the cells will have an impact on the total travel time. If the lateral mixing is assumed to be limited, since it is mainly caused by wind shear effects that are also limited trough the planted

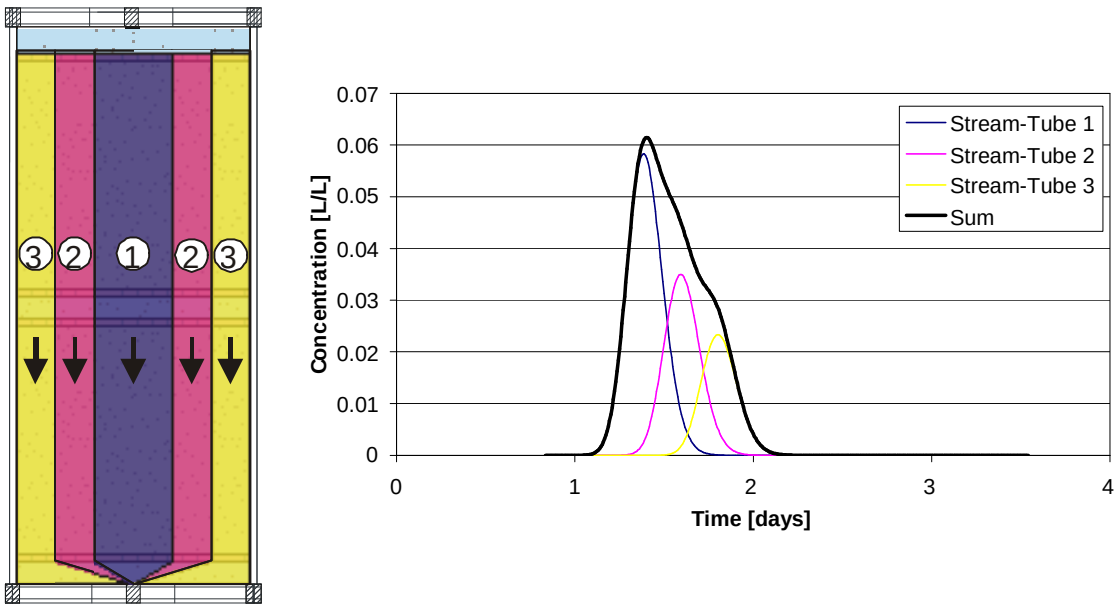

Figure 6.2. Stream-tube model of subsurface flow reed bed

reeds, then this will maximise the difference in the travel times between the outer and the inner stream-tubes. The longitudinal dispersion, as shown in Table 5.4, will be similar in each stream-tube. Considering the pollutant reaching each stream-tube to have the same mass and considering the dispersion to be negligible in the open channel sections, then the combined concentration distribution at the outlet will just produce a more or less gaussian-shaped distribution, that has a wider base than each of the distributions measured at the end of each stream-tube (see Figure 6.2). In comparison to the observed residence time distribution (Figure 5.15 to Figure 5.23) do the computed residence time distribution for the stream-tube model (Figure 6.2) not show the same distinctive tail.

Clearly, not all previous mentioned conditions for this hypothetical model case are true. The concentrations in front of the first cell do vary in time and space and the magnitude of the concentrations will not reach the same hypothetical levels in the channel. Due to the inlet conditions in the first open channel section, as illustrated in Figure 5.24, Figure 5.25 and Figure 5.26, the proportion of the dye entering the middle section of the first cell is higher than the proportion entering the outer sections of the cell. Further, the distance from the outer sections are much greater and thus the travel time to the outlet structure of the bed. This leads to a staggered arrival of the distributions (Figure 6.2). It causes the spread of the distribution and development of some kind of tail.

However, this model cannot reproduce the long tail of the observed distributions of the field tests. Those long tails of the distribution suggests, that some of the pollutant is affected by some "dead zone" effect, where a proportion of tracer is trapped and slowly released. The visual observations, shown in Figure 5.24, Figure 5.25 and Figure 5.26, suggest that this process takes place in the first open channel section of each bed. The impact of the water entering the reed bed causes a transverse circular movement of the water body, that enhances the mixing of the pollutant with the water in this first open channel section. These physical mixing processes in the open channel are therefore similar to the processes that take place in a Continuous Stirred Tank Reactor, as highlighted in Equation 2.65 in Chapter 2.4.9. However, the "tank reactor" must be considered not to be completely mixed.

6.2.1.3 Conclusions and summary of the a priori knowledge

The assessment of the measured data allows the following conclusions to be drawn as a priori knowledge to the modelling process:

- The measured discharges for the test of Series 0 and 2 are associated with a low uncertainty, while the discharges for the test of Series 1 are associated with a high uncertainty.

- The uncertainties of the hydraulic conductivities are associated with those of the discharges.
- The uncertainties in the porosities for the test Series 1 and 2 are high. Nevertheless, the absolute values are represented by the hydraulic conductivities.
- Low longitudinal dispersivity suggests that advection dominates longitudinal dispersion within the gravel cells.
- Low transverse dispersion suggests limited transverse exchange of pollutant within the gravel cells, which may imply parallel flow paths.
- The first open channel section delays transport of pollutant to the outer parts of the beds.
- The first open channel section may act as an imperfectly mixed CSTR.

6.2.2 Pollutant transport model with an aggregated dead zone approach

6.2.2.1 Residence time data preparation for flow modelling

As mentioned before, organic matter started to grow on the optics of the fluorometer during each test. The observed amount of organic matter on the optics was larger during the tests of Series 1 and 2. The growth of the organic matter did influence the reading of the turbidity channel of the instrument as well as the fluorescence channel of the instrument. As can be seen exemplarily in Figure 6.3, the growth of the organic matter had a noticeable effect on the fluorescence and turbidity readings after approximately from three days and reached a constant level at approximately 5.8 days. Since it is well known that turbidity influences the fluorescence readings in fluorometry (Turner-Designs, 2003), the change in turbidity reading was used to compensate for the increase in fluorescence using a linear relationship. The "corrected"

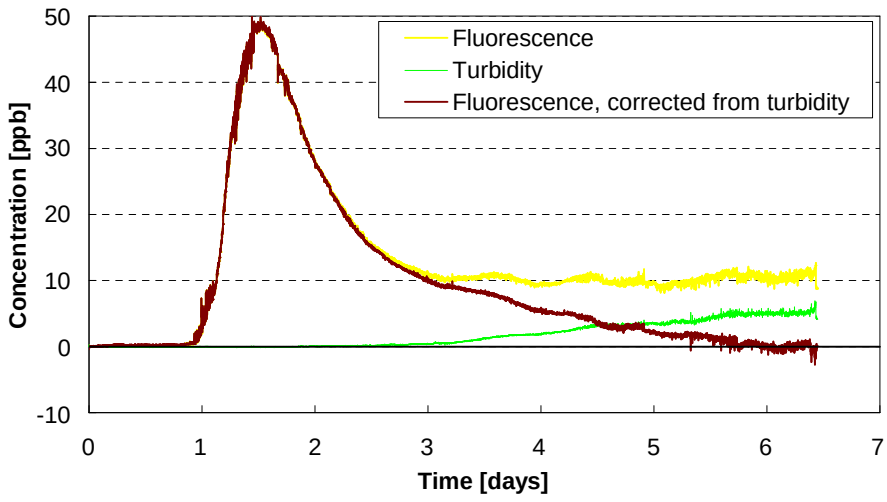

Figure 6.3. Correction of the influenced fluorescence reading trough build-up of organic matter on the optics of the instrument

fluorescence readings are also presented in Figure 6.3. While the confidence in the fluorescence readings before the increase in turbidity after 3 days is high, the confidence in the corrected fluorescence readingsfrom 3 days onwards is, obviously, less, since the no cross calibration of the effect of turbidity to the fluorescence could be performed under controlled conditions.

From the "corrected" residence time distributions the recovery rates of the tracer were calculated. The mass of the tracer M can be calculated from the residence time distributions by multiplication of the area under the residence time distributions with the flow rate Q as

$$M = \sum C_i \, Q \Delta t \qquad 6.1$$

where

C_i tracer concentration at time i

Q discharge rate

Δt time step

Table 6.3. Recovery rates of injected tracer

	Test Series 0	Test Series 1	Test Series 2
Bed 2		118.5%	111.3%
Bed 4	68.3%	105.1%	71.7%
Bed 10	67.3%	66.4%	125.3%

The obtained recovery rates for the tests are shown in Table 6.3. There are three main reasons for poor recovery rates. The first reason is that effluent being monitored was not completely representative for the whole effluent, e.g. it was not completely mixed. At the time of the tests of Series 0, the building work of the outlet structures of the reed beds was not completed. Thus it is likely that the whole effluent was not being monitored. This does not hold true for the tests of Series 1 and 2. The second reason is, as mentioned before, the uncertainty associated with the "correction" of the readings of fluorescence by the measured increase in turbidity reading. This did influence all test series. The third reason lies in the calculation of the recovery rate itself, since the flow rate Q is needed for the calculation. The discharge rated were measured for the tests of Series 0 and 2, thus tests of Series 1 have a higher uncertainty.

The concentration readings for the residence time distributions were recorded every minute for approximately 7 to 8 days. The large number of data points in each data set was reduced according to the procedure described in Chapter 3.5.2. The data was sampled down with a rate of 1 sample in 50 samples. A moving average filter was applied prior to the down sampling of

the data, utilising the same sampling rate. The number of samples describing the rising limb of each distribution is in the range of 20 samples.

6.2.2.2 Flow modelling with the SRIV method

The SRIV-method (Chapter 3.3) was applied to the resampled and filtered data sets of the observed residence time distributions. For each observed residence time distribution a SRIV-model was evaluated for the each possible permutation in the parameter range of m = 1...10, n = 1...10 and δ of approximately ±7 time steps of the time lag gained by visual inspection. As model input a direc-delta function was used to represent the instantaneous tracer injection. From the results of the model evaluations a parameter table was compiled for each residence time distribution and then ranked for the parameters of the coefficient of determination R_T^2, the YIC-information criterion and the AIC-information criterion (Chapter 3.3.2; Young, 1985; Ljung 1999; Young,1992). The top ten results of ranking for the models for the test Series 0, Bed 11 is shown as an example in Table 6.4. The coefficient of determination and the AIC information criterion give the same ranking of the models, where the results of the YIC criterion give a different ranking. The "best" R_T^2- and AIC-identified models are not within the list of the best ten YIC-identified models and vice versa. The B-polynom of the "best" identified model with the criteria of the coefficient of determination and the AIC have more parameters than the "best" YIC-identified model. Further on, the standard errors for all identified parameters of the transfer function are lower for the YIC-identified model, resulting in the lower YIC-value (see Table 6.5). Obviously the "best" YIC-identified model is more efficient with respect to the number of parameters and their associated errors from the process of estimation.

Apart from the tests of Series 1, Bed 11 and Series 2, Bed 2, the [4 2 δ] model structure was the parametric most efficient model of all evaluated models in terms of the YIC identification criterion. The criteria of the coefficient of determination and the AIC-criterion showed a non-uniform picture, evaluating different model structures as their "best" structure. The best-identified model structure for the Series 1, Bed 11 test is the [3 1 20] model and for the test Series 1, Bed 2 is the [2 1 20] model. However, apart from test Series2, Bed 2 all residence time distributions share the same characteristic shape, with a similar distinctive gaussian shape around the peak and a long tailed falling limb. In terms of transfer function modelling, these distributions generally indicate parallel flow patterns.

As shown previously, parallel flow patterns are modelled with a serial and parallel combination of single ADZ-cells. Some of those combinations are shown examplarily in Table 6.6. The a priori knowledge and the results of the process of model identification suggest that the [4 2 δ] model should therefore be used as an appropriate transfer function model for the flow in the reed beds. Further, the limitation to this one model structure makes it easier to compare

Table 6.4. Results of the SRIV model structure identification for test Series 0, Bed 11 (each identified structure is only shown for its "best" time lag δ)

Model structure [m n δ]	R_T^2-values	R_T^2-ordering	YIC-values	YIC-ordering	AIC-values	AIC-ordering
[4 6 29]	0.99755	1	-15.2153		-8.5606	1
[4 5 30]	0.99746	2	-16.4442		-8.5317	2
[5 5 31]	0.99741	3	-17.1558		-8.5004	3
[5 6 28]	0.99717	4	-14.2539		-8.4236	5
[4 4 31]	0.99715	5	-18.1362	8	-8.4246	4
[4 3 31]	0.99681	6	-19.0235		-8.3260	6
[5 3 30]	0.99674	7	-17.8045	9	-8.3116	7
[4 2 31]	0.99654	8	-22.8513	1	-8.2570	9
[5 2 30]	0.99650	9	-15.2021		-8.2579	8
[6 2 31]	0.99609	10	-14.8911		-8.1528	10
[4 3 30]	0.99661		-19.7194	4	-8.268	
[3 3 31]	0.99445		-18.3783	7	-7.8099	
[3 1 31]	0.99276		-22.6090	2	-7.5753	
[4 1 28]	0.99198		-20.3949	3	-7.4654	
[5 2 27]	0.99009		-17.4816	10	-7.2638	
[3 2 26]	0.98115		-19.5514	5	-6.6378	
[2 1 31]	0.95073		-19.5165	6	-5.6557	

Table 6.5. Standard errors SRIV model structure identification for test Series 0, Bed 11 (Errors shown are for the "best" coefficient of determination and the AIC-criterion identified models (row 1) and the best SRIV identified model (row2))

Model	a_1	a_2	a_3	a_4		
[4 6 29]	0.00805	0.02235	0.02070	0.00640		
[4 2 31]	0.00530	0.01485	0.01399	0.00442		
	b_0	b_1	b_3	b_4	b_5	b_6
[4 6 29]	0.00051	0.00195	0.00325	0.00335	0.00221	0.00067
[4 2 31]	0.00002	0.00003	-	-	-	-

Table 6.6. Structures of transfer functions for various connected ADZ-cells

No.	System	Transfer Function	$[m\ n\ \delta]$
1.		$x(k) = \frac{[b_0]z^{-\delta}}{1 - a_1 z^{-1}} u(k)$	[1 1 δ]
2.	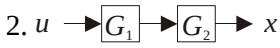	$x(k) = \frac{[b_0]z^{-\delta}}{1 + a_1 z^{-1} + a_2 z^{-2}} u(k)$	[2 1 δ]
3.		$x(k) = \frac{[b_0]z^{-\delta}}{1 + a_1 z^{-1} + a_2 z^{-2} + a_3 z^{-3}} u(k)$	[3 1 δ]
4.		$x(k) = \frac{[b_0]z^{-\delta}}{1 + a_1 z^{-1} + a_2 z^{-2} + a_3 z^{-3}} u(k)$	[3 1 δ]
5.	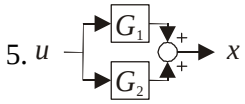	$x(k) = \frac{[b_0 + b_1 z^{-1}]z^{-\delta}}{1 + a_1 z^{-1} + a_2 z^{-2}} u(k)$	[2 2 δ]
6.	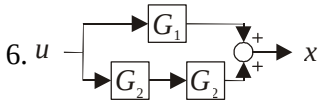	$x(k) = \frac{[b_0 + b_1 z^{-1} + b_2 z^{-2}]z^{-\delta}}{1 + a_1 z^{-1} + a_2 z^{-2} + a_3 z^{-3}} u(k)$	[3 3 δ]
7.	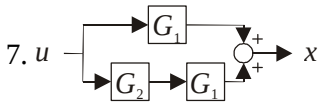	$x(k) = \frac{[b_0 + b_1 z^{-1}]z^{-\delta}}{1 + a_1 z^{-1} + a_2 z^{-2} + a_3 z^{-3}} u(k)$	[3 2 δ]
8.	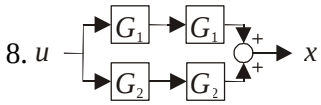	$x(k) = \frac{[b_0 + b_1 z^{-1} + b_2 z^{-2}]z^{-\delta}}{1 + a_1 z^{-1} + a_2 z^{-2} + a_3 z^{-3} + a_4 z^{-4}} u(k)$	[4 3 δ]
9.	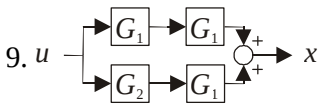	$x(k) = \frac{[b_0 + b_1 z^{-1}]z^{-\delta}}{1 + a_1 z^{-1} + a_2 z^{-2} + a_3 z^{-3}} u(k)$	[3 2 δ]
10.	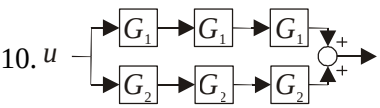	$x(k) = \frac{[b_0 + b_1 z^{-1} + b_2 z^{-2} + b_3 z^{-3}]z^{-\delta}}{1 + a_1 z^{-1} + a_2 z^{-2} + a_3 z^{-3} + a_4 z^{-4} + a_5 z^{-5} + a_6 z^{-6}} u(k)$	[6 4 δ]
11.	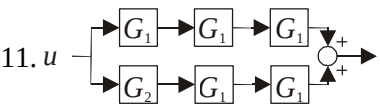	$x(k) = \frac{[b_0 + b_1 z^{-1}]z^{-\delta}}{1 + a_1 z^{-1} + a_2 z^{-2} + a_3 z^{-3} + a_4 z^{-4}} u(k)$	[4 2 δ]
12.	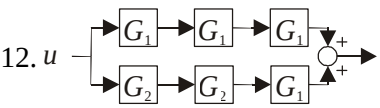	$x(k) = \frac{[b_0 + b_1 z^{-1} + b_2 z^{2}]z^{-\delta}}{1 + a_1 z^{-1} + a_2 z^{-2} + a_3 z^{-3} + a_4 z^{-4} + a_5 z^{-5}} u(k)$	[5 3 δ]

the results of the modelling process. The test of Series 1, Bed 2 showed a characteristically different residence time distribution (Figure 5.18). This was physically explained because of the short-circuiting pipes, which had been installed in that bed. Since the physical flow structure was different to the other beds, the best-identified model of [2 1 δ] was used for this test for further evaluation.

The obtained transfer functions from the identification process are shown in Table 6.7, while the associated standard errors (Equation 3.42) are compiled in Table 6.8. The residence time distributions gained by the identified transfer function models are shown in the graphs of Figure 6.4 to Figure 6.18. The coefficients of determination show that all models explain the data very well, where the value of R_T^2 is found to be between 0.987 and 0.998 (see Table 6.9). Anyhow, most of the SRIV models are not readily acceptable for the modelling of the dispersion of pollutants in the reed beds, since their eigenvalues of the denominators of the *A*-polynomial are complex numbers. As shown before, a single ADZ-cell is described by a first order differential equation. Thus from the ADZ-modelling point of view, the transfer function describing the reed bed as a combination of single ADZ-cells should be characterised by real eigenvalues.

An approach to deal with these circumstances is to re-estimate the model by constraining the eigenvalues of the transfer function to real values. From Table 6.6 it can be seen, that the structure of the [4 2 δ] transfer function model can be broken down in a combination of ADZ-cells with just two different residence times T_c. The constrained model can therefore be rewritten in the following form, where the parameter a_1 corresponds to the residence time T_c of the five ADZ-cells G_1 and the parameter c_1 corresponds to the residence time T_c of the cell G_2, as shown in their combination in row 11 of Table 6.6.

$$y(k) = \frac{b_0 + b_1 z^{-1}}{(1 + c\, z^{-1})(1 + a\, z^{-1})^3} u(k - \delta) + e(k) \qquad 6.2$$

Again, the a priori knowledge suggested a time delay in the outer regions of the reed beds through the mixing processes in the first open channel section. To take this into account, a second constrained model was obtained by including a further advective time lag Δ in the flow path of the cell represented by the ADZ-cell G_1, thus both paths of the dispersive flow are then represented by the following combination of single ADZ-cells:

$$y_1(k) = \frac{b}{(1 + a z^{-1})} \frac{b}{(1 + a z^{-1})} \frac{b}{(1 + a z^{-1})} u(k - \delta) + e(k) \qquad 6.3$$

$$y_2(k) = \frac{[d]\,z^{-\Delta}}{(1+c\,z^{-1})}\,\frac{b}{(1+a\,z^{-1})}\,\frac{b}{(1+a\,z^{-1})}u(k-\delta)+e(k) \qquad 6.4$$

The added time lag Δ just alters the *B*-polynom of the transfer function, when the single transfer functions are being multiplied. Thus a structure like this could explain the best identified model structure from the R_T^2 value as shown in row 1 of Table 6.4, where the order of the *B*-polynom is higher than that of the *A*-polynom. The parameters of the constrained models were estimated using the numerical optimisation routine as described for the parameter estimation process for the ADE-model in Chapter 3.2. The models described by Equation 6.2 will be referred to as "decomposed model A", where the model described by Equations 6.3 and 6.4 will be referred to as "decomposed model B". While the parameters for the decomposed model A were estimated with the time lag δ gained from the SRIV estimation process, the time lag δ for the decomposed model B was also subject to the optimisation.

The *A*-polynom of the [2 1 δ] model of the test Series 2, Bed 2 has real eigenvalues, as can be seen in Table 6.10. Therefore these eigenvalues can be used to set-up an ADZ model with two cells in series, as can be seen from row 2 of Table 6.6.

The residence time distributions gained by the decomposed models from an instantaneous tracer injection are shown in the graphs of Figure 6.4 to Figure 6.18. In most cases, the data is much less well explained by the decomposed models A. This can also be taken from the coefficients of determination in Table 6.9 with values between 0.949 and 0.992. The explanation of the data is much better with the decomposed model B, where the computed values of the coefficients of determination are between 0.975 and 0.996 and only slightly worse than those from the SRIV identification.

The further decomposition of the decomposed model A, as described by Equation 6.2, into the discrete ADZ cells model with two parallel pathways each consisting of three ADZ reaches, as described in row 11 of Table 6.6, is done by partial fraction expansion. The decomposed model B, as described by Equations 6.3 and 6.4, gives readily the ADZ parameters, from which the residence times (time constants) for each ADZ-cell can be computed.

The residence times T_c for the five identical G_1-cells for the [4 2 δ] structure of the decomposed model A are in the range of 0.19 to 0.33 days, except for the test of Series 0 on Bed 4, which were calculated to be 0.13 days. The residence time T_c of the single G_2 cell is not in a similar narrow bandwidth. While T_c is in the range between 1.41 days and 1.60 days for the tests of Series 1, Beds 2 and 4 and Series 2, Beds 4 and 10, it is quite different for the other beds. The value was computed with 0.96 days for the test of Series 0, Bed 11. Further, the value for the test of Series 1, Bed 11 is similar to its value of the G_1-cells. As highlighted earlier, the SRIV-algorithm identified a [3 1 δ] model for this test. The identical residence times for the cells show that data indicates as well, that a structure with a parallel pathway does not result in a better

model fit, but in a over-parameterisation. For the computed value for T_c of 2.18 days for the test of Series 0, Bed 4 the uncertainties of the incomplete recorded tail of the distribution has to be taken into account.

The computed residence times T_c for the five G_1-cells of the decomposed model B are much smaller with values between 0.12 days and 0.18 days. The residence times for the G_2-cell, in the range of 1.32 days and 1.43 days, are similar to the values computed for model A. Interestingly, the residence times for the tests of Series 1, Bed 2 and 4, and the tests of Series2, Bed 4 and 10, show nearly identical values for the G_1-cells as well as for the G_2-cells. Obviously, this confirms the similarity in the shape of the observed residence time distributions for theses tests. It is also an indication that the design philosophy of a similar hydraulic load results in similar flow patterns within the different bed layouts.

Table 6.12 shows the advective time delays δ and Δ in time steps and τ in days for the models. The optimised time delays δ from the decomposed model B (column 6) are two to three time steps more than the time delay gained from the SRIV-identification (column 2). The additional time delay Δ for the slow flow path was computed with three to six time steps for the test of Series 0, 1 and 2.

The good fit of the data with the SRIV model is due to the imaginary eigenvalues of the models. This can be seen especially at the leading front of the residence time distributions (Figure 6.4 to Figure 6.18). The decomposed and re-estimated models fit the data at the very beginning of the distribution much worse than the SRIV-models.

The addition of the advective time delays τ and the ADZ-cell residence times T_c results in the total travel times $\bar{t}$ for the slow and fast pathways and also for the whole model (Table 6.12, columns 11 to 17). The travel times for the slow pathway are around 60% to 70% longer than those of the quick pathway.

Table 6.13 shows the fractions of the flow in the slow pathway. Leaving tests Series 0, Bed 4 and Series 1, Bed 11 aside, then the fractions computed from the decomposed model A are around 70% for tests Series 0 Bed 11 and Series 1, Bed 2 and with around 55% for the tests of Series 1, Bed 4 an d Series 2, Bed 4 and Series 2, Bed 10. The fractions computed from the model B are all in the range of 70%, again with the exception of Series 0, Bed 4. As before, this indicates similarities in the flow patterns due to the physical similarities in the bed layouts.

Further shown in Table 6.13 are the dispersive fractions (Chapter 2.4.9). The values for the SRIV-identified models with the [4 2 δ] structure are in the range of 0.5 to 0.68. The [2 1 δ] model for test Series 2, Bed 2 has a much higher value of 0.76. The values calculated from the modelled residence time distributions of the decomposed models (columns 8 and 12) are identical to the values obtained from the SRIV-models (column 4). Further, the dispersive fraction of the flow in the quick pathways is with values of 0.25 to 0.49 much lower than the dispersive fraction in the slow pathways of 0.49 to 0.73. Obviously, the slow pathway causes

more dispersion than the quick pathway. This results from the longer residence time of the ADZ-cell $G_{2,}$ where the pollutants are retained much longer, and thus disperse within this cell. The dispersive fractions for both pathways of the model B are also smaller than those of the model A. This is caused by the longer advective time delays δ obtained for all models B (columns 5 and 9 of Table 6.12).

Since the flow rate was measured, it is possible to calculate the theoretical mixing volumes of the ADZ-cells from their residence times, simply by using the formula $V = T \times Q$. These theoretical mixing volumes are shown in Table 6.14. From water head observations mixing volumes can be computed with values of approximately 1,200 m^3 for Bed 2, with 800 m^3 for Bed 4 and with 400 m^3 for Bed 11 (last column of Table 6.14). The theoretical mixing volumes for the decomposed model A are approximately in the range of 50% to 83% of the values computed from the water head observations (column 3 to 5 of Table 6.14). The mixing volumes computed from the decomposed model B are even lower with values between 43% and 67% (column 6 to 8 of Table 6.14). The smaller values for model B are caused by lower residence times in the ADZ-cells and by longer advective time delays of model B compared to model A. Further, the ratio of the theoretical mixing volumes V to the computed mixing volume V_a from the water head observations is up to 18% higher than the computed dispersive fractions. This leads to the conclusion, that approximately 50% of the volume of the water in the wetland is important in dispersing the solutes.

The physical interpretations of the estimated ADZ-models for the observed residence time distributions are rather satisfying. The partitioned flow patterns of a slow pathway and a fast pathway match with the observations of the mixing behaviour made in the first open channel sections and the longer distances of the flow through the wetland in the outer regions of the reed bed compared to the inner region. Further, the identical two "quick" ADZ-cells in series in both pathways can be interpreted in terms of the dispersion affecting the water as it travels through the reed bed, whereas the single "quick" and "slow" cell may be interpreted as mixing at the front and at the end of the beds. The interpretations of the computed dispersive fractions have to be assessed in the light of the porosity of the gravel matrix. On one hand the porosity affects the seepage velocity. Here, only the effective cross-sectional area affects the transport velocity. On the other hand the porosity affects the dispersion. Here, also the interstitial water might affect the dispersion of the pollutant within the gravel matrix. However, the dispersive fractions, as well as the computed volumes of the ADZ-cells, suggest that only 50% up to 80% of the water are taking part in the dispersive process in the wetland. The interpretation of these low fractions might be, that the interstitial water plays only a minor role in the mixing within the wetland. This holds especially true, when considering that the first open channel section might be a main reason for the process of dispersion. To take this further, the dispersion in the wetland might then be just subject to the "quick" ADZ-cells. Taking this into account, then the dispersive

fractions or the fraction of the mixing volume computed from the "quick" cells to total theoretical volume of water in the wetlands reach values between 25% and 50%.

Table 6.7. Transfer functions estimated by the SRIV algorithm

Test Name	
Series 0, Bed 4	$A(z^{-1}) = 1 - 3.44\, z^{-1} + 4.48\, z^{-2} - 2.62\, z^{-3} + 0.58\, z^{-4}$ $B(z^{-1}) = 0.00193\, z^{-1} + -0.00149\, z^{-2}$
Series 0, Bed 11	$A(z^{-1}) = 1 - 3.72\, z^{-1} + 5.22\, z^{-2} - 3.28\, z^{-3} + 0.78\, z^{-4}$ $B(z^{-1}) = 0.00136\, z^{-1} + -0.00131\, z^{-2}$
Series 1, Bed 2	$A(z^{-1}) = 1 - 3.77\, z^{-1} + 5.33\, z\text{-}2 - 3.37\, z\text{-}3 + 0.80\, z^{-4}$ $B(z^{-1}) = 0.00075\, z^{-1} + -0.00075\, z^{-2}$
Series 1, Bed 4	$A(z^{-1}) = 1 - 3.65\, z^{-1} + 5.01\, z^{-2} - 3.08\, z^{-3} + 0.71\, z^{-4}$ $B(z^{-1}) = 0.00002\, z^{-1} + 0.00013\, z^{-2}$
Series 1, Bed 11	$A(z^{-1}) = 1 - 3.54\, z^{-1} + 4.71\, z\text{-}2 - 2.8\, z\text{-}3 + 0.63\, z^{-4}$ $B(z^{-1}) = 0.00007\, z^{-1} + 0.00025\, z^{-2}$
Series 2, Bed 2	$A(z^{-1}) = 1 - 1.9\, z^{-1} + 0.91\, z^{-2}$ $B(z^{-1}) = 0.00192\, z^{-1}$
Series 2, Bed 4	$A(z^{-1}) = 1 - 3.74\, z^{-1} + 5.26\, z^{-2} - 3.31\, z^{-3} + 0.78\, z^{-4}$ $B(z^{-1}) = 0.00116\, z^{-1} + -0.00115\, z^{-2}$
Series 2, Bed 10	$A(z^{-1}) = 1 - 3.75\, z^{-1} + 5.3\, z^{-2} - 3.34\, z^{-3} + 0.79\, z^{-4}$ $B(z^{-1}) = 0.00102\, z^{-1} + -0.00102\, z^{-2}$

Table 6.8. Standard errors associated with the parameters of the transfer functions

Test Name	a_1	a_2	a_3	a_4	b_0	b_1
Series 0, Bed 4	0.08977	0.24528	0.22829	0.07262	0.00022	0.00021
Series 0, Bed 11	0.00530	0.01485	0.01399	0.00442	0.00002	0.00003
Series 1, Bed 2	0.11154	0.30059	0.27151	0.08234	0.00008	0.00019
Series 1, Bed 4	0.01023	0.02859	0.02677	0.00841	0.00002	0.00002
Series 1, Bed 11	0.03271	0.09055	0.08399	0.02612	0.00007	0.0001
Series 2, Bed 2	0.00131	0.00129	-	-	0.00002	-
Series 2, Bed 4	0.00334	0.00952	0.0091	0.00291	0.00001	0.00001
Series 2, Bed 10	0.00532	0.01504	0.01424	0.00452	0.00001	0.00001

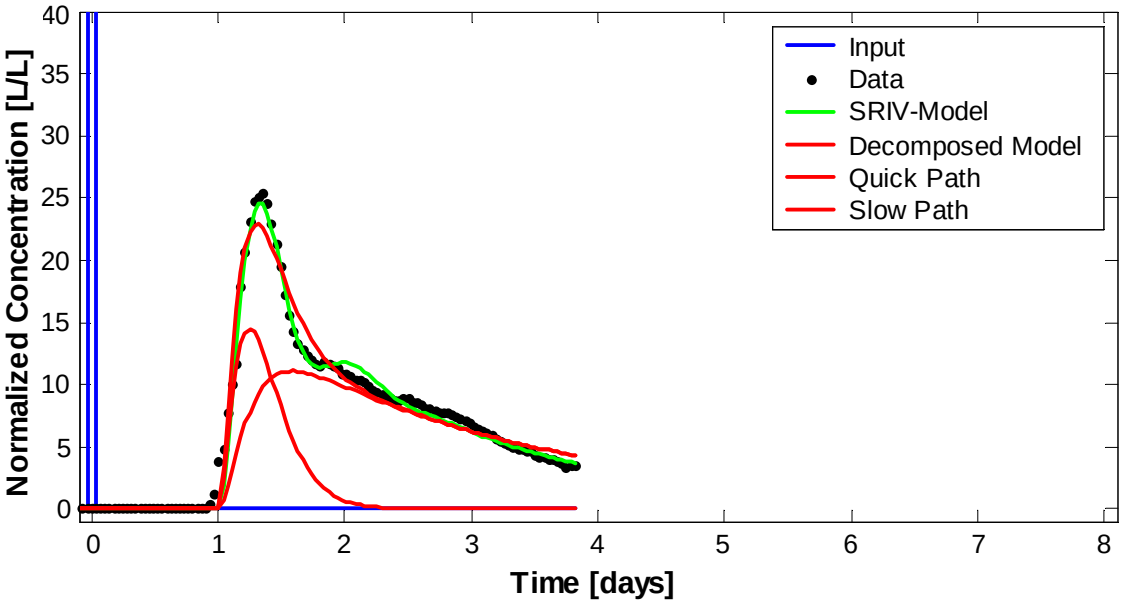

Figure 6.4. Series 0, Bed 4: SRIV identified model and decomposed model A

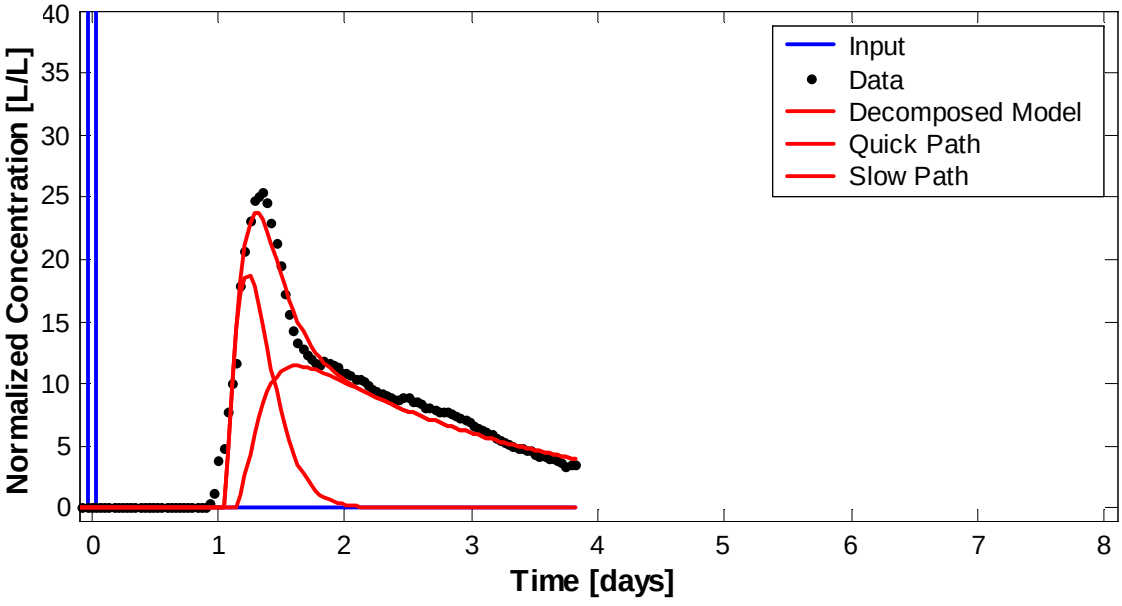

Figure 6.5. Series 0, Bed 4: Decomposed model B with optimised time lag Δ

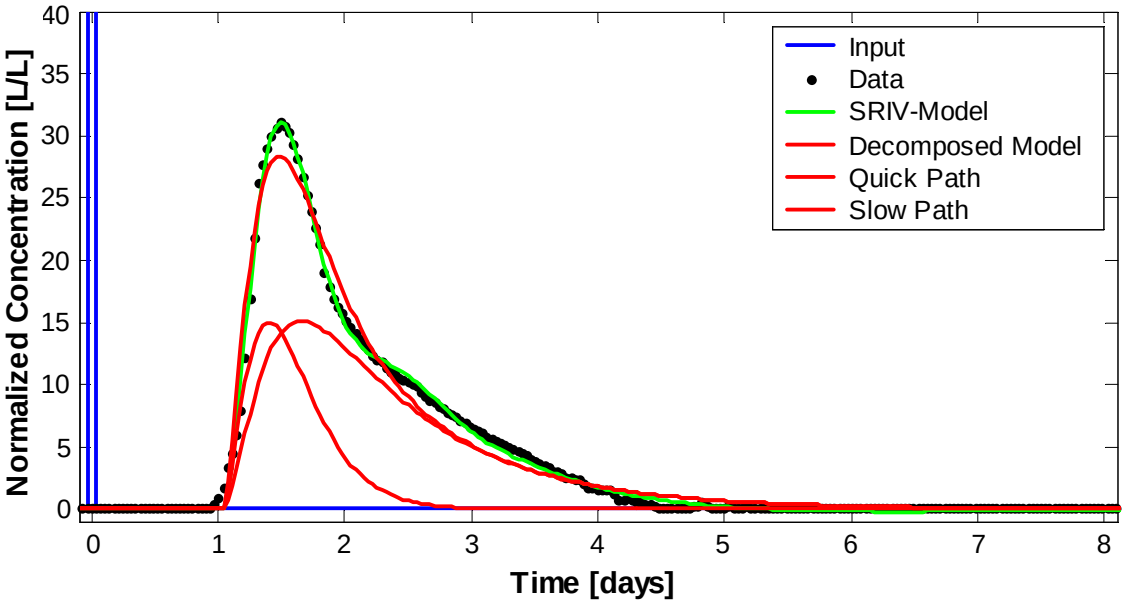

Figure 6.6. Series 0, Bed 11: SRIV identified model and decomposed model A

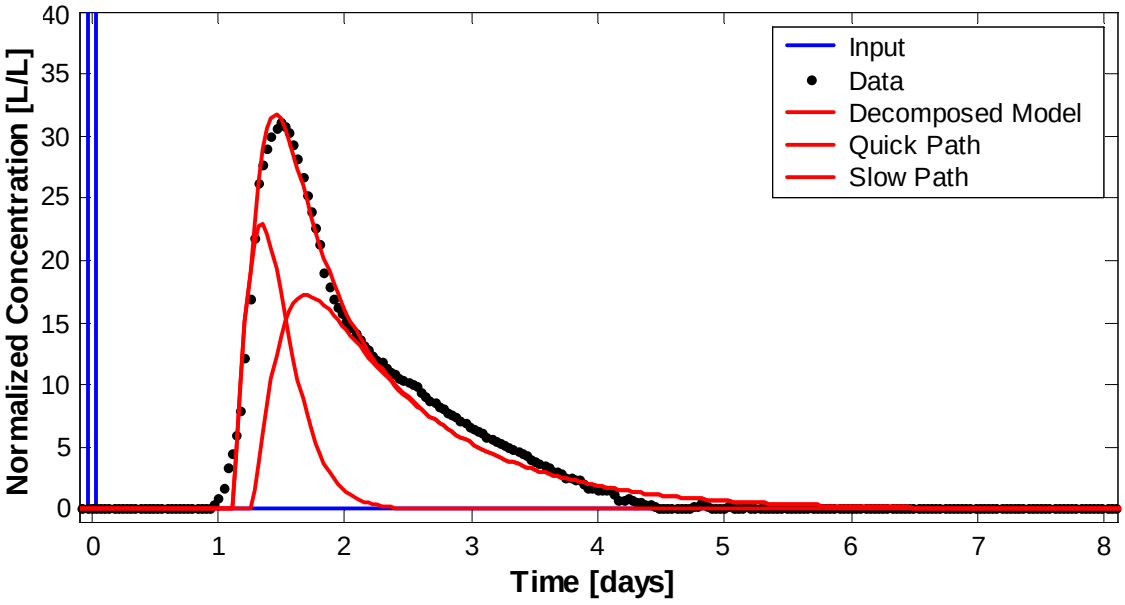

Figure 6.7. Series 0, Bed 11: Decomposed model B with optimised time lag Δ

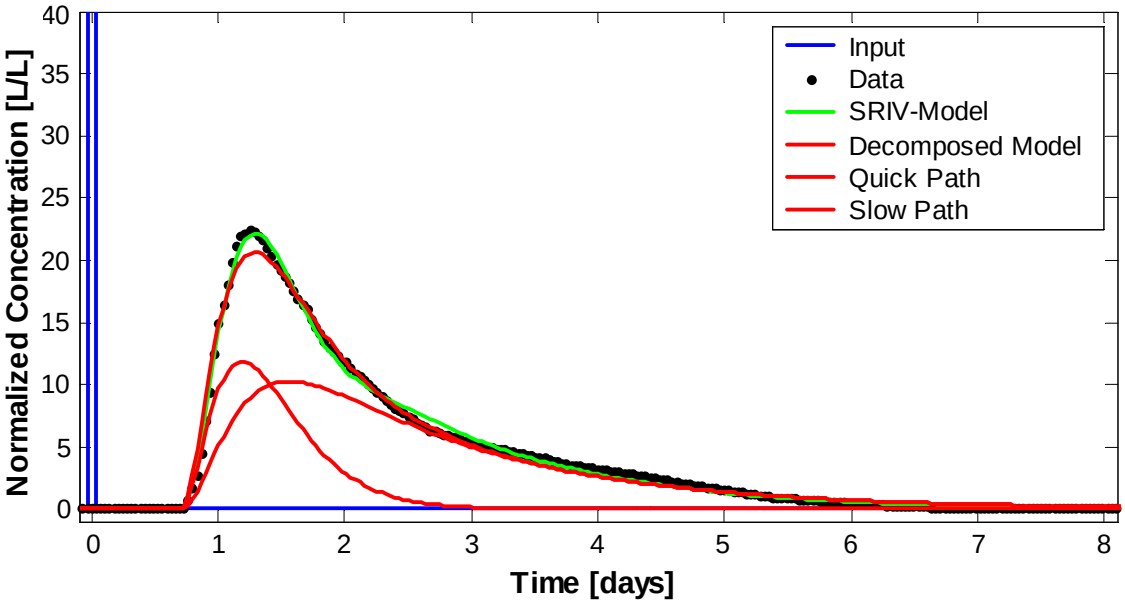

Figure 6.8. Series 1, Bed 2: SRIV identified model and decomposed model A

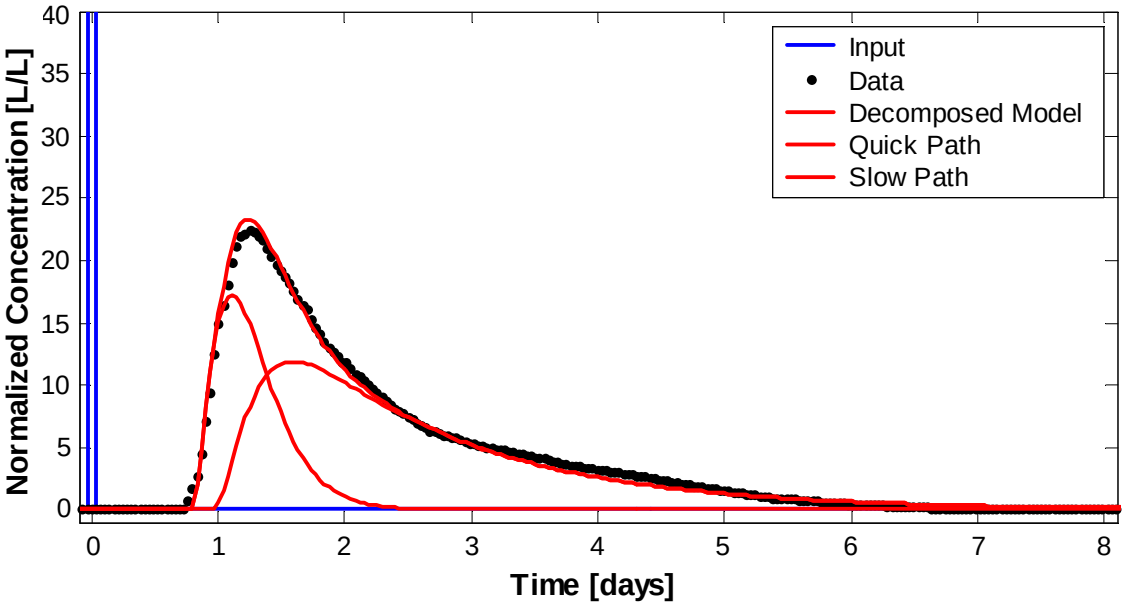

Figure 6.9. Series 1, Bed 2: Decomposed model B with optimised time lag Δ

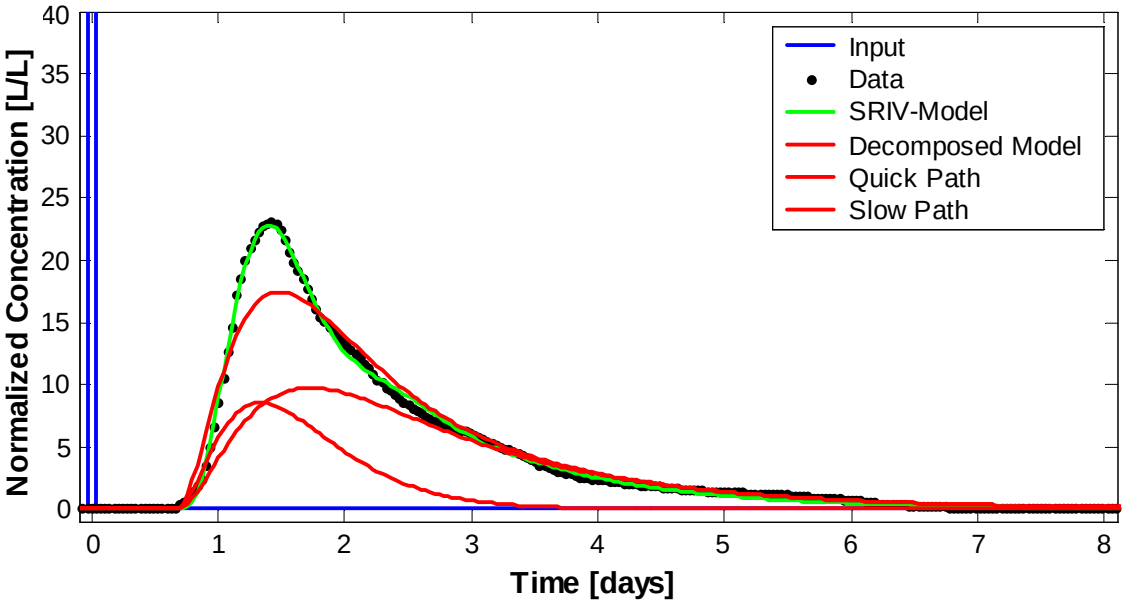

Figure 6.10. Series 1, Bed 4: SRIV identified model and decomposed model A

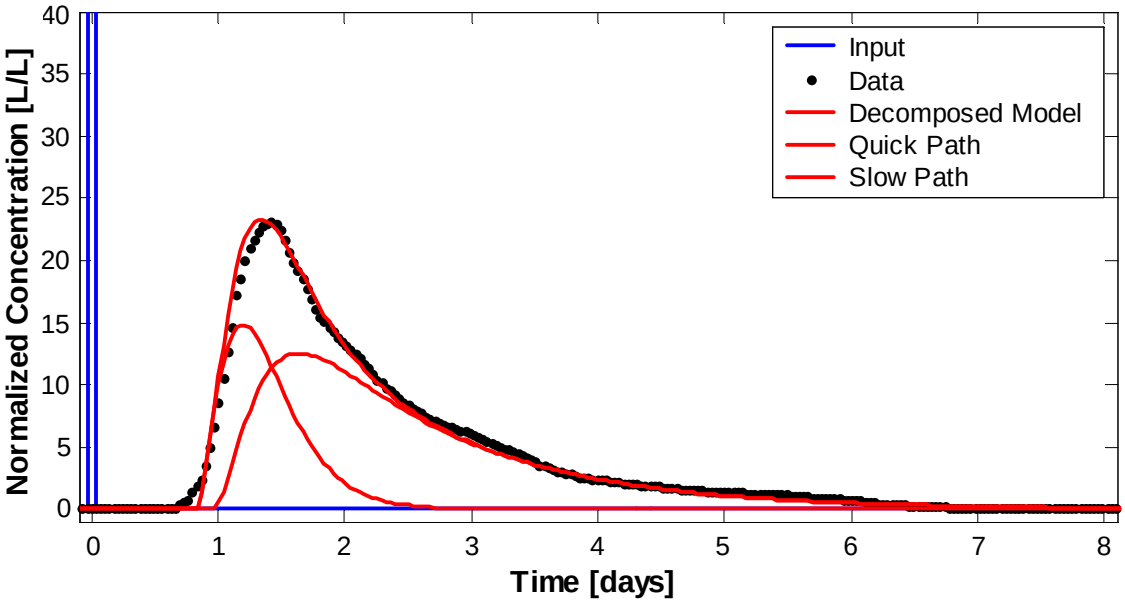

Figure 6.11. Series 1, Bed 4: Decomposed model B with optimised time lag Δ

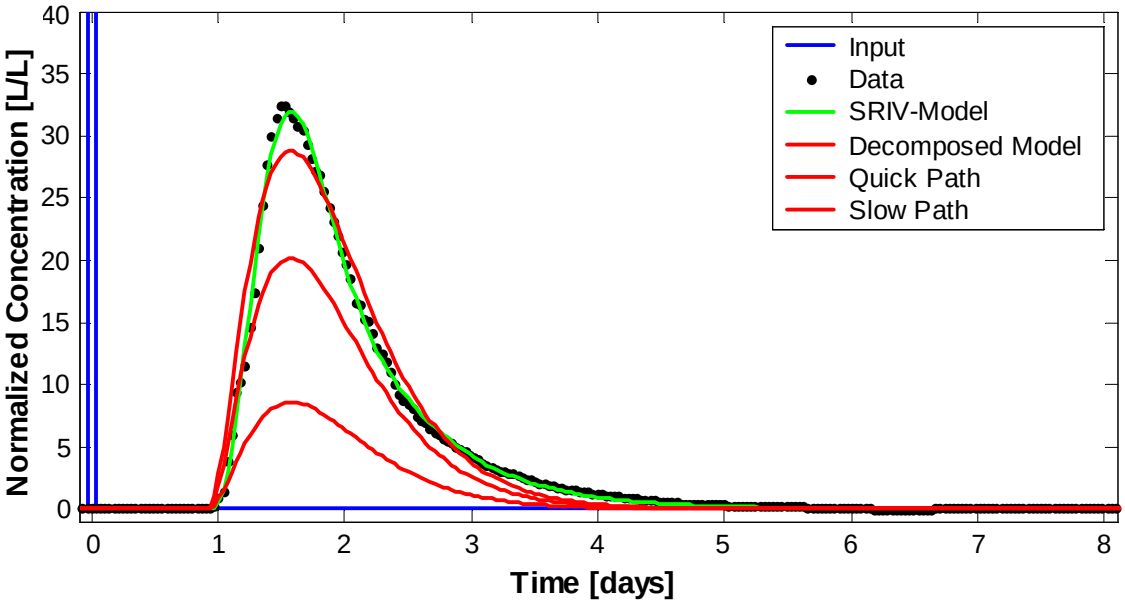

Figure 6.12. Series 1, Bed 11: SRIV identified model and decomposed model A

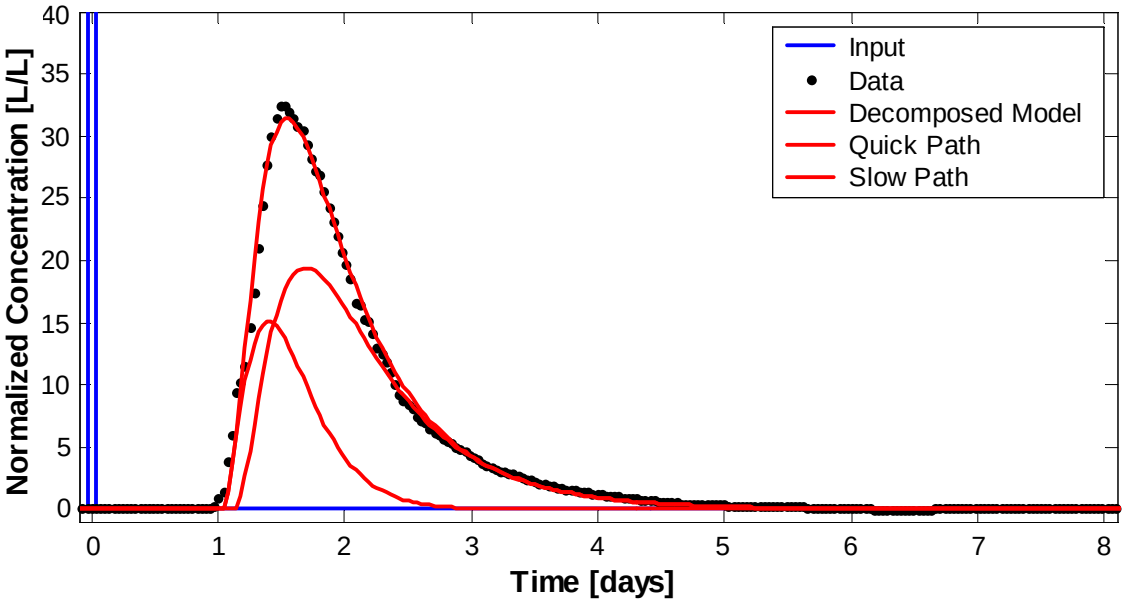

Figure 6.13. Series 1, Bed 11: Decomposed model B with optimised time lag Δ

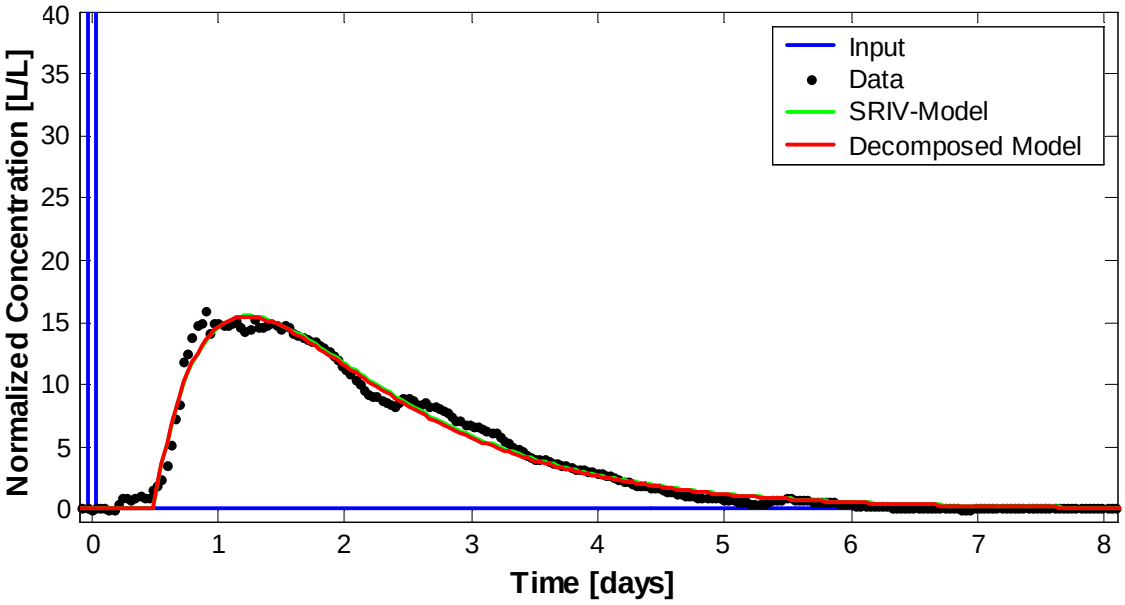

Figure 6.14. Series 2, Bed 2: SRIV identified model and decomposed model

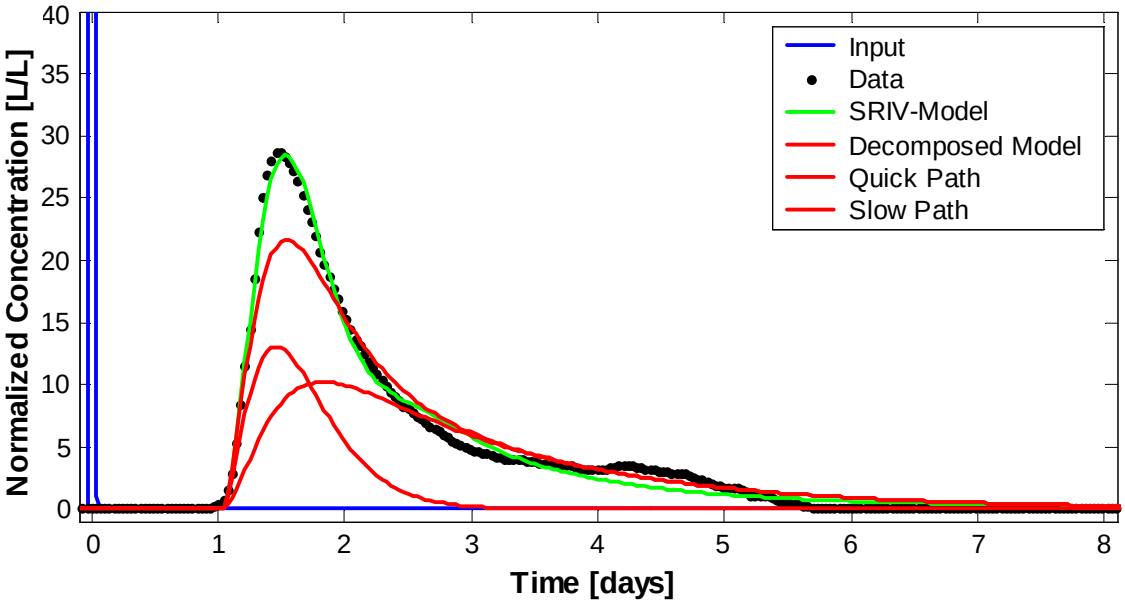

Figure 6.15. Series 2, Bed 4: SRIV identified model and decomposed model A

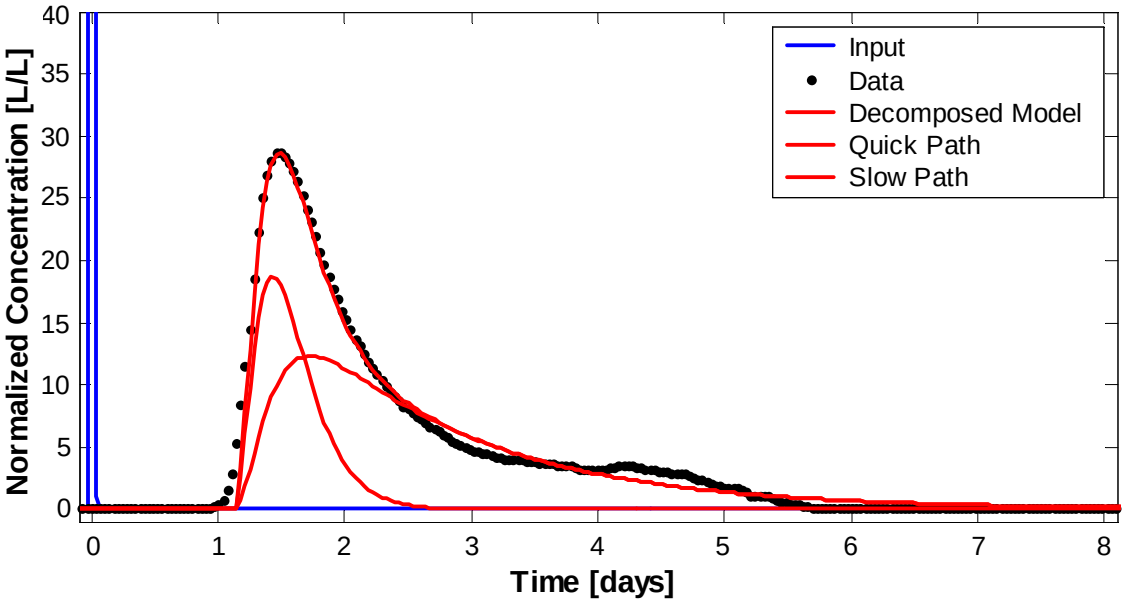

Figure 6.16. Series 2, Bed 4: Decomposed model B with optimised time lag Δ

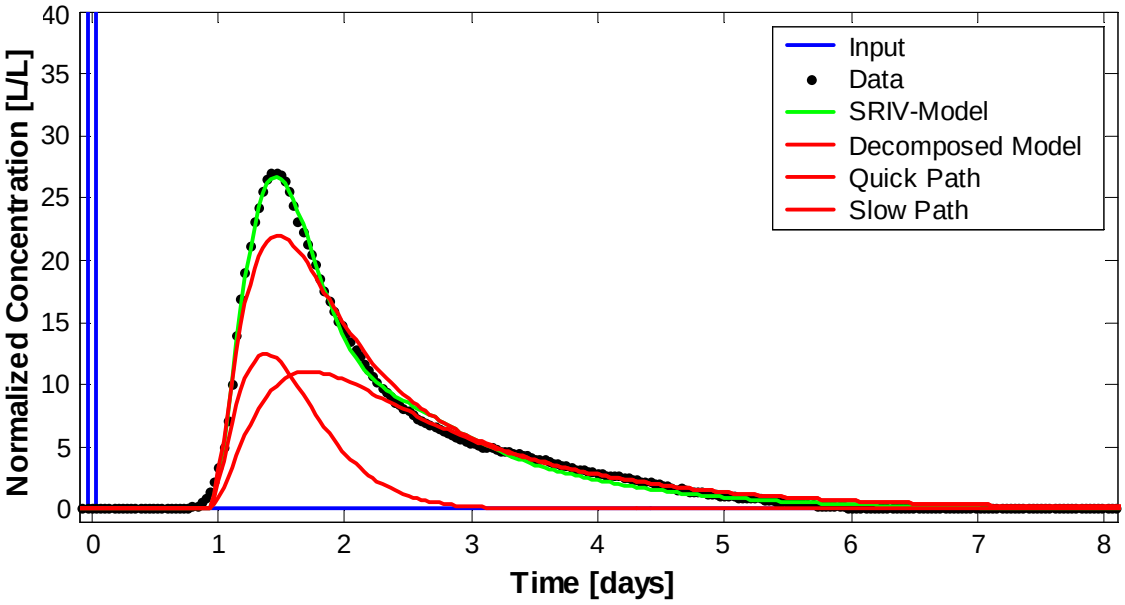

Figure 6.17. Series 2, Bed 10: SRIV identified model and decomposed model A

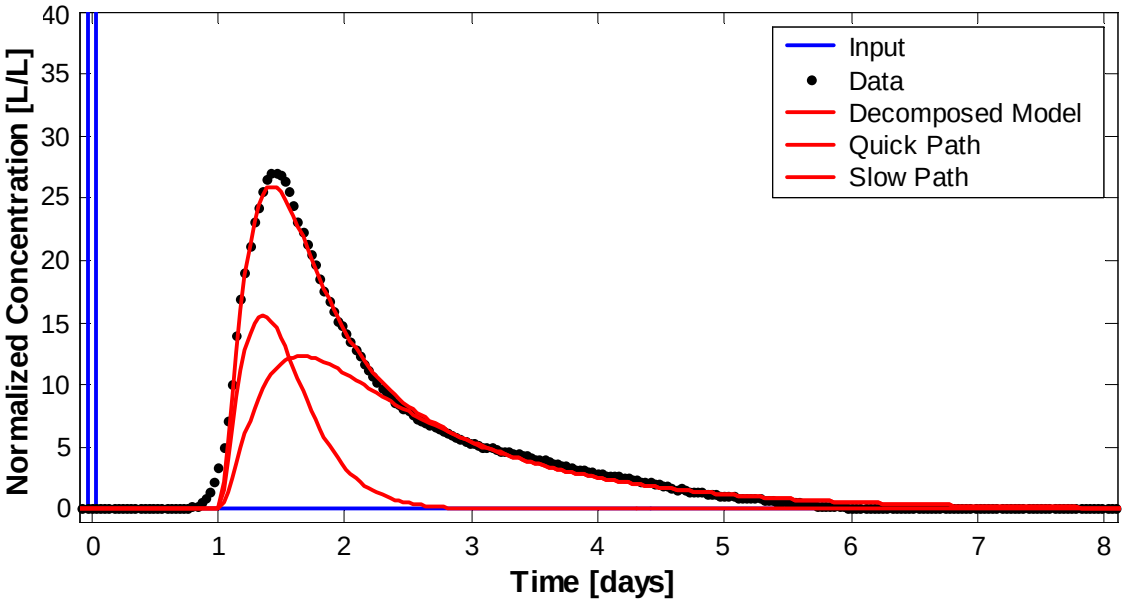

Figure 6.18. Series 2, Bed 10: Decomposed model B with optimised time lag Δ

Table 6.9. Coefficient of determination for "best" identified transfer function models

Test Name	SRIV model [-]	Decomposed model A [-]	Decomposed model B [-]
Series 0, Bed 4	0.98839	0.95681	0.96007
Series 0, Bed 11	0.99701	0.98391	0.99198
Series 1, Bed 2	0.99636	0.99282	0.99746
Series 1, Bed 4	0.99799	0.95739	0.99685
Series 1, Bed 11	0.99796	0.97923	0.99872
Series 2, Bed 2	0.98738	0.98786	-
Series 2, Bed 4	0.99010	0.94940	0.99051
Series 2, Bed 10	0.99689	0.97559	0.99694

Table 6.10. Eigenvalues of the *A*-polynom of the transfer functions

Test Name	Eigenvalues of *A*-polynomial [-]
Series 0, Bed 4	0.982, 0.855 ± 0.252i, 0.744
Series 0, Bed 11	0.890 ± 0.184i, 0.970 ± 0.0143i
Series 1, Bed 2	1.016, 0.960, 0.895 ± 0.140i
Series 1, Bed 4	0.900 ± 0.180i, 0.983, 0.863
Series 1, Bed 11	0.868 ± 0.166i, 0.965, 0.835
Series 2, Bed 2	0.972, 0.932
Series 2, Bed 4	0.980 ± 0.036i, 0.889 ± 0.154i
Series 2, Bed 10	0.989 ± 0.037i, 0.889 ± 0.146i

Table 6.11. ADZ-cell residence times

Test Name	Decomposed model A				Decomposed model B			
	Eigen-values	$T_c(G_1)$	Eigen-values	$T_c(G_2)$	Eigen-values	$T_c(G_1)$	Eigen-values	$T_c(G_2)$
	[-]	[days]	[-]	[days]	[-]	[days]	[-]	[days]
Series 0, Bed 4	0.743	0.12	0.971	1.90	0.682	0.09	0.971	1.2
Series 0, Bed 11	0.830	0.19	0.965	0.96	0.75	0.12	0.964	0.96
Series 1, Bed 2	0.865	0.24	0.978	1.53	0.836	0.19	0.977	1.47
Series 1, Bed 4	0.900	0.33	0.976	1.41	0.846	0.21	0.974	1.34
Series 1, Bed 11	0.900	0.33	0.898	0.32	0.751	0.12	0.947	0.63
Series 2, Bed 2	0.930	1.22	0.972	0.49	-	-	-	-
Series 2, Bed 4	0.852	0.22	0.979	1.60	0.845	0.21	0.978	1.53
Series 2, Bed 10	0.858	0.23	0.976	1.41	0.832	0.19	0.97	1.32

Table 6.12. Travel times of "best" identified and decomposed models

Test Name	advective time delay τ								Travel Time $\bar{t}$							
	SRIV-model		Decomposed model A		Decomposed model B				Centroid of RTD	SRIV model	Decomposed model A			Decomposed model B		
					quick path		slow path				quick path	slow path	sum	quick path	slow path	sum
	δ [time steps]	τ [days]	δ [time steps]	τ [days]	δ [time steps]	τ [days]	$\delta+\Delta$ [time steps]	τ [days]	[days]	[days]	[days]	[days]	[days]	[days]	[days]	[days]
Series 0, Bed 4	30	1.04	30	1.04	31	1.08	33 (+2)	1.15	-	2.91	1.38	3.20	2.86	1.35	2.52	2.32
Series 0, Bed 11	31	1.08	31	1.08	33	1.15	36 (+3)	1.25	2.07	2.02	1.58	2.36	2.12	1.51	2.45	2.22
Series 1, Bed 2	22	0.76	22	0.76	23	0.80	26 (+3)	0.90	2.23	2.24	1.43	2.67	2.30	1.38	2.76	2.38
Series 1, Bed 4	21	0.73	21	0.73	25	0.87	29 (+4)	1.01	2.25	2.25	1.67	2.72	2.40	1.49	2.76	2.37
Series 1, Bed 11	28	0.97	28	0.97	30	1.04	36 (+6)	1.25	2.00	1.99	1.90	1.91	1.90	1.41	2.13	2.02
Series 2, Bed 2	15	0.52	15	0.52	-	-	-	-	2.09	-	-	-	2.19	-	-	-
Series 2, Bed 4	31	1.08	31	1.08	31	1.08	35 (+4)	1.22	2.30	2.40	1.68	2.99	2.59	1.70	3.16	2.44
Series 2, Bed 10	28	0.97	28	0.97	29	1.01	33 (+4)	1.15	2.19	2.21	1.60	2.75	2.40	1.57	2.84	2.34

Table 6.13. Flow fractions and dispersive fractions of models

Test Name	Fractions of flow in slow path		Dispersive Fraction								
	Deomp. Model A	Decomp. Model B	SRIV model	Decomposed model A				Decomposed model B			
				quick path	slow path	sum	model	quick path	slow path	sum	model
	[-]	[-]	[s/s]	[s/s]	[s/s]	[s/s]	[s/s]	[s/s]	[s/s]	[s/s]	[s/s]
Series 0, Bed 4	0.81	0.83	0.64	0.25	0.67	0.59	0.64	0.20	0.55	0.49	0.54
Series 0, Bed 11	0.72	0.76	0.47	0.32	0.54	0.48	0.48	0.24	0.49	0.43	0.48
Series 1, Bed 2	0.69	0.72	0.66	0.47	0.71	0.64	0.66	0.42	0.67	0.60	0.66
Series 1, Bed 4	0.54	0.69	0.68	0.56	0.73	0.65	0.68	0.42	0.64	0.57	0.63
Series 1, Bed 11	0.76	0.86	0.51	0.49	0.49	0.49	0.51	0.26	0.41	0.39	0.49
Series 2, Bed 2		-	0.76	-	-	-	0.76	-	-	-	-
Series 2, Bed 4	0.53	0.51	0.55	0.36	0.64	0.51	0.53	0.37	0.62	0.49	0.56
Series 2, Bed 10	0.58	0.60	0.56	0.39	0.65	0.54	0.56	0.36	0.60	0.50	0.57

Table 6.14. Theoretical volumes of the ADZ-cells V_G and the model V_{Sum} calculated from the residence times in comparison to the volumes V_a calculated from water head observations

Test Name	Discharge	Decomposed model A			Decomposed model B			Water head observations
	Q [L/s]	V_{G1} [m^3]	V_{G2} [m^3]	V_{Sum} [m^3]	V_{G1} [m^3]	V_{G2} [m^3]	V_{Sum} [m^3]	V_a [m^3]
Series 0, Bed 4	3.96	44	746	688	31	409	407	710
Series 0, Bed 11	2.05	34	170	199	21	169	176	400
Series 1, Bed 2	5.55	115	734	797	93	704	721	1,200
Series 1, Bed 4	4.24	121	517	659	76	491	514	810
Series 1, Bed 11	2.10	60	58	178	22	115	146	380
Series 2, Bed 2	5.16	544	218	762	-	-	0	1,200
Series 2, Bed 4	3.87	74	535	534	69	511	433	790
Series 2, Bed 10	2.33	46	284	300	38	265	251	360

6.2.2.3 Monte Carlo evaluation of uncertainty

The parameters of advective time delay, ADZ-cell residence times and partition percentages of the parallel pathway [4 2 δ] model structure have been subject to the Monte Carlo analysis (Chapter 3.4). The process parameter estimation showed for model B, that a better fit can be achieved when the advective time delay is subject to the estimation process and not fixed to the value gained through the SRIV-estimation process. To highlight this effect, the parameter of advective time delay of the model A is as well subject to the Monte Carlo analysis. Up to 50,000 evaluations for model and test were needed to produce at least 2,000 evaluations with a coefficient of determination above a chosen threshold. The thresholds as well as the "dotty plots" and the computed frequency plots of the evaluations are shown in Figure 6.19 to Figure 6.25 for the model A and Figure 6.26 to Figure 6.32 for the model B. The results of the Monte Carlo analysis are shown in Table 6.15 for the model A and in Table 6.16 for the model B.

The surface of the dotty plots and the shape of the frequency plots are not in all cases very smooth, indicating that the 2,000 selected evaluations are not sufficient enough to fully converge the Monte Carlo analysis. However, the qualitative shape of the dotty plots as well as the standard deviations of the frequency plots indicates how "narrow" each parameter is defined within that model to simulate the observed residence time distributions. Since not all dotty plots and frequency plots have a symmetrical shape (e.g. the residence time of Figure 6.23), the computed mean values won't correspond to the values with the highest coefficient of

determination. Therefore the "best" computed evaluations are given as well for comparison in those tables.

The advective time delay τ for the model A (Figure 6.19 to Figure 6.25) is for all tests quite well defined and shows only a narrow span width. Further, the Monte Carlo evaluated advective time delays are longer than those identified with the SRIV model. The additional time delay is between one and three time steps (see Table 6.12 and Table 6.15). As seen before at the estimation process of the model B, the additional time delay promotes a better fit of the model to the peak of the distribution but is resulting in models that are even more unable to describe the first section of the rising limbs. Since the total travel time of the MCS evaluated model is more or less equivalent to the travel times gained from the data themselves or the model estimation, the longer advective time delays result in shorter ADZ-cell residence times. Additionally, longer advective time delays result in smaller dispersive fractions.

Interestingly, the Monte Carlo analysis of the test Series 1 Bed 11 (Figure 6.23) shows quite broad defined residence times for the slow ADZ-cell $T_c(G_2)$ and for the partition percentage. Initially, the SRIV algorithm identified a [3 1 δ] model as a best model and the [4 2 δ] model was just chosen to simplify the comparison with the models for the other tests.

The Monte Carlo analysis for the model B (Figure 6.26 to Figure 6.32) gives similar results for the "best" parameters compared to the parameter estimation process. Generally, the advective time delays for the quick flow path, the residence time for the quick ADZ-cells $T_c(G_1)$ and for the partition percentage are quite well defined from the peak of the dotty plots. The advective time delays for the slow flow path and the residence time for the slow ADZ-cells $T_c(G_2)$ are generally less well defined. The dotty plots of the test Series 0, Bed 11 (Figure 6.27) show two peaks for the residence time $T_c(G_1)$ and the partition percentage, while dotty plots and the frequency plots of test Series 1, Bed 2 (Figure 6.28) indicate two peaks for the advective time delay of the slow flow path, the residence time $T_c(G_1)$ and the partition percentage. In both cases, the "best" parameters can be easily identified from the absolute maximum of the peaks. However, without this knowledge, the algorithm for the model parameter estimation can converge on a local maximum rather than on the absolute maximum.

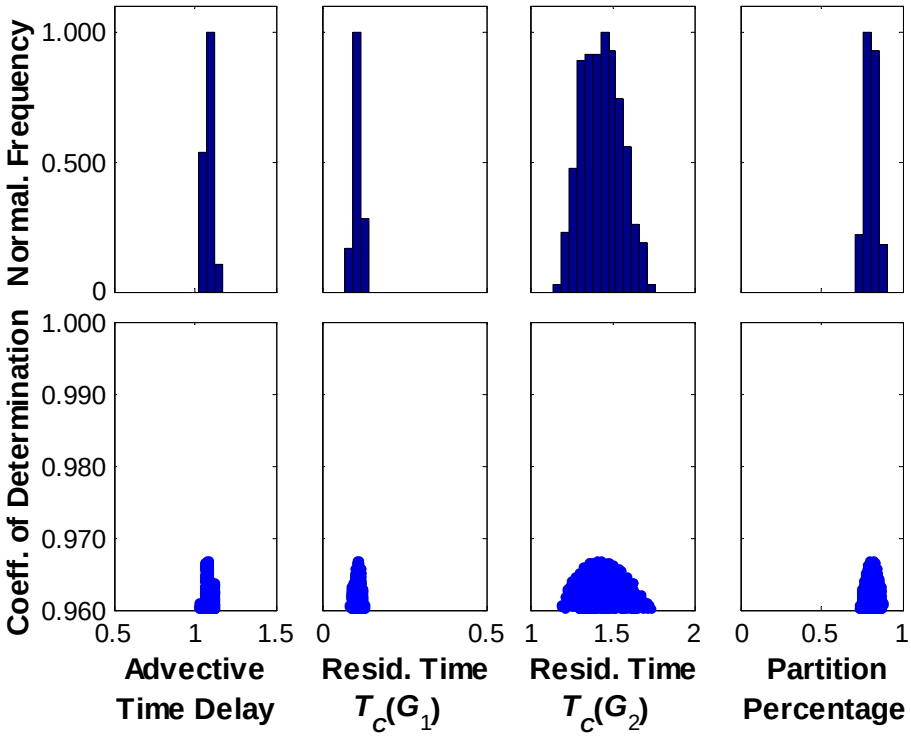

Figure 6.19. Series 0, Bed 04: Monte Carlo analysis of model A

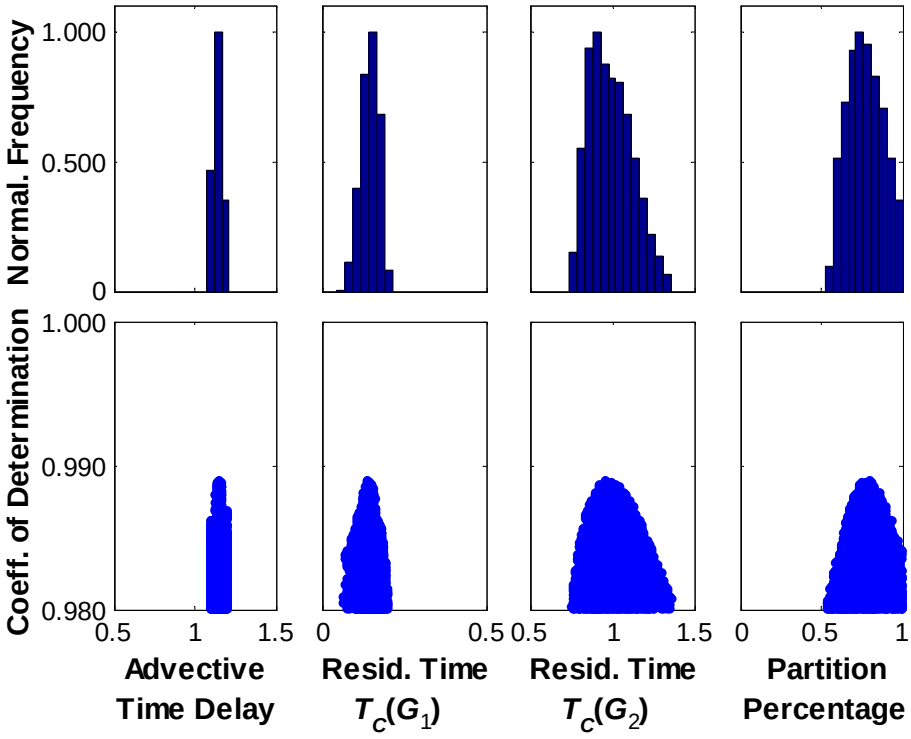

Figure 6.20. Series 0, Bed 11: Monte Carlo analysis of model A

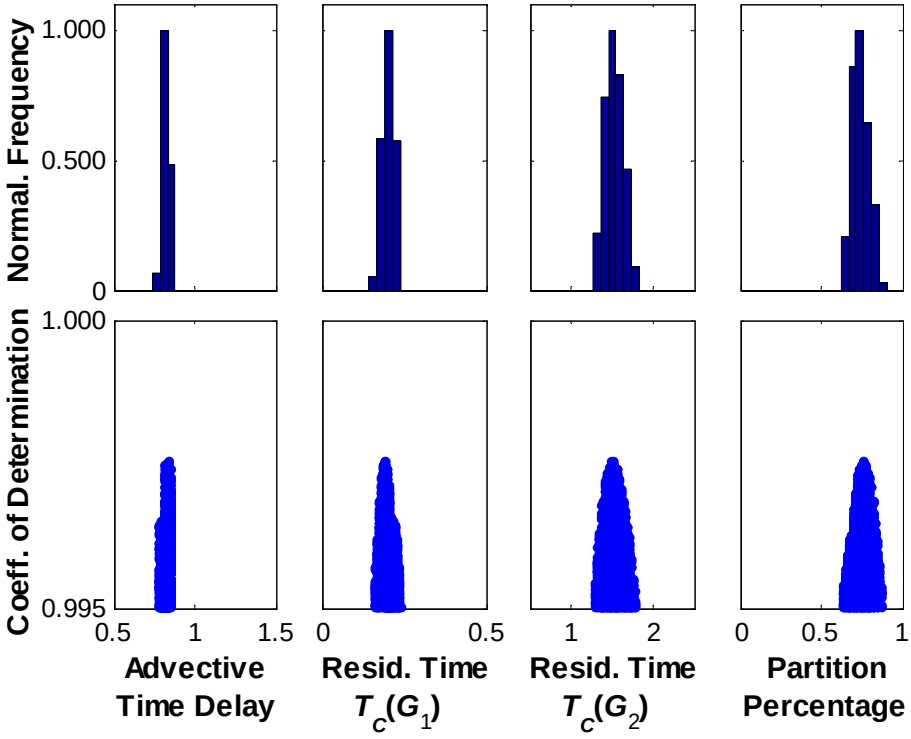

Figure 6.21. Series 1, Bed 02: Monte Carlo analysis of model A

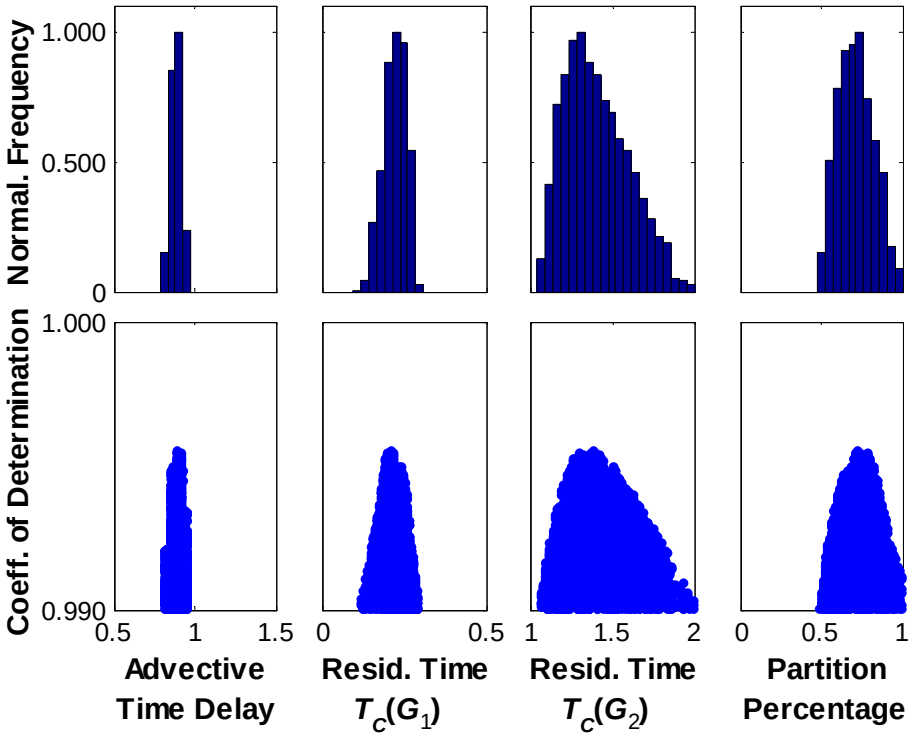

Figure 6.22. Series 1, Bed 04: Monte Carlo analysis of model A

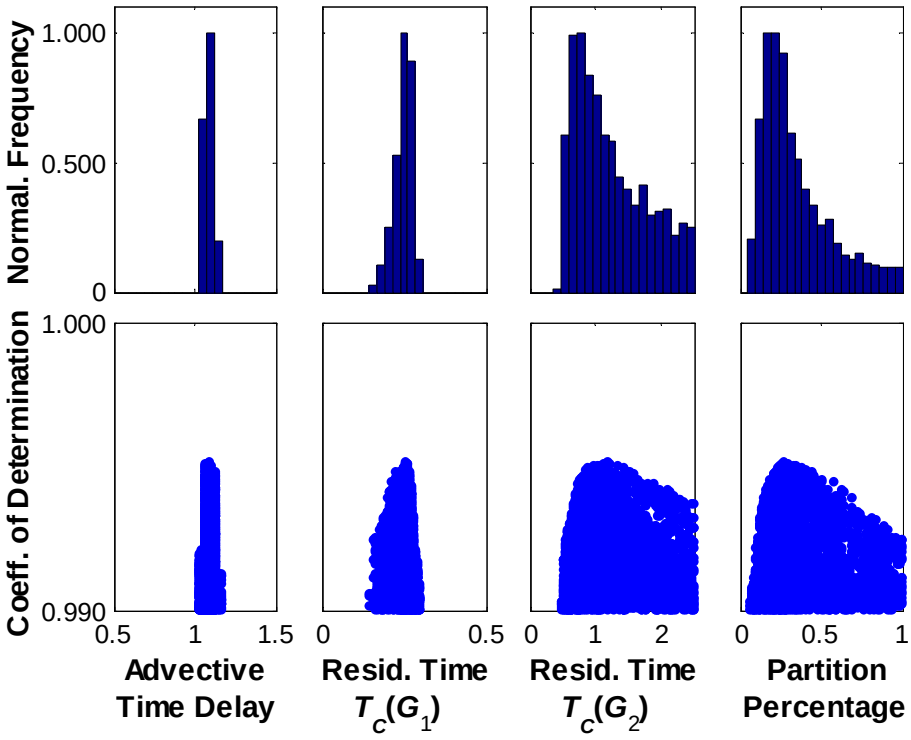

Figure 6.23. Series 1, Bed 11: Monte Carlo analysis of model A

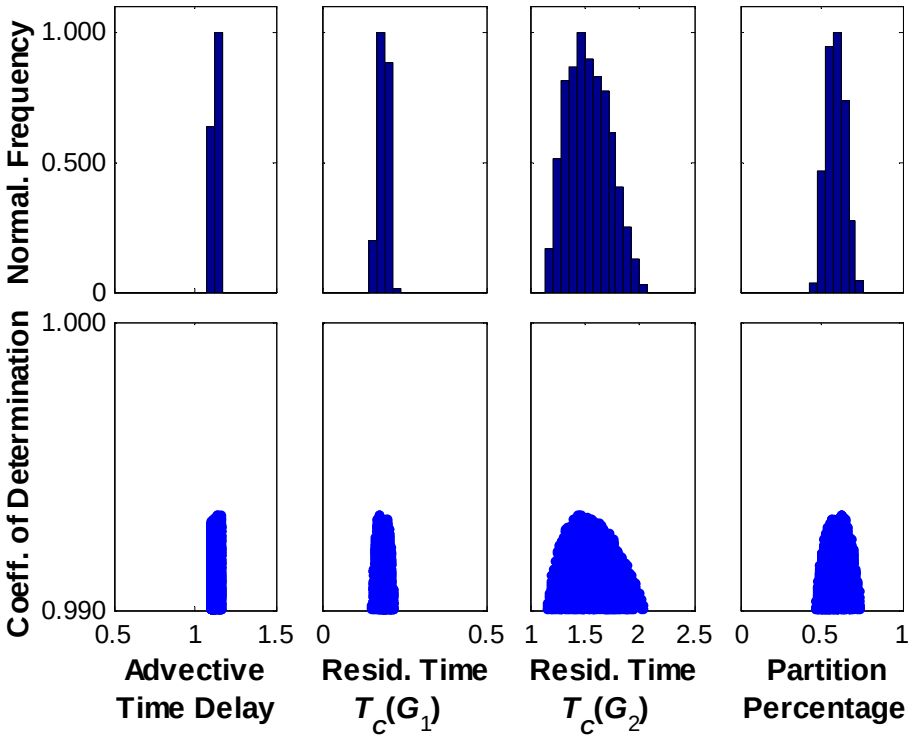

Figure 6.24. Series 2, Bed 04: Monte Carlo analysis of model A

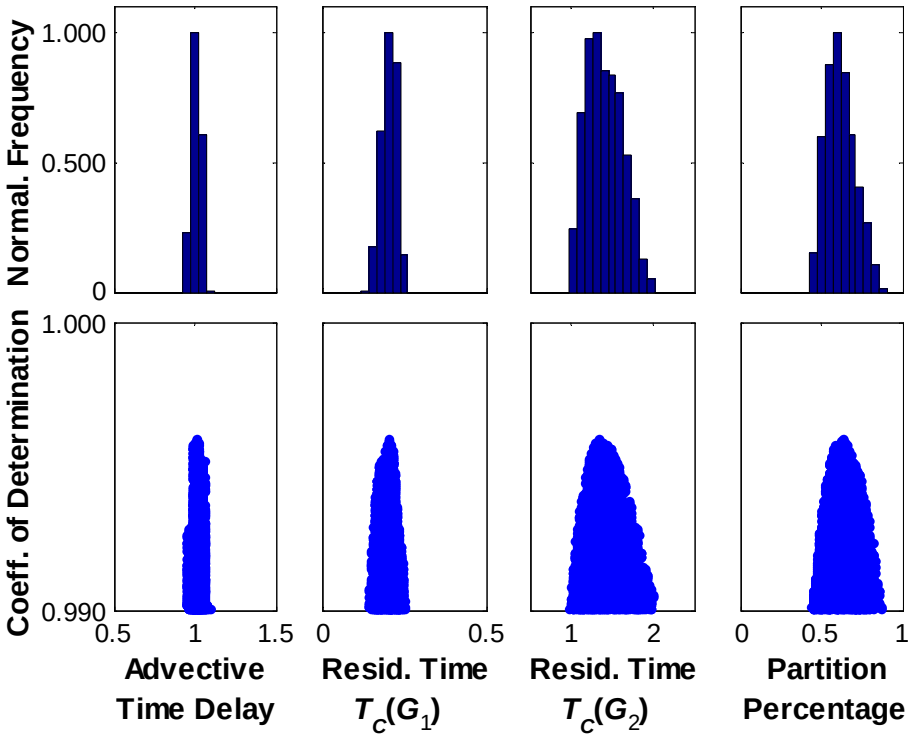

Figure 6.25. Series 2, Bed 10: Monte Carlo analysis of model A

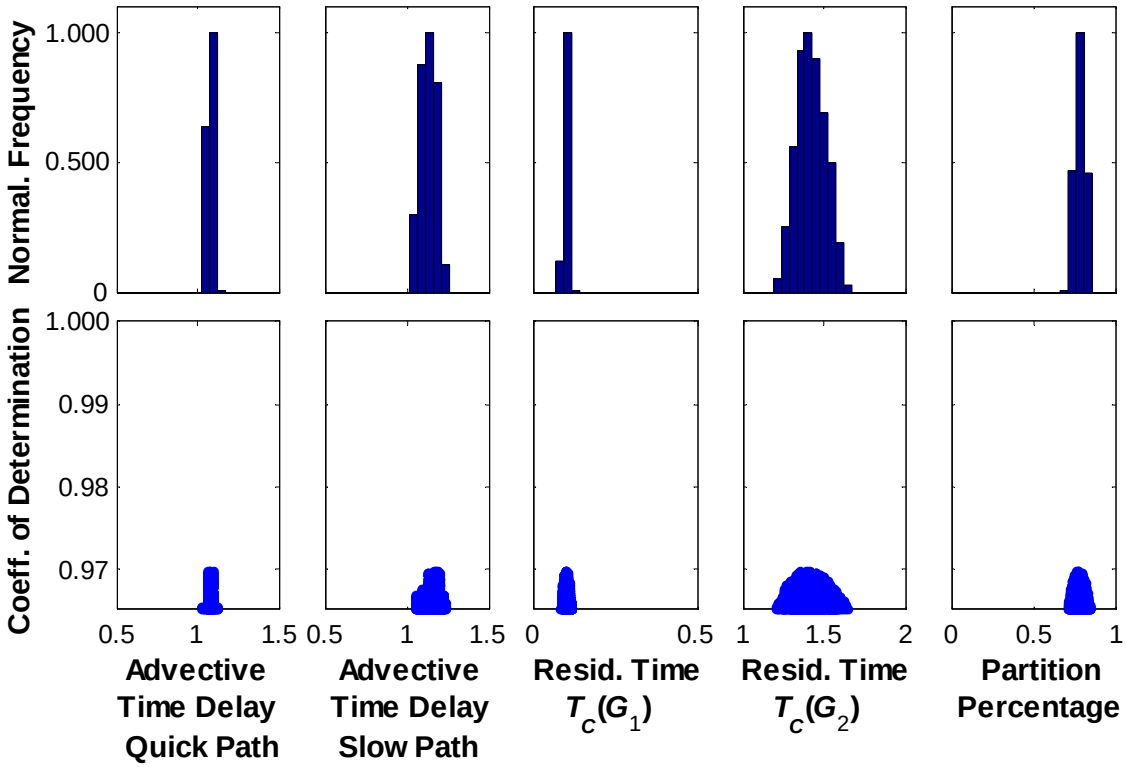

Figure 6.26. Series 0, Bed 04: Monte Carlo analysis of model B

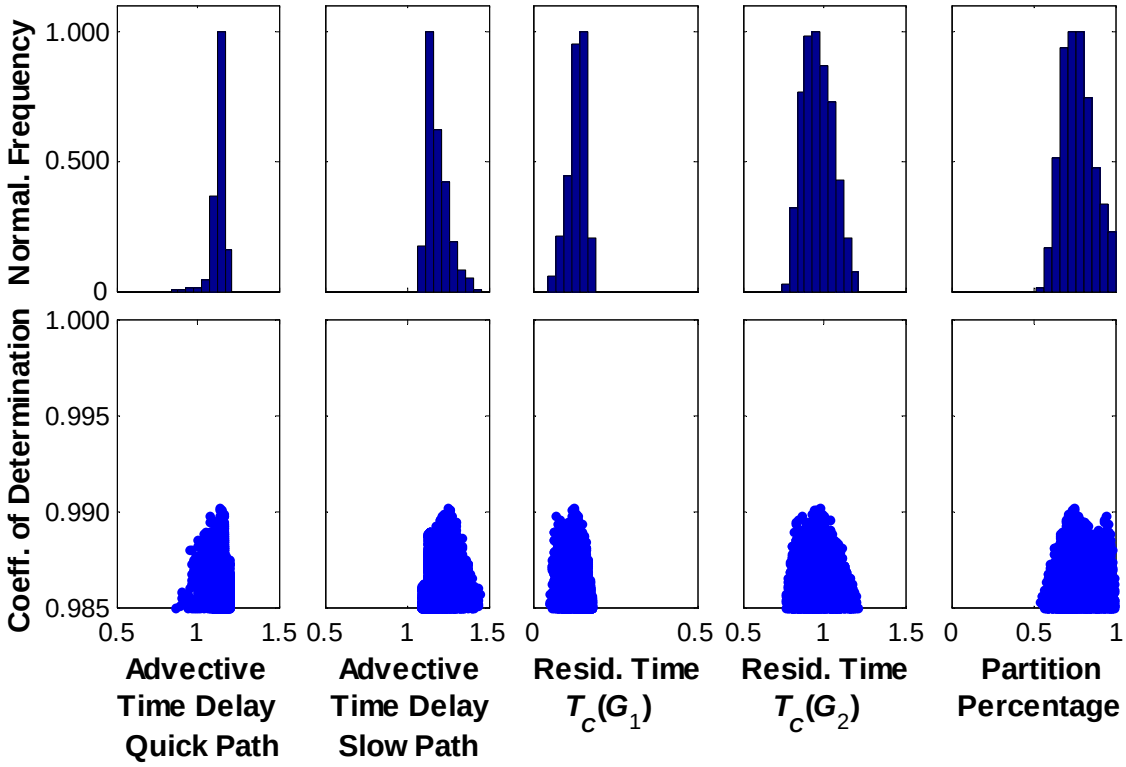

Figure 6.27. Series 0, Bed 11: Monte Carlo analysis of model B

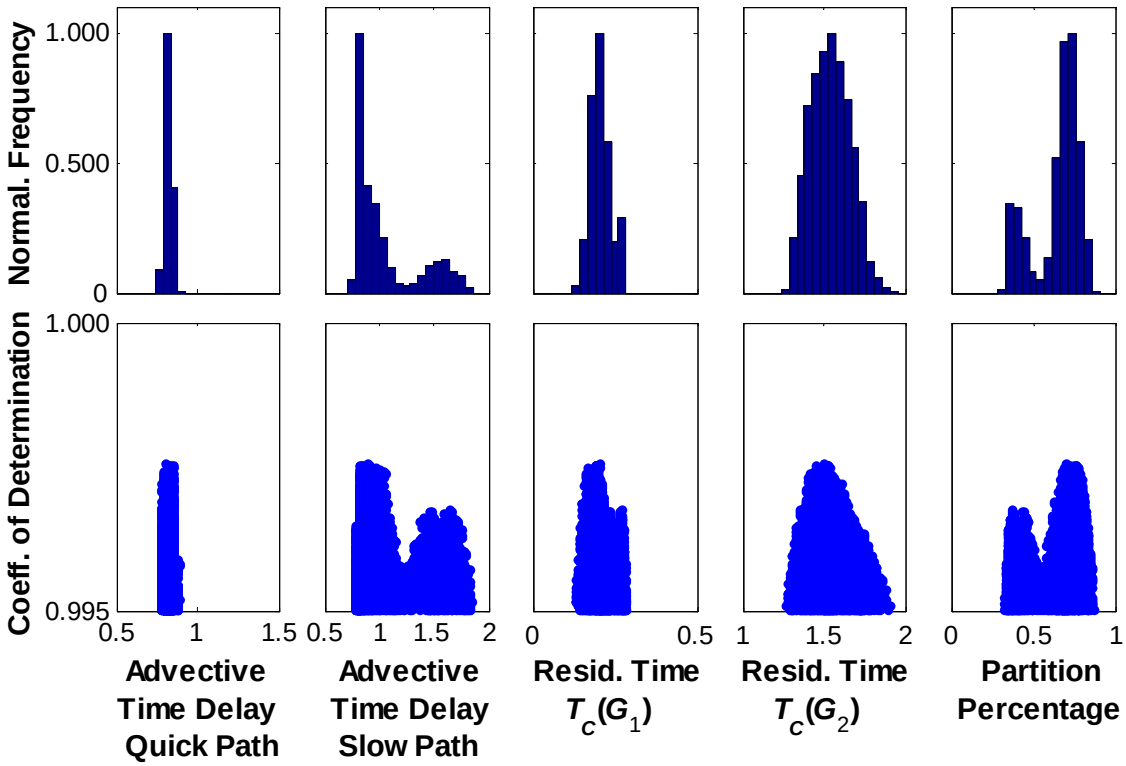

Figure 6.28. Series 1, Bed 02: Monte Carlo analysis of model B

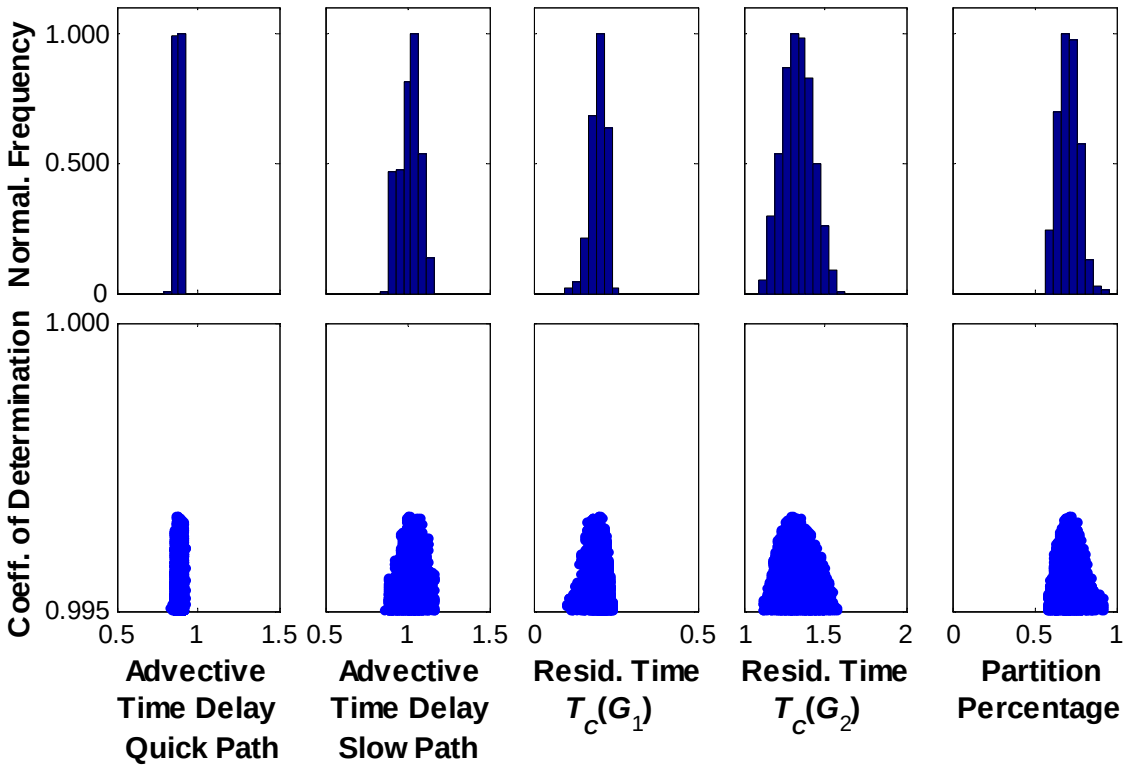

Figure 6.29. Series 1, Bed 04: Monte Carlo analysis of model B

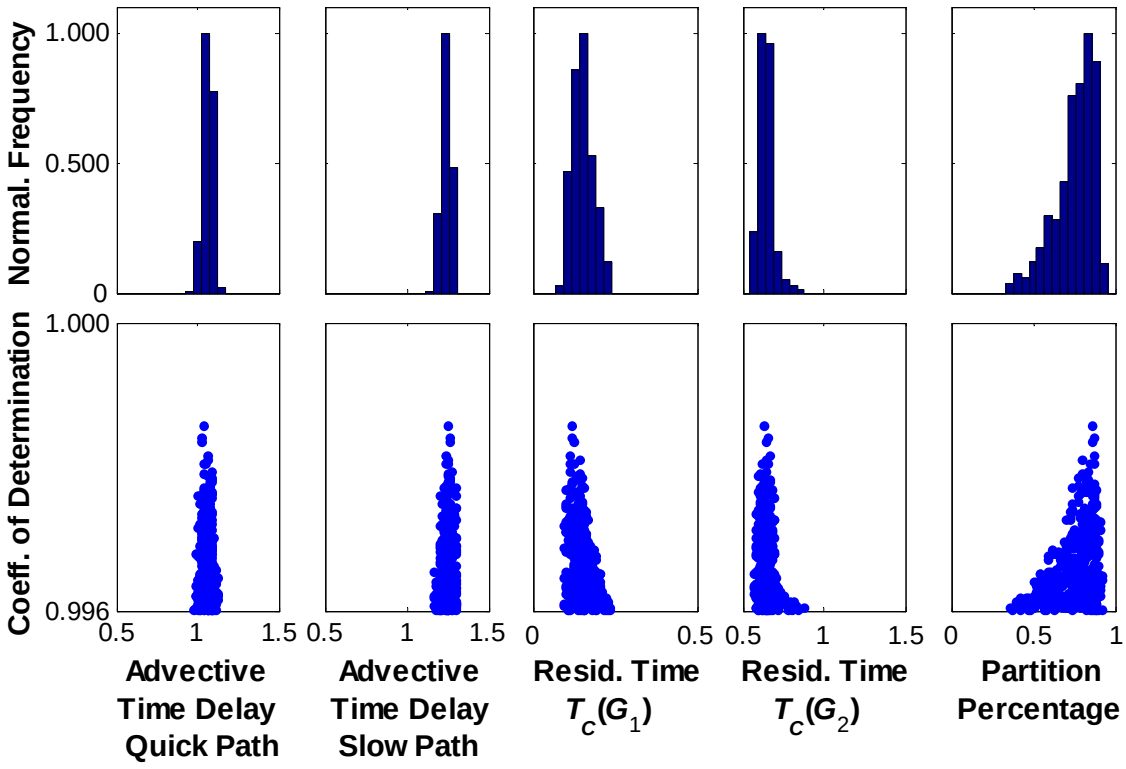

Figure 6.30. Series 1, Bed 11: Monte Carlo analysis of model B

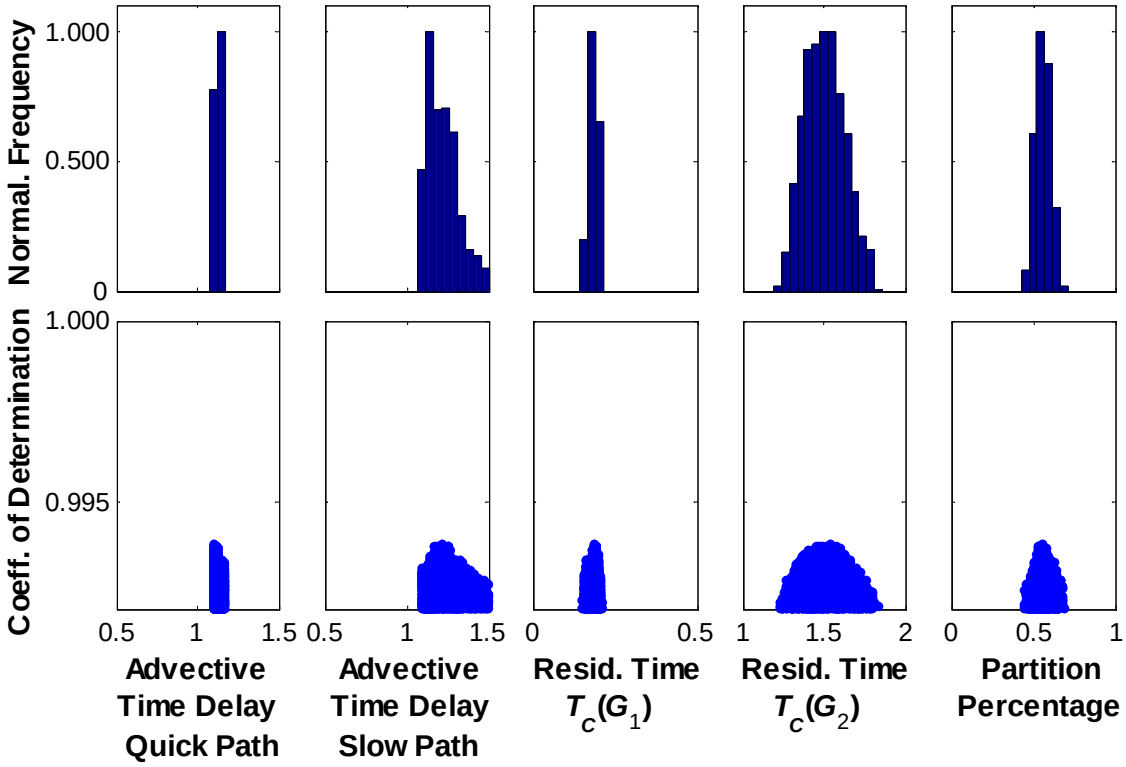

Figure 6.31. Series 2, Bed 04: Monte Carlo analysis of model B

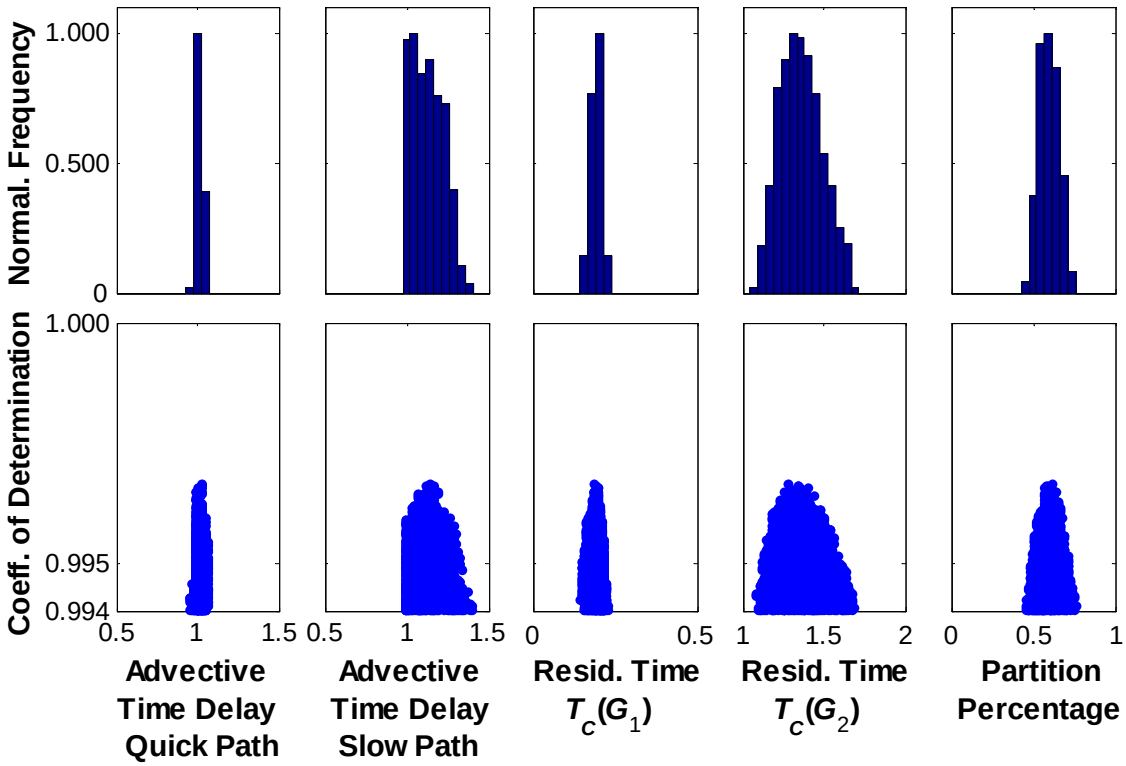

Figure 6.32. Series 2, Bed 10: Monte Carlo analysis of model B

Table 6.15. Results of Monte Carlo analysis for decomposed model A

Test Name	advective time delay quick path			ADZ-cell residence times				Fractions of flow in slow path		Total travel time	
	mean δ [time steps]	mean τ [days]	best τ [days]	mean $T_c(G_1)$ [days]	best $T_c(G_1)$ [days]	mean $T_c(G_2)$ [days]	best $T_c(G_2)$ [days]	mean value [-]	best value [-]	mean $\bar{t}$ [days]	best $\bar{t}$ [days]
Series 0, Bed 4	31	1.08 (0.03)	1.08	0.11 (0.01)	0.11	1.44 (0.12)	1.41	0.81 (0.04)	0.82	2.48	2.47
Series 0, Bed 11	33	1.14 (0.03)	1.15	0.15 (0.03)	0.14	0.99 (0.13)	0.95	0.77 (0.11)	0.80	2.23	2.22
Series 1, Bed 2	24	0.82 (0.03)	0.84	0.20 (0.02)	0.19	1.52 (0.11)	1.50	0.74 (0.05)	0.76	2.40	2.41
Series 1, Bed 4	25	0.89 (0.04)	0.89	0.22 (0.04)	0.21	1.41 (0.19)	1.38	0.71 (0.11)	0.73	2.40	2.38
Series 1, Bed 11	31	1.08 (0.03)	1.08	0.25 (0.03)	0.25	1.24 (0.54)	1.17	0.35 (0.22)	0.27	2.17	2.09
Series 2, Bed 4	32	1.12 (0.02)	1.14	0.19 (0.02)	0.17	1.54 (0.19)	1.46	0.59 (0.06)	0.62	2.48	2.46
Series 2, Bed 10	29	1.01 (0.03)	1.01	0.20 (0.02)	0.20	1.41 (0.22)	1.35	0.62 (0.09)	0.63	2.37	2.34

Table 6.16. Results of Monte Carlo analysis for decomposed model B

Test Name	advective time delay quick path			advective time delay slow path			ADZ-cell residence times				Fractions of flow in slow path		Total travel time	
	mean δ [time steps]	mean τ [days]	best τ [days]	mean δ [time steps]	mean τ [days]	best τ [days]	mean $T_c(G_1)$ [days]	best $T_c(G_1)$ [days]	mean $T_c(G_2)$ [days]	best $T_c(G_2)$ [days]	mean value [-]	best value [-]	mean $\bar{t}$ [days]	best $\bar{t}$ [days]
Series 0, Bed 4	31	1.08 (0.02)	1.08	33	1.14 (0.05)	1.18	0.10 (0.01)	0.10	1.42 (0.09)	1.40	0.79 (0.03)	0.77	2.47	2.46
Series 0, Bed 11	33	1.13 (0.04)	1.14	34	1.19 (0.06)	1.25	0.13 (0.03)	0.12	0.96 (0.09)	0.98	0.77 (0.09)	0.75	2.22	2.24
Series 1, Bed 2	24	0.82 (0.03)	0.80	30	1.04 (0.29)	0.90	0.21 (0.03)	0.20	1.53 (0.12)	1.50	0.65 (0.14)	0.70	2.38	2.38
Series 1, Bed 4	25	0.88 (0.02	0.87	29	1.01 (0.07)	1.01	0.20 (0.02)	0.20	1.33 (0.09)	1.30	0.71 (0.06)	0.71	2.37	2.36
Series 1, Bed 11	31	1.06 (0.03)	1.03	35	1.24 (0.03)	1.25	0.15 (0.03)	0.12	0.65 (0.05)	0.63	0.75 (0.05)	0.86	2.02	2.02
Series 2, Bed 4	32	1.12 (0.02)	1.09	35	1.22 (0.09)	1.21	0.18 (0.02)	0.19	1.50 (0.12)	1.53	0.56 (0.05)	0.55	2.47	2.46
Series 2, Bed 10	29	1.01 (0.02)	1.02	32	1.13 (0.09)	1.14	0.19 (0.02)	0.19	1.36 (0.13)	1.28	0.60 (0.06)	0.62	2.35	2.32

6.2.3 Pollutant transport model with an advective-dispersive approach

The physics of flow of contaminated water through the subsurface gravel beds in the wetlands is similar to that of flow and contaminant transport in groundwater. In the research field of groundwater studies software-packages have been developed to simulate the processes in the underground, utilising two- or three-dimensional models (e.g. Zheng and Bennett, 2002). These software-packages are using different numerical approaches to solve the advection-dispersion equation. To check the usability of those packages for the modelling of the pollutants in the subsurface reed beds, trials were performed with the groundwater flow- and transport-modelling package "Modflow" (e.g. Zheng and Bennett, 2002), which is well known and widely used for groundwater modelling. While the simulated levels of the water head were consistent with the measurements in the field, the calculated residence time distributions from the "Modflow"-model could not be matched with the observed distributions.

The residence time distributions obtained were rather gaussian-shaped and did not show the distinctive tails of the observed residence time distributions. As discussed before, the dispersive effect of the gravel beds more likely to cause gaussian shaped residence time distributions, since the observations of longitudinal dispersion within the gravel bed did not show any significant build-up of tail of the residence time distributions. Obviously, the "Modflow"-model has to be much more detailed to be able to describe the flow and mixing patterns in the first open channel section. Further, the effect of the impulse of the inflowing water has to be modelled. Since such an impulse is not a "normal" boundary condition and since the necessary refinement of the model will not guarantee a working and, more important, realistic model, the use of groundwater software packages for these modelling purposes was not taken any further.

While the flow of the water, as soon as it leaves the first open channel section, is mainly unidirectional it seems reasonable to use a one-dimensional model that is based on the advection-dispersion equation. The one-dimensional model has to be extended with a module that is capable to model the turbulent flow conditions or to model the mixing in the first open channel section. The knowledge about the mixing behaviour was only deduced from visual observations and conclusions rather than from physical measurements. It therefore seems reasonable for this modelling purpose to use a simple approach instead of computational intensive numerical schemes such as finite-volume/finite-element models.

Idealising the first open channel sections as a mixing zone with a constant inflow and outflow, then a quite simple module describing the mixing behaviour is the continuously stirred tank reactor (CSTR), as described in Chapter 2.4.9. Clearly, this idealisation cannot hold true since the zone is not fully mixed. Further on, only one CSTR-module will be used in this combined CSTR/ADE model. The CSTR module will therefore also incorporate the effects of mixing of all other open channel sections. For the transport modelling in the gravel cells the

analytical solution of the ADE-equation in form of the routing procedure is used (Equation 2.58). The complete concept of this modelling approach is shown in Figure 6.33.

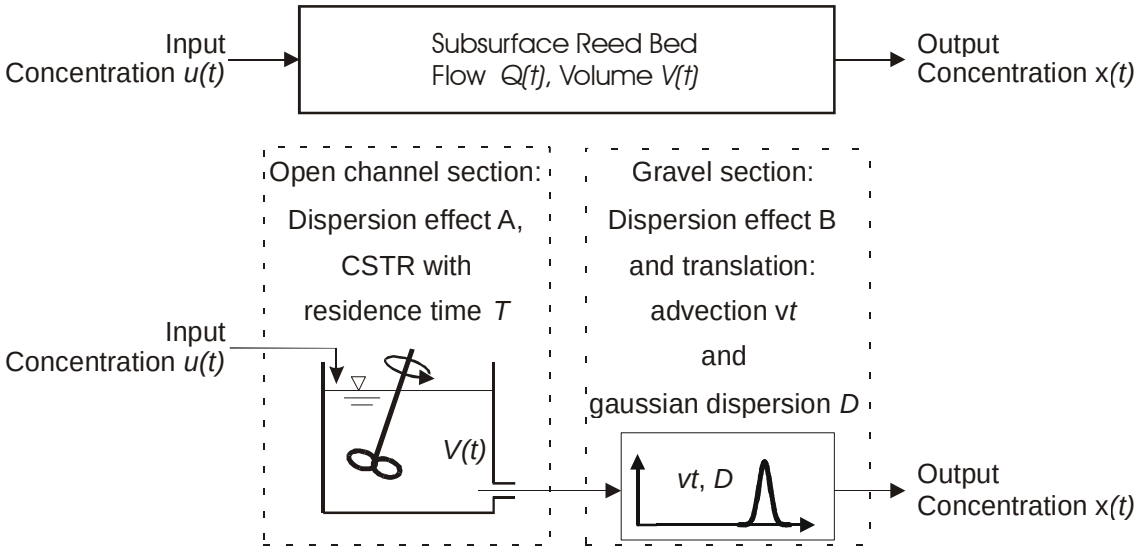

Figure 6.33. Conceptual model for a combined CSTR/ADE model for the transport of pollutant in the subsurface reed beds

6.2.3.1 Sensitivities to the parameters

Prior to the modelling procedure, it might be of interest to explore the sensitivity (Chapter 3.4.1) of the travel time to some parameters that had been observed or computed. The parameter of retention time of the CSTR of the previously explained conceptual model is gained in the model estimation process. Therefore it is not subject of the sensitivity analysis. Relevant factors for the travel time of the ADE-part of the conceptual model are observed parameters of the discharge Q, the porosity n and the water head h at the beginning of the reed bed as well as the hydraulic conductivity k that was calculated from observations but is related to the discharge Q. The routing procedure solution of the ADE was used to calculate the travel time of a pollutant through the reed bed. To compensate for the head loss and the increasing flow velocities, the whole reach of the bed was subdivided with a one-dimensional mesh. For each element of the mesh the water head and the transport of the pollutant were computed. While for the gravel cells and the open water sections a mesh-length of 2 m was chosen, for the gabions a mesh length of 0.6 m was chosen. The initial values of the parameters for the sensitivity analysis have been selected as typical values from the tables of Chapter 5 for the bed types equivalent to Bed 4 and Bed 11. For the computations of the sensitivity a parameter perturbation of 5% was selected and the sensitivities were calculated according to the procedures in Chapter 3.4. The computed sensitivities are shown in Table 6.17.

The results show that the highest sensitivity is associated with the measurement of the water head at the beginning of the subsurface reed bed for both bed types. Since it was shown in

Chapter 6.2.1.1 that the error in the measurement of this value is quite low with 5%, the sensitivity to this parameter is not as important as the sensitivity to the discharge. Here the sensitivity is slightly less for Bed 4 or nearly similar for Bed 11, but the error in the measurement is much higher and was estimated to be approximately 10%. The sensitivity of the hydraulic conductivity to the travel time is much lower for both beds. The error in the computation of the hydraulic conductivity was estimated to be 15%, but since the sensitivity is so low it has much less impact on the travel time than the discharge or the water head. The porosity is associated with a quite high uncertainty, as shown in Chapter 6.2.1.1. Assuming an error in the range of 10%, then the impact on the travel time will still be less than the impact of the discharge, but with an error in the range of 15 to 20%, the impact of the porosity is similar to the impact the discharge has on the travel time.

Table 6.17. Sensitivity of travel time of ADE model of Bed 4 and Bed 11 to different parameters (With a parameter perturbation of 5%)

	Bed 04		Bed 11	
Parameter	Initial Value	Sensitivity	Initial Value	Sensitivity
Discharge Q	3.8 l/s	1.65	2.05 l/s	1.51
Hydraulic Conductivity k	0.15 m/s	0.35	0.15 m/s	0.08
Porosity n	0.45	1.10	0.45	1.17
Water Head h	0.60 m	2.03	0.60 m	1.65

6.2.3.2 Modelling of observed residence time distributions with a combined CSTR/ADE model

The mathematical formulation for the CSTR module and the ADE module of the model was shown in Chapter 2. The CSTR is formulated as an ADZ-cell according to Equation 2.74 with an advective time delay δ = 0 time steps, while the routing procedure for the ADE was presented with Equation 2.58. Three parameters were subject to the process of parameter estimation, the ADZ cell residence time T_c of the CSTR module and the dispersion coefficient D and the travel time $\bar{t}$ of the ADE module. The parameters were estimated by means of a least square minimisation as shown in Chapter 3.2. The estimated values of dispersion coefficient D and travel time $\bar{t}$ are averaged numbers for the total length of the gravel cells. The effects of change in head and flow velocity are over the length of the gravel cells are included in those averaged values. The estimated parameters are summarised in Table 6.18 while the associated residence time distributions for the CSTR module and the whole model are shown in Figure 6.34 to Figure 6.40.

The models fit the observed data quite well, with coefficient of determinations of 0.98 and higher. The fit for the model for the test Series 0 Bed 4 is less good, with a coefficient of determination of 0.95. Despite the high numbers for the coefficients of determinations, the models fail to accurately fit the falling limbs of the observed distributions. Anyhow, the falling limbs of the observed residence time distributions are associated with a higher uncertainty than the rising limb or peak of the distributions. Contrary to the ADZ models, the CSTR/ADE model can explain the first sections of the rising limb quite well. The reason for this is, that the ADE-equation describes the process of dispersion in terms of the spread of a normal equation rather than the ADZ-model that utilises a fully mixed tank. The estimated CSTR residence times are approximately between 1.0 and 1.2 days, except for the test Series 1 Bed 11 with a much shorter residence time of 0.66 days. The estimated travel times and dispersion coefficients of the ADE module were converted into dispersivities. These computed dispersivities are in the range of 0.1 to 1.0 m and compare quite well with the measured value of 0.12 m from the longitudinal dispersion coefficient test.

Rather satisfying about this CSTR/ADE conceptual model is, that it is not only able to explain the observed residence time distributions of all tests very well but that it is as well a deterministic model that is based on physical principles. Thus, this model is able to describe processes of transport and dispersion within the bed of the subsurface wetlands. Unfortunately it is not possible to fully verify this model from the current data, since the past tests have not been designed under the aspects of this deterministic model. Nevertheless, even without taking the CSTR module into account, the ADE module of this model is able to describe the rising limb and the peak of the observed residence time distribution. And since the estimated dispersivities and travel times as well as the chosen porosity are reasonable values compared to values gained from others tests (Table 5.4) or from the literature (Freeze and Cherry, l979; Bear and Corapcioglu, 1991; Zheng and Bennett, 2002;), this part of the model does make sense and is reasonable.

The CSTR part of the model cannot be readily verified from literature, since the layout of the reed beds is unique and no or only little literature exists about such a layout. The visual observations of the mixing in the first open channel section had not been proved by measurements, since it was not primarily a goal of the research. However, the CSTR module for describing the mixing in the first open channel section seems to be physically reasonable when being aware of the following two facts. The water in the open channel section is not fully mixed and cannot be, because the area of the outflow is a large part of the total surface area of the mixing zone. The CSTR includes as well further mixing effects of downstream open channel sections.

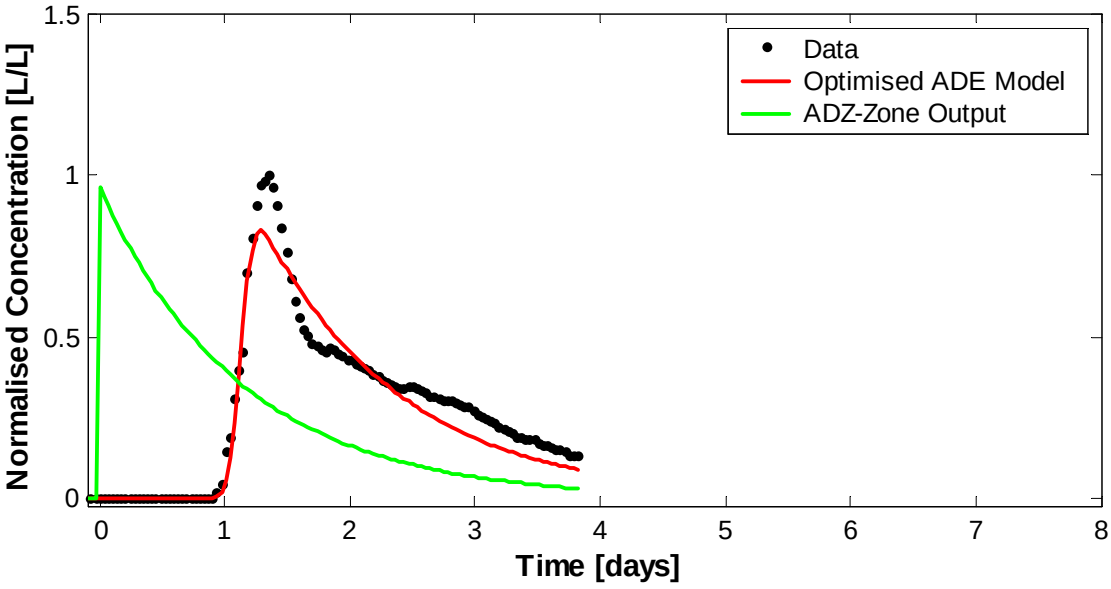

Figure 6.34. Series 0, Bed 04: residence time distribution of combined CSTR/ADE model

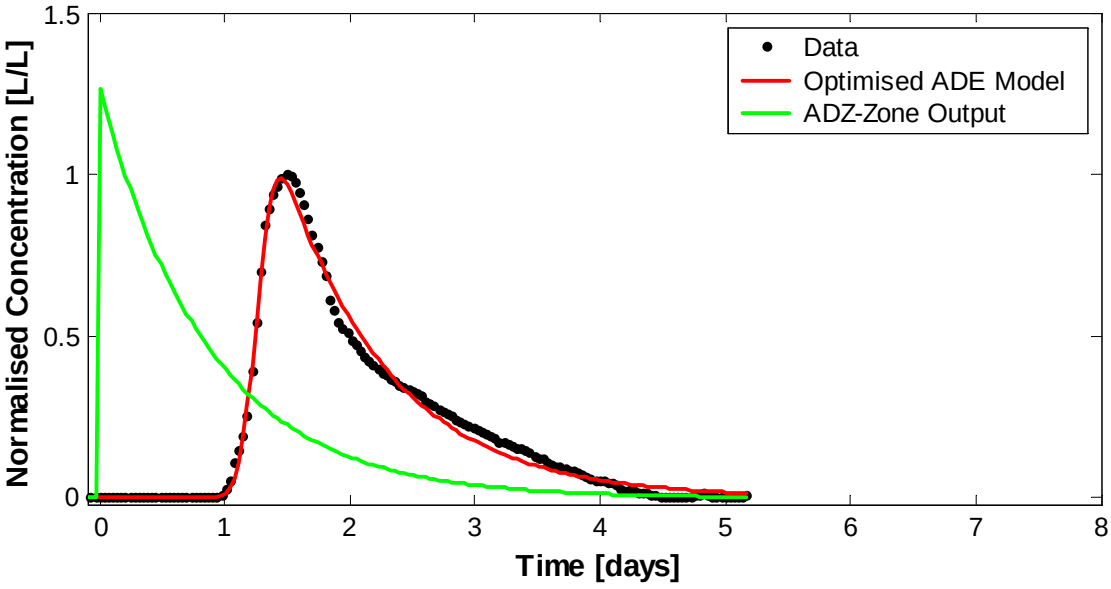

Figure 6.35. Series 0, Bed 11: residence time distribution of combined CSTR/ADE model

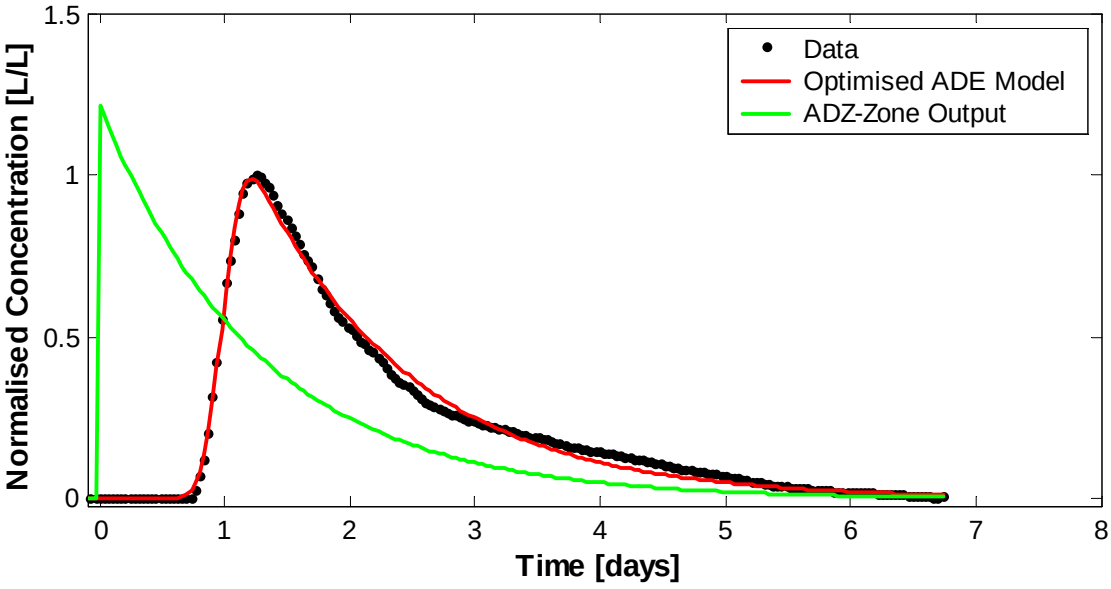

Figure 6.36. Series 1, Bed 02: residence time distribution of combined CSTR/ADE model

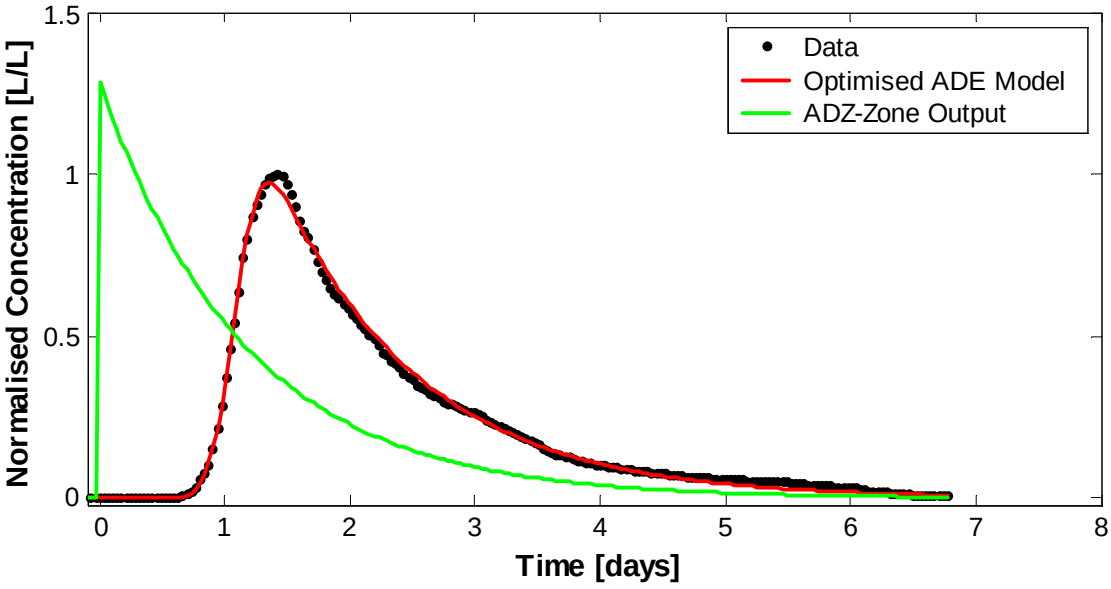

Figure 6.37. Series 1, Bed 04: residence time distribution of combined CSTR/ADE model

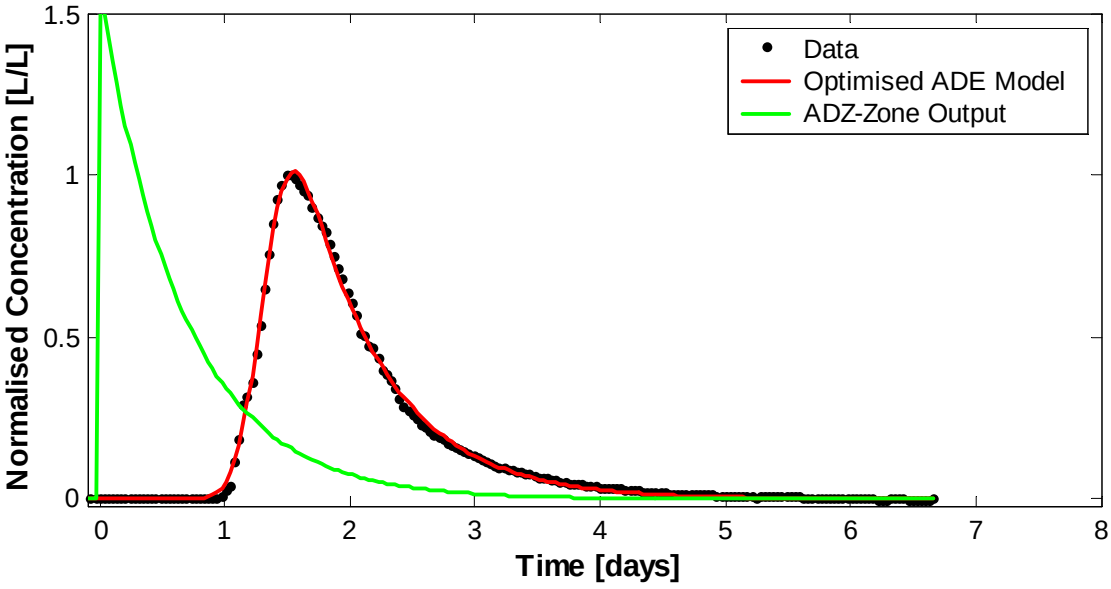

Figure 6.38. Series 1, Bed 11: residence time distribution of combined CSTR/ADE model

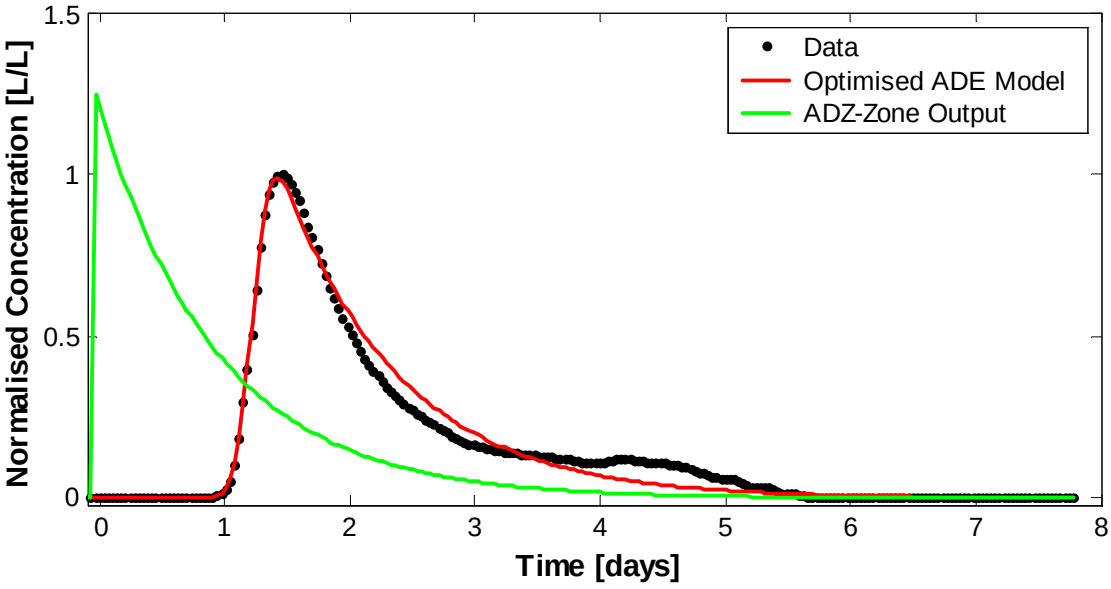

Figure 6.39. Series 2, Bed 04: residence time distribution of combined CSTR/ADE model

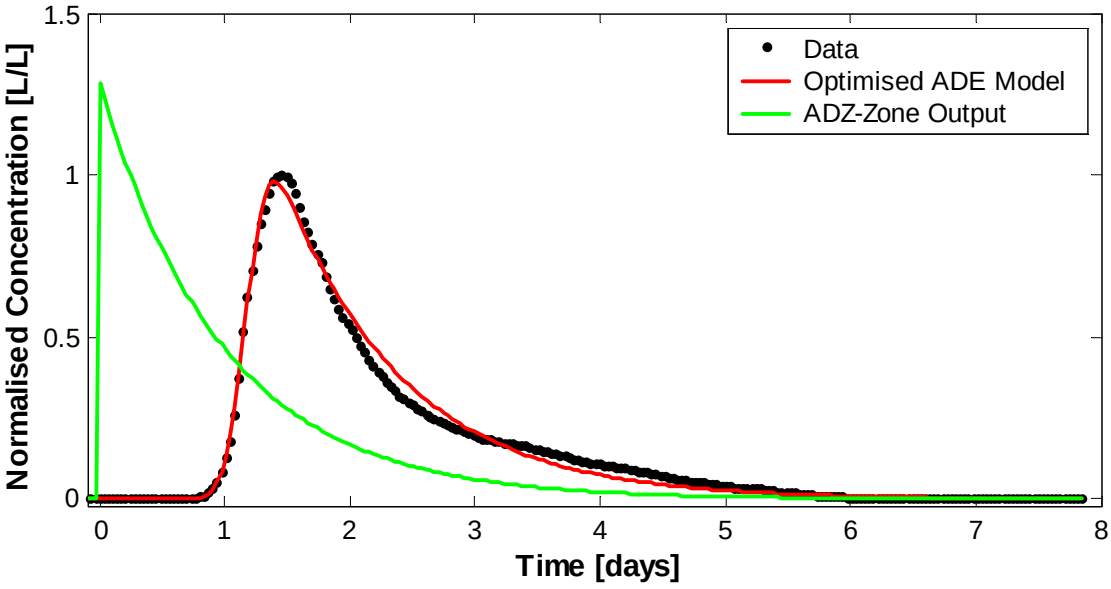

Figure 6.40. Series 2, Bed 10: residence time distribution of combined CSTR/ADE model

Table 6.18. Estimated parameters for the CSTR/ADE model

Test Name	Coefficient of determination R_T^2 [-]	CSTR residence time T_c [days]	ADE-reach travel-time $\bar{t}$ [days]	Longitud. dispersion coefficient D_L [m^2/s]	Longitud. dispersivity α_L [m]	Total travel time t [days]
Series 0, Bed 4	0.95407	1.13	1.15	1.53E-04	1.90E-01	2.28
Series 0, Bed 11	0.99100	0.87	1.28	5.54E-05	1.53E-01	2.14
Series 1, Bed 2	0.99389	1.26	1.00	1.37E-03	9.91E-01	2.26
Series 1, Bed 4	0.99714	1.16	1.10	7.07E-04	8.43E-01	2.26
Series 1, Bed 11	0.99817	0.66	1.34	1.20E-04	3.46E-01	2.00
Series 2, Bed 4	0.98142	0.95	1.28	2.25E-04	3.11E-01	2.23
Series 2, Bed 10	0.99118	0.98	1.19	1.03E-04	2.64E-01	2.18

6.2.3.3 Monte Carlo analysis of the CSTR/ADE model

The "dotty plots" and the frequency plots of the Monte Carlo analysis are shown in Figure 6.41 to Figure 6.47 and the results are summarised in Table 6.18. The travel time is for all data sets quite sharply defined with times around the peak times of each residence time distribution, indicating, as previously mentioned, the good fit of the model with the rising limb and the peak of the distributions. The dispersivities show a broader shape, as being indicated by their bigger standard deviation, but a clear peak defines all. The dispersivities of the tests of Series 1, Bed 2 and Series 1, Bed 4 are less well defined than the others, with a standard deviation of approximately four times greater than the standard deviations of the others. Further, the CSTR residence times are quite well defined, having for all tests a similar standard deviation.

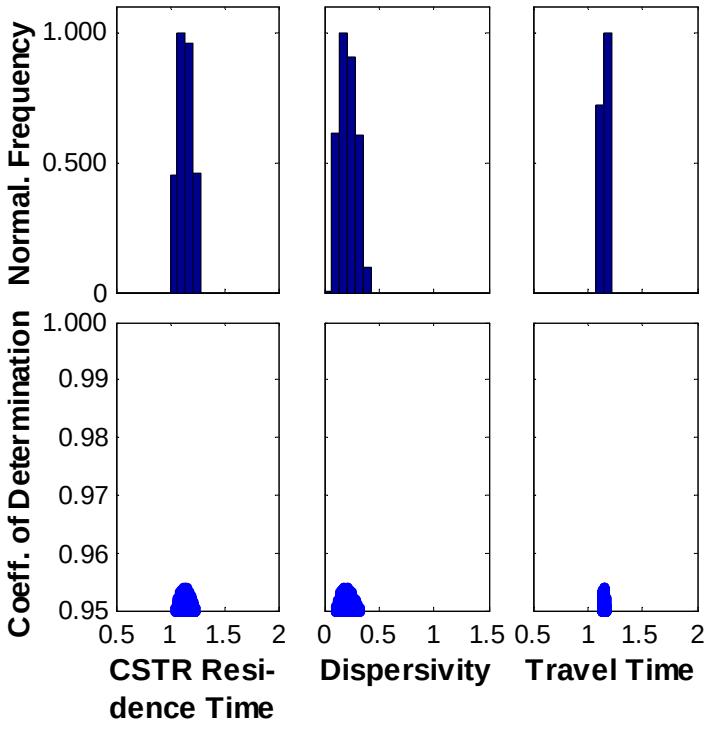

Figure 6.41. Series 0, Bed 04: Monte Carlo analysis of CSTR/ADE model

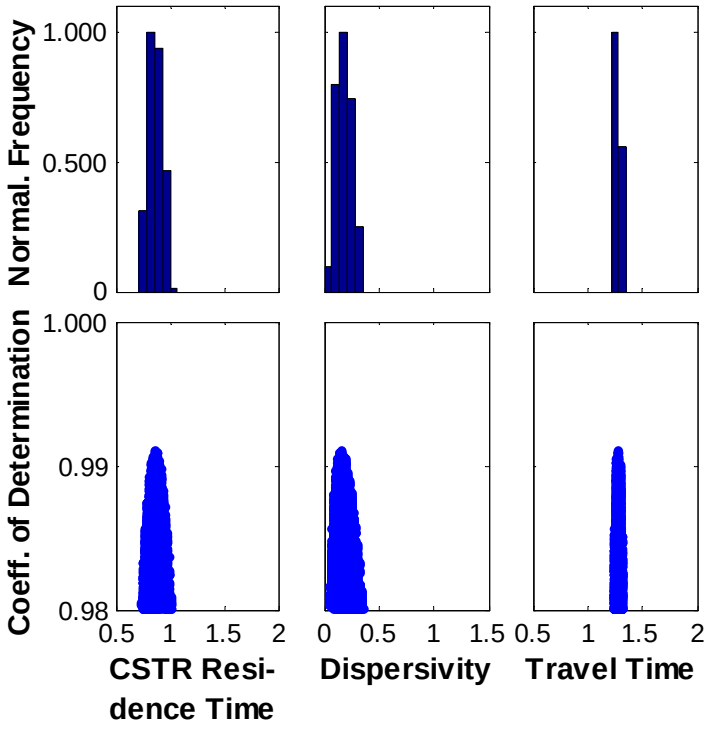

Figure 6.42. Series 0, Bed 11: Monte Carlo analysis of CSTR/ADE model

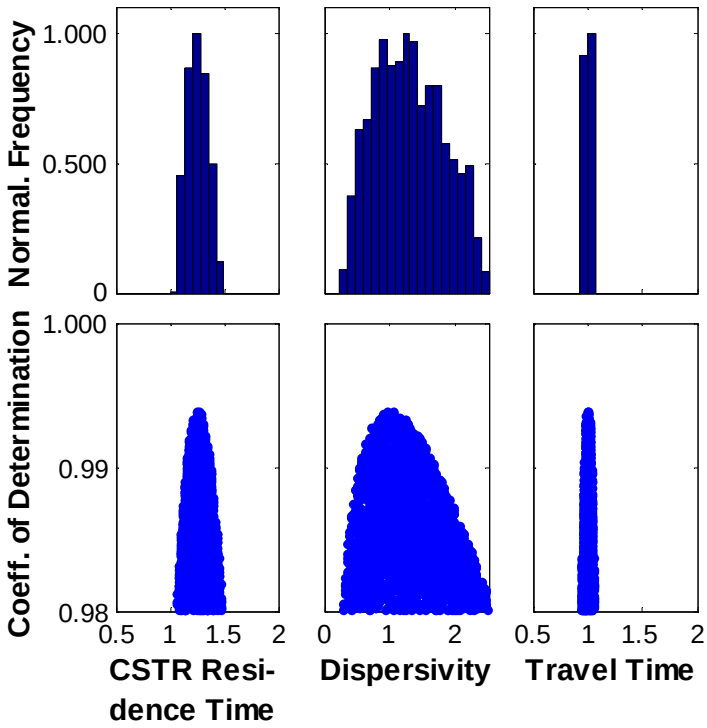

Figure 6.43. Series 1, Bed 02: Monte Carlo analysis of CSTR/ADE model

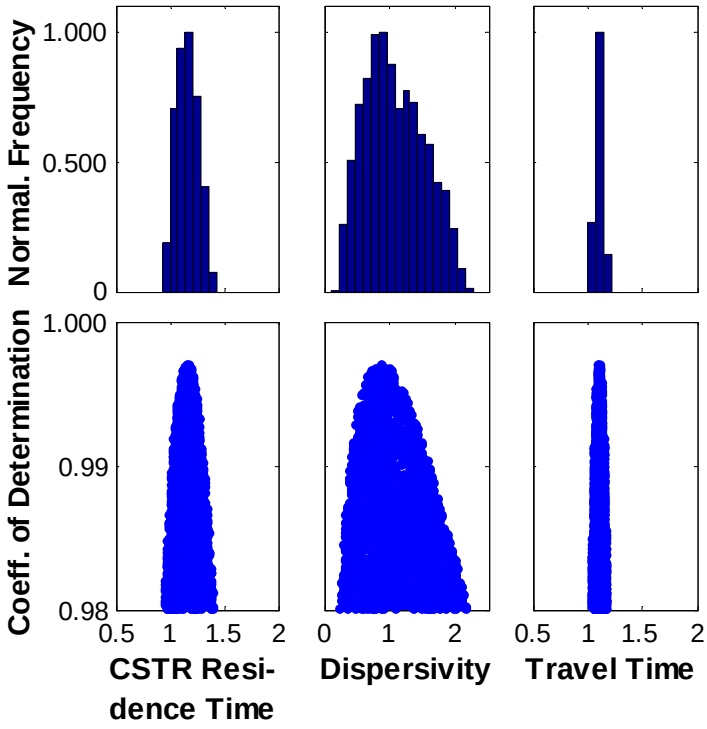

Figure 6.44. Series 1, Bed 04: Monte Carlo analysis of CSTR/ADE model

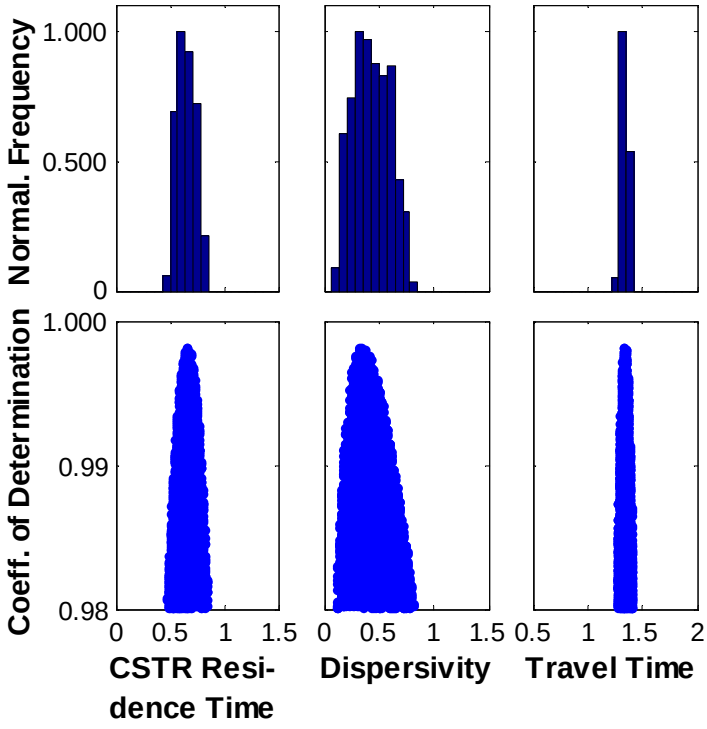

Figure 6.45. Series 1, Bed 11: Monte Carlo analysis of CSTR/ADE model

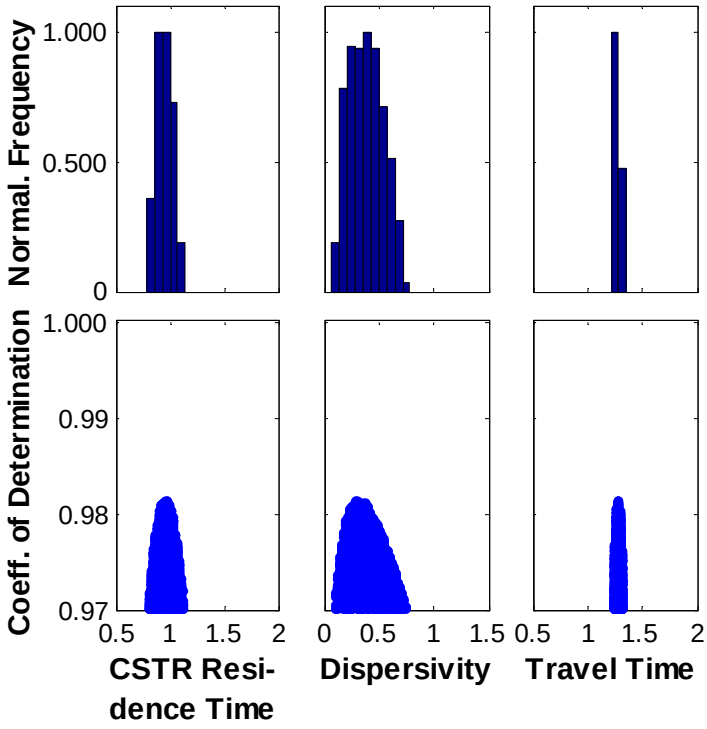

Figure 6.46. Series 2, Bed 04: Monte Carlo analysis of CSTR/ADE model

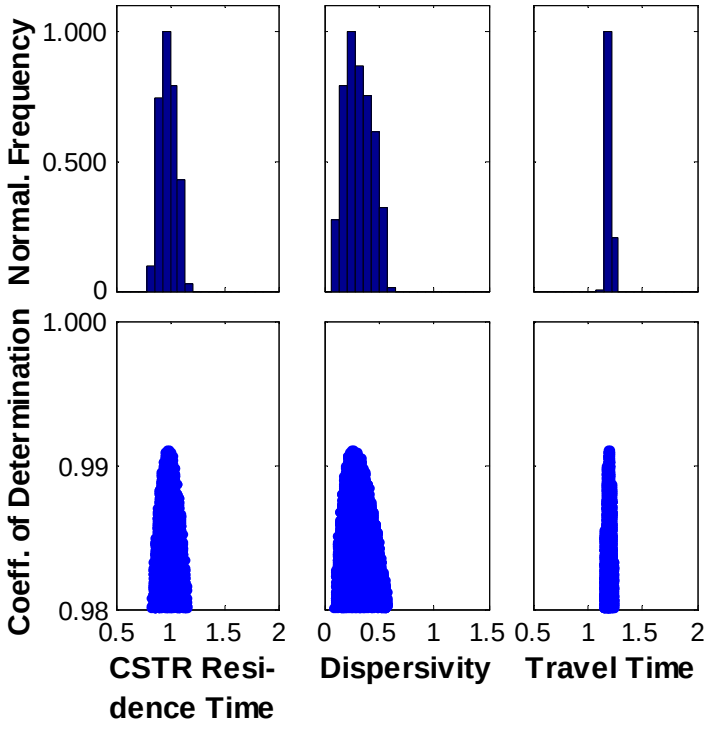

Figure 6.47. Series 2, Bed 10: Monte Carlo analysis of CSTR/ADE model

Table 6.19. Results of Monte Carlo Simulation for CSTR/ADE model

Test Name	CSTR residence Time		Longitudinal Dispersivity		ADE-reach travel time		Total travel time	
	mean T_c [time steps]	best T_c [days]	mean α_L [days]	best α_L [days]	mean $\bar{t}$ [days]	best $\bar{t}$ [days]	mean $\bar{t}$ [days]	best $\bar{t}$ [days]
Series 0, Bed 4	1.14 (0.07)	1.13	0.22 (0.08)	0.19	1.15 (0.04)	1.15	2.29	2.28
Series 0, Bed 11	0.86 (0.07)	0.86	0.18 (0.07)	0.15	1.28 (0.03)	1.28	2.14	2.14
Series 1, Bed 2	1.26 (0.09)	1.26	1.29 (0.52)	1.04	1.00 (0.04)	1.00	2.26	2.26
Series 1, Bed 4	1.16 (0.10)	1.15	1.08 (0.44)	0.88	1.10 (0.04)	1.11	2.26	2.26
Series 1, Bed 11	0.65 (0.09)	0.66	0.43 (0.17)	0.34	1.34 (0.04)	1.34	1.99	2.00
Series 2, Bed 4	0.95 (0.08)	0.96	0.38 (0.15)	0.28	1.27 (0.03)	1.28	2.22	2.24
Series 2, Bed 10	0.98 (0.08)	0.98	0.31 (0.12)	0.26	1.19 (0.03)	1.20	2.17	2.18

6.2.4 Summary of pollutant transport modelling

The SRIV identified models describe the observed residence time distributions well. The SRIV identification method did identify for nearly all cases an identical model structure that seems a physically reasonable explanation for the pollutant transport in the subsurface wetlands. This identified model has one slow and one quick parallel flow path. Since all identified models of this structure have complex roots the model parameters have been re-estimated by means of a least-squares optimisation procedure. The re-estimated model with the advective time delay from the SRIV identification explains the data well (Model A), but a better fit is gained when the advective time delays for the slow and quick flow paths are also subject of the optimisation procedure (Model B). The fraction of flow in the slow flow path is for the tests of Series 0 and 1 higher than 70% while it is 50 to 60% for the tests of Series 2. The dispersive fractions indicate for all tests that only 50 to 60% of the saturated wetland volume is used for the mixing of the water. A similar relationship exists between the sum of all theoretical ADZ-cell volumes and the water volume computed from field observations. The re-estimated models explain the data well and can further be related to physical properties. However, the ADZ-model can only be used to explain the mixing between an up- and downstream observations. Being a stochastic "Grey-Box" model, is it not able to describe the mixing processes with distance while the water moves through the wetland.

The CSTR/ADE model is a combined stochastic-deterministic model, where the deterministic ADE-module describes the flow through the gravel cells and the stochastic CSTR-module summarises the mixing effects of the open water sections. The modelling of all observed residence time distributions gave equally good results compared to the ADZ-model (Model B). The estimated parameters for the ADE module of the model compare well to observed values. The estimated longitudinal dispersivities are in the range of 0.1 to 0.9 m and compare well with values from literature. This gives a reasonable high confidence about the ability of that module to explain the physical movement and mixing of the water while moving through the gravel cells of the wetland. Nevertheless, this module is subject to some inaccuracies, since it does not take the draw down of the water head into account. Actually this has an effect on the value of the dispersivity. Therefore the dispersivity shown here should be taken as an averaged value over the length of the bed. The estimated residence times of the CSTR of all tests are similar and in a range between 0.9 and 1.1 days, except of one value with 0.66 days. However, the CSTR module is not backed by physical measurements and was deduced from visual observations about the mixing processes in the first open channel section of each wetland-bed. Nevertheless, approach of modelling this open channel section as a CSTR seems physically reasonable.

6.3 PART B: TREATMENT PERFORMANCE OF GLYCOL

In this section the decay constants of the degradation tests will be evaluated. First the pollutant transport models that were previously developed are assessed for the evaluation of pollutant decay constants. Especially investigated are the implications of the flow models to the spatial and temporal distribution of a neutral pollutant within a wetland subject to temporal changes of the inflowing pollutant concentration. Naturally, this assessment is mainly subject to the CSTR/ADE model, since it has been shown that the ADZ model is not able to describe the movement of pollutants within the wetland. Hereafter, the degradation rates are evaluated.

6.3.1 Assessment of the pollutant transport model for the evaluation of pollutant decay constants

For the evaluation of more meaningful pollutant degradation constants, it might be useful to assess the transport models with respect to the temporal change in pollutant influent concentration. The simplest case is an inflowing pollutant of a constant concentration. Considering that the degradation only takes place in the gravel matrix of the reedbeds and assuming that the flow velocity in each cross-section along the gravel cell beds is constant, than obviously all mixing and dispersion effects outside the reedbeds have no impact. The transport of a conservative pollutant through the gravel matrix may under these circumstances be modelled with purely advective transport (AT).

This is different for non-conservative pollutants, since the pollutant in the slower fraction spends more time in the gravel matrix than the pollutant in the faster fraction of the flow. The pollutant in the slower fraction is therefore subject to more degradation. It was previously shown, that the flow through the gravel cells is advection dominated (Chapter 6.2.1.2). Computing the relationship of advection/dispersion (Equation 2.55) with the estimated parameters of the ADE-reach travel time $\bar{t}$ and the longitudinal dispersion coefficient D_L from the tests of Series 2, Bed 4 (Table 6.18) gives that the advection term of the equation is 260 times larger than the dispersive term. For Bed 10 it is 150 times greater. Thus it can be assumed, that an advective transport model with an average travel time describes the movement of the pollutant within the gravel matrix with sufficient accuracy. This will simplify the modelling procedure significantly, since no dispersive transport has to be computed. A further advantage of this simplification is, that the draw down of the water head can still easily be computed and included in the plug-flow model. Inclusion of the draw down effect will increase the accuracy of the computation of the travel times of pollutants within the gravel cells. From Equation 2.27 the advective transport term of the now gained CSTR/AT model can be defined as

$$C(\bar{t}_2, x_2) = C(\bar{t}_1, x_1) \qquad 6.5$$

where

$C(\bar{t}_i, x_j)$ concentration at the temporal centroid of the distribution i at the location j

and the time t_2 is defined as

$$\bar{t}_2 = \bar{t}_1 + \int_{x_1}^{x_2} \frac{1}{v(x)} dx \qquad 6.6$$

where

$v(x)$ fluid velocity at location x (L T^{-1})

Comparative computations with the different models show the ability of the model to describe the transport within the gravel cells with advective transport model for the Heathrow wetlands. The ADE-module and the AT module were applied to the averaged values of the observed temporal concentrations obtained at the inflow of the reed beds (see Figure 5.37). Here, the observed temporal concentrations have been resampled to obtain a uniform sample interval to simplify the modelling. The computations were performed with the estimated parameters of the tests Series 2, Bed 4 and Series 2, Bed 10. The results are shown in Figure 6.48, where the predictions of both models are very similar for Bed 4 and are differing slightly for Bed 10. An explanation for this might be the difference in flow velocities between those beds that results in different ratios of advection to dispersion (Table 6.2).

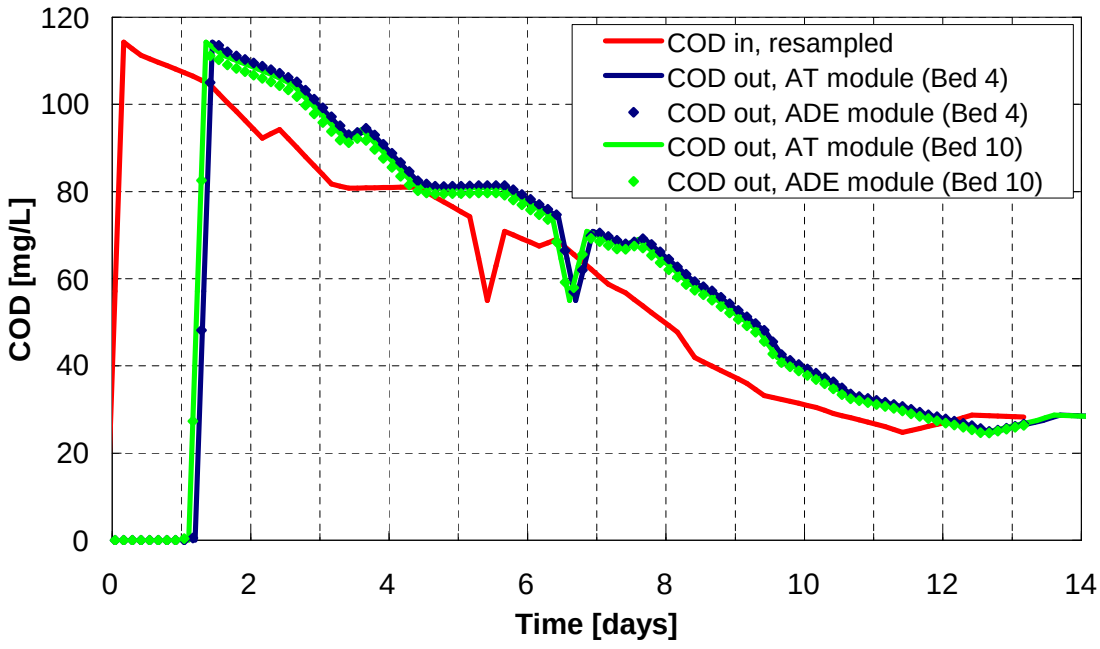

Figure 6.48. Comparison of modelled COD variations with the ADE module and the AT module

The mixing in the first open channel section, as described by the CSTR module, may well have an impact on the concentrations of the pollutants entering the wetland. The residence times for the CSTR module were estimated at 0.95 and 0.98 days for the tests of Series 2, Bed 4 and Bed 10 (Table 6.18). The CSTR module of Bed 4 is applied to the averaged and resampled temporal observations of COD. The prediction of the module for this data is shown in Figure 6.49. The CSTR shows the typical initially rising concentration and reaches a steady state after approximately 5 days. This is, when the predictions and the influent concentrations show a parallel trend. Further, the concentration leaving the CSTR is higher than the actual influent concentration. Since these differences in concentration are not neglectable, this effect has to be taken into account when evaluating the pollutant decay rates from temporal observations of pollutant concentrations as well as for spatial concentrations within the wetland.

The previous remarks give a much greater insight into the mixing and transport of pollutant within the reed beds of the wetland. Therefore the ADZ model will be investigated likewise in the following. The visual examination of the quick and slow ADZ-cell residence times might suggest that a residence time gained by subtracting the quick cell from the slow cell (1.4 - 0.2 = 1.2 days for Series 2, Bed 10; Table 6.11) will give residence time of similar magnitude when being compared with the CSTR residence time (0.98 days; Table 6.18). This might then suggest, that the quick flow path describes the mixing within the gravel cells. However, this does not hold true. The plots of the quick flow paths show (e.g. Figure 6.17), that the dispersion modelled with this flow path is much larger than those gained from the ADE-

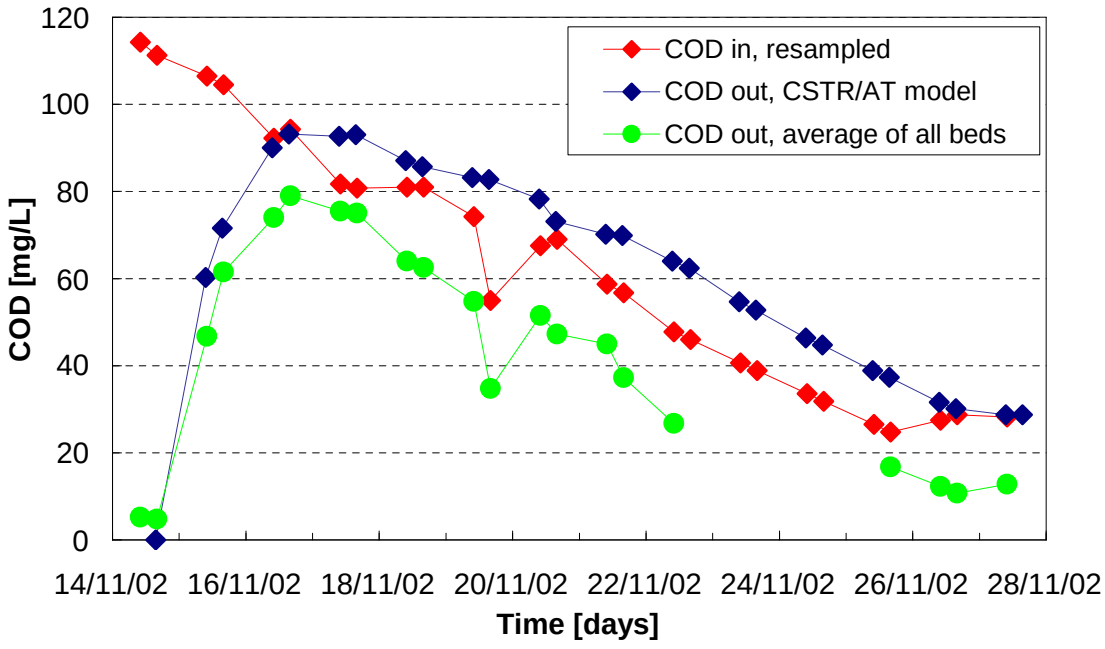

Figure 6.49. CSTR/AT model applied to the averaged and resampled temporal observations of COD at the inlets of the beds; further shown are the COD concentrations at the bed outlets.

module. Since here the advection dominates the dispersion, it might be suitable to compare the advective time delays of the ADZ-models with the advective transport model of the CSTR/AT model. Thus the ADZ-model describes the mixing in the first open channel section.

The step response and the impulse response of the ADZ model and of the CSTR module are shown in Figure 6.50. The step impulse shows for both models a similar magnitude in rise, where the ADZ model has a short time delay. The impulse responses of both models show a very different behaviour during the first period of time. The impulse response of the CSTR module shows simply a decaying concentration while the response of the ADZ model initially rises rather quickly to a peak, before beginning to decay. After a time of 1.5 days the predicted decay is similar to the decay predicted with the CSTR module at that time.

Obviously, the time step for the real data is much larger than those used for these computations of the step- and impulse response. The data of the daily temporal observations was collected around 10.00 hours and 16.00 hours. It is therefore reasonable to investigate into the effect of greater time steps of dt = 0.25 days and dt = 0.75 days on the impulse response. The impulse responses for these time steps are shown in Figure 6.51. The CSTR model described the data well; of course the peak cannot be described as accurately due to the greater time step. Similarly, the ADZ model cannot predict the peak for either the greater or for the smaller time steps. Nevertheless, the general dynamics of the model is reasonably well defined.

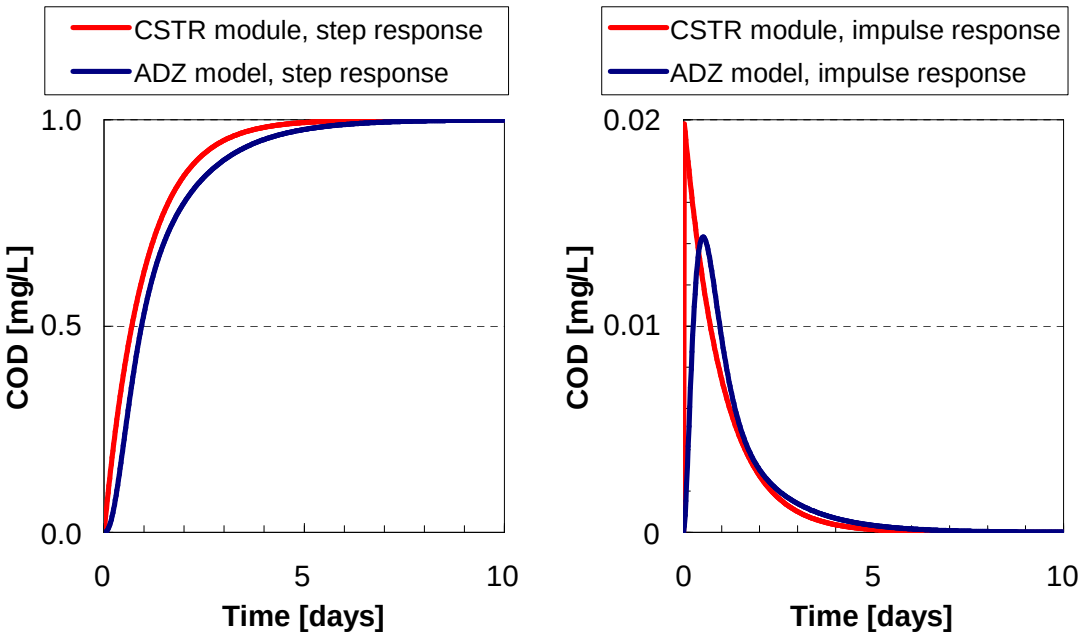

Figure 6.50. Step and impulse response of CSTR module and ADZ model of the estimated models for test Series 2, Bed 10

Since the temporal changes of concentration during the observations are less drastic compared with the impulse or step response, larger time steps may be sufficient to model the observed data. The largest observed change in concentration of influent is approximately 16.7 mg COD/L within 0.25 days. To simulate this change of concentration, the models were applied to artificial data, using the same time step intervals as before. The predictions are shown in Figure 6.52. The predictions show an initial sharp increase of concentration. Both models achieve a steady state condition after approximately 5 days. This time is approximately five times greater than the residence time and is therefore equivalent to the time to reach 99% of the steady state of a step impulse. The models predict the second change in concentration for all time steps with a similar accuracy. The small time difference between the ADZ modelled data and the CSTR modelled data results from the different residence times of the models (0.98 days for the CSTR- and 1.43 days for the ADZ model). This evaluation shows that a time step of 0.25 days or 0.75 days can be selected to model pollutant transport with considerably small changes in concentration with sufficient accuracy.

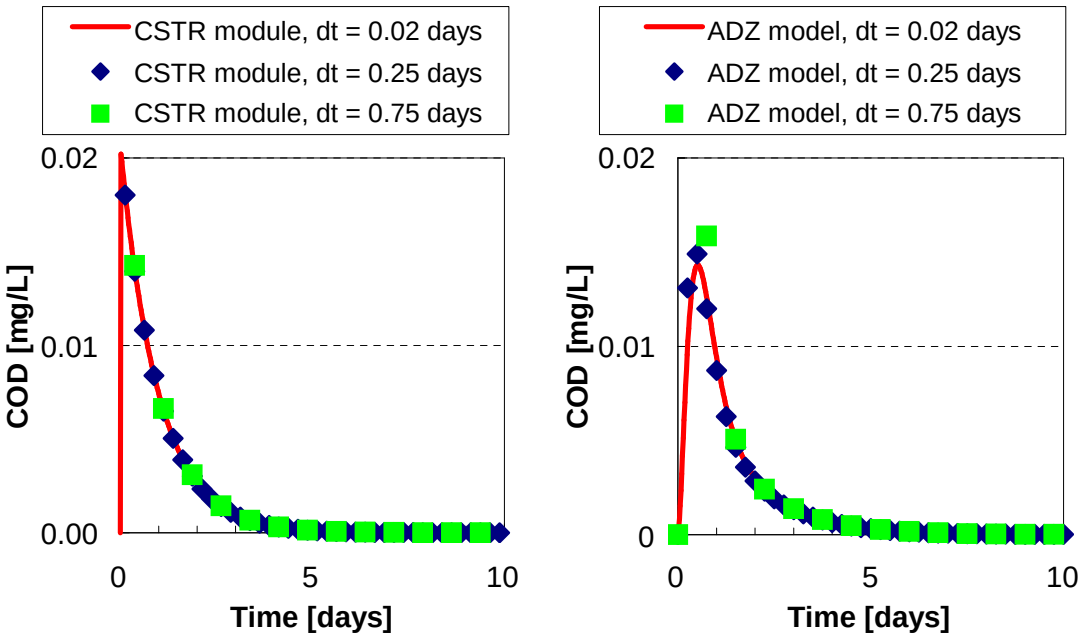

Figure 6.51. Impulse response of CSTR module and ADZ model with different time steps of *dt* = 0.02 days and *dt* = 0.25 days and *dt* = 0.75 days for the estimated models of test Series 2, Bed 10

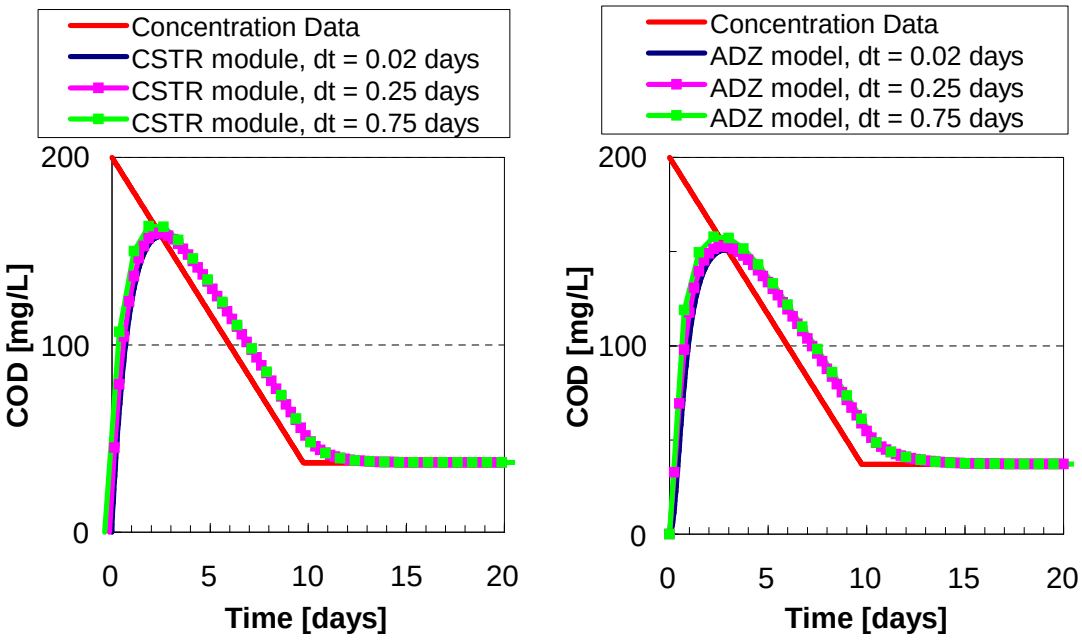

Figure 6.52. Model response to slow change in concentration for different time step intervals.

6.3.2 Laboratory test of glycol degradation in a gravel matrix

Laboratory tests were undertaken to get a better insight in the processes of aerobic and anaerobic glycol degradation within a gravel matrix. Here, the depletion of dissolved oxygen can be assumed to be identical with the amount of aerobic reduction in BOD or COD of the glycol, since glycol was the only pollutant in the system and therefore its reduction the main sink for oxygen. The test results were presented in Chapter 5.3.4. The relation of oxygen concentration to residence time is shown in Figure 6.53. The level of oxygen leaving the reactor decays exponentially with time and approaches asymptotically a residual oxygen level of approximately 1 mg/L. This level is reached after approximately 0.1 days. A residual oxygen level was also detected during the anaerobic laboratory test (Chapter 5.3.4), and during field tests (see Figure 5.30, Figure 5.31, Figure 5.34 and Figure 5.35). It is not clear if dissolved oxygen of concentrations less than approximately 1 mg/L cannot be used in the aerobic degradation processes or if this values is caused by the inaccuracy of the measurement method.

Since the aerobic degradation of organics is usually a first order reaction (Chapter 2.2), a first order reaction rate for the depletion of oxygen can be computed. A linear regression is used to fit Equation 2.79 to the data. The result of the regression analysis is presented in Table 6.20. The estimated reaction rate k is 51 d^{-1}. The depletion of oxygen cannot be related to the degradation of COD. The measured COD concentrations show a wide scattering, even at similar residence times (Figure 5.43). This is probably caused by the measurement error associated with the COD test, that is in the range of 5 mg COD/L (see Chapter 2.2). Since the error is attributed

to the measured concentrations of the inlet and the outlet, the overall error of the difference in the measured concentration is twice as high. Since this error has the same magnitude as the absolute difference between in concentration of the inlet and outlet the computation of a reaction rate from this data is impracticable and unreliable.

In Figure 6.54 the relation of observed COD concentrations against residence time is shown for the anaerobic test of glycol degradation. The observed COD concentrations have a great variation. Similarly, the level of observed COD degradation is within the range of the COD determination method. Thus the results of the anaerobic degradation tests for glycol cannot be used to compute a degradation rate. Nevertheless, the observed degradation of COD clusters around low values when being compared to the observed values of oxygen depletion of the aerobic test. This might indicate that the reaction rate for the anaerobic degradation of glycol is much lower than the reaction rate for aerobic degradation.

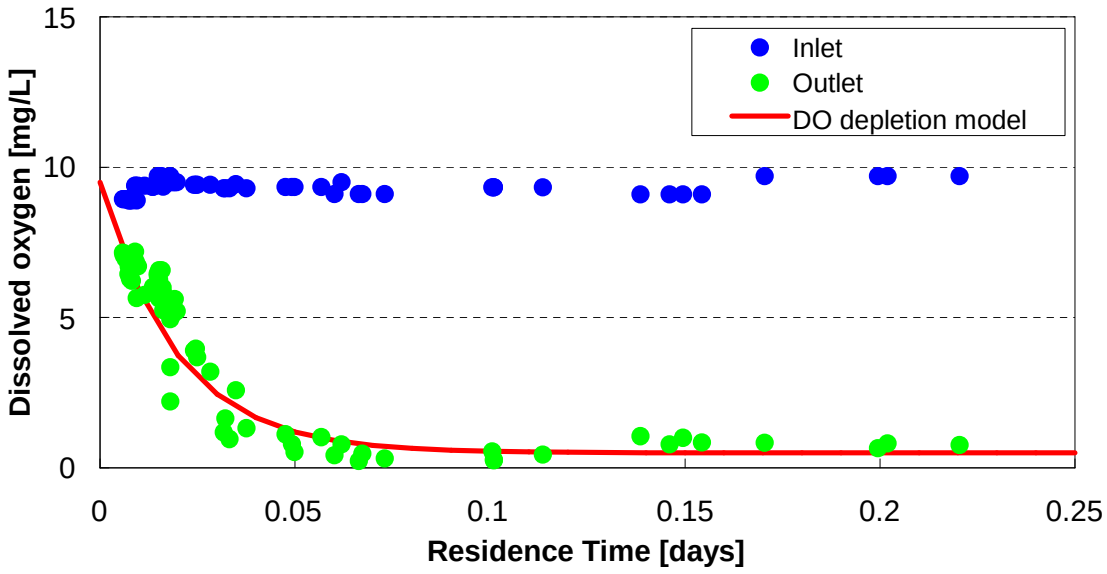

Figure 6.53. Dissolved oxygen depletion in a gravel matrix with a glycol pollutant load in a laboratory reactor and its first order reaction model of depletion

Table 6.20. Reaction rates for laboratory tests of oxygen depletion

Test	First order reaction rate *k* [day-1]	Coefficient of determination *R* [-]
Aerobic glycol degradation, oxygen depletion	51.1	0.92

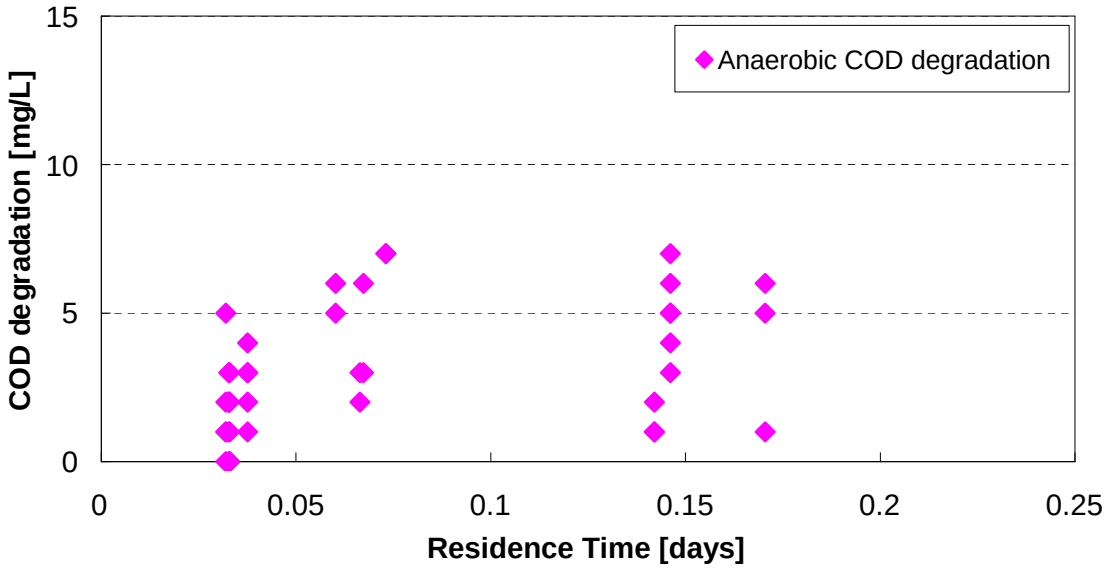

Figure 6.54. Anaerobic degradation of glycol in a gravel matrix of a laboratory reactor

6.3.3 Temporal BOD observations

The temporal observations of BOD_5 were presented in Figure 5.38. The observed concentrations of the influent show a large variation for each sample time, while the effluent concentrations have a significant smaller variation. The analysed samples had not been filtered. The larger variation of BOD_5 of the influent concentrations is likely to be caused by a combination of measurement error and different amounts of suspended solids in the samples (see Chapter 2.2). The effluent has a smaller variation, since the reedbeds act as a filter. It can therefore be assumed, that the measurement error has a larger impact on the variation in effluent concentration. The average standard deviation for the influent concentration is 8.23 mg BOD_5/L, with a maximum deviation of 19.8 mg BOD_5/L. For the effluent the averaged standard deviation was computed at 3.77 mg BOD_5/L and the maximum deviation was computed at 9.8 mg BOD_5/L.

Only little variation in the influent concentration of COD was observed for the different sample times. The variation in effluent concentration was slightly higher. Therefore it does seem more reasonable to average the concentrations of all sample locations for further computations.

Figure 6.55 shows the graph of the averaged BOD_5 against COD. The linear regression for the relation of BOD_5/COD gives a ratio of 0.7 for the influent while the ratio for the effluent is 0.55. The regression for all data gives a ratio of 0.65. In the literature relations for propylene glycol are given in the range of 0.5 to 0.73 (Cyrotech, 2002; Cyrotech, 2002a). The coefficients of determination for the regressions of BOD_5/COD for the influent and effluent are 0.79 and 0.77. Different BOD_5/COD ratios for the influent and effluent could imply that the BOD_5 test

does not detect the intermediate products of glycol degradation in the effluent (Chapter 2.3.2). This might be indicated by the lower ratio of BOD_5/COD of the effluent compared to the influent but it is uncertain due to the rather poor coefficients of determination.

However, the general trend for a linear relationship of BOD_5/COD is clearly visible from Figure 6.55, for the influent and effluent data as well as for the combination of their values. A regression for the combined data of influent and effluent shows a ratio of 0.66 with a slightly stronger coefficient of determination of 0.83 (Table 6.21).

The computation of efficiencies and reduction rates from the temporal BOD_5 observations will be less accurate than the computed values from the COD observations due to relatively large variation in the BOD_5 data. Since a linear relationship between BOD_5 and COD was established, a separate assessment of the temporal COD and BOD_5 data brings no further insight in the treatment process. Thus computations are only performed on the COD data. Efficiencies or reduction rates for BOD_5 can then be computed from the COD data in conjunction with the combined influent and effluent BOD_5/COD ratio of 0.66.

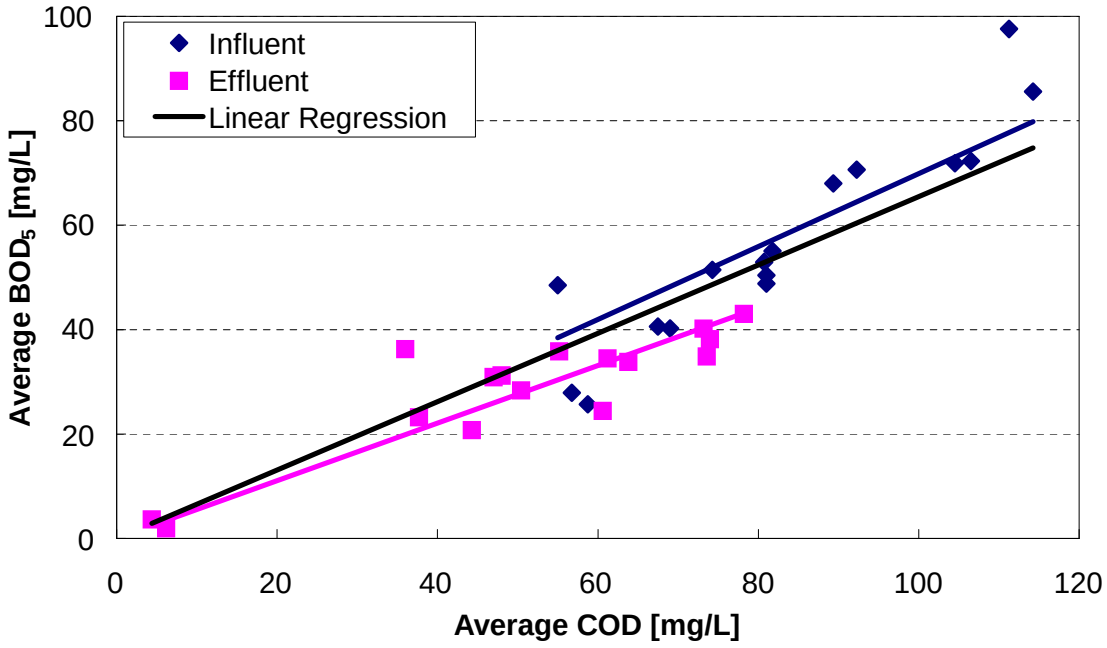

Figure 6.55. Relation between COD and BOD_5 of influent and effluent

Table 6.21. Linear regression of COD/BOD_5 relation

	COD/BOD_5 ratio [%]	R_t^2 [-]
Influent	69.9	0.7944
Effluent	55.2	0.7654
Influent + Effluent	65.5	0.8292

6.3.4 Temporal glycol observations

The temporal observed concentrations of glycol of the influent and effluent of the Bed 4 were presented in Figure 5.41. Figure 6.56 shows the relation of measured glycol concentration to measured COD concentration. Obviously, the relation between glycol and COD is not linear. In Figure 6.57 the temporal observations of glycol and COD are shown. Clearly the observed glycol show a faster decay than the observed COD. A linear relation of COD concentration measured with the COD test and glycol concentration measured with the glycol test was observed in the laboratory using fresh glycol. This might lead to the conclusion that the glycol test method, in contrary to the BOD_5 test method, cannot pick up the metabolic intermediates of the degradation processes (Chapter 2.3.2). Further, the non-linearity of the measured influent concentrations might indicate that some degradation does happen in the reservoirs before the polluted water is actually being discharged into the wetland system.

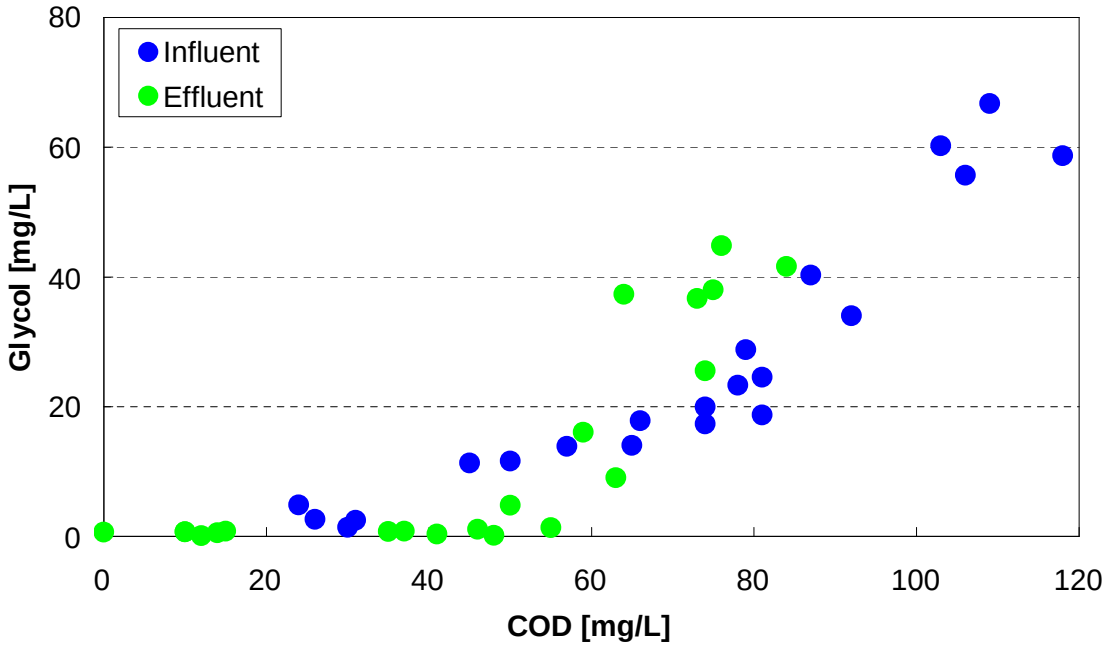

Figure 6.56. Relation between COD and glycol of influent and effluent

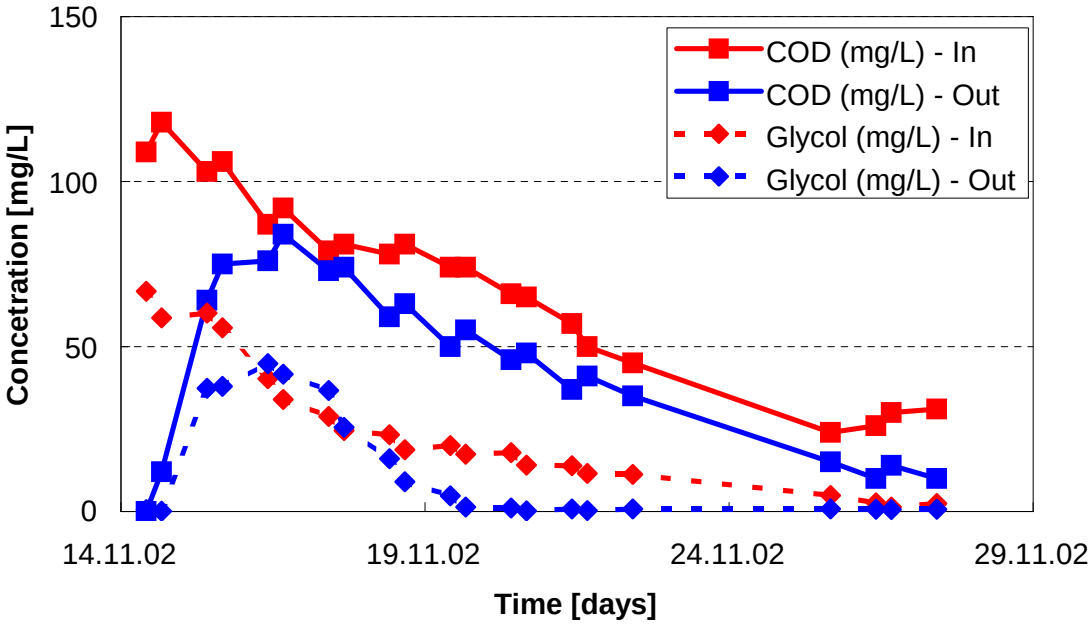

Figure 6.57. COD and glycol concentration of influent and effluent

6.3.5 Derivation of glycol degradation performance from temporal COD observations

The temporal observations of COD in the influent and effluent were presented in Figure 5.37. The observed COD concentrations in the influent of the beds are approximately uniformly decreasing with time. The effluent concentration rises first and decreases later at a similar rate as the influent concentrations. After removing the erroneous value from the 16/11/02, the observed influent concentrations show little variation, with a standard deviation averaged for all observation of in- and effluent of 1.7 mg/L and a maximum deviation of 3.5 mg/L. This variation is smaller than the accuracy of the COD-test itself. The averaged standard deviation of the observed effluent concentrations is 3.9 mg/L with a maximum deviation of 13 mg/L. The small standard deviations of the influent observations suggest that the concentration of COD that enters the reed beds is identical for each time of observation. This is clearly not true for the outlet. The differences in observed concentration of COD leaving the beds is not only caused by different efficiencies. The different discharge rates and layout of the beds will obviously have an impact on the effluent concentration. Therefore the different travel times and the pollutant transport models have to be taken into account.

For the computation of total reduction of COD and the COD reduction efficiency the influent and effluent concentration were related to each other by applying both transport models, the CSTR/AT model and the AT model as shown in Chapter 6.3.1, to the observed inlet concentration data. The obvious erroneous measurement errors from the 16/11/02 (Bed 2 Inlet)

and the 22/11/02 (Bed 10 Outlet) were replaced by interpolated values. All values from the 19/11/02 16:00 observation were also replaced by interpolated values. Since the sudden drop in concentration was observed simultaneously and there is no simultaneous relation between influent and effluent concentration. This is clearly a measurement error.

It was shown, that the CSTR and ADZ models would reach the steady state conditions after approximately five days. To allow a reasonable comparison between influent and effluent concentrations, the observation of the effluent should be taken into account six days after the start of the water flow (five days plus one day of advective transport). Since the pumps were switched on at 13/11/2002 (see Chapter 5.3.3), in the following section only the data that relates to the outlet observations from the 19/11/2002 and later will be taken into account.

The orifices of Bed 5 and Bed 11 were exchanged. Since no residence time distribution was measured for either bed, the following assumptions are made. For the CSTR model of Bed 5 the discharge rate and the CSTR-zone is assumed to be identical to those of Bed 10, since orifices and dimensions of inlet zone are identical. The advective time delay was assumed to be twice as long to take into account the double length of the bed. For simplicity the effects of a change in water head to the travel time was not taken into account. For Bed 11 the CSTR zone was assumed to be identical to those of Bed 4. The advective travel time was assumed to be half of those of Bed 4, similarly without taking the effects of the water head into account. It can be assumed that the simplification for the computation on the travel time has an inaccuracy of less than 0.25 days. This inaccuracy of observed inlet concentrations will result in an acceptable error in COD of approximately 2 mg COD/L at the outlet, when being computed from an average change of concentration with time.

The effluent concentration predicted with the CSTR/AT and AT model for pure transport without degradation is shown for Bed 4 in Figure 6.58. The AT model is simply a time-shifted version of the inlet data (see Chapter 6.3.1). The CSTR/AT model predicts a concentration distribution similarly to the observed COD concentration of the outlet that reaches asymptotically the concentration predicted with the AT model. From these predictions the efficiencies and absolute reduction of COD are computed from the difference of the observed concentrations and the predicted concentrations.

The computed efficiencies and absolute reductions of COD are shown in Table 6.22 and are given in a range of minimum and maximum values. The efficiencies and reduction rates of COD computed with both transport models are quite similar. For example, the efficiency for the observations of the outlet (Total Out) of the reed beds were computed in the range of 31 to 66 % with the CSTR/AT model and in the range of 30 to 68 % with the AT model. The absolute reduction rates were computed in the range of 14 to 36 mg COD/L with the CSTR/AT model

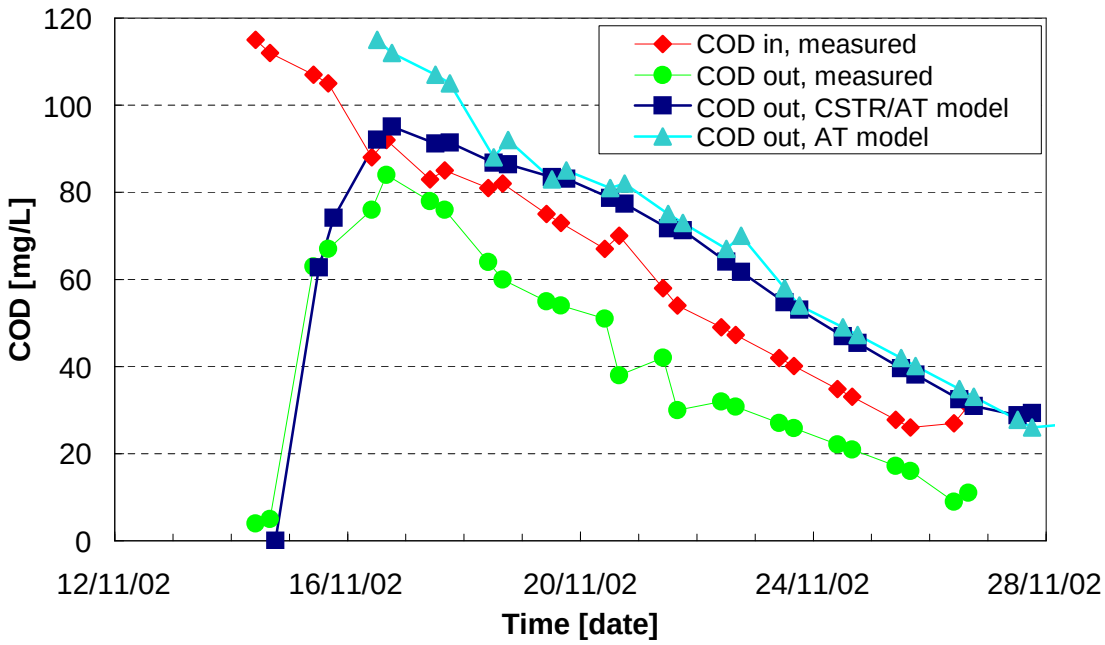

Figure 6.58. Temporal concentration of COD for Bed 4; observed influent and effluent concentration and transport-modelled effluent concentration

and 12 to 30 mg COD/L with the AT model. These similar values show that both models can be used to model the transport of pollutant through the reed beds, when the change in concentration is fairly small. However, it has to be stated, that the lowest or highest computed value of reduction efficiency were not computed at times of lowest or highest absolute COD reduction. While the higher efficiencies tend to be related with the lower influent concentration at later observations, the higher values of absolute COD reduction tend to be related to the observations in the temporal middle.

The highest efficiencies and absolute reduction rates were computed for Bed 2 and Bed 4 in an approximately identical range (Table 6.22). The values computed for Bed 10 and 12 are also in similar ranges but lower than Bed 2 and Bed 4. The efficiencies and absolute reduction rates for the Total Out are between the values of Bed 2/Bed 4 and Bed 10/Bed 12.

The different efficiencies and total reduction rates can be related to the hydraulic load of the beds. The measured discharge for Bed 2 (Table 6.22) is 2% lower than the design value (Table 5.7) and the measured discharge for Bed 4 is approximately 7% higher than the design value, thus these discharge rates are quite similar to the design value. The discharge rates for Bed 10 and Bed 12 are 43% and 67%, respectively higher than the design value. Since the design discharge rates are derived from identical hydraulic load for all beds it can be assumed, that the beds with the higher hydraulic load are not performing as well as the beds with the design load.

Table 6.22. Range of absolute, daily reduction and reduction per area of COD, computed from temporal observations

Location	Discharge	Area	Efficiency of COD reduction		Absolute reduction of COD, computed with		Mass of daily reduced COD, computed with		COD reduction per plan area, computed with	
			CSRT/AT model	AT model	CSRT/AT model	AT model	CSRT/AT model	AT model	CSRT/AT model	AT model
	[L s^{-1}]	[m^2]	[-]	[-]	[mg L^{-1}]	[mg L^{-1}]	[kg d^{-1}]	[kg d^{-1}]	[kg d^{-1} ha^{-1}]	[kg d^{-1} ha^{-1}]
Total Out	40	17561	31 - 66	30 - 68	14 - 36	12 - 39	48 - 124	41 - 135	28 - 71	24 - 77
Bed 2	5.16	2291	34 - 73	33 - 74	18 - 35	16 - 40	8 - 16	7 - 18	35 - 68	31 - 78
Bed 4	3.87	1526	34 - 72	34 - 74	16 - 41	15 - 44	5 - 14	5 - 15	35 - 90	33 - 96
Bed 10	1.99	765	26 - 65	30 - 67	15 - 32	13 - 32	3 - 6	2 - 6	34 - 72	29 - 72
Bed 12	2.33	767	29 - 54	27 - 57	14 - 31	12 - 33	3 - 6	2 - 7	37 - 81	31 - 87
Bed 5	1.99	1526	48 - 69	47 - 71	23 - 43	25 - 46	4 - 7	4 - 8	26 - 48	28 - 52
Bed 11	4.21	765	26 - 56	25 - 54	10 - 24	8 - 23	4 -9	3 - 8	48 - 114	38 - 109
Sum of all Beds	42.18						61 - 141	56 - 152		

The discharge through Bed 5 is approximately 50% of the discharge through Bed 4. While the higher values of the computed efficiencies and absolute reduction of COD are approximately similar to those of Bed 4, the lower values are approximately 14% or 10 mg COD/L higher. Bed 11, with a discharge approximately twice as high as the discharge of Bed 10 or Bed 12, shows an efficiency that is comparable to Bed 12 and that is around 10% lower than the efficiency of Bed 10. The absolute reduction in COD is around 4 mg/L to 10 mg/L. This is lower than those of Beds 10 and 12.

Interestingly, the fertilisation of Bed 12 did not show a significant change in treatment performance. The efficiency and absolute COD reduction of Bed 12 is even slightly lower than Bed 10. This difference is most likely caused by the difference in discharge rate.

In general it can be stated, that a longer residence time leads to a higher treatment performance and more reduction in COD. The longer beds (Bed 2, Bed 4) or beds with a lower discharge rate (Bed 5) did perform better compared to the other beds and to the average observed value at the outlet (Total Out). However, the magnification in bed size or discharge has not a similar magnification effect on the treatment performance.

However, from an engineering point of view, optimum removal rates in relation to the costs (here in terms of plan area) are favourable. Therefore the reduced mass per day and reduced mass of COD per area and day are shown in Table 6.22. For Bed 2 the largest total amount of COD reduction per day was observed. Bed 2 and Bed 4 are performing better for the mass removed per day. However, the highest COD reduction per area and day was observed for Bed 11, where Bed 2, Bed 4 Bed 10 and Bed 12 have a lower COD reduction per area and day.

Clearly, the smallest bed with the highest flow rate shows the highest reduction in COD per area and day.

Since the computation of efficiencies and absolute reduction of COD gave ranges and not single values, it is of interest to investigate the relationship of the concentrations of influent and effluent. In Figure 6.59 the influent concentrations of all temporal observations are plotted against the effluent for all observations. All plots show similar trends that tend to be not linear. The observed concentrations of Total Out, Bed 2 and Bed 12 show a logarithmic trend. Linear and logarithmic regressions were calculated for this data. The results are shown in Table 6.23a for the linear regression and Table 6.23b for the exponential regression, where the parameters for the Equations 6.7 and 6.8 and the coefficients of determination are given.

$$C_{out} = a\,C_{in} + b \qquad 6.7$$

$$C_{out} = a\,e^{b\,C_{in}} \qquad 6.8$$

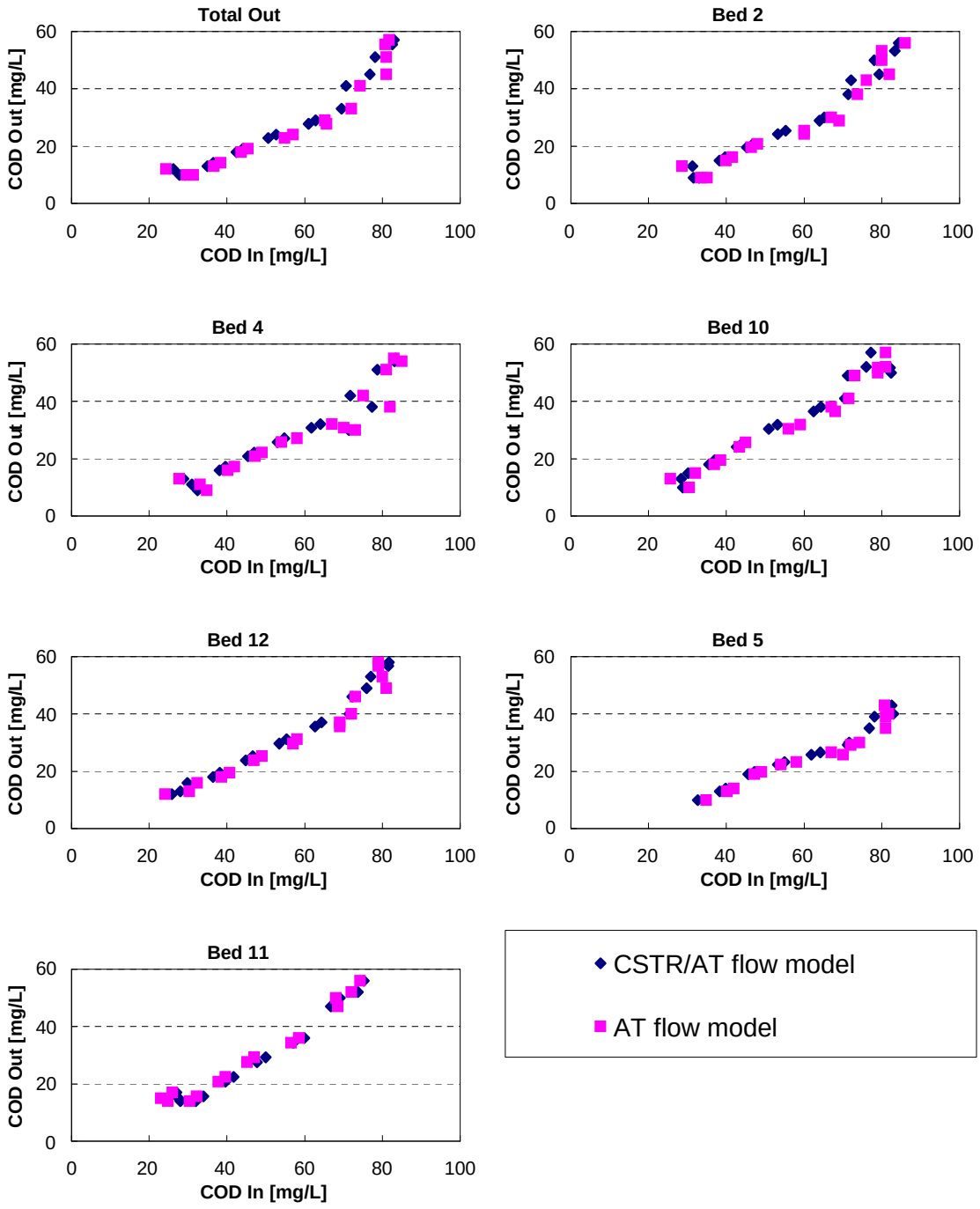

Figure 6.59. COD influent and effluent relation of temporal observations

Table 6.23. a) Relation of influent and effluent concentration of COD reduction of temporal observations; linear regression

Bed	Linear data regression					
	CSTR/AT model			AT model		
	a [-]	b [-]	R_t^2 [-]	a [-]	b [-]	R_t^2 [-]
Total	0.781	-14.283	0.9375	0.753	-14.261	0.8941
Bed 2	0.808	-17.010	0.9587	0.777	-16.825	0.9147
Bed 4	0.744	-12.983	0.9196	0.713	-12.886	0.8868
Bed 10	0.772	-9.435	0.9663	0.762	-10.243	0.9646
Bed 12	0.778	-10.113	0.9702	0.765	-10.909	0.9308
Bed 5	0.590	-9.438	0.9658	0.586	-10.447	0.9283
Bed 11	0.851	-11.289	0.9679	0.812	-8.008	0.9657

Table 6.23. b) Relation of influent and effluent concentration of COD reduction of temporal observations; exponential regression

Bed	Exponential data regression					
	CSTR/AT model			AT model		
	a [-]	b [-]	R_t^2 [-]	a [-]	b [-]	R_t^2 [-]
Total	4.815	0.030	0.9835	4.699	0.029	0.9674
Bed 2	4.339	0.031	0.9564	4.257	0.030	0.9399
Bed 4	5.239	0.028	0.9308	5.175	0.027	0.9159
Bed 10	6.773	0.027	0.9304	6.485	0.027	0.9483
Bed 12	6.907	0.026	0.9849	6.544	0.026	0.9799
Bed 5	5.338	0.025	0.9563	5.019	0.025	0.9417
Bed 11	6.560	0.029	0.9758	7.332	0.028	0.9736

For all cases the exponential trend has the better fit. The parameter *a* of the exponential regression can be interpreted as an initial reduction in COD and is for all observations of a similar magnitude between 4.3 to 6.9 mg COD/L. The parameter *b* of the regression equation was computed in the range of 0.025 to 0.031.

The linear regression is easier to interpret. The parameter *b* gives an initial reduction in concentration, in the range of 9 to 17 mg COD/L. The parameter *a* is then the additional reduction in COD with an increase in influent concentration.

It should be noted, that this test was performed at the beginning of the de-icing season. Therefore it is not clear, if the change in observed influent/effluent relation is due to an improvement in treatment efficiency during this test.

Clearly, a single efficiency, that is often stated in the literature (e.g. Revitt *et al.*, 1997; Vymazal, 2002) without further information about influent concentrations and conditions of the wetland system, is insufficient to describe the treatment performance. Vymazal (2002) observed very poor coefficients of determination between influent and effluent concentrations of several wetlands. The author goes on that efficiencies expressed as a percentage of removal could be misleading.

Literature reports that propylene glycol (PG) is readily degradable in laboratory tests (Chapter 2.3.2; Cox, 1978;Lamb and Jenkins, 1952; Price *et al.*, 1974; Briedie *et al.*, 1979). The propylene glycol used in this test was similarly readily biodegradable in the constructed wetlands. Further, PG degrades quicker under aerobic conditions than under anaerobic conditions. Kaplan *et al.* (1982) found in laboratory tests a complete degradation of PG within 2 to 4 days under aerobic conditions and within 4 to 9 days under anaerobic conditions. With observed residence times of approximately 2.5 days in the wetland and travel times through the gravel of approximately 1 day the computed efficiencies of 30 to 70 percent from the temporal observations seem to be comparable to the reported times needed for degradation. The efficiencies reported for anaerobic treatment in a bench scale reactor of 93% to 97% were achieved with residence times of 12 hours or 24 hours (Jank *et al.*, 1974) and are much higher than those observed in this test.

At the two stage experimental wetland system at Zurich airport the water was treated from 600 to 900 mg COD/L to below 40 mg COD/L after two month of operation and below the discharge consent of 20 mg COD/L during several month of operation (Flughafen Direktion Zürich, 1999). The removal rate per plan area reported for this experimental wetland of 320 kg COD ha^{-1} d^{-1} is approximately 3 to 4 times higher than the observed removal rate per plan area in test Series 2 of up to 70 to 110 kg COD ha^{-1} d^{-1} (Table 6.22). For the pilot constructed wetland at Heathrow airport efficiencies in the range of 59 to 99% were observed for PG (Revitt *et al.*, 1997). The tests at the real-scale wetland cannot confirm such high removal rates or

efficiencies. Furthermore, the data gained in the tests on the real-scale wetland system generally indicate a trend of a fairly steady removal in the range of 30 to 40 mg COD/L.

The design worst case, a reduction of BOD_5 from 108 mg/L to 40 mg/L with an efficiency of 63% was not reached during the tests on the real-scale wetland. Nevertheless, the tests were performed at the beginning of the de-icing season. Thus an increase of performance might be expected after a longer time of operation. However, the here obtained efficiencies and absolute reductions of glycol can be taken as worst-case removal efficiencies and rates.

6.3.6 Derivation of glycol degradation constants from spatial COD observations

The derivation of the rate constants of glycol degradation from the spatial tests at the reedbeds have to be computed by taking the travel times of water through the reed bed to each observation point into account. Further, the spatially measured concentrations have to be related to their initial concentration when entering the gravel beds. This is easy for the tests of Series 1, since a constant injection with a fixed concentration was used and therefore only the travel times through the gravel cells have to be computed. As shown before, the advective transport (AT) model is sufficient for this. Do to the changing inflow concentration of glycol in tests of Series 2 the CSTR/AT model will be used to relate the observed concentrations to their initial value. Also, the loss in head while the waters flows through the gravel cells will be taken into account. Intermediate water levels are computed from the estimated k-values (see Table 5.2) and observed water heads.

Test Series 1. The spatially observed COD profiles on Bed 4 of the Test Series 1 were presented in Figure 5.30. While the measured and fluorescence corrected COD concentrations are very similar in the cells 1 and 2 of Bed 4, they differ quite drastically for cell 3 and cell 4. A similar observation can be made for the test on Bed 11 (Figure 5.31). Here, the observed and corrected values are similar for cell 1 and they differ for cell 2. This might indicate that the time span between the start of the constant injection and the time of taking the actual measurements was not long enough to exchange and mix the whole water throughout the bed. Interestingly, the deviation of the observed and corrected concentration values seems to start at the middle of both beds. Here, from the design criterion of a similar hydraulic load, these locations within the two beds have similar travel times. Therefore, only the data of cells 1 and 2 of the test of Bed 4 and the data for the cell 1 of the test of Bed 11 will be taken into account for further computations of glycol degradation rates.

The COD concentrations on Bed 4 show an immediate decrease of approximately 10 mg COD/L in the first half of cell 1 and then a nearly linear decrease over a magnitude of approximately 12 mg COD /L up to the end of cell 2. The observed concentrations of COD on

Bed 11 follow a similar trend. Here, the initial decrease of approximately 12 mg COD/L is in the first quarter or so of cell 1 and thereafter the concentration decreases nearly linearly to a magnitude of 10 mg COD/L.

The associated measured oxygen concentrations for cell 1 of Bed 4 show depletion in magnitude from approximately 6 mg O_2/L to 2 mg O_2/L. It follows a linear decreasing trend for around three quarters of the length of the cell before becoming constant at 2 mg O_2/L. The observed oxygen level at the beginning of cell 2 is 3.4 mg O_2/L and higher than the level observed at the end of cell 1. The depletion in cell 2 follows a similar trend compared to cell 1. It decreases linearly in the first half of the cell and is thereafter constant at approximately 1.5 mg O_2/L. A nearly identical constant level is measured at cell 3. Literature (Chapra, 1997; Hammer, 1986) and the laboratory test (Chapter 6.3.2) show that the decay of oxygen in aerobic treatment processes follows an exponential trend. However, here observed oxygen depletion follows a linear decaying trend. Compared to the laboratory test the observed decay is quite slow and stops at a level between 1 and 2 mg O_2/L. The remaining low oxygen content in the water may indicate that low oxygen levels cannot be utilised in treatment processes.

The rise in oxygen at the beginning of the second cell cannot be explained with re-aeration, since the re-aeration rates for slow and laminar flowing water are too low for this magnitude of increase. An explanation for this might be that at this early stage the bacteria and biomass had not been fully developed over the whole depth of the gravel cells throughout the beds and that therefore the water was only partially treated. This would also explain the rise in oxygen concentration at the beginning of cell 2, which might then be caused by the redistribution of partially untreated water with higher oxygen content.

The oxygen concentrations for Bed 11 were only measured in the open channel sections, thus only the general trend in oxygen depletion is comparable to the measurements of Bed 4. The general trend of oxygen depletion seems to be similar. After the first half of the bed the oxygen concentration is at a level of approximately 1.8 mg O_2/L and similarly at the end of the bed with 1.4 mg O_2/L. The high initial value of 12 mg O_2/L is most likely caused by super-saturation of the water in the inlet channel due to the water cascading into it when entering the reedbed.

Since in the controlled test environment the only pollutant entering the reedbed was the injected glycol, it can be assumed that the oxygen depletion in the gravel cells is equivalent to the aerobic degradation of this glycol. Further, it can be assumed that the observed degradation in COD is equivalent to the biological degradation of glycol.

The reaction rates for the degradation of COD were computed as a first-order reaction. Since COD was not degraded completely within the reed beds, Equation 2.81 will be used for computation of the first order reaction rate k and the background concentration C^*. Estimation of these parameters is done by means of a least squares optimisation. The results of the

estimation process are shown in Table 6.24. The results of applying degradation models are shown in Figure 6.60 and Figure 6.61.

Table 6.24. Estimated glycol degradation rates for the spatial tests

Test	First order reaction rate k [day^{-1}]	Background Concentration C^* [mg COD/L]	Coefficient of determination R_t^2 [-]	Total reduction in COD of model [mg COD/L]
Test Series 1, Bed 4	5.1	33.0	0.7863	18.9
Test Series 1, Bed 11	5.6	110.3	0.7352	22.6
Test Series 2, Bed 4 Test 1	8.4	46.6	-0.0550	36.3
Test Series 2, Bed 4 Test 2	8.3	13.7	0.7331	14.8
Test Series 2, Bed 10 Test 1	8.3	51.1	0.1906	20.4
Test Series 2, Bed 10 Test 2	-	10.0	-9.7954	20.6

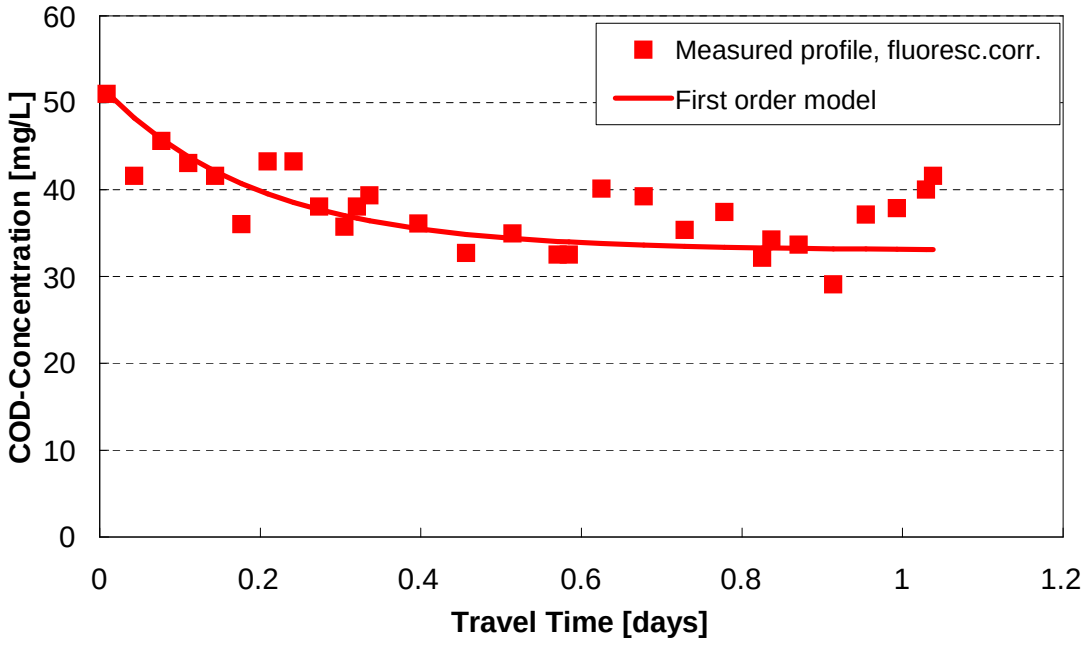

Figure 6.60. First order COD degradation model for Test Series 1, Bed 4

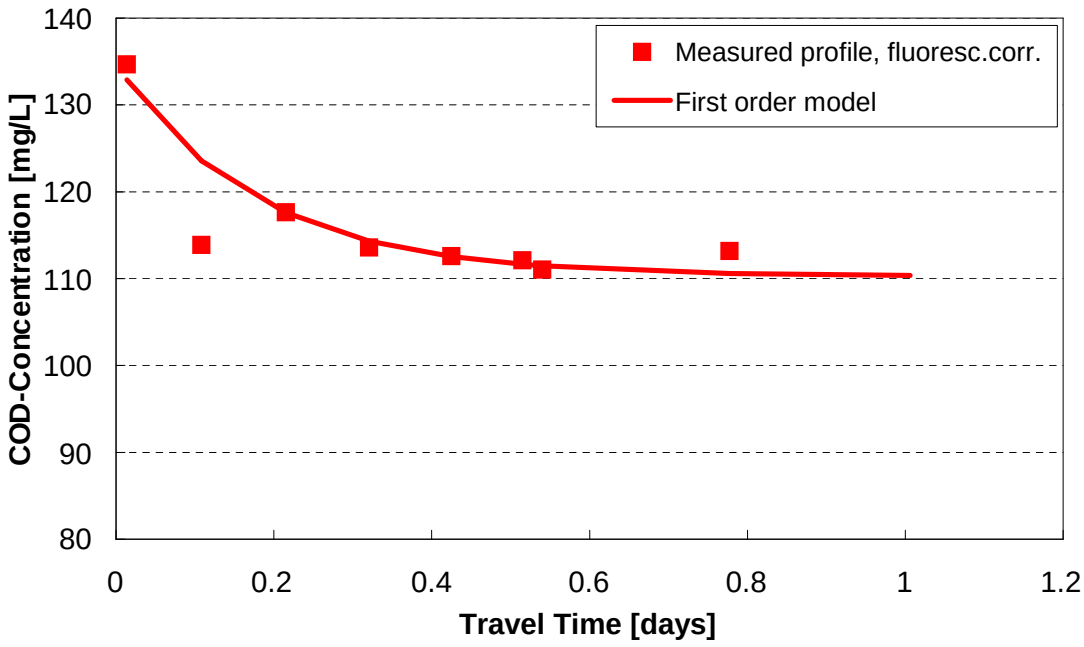

Figure 6.61. First order COD degradation model for Test Series 1, Bed 11

Test Series 2. The observed COD profiles of the spatial tests of the Test Series 2 were presented in Figure 5.34 and Figure 5.35. The observed COD profiles for Bed 4 shows for both test of Series 2 a clear trend of exponential decay. As in Test Series 1, no total reduction of COD was observed. The observations of Bed 10 show for both tests a nearly constant concentration of COD throughout the bed. The reason for this observed profile is uncertain, but might have been caused by surface flow since some surface ponding was visible. However, the temporal observations (Figure 5.37) show that the influent concentration of COD for these test were with levels of approximately 30 mg COD/L clearly above the observed concentration of 10 to 15 mg/L. Observed oxygen levels for Bed 4, as well as for Bed 10, were below 2 mg O_2/L throughout the bed. Higher levels of 6 to 8 mg O_2/L were only observed in the inlet channel of the beds.

The computation of the first order reaction rates was performed identical to the computations for Test Series 1. Since the concentration of COD in the influent was changing, these changes were taken into account by computation of the related influent concentration for each observation point in the profiles from the temporal COD observations. Concentrations were calculated by means of the CSTR/AT model as described in Chapter 6.3.3.

Computed parameters are shown in Table 6.24. Degradation models and related influent concentration are presented in Figure 6.62 to Figure 6.65. Since a meaningful computation of the first order degradation rate k could not be obtained from the data set of Bed 10, the rate estimated for Bed 10, Test 1 was used to estimate the value of background concentration C^*.

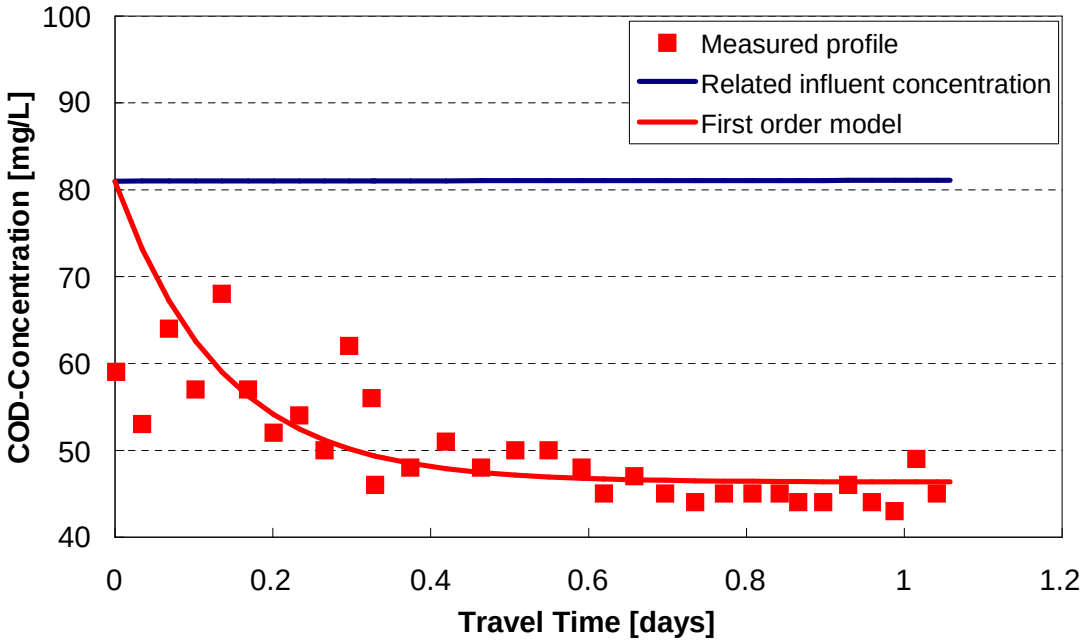

Figure 6.62. First order COD degradation model for Test Series 2, Bed 4 - Test 1

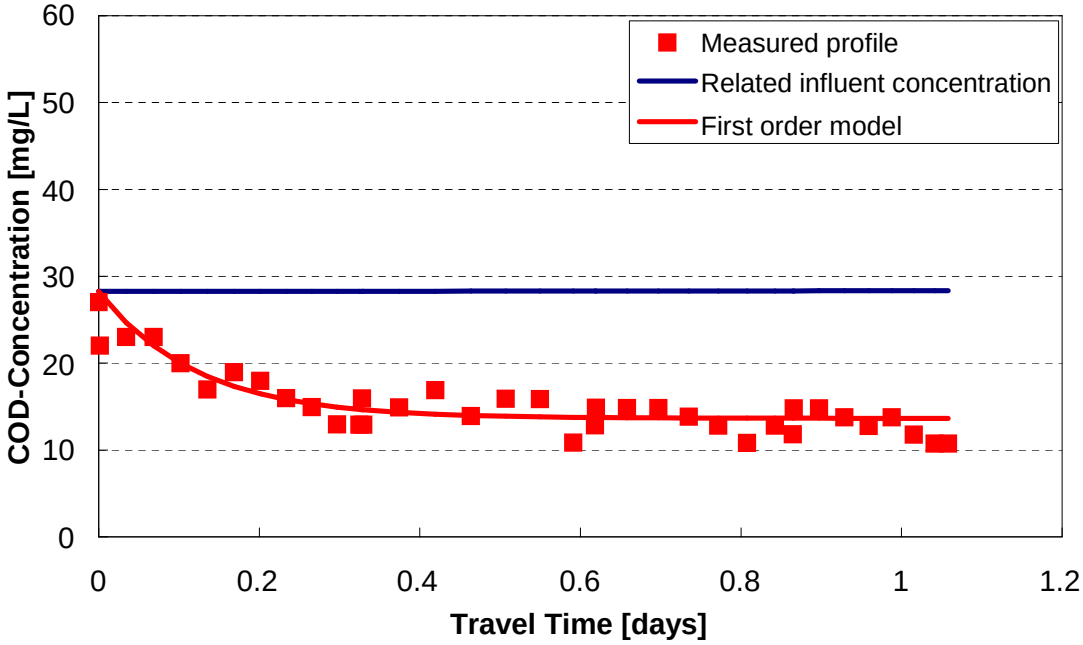

Figure 6.63. First order COD degradation model for Test Series 2, Bed 4 - Test 2

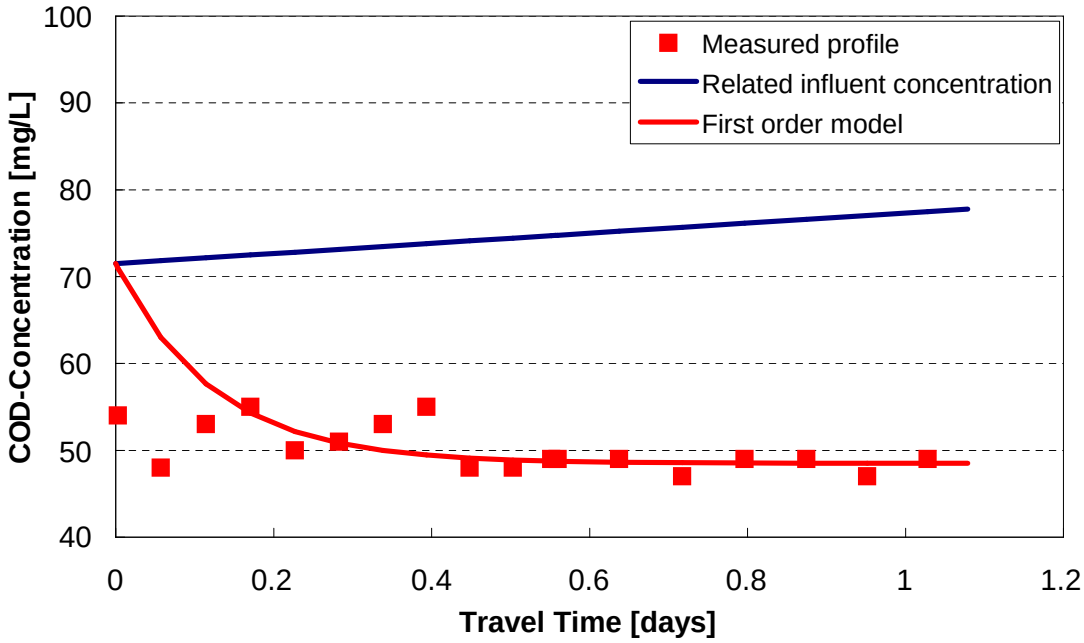

Figure 6.64. First order COD degradation model for Test Series 2, Bed 10 - Test 1

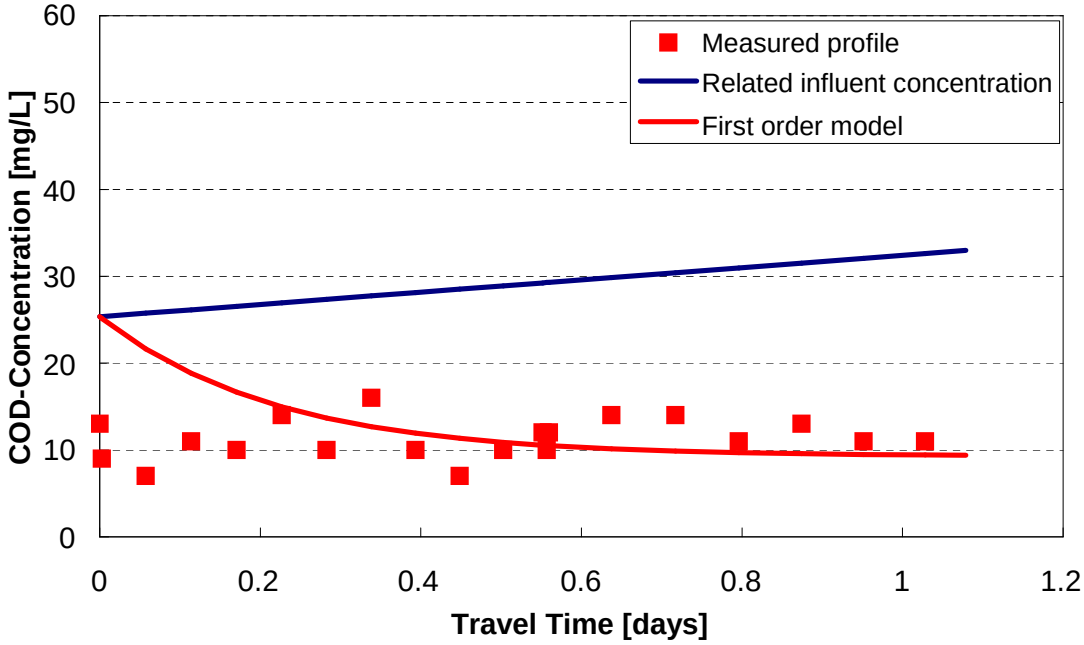

Figure 6.65. First order COD degradation model for Test Series 2, Bed 10 - Test 2

The tests of Test Series 1 show similar first order degradation rates k of 5.1 d^{-1} and 5.6 d^{-1}. Different initial concentrations of COD cause different levels of background concentration *C**. The total rates of COD reduction computed for both beds show a similar level of approximately 20 mg COD/L. The first order reaction rate model fits the data well with coefficients of determination of 0.79 for Bed 4 and 0.74 for Bed 11 respectively. The tests on Bed 4 Test Series

2 show nearly identical first order reaction rates of 8.3 d^{-1} to 8.4 d^{-1}. The rate of COD degradation is significantly larger compared to the rate computed for the tests of Test Series 1. However, the fit of the first order reaction rate models to the observed profile data is much poorer. Only for the data of Test 2 on Bed 4 a coefficient of determination could be computed in similar magnitude compared to Test Series 1. Again, the background concentration C^* is higher for the tests with the higher concentration of COD in the influent. This suggests, that for the application of wetlands for glycol treatment the value of C^* depends strongly on the influent concentration of COD. A relationship between influent concentration C and C^* is shown in Figure 6.66. The regression equation for this relationship is

$$C^* = 0.9172\, C - 16.8 \qquad 6.9$$

and has a coefficient of determination of 0.97. Kadlec and Knight (1996) computed a similar regression for BOD_5 of municipal wastewater. The authors state a weakly relationship between those parameters with an equation of

$$C^* = 0.053\, C + 3.5 \qquad 6.10$$

and a coefficient of determination of 0.67.

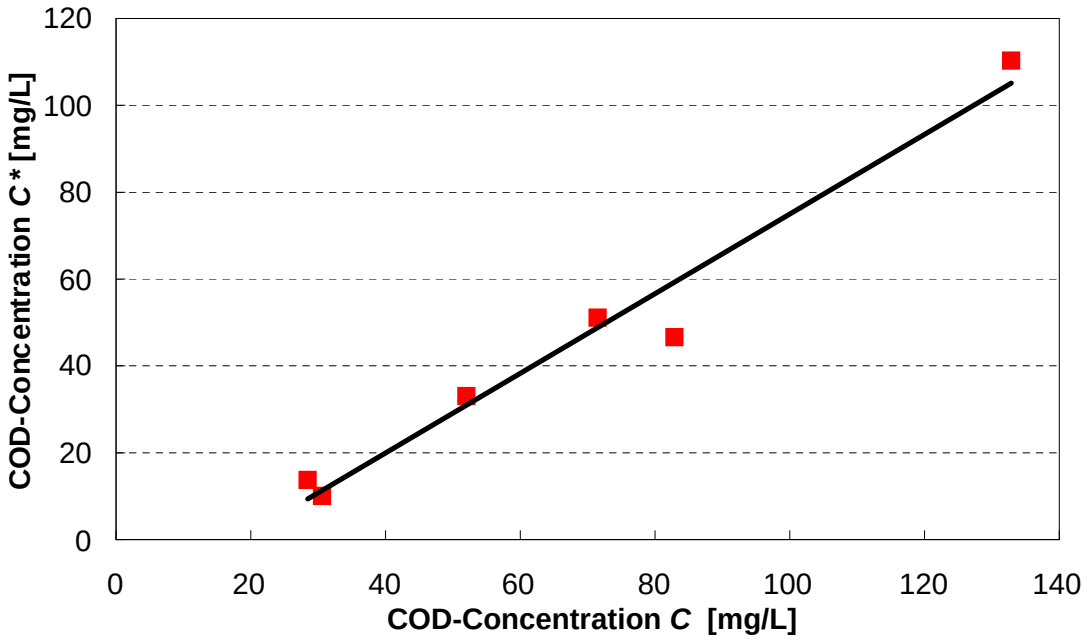

Figure 6.66. Relation of influent concentration C and background concentration C^* for all tests of Test Series 1 and Test Series 2

Table 6.25. Efficiency and total reduction of COD from temporal observations at the time of spatial tests

Test	Efficiency of COD reduction [-]	Total reduction of COD [mg COD/L]
Test Series 2, Bed 4 Test 1	30-35	26-32
Test Series 2, Bed 4 Test 2	55-64	15-19
Test Series 2, Bed 10 Test 1	36-32	20-23
Test Series 2, Bed 10 Test 2	47-51	17-19

The total reduction of COD varies between the tests. For the first test on Bed 4 a reduction of 36 mg COD/L was computed from the model. This compares quite well with the temporal observations, where a total reduction of approximately 32 mg COD/L was computed (see Chapter 6.3.5, Table 6.24 and Table 6.25). The reduction rates for the second test on Bed 4 are also of a similar magnitude of 15 mg COD/L. For both tests on Bed 10 total reduction rates of approximately 20 mg COD/L were determined. These values can be confirmed with the temporal COD observations; for both times a reduction rate of COD in the range of 20 mg/L was obtained for Bed 10. Both second tests on Bed 4 and Bed 10 indicate that the observed concentration of COD within the beds is not falling below a threshold of approximately 10 to 15 mg COD/L. The literature shows, that there is a certain background production of COD from the wetland itself, that is in a similar magnitude (e.g. Kadlec and Knight, IWA). However, the samples for the COD test were filtered before analysis, therefore it is quite certain that the measured COD is mainly due to the glycol and not to particulate organics carried in or produced within the wetland.

First order reaction rates for glycol removal were only reported for anaerobic treatment (Schoenberg *et al.*). The author states a first order degradation constant of 3.5 d^{-1} for PG-based de-icer and 5.2 d^{-1} for EG-based de-icer. Kadlec and Knight (1996) summarise rate constants for the degradation of BOD_5 in subsurface wetlands. They report first order rates in the range of 0.3 d^{-1} to 6.1 d^{-1} and compute a weighted mean of 1.96 d^{-1}. The here computed rate constants of 5.1 d^{-1} to 5.6 d^{-1} for Test Series 1 and 8.3 d^{-1} for Test Series 2 are much higher. This indicates that the process of degradation is faster compared to the values given in literature.

However, the high background concentrations of C^* show that the total reduction of COD is not comparable. It was previously stated in Chapter 6.3.5, that the performance of total COD reduction is lower than values reported in literature. As it can be seen in Figure 6.60 to Figure 6.65 takes the main reduction of COD place in the first third or quarter of the total time of travel

through the beds. It was gained from the temporal observations, that Bed 11, with the highest hydraulic load and the lowest residence time, had a significantly higher efficiency of COD removal per area and time. This and the rapid exponential reduction of COD while the water moves through the wetland may imply that a shorter construction of wetlands is generally more efficient for the purpose of treating glycol laden water. An even more rapid degradation in oxygen was observed in the laboratory tests with a first order degradation rate of 51 d^{-1} for a reduction of approximately 9 mg O_2/L. Since it can be assumed that the oxygen in the water allows for aerobic treatment of the glycol, it is not quite clear where this consumption of oxygen takes place. While this can be related to the observed level of oxygen in Test Series 1, a similar statement cannot be made for Test Series 2. However, the oxygen is depleted within the first quarter of the beds and it can be assumed that this will result in one-fifth to one-third of the total reduction in COD of glycol.

6.3.7 Summary of the evaluation of glycol treatment performance

It was highlighted, that the observed concentration of COD of the temporal observations did change slowly. For this slow change in concentrations both, the ADZ model and the CSTR models can describe the pollutant transport between inlet and outlet of the gravel beds with sufficient accuracy for model time intervals of 0.25 days or 0.75 days.

A comparison of temporal observation data between measured BOD_5 and COD concentrations showed a linear relationship with a BOD_5/COD ratio of 0.66 and indicate that the magnitude of glycol removal can be measured in terms of BOD_5 or COD.

The temporal observations of glycol removal showed treatment efficiencies in the range of 30% to 70 %, but only absolute reductions of up to 45 mg COD/L. The absolute reduction is therefore smaller than the design worst case of 68 mg BOD_5/L (Worrall *et al.*, 2001) and its equivalent of 103 mg COD/L.

The spatial observations of COD within the wetlands showed similar absolute removal rates and efficiencies. The removal could be described best by a first order trend. The observed oxygen levels could not be directly related to the COD removal. However, the removal of COD was observed to be slower in regions further downstream, e.g. in the second half of the beds, where little or no oxygen was measured. The depletion of oxygen in the field was much slower compared to the laboratory test.

The removal of COD per area and flow rate was highest for the smallest bed with the greatest flow rate. This is consistent with the previous observation that the main removal of COD takes place within the first half of the beds.

From temporal and spatial observations it was concluded, that the absolute removal of COD is higher with higher influent concentrations of COD into the wetland system.

The effect of temperature will obviously affect the kinetic rates for glycol degradation and oxygen depletion. While the air temperatures for both field tests were approximately similar with temperatures in the range of +5 to 10°C and approximately +15°C for the laboratory test, no test was performed at the freezing point.

6.4 PART C: A MODEL FOR GLYCOL REMOVAL IN THE SSF CONSTRUCTED WETLAND

6.4.1 Development of a temporal glycol removal model and application to observed data

For the prediction of glycol or COD effluent concentrations a degradation component has to be added to the flow models developed previously and shown in Chapter 6.3.1. While the degradation of glycol within a bed of the wetland can be sufficiently described by a first order reaction, the aim here is to predict the effluent concentration of the whole system.

Efficiencies and absolute reduction rates for COD were presented in Table 6.22. However, it was observed that the efficiencies or absolute reduction rates depend on the magnitude of the concentration of COD in the influent. Further, it was shown that a fixed COD reduction rate was not suitable to describe the observed system. Nevertheless, the developed CSTR/AT transport model will be used and the degradation of COD will be modelled with a fixed reduction rate and a reduction rate that depends on the actual COD concentration of the influent. This model will be applied to the observed temporal concentrations of influent (Total In) and effluent (Total Out) of the wetland system.

Since all beds have nearly similar residence times and mixing behaviour (Chapter 6.2.3), the transport for the whole system is modelled with the CSTR/AT model obtained for Bed 4. The obtained concentration/time distributions are shown in Figure 6.67. COD reduction efficiencies were observed in the range of 30% to 70% (Table 6.22). Fixed efficiencies of 30%, 50% and 70% are the transport-modelled data. The resulting effluent concentrations are shown in Figure 6.68 for each efficiency. The graphs show clearly, that no such model can describe the full-observed concentration distribution at the outlet. While the model with the lower efficiency of 30% fits the higher concentrations, the 50% and 70% efficiency models describe the lower concentrations much better.

A relationship between influent concentration and background concentration for the fit of a first order reaction rate was gained from Figure 6.66 and presented as Equation 6.10. This equation can be interpreted in terms of a level of treatment that is achievable depending on the influent concentration during the observed residence times. The background concentration C^* is then simply the effluent concentration that depends on the influent concentration. Similar to the fixed efficiency model, the equation is added for the computation of COD reduction is added

after the computation of the pollutant transport. The computed effluent concentrations for this model are presented in Figure 6.69 as the *C** treatment model. A reasonably well-defined coefficient of determination R_T^2 of 0.7381 underlines the good fit of this model to the observed data.

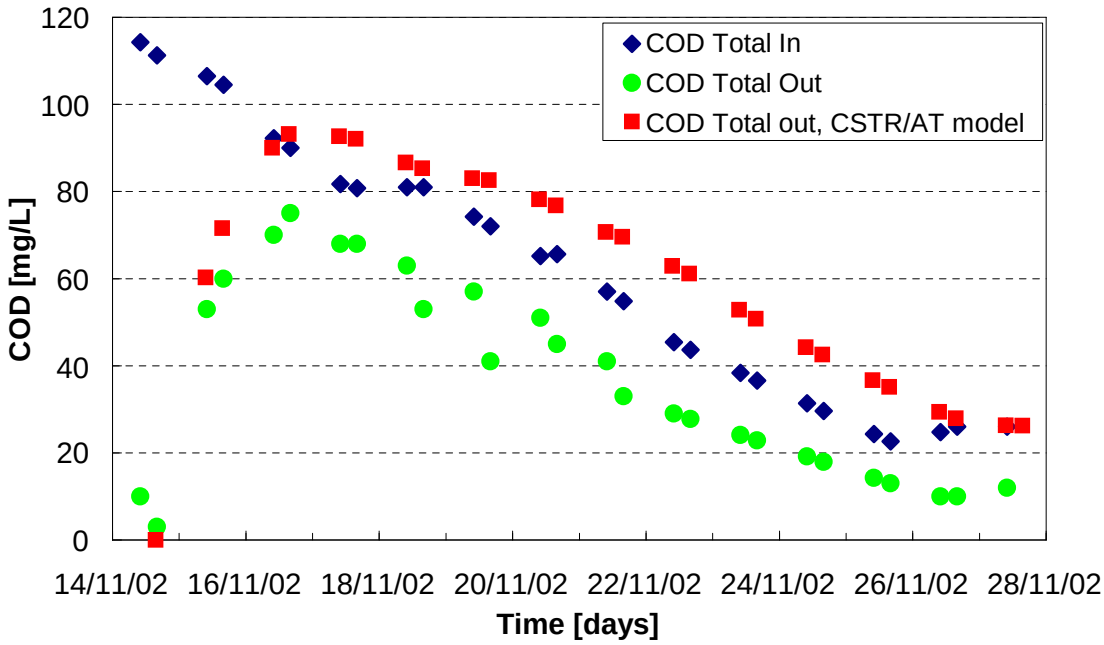

Figure 6.67. Observed and transport modelled COD concentrations

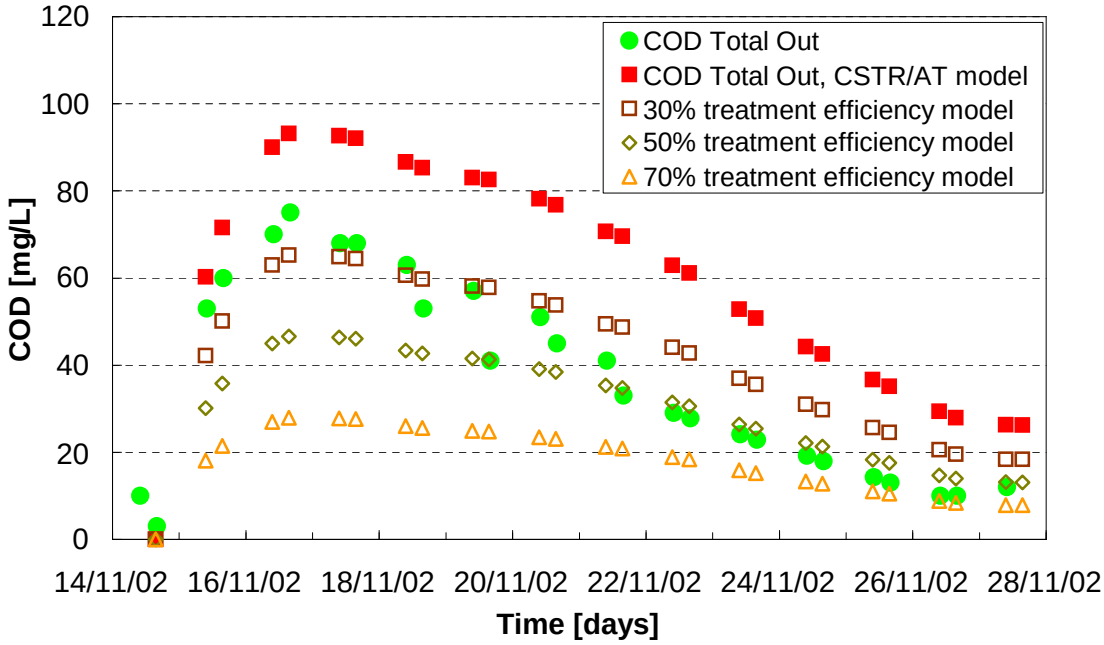

Figure 6.68. COD reduction model with fixed removal efficiencies of 30%, 50% and 70%

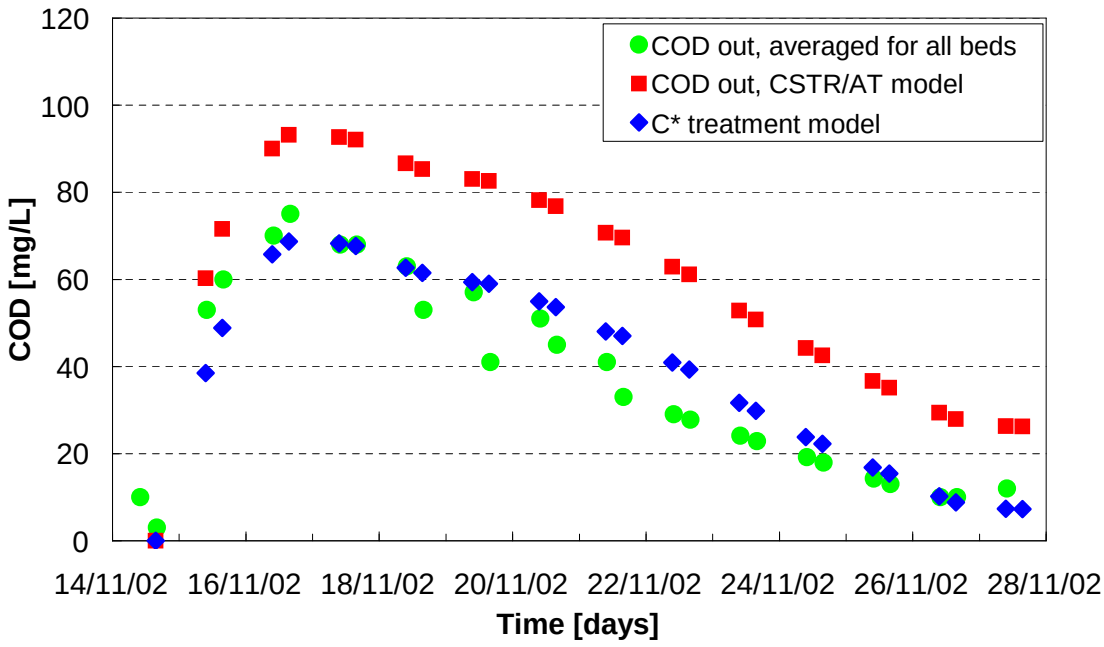

Figure 6.69. COD reduction model with *C** related reduction rates

In a similar manner the CSTR/AT transport model and *C** pollutant reduction model will be applied to the recordings of BOD from the BiOX-meters. The reading from the Balancing Pond will be taken as influent concentrations and the readings at the Site Outlet (note that it is not identical with the observation point of the wetland outlet "Total Out") are taken for the effluent concentrations. Since a linear relationship between BOD_5 and COD was found between the BOD_5 and COD measurements of the temporal observation test (Chapter 6.3.3), this model might be directly applied to the BiOX-data. However, the BiOX-meter of the Balancing Pond does monitor the BOD level in the bulk water in the area of the transfer pumps and not in the water that is transferred into the subsurface wetland system.

Figure 6.70 shows the temporal observed concentrations of the BiOX-meter, the BOD_5 and the COD, while Figure 6.71 shows the values for the effluent. The shown BOD_5 concentrations are the averaged values for the influents and the effluents of all beds (Chapter 6.3.3). The COD values are taken from the observation location "Total In" and "Total Out" at the wetlands inlet and outlet. The BiOX-readings show a great variation for both, influent and effluent. Even throughout the day readings show a variation in a magnitude of 10 to 20 mg BOD/L. Nevertheless, both BiOX-meters clearly show a general trend for the concentrations of BOD. The influent observations for BOD_5 and COD do not match closely with the BiOX-readings from the Balancing Pond (Figure 6.70). A similar decaying trend is visible from the 16/11/02 onwards. The magnitudes of the BiOX-BOD readings tend to be at a similar level as the COD concentrations. The observations for the effluent concentrations are more closely matched (Figure 6.71). BOD, COD and BiOX-BOD show similar trends for the effluent. The magnitude

of the BiOX-BOD readings is between the observed BOD_5 and COD concentrations. Further, a small time shift of the BiOX-readings compared to the other concentrations is visible. Obviously is this an advective time delay for the water covering the distance between the outlet of the subsurface reedbed and the sampling station of the BiOX-meter. The magnitude of this advective time delay can roughly be estimated from the data as approximately 12 hours. It is not clear, what further reduction of pollutant is achieved during this advection.

In Figure 6.72 the computed effluent concentrations are shown after applying the CSTR/AT model for pollutant transport, the C^*-model for pollutant reduction and the 12 hours advective time delay to the BiOX-data and the COD data. While the shape of the modelled COD effluent concentrations match the observed BiOX-meter readings at the outlet, the COD concentrations are much higher than the observed BOD concentrations of the BiOX-meter. When applying the BOD_5/COD correlation factor of 0.656 (Table 6.21) to the modelled COD effluent data, then the BiOX-BOD and the gained BOD_5 data match quite well. The modelled effluent concentration from the BiOX-meter influent readings of the Balancing Pond do not compare well with the observed effluent concentrations. Only the rising limb of the modelled distribution matches the observations, but this is mainly caused the modelling process itself.

The reasons for the poor predictions, when using the Balancing Pond BiOX data, and the rather successful modelling, when using the COD data, may lie in the different preparation of both BiOX meters. The BiOX-meter at the wetland systems outlet was continuously conditioned and acclimatised to glycol by injecting glycol of a concentration of approximately 10 mg BOD_5/L as soon as the measured effluent concentration dropped below this value. This was not done for the BiOX-meter of the Balancing Pond. Further, as already mentioned before, the bulk water is monitored by the Balancing Pond BiOX-meter. Therefore the immediate relation of both BiOX-meter by a pollutant-transport/pollutant-degradation model is quite uncertain.

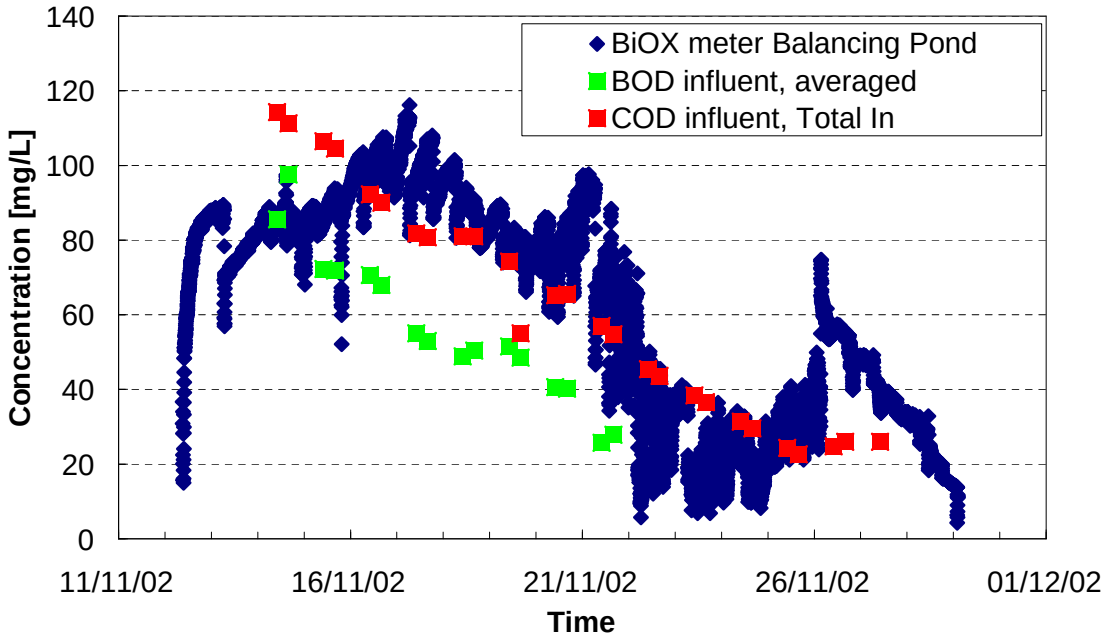

Figure 6.70. Temporal observed influent concentrations: BiOX-meter, BOD_5 and COD

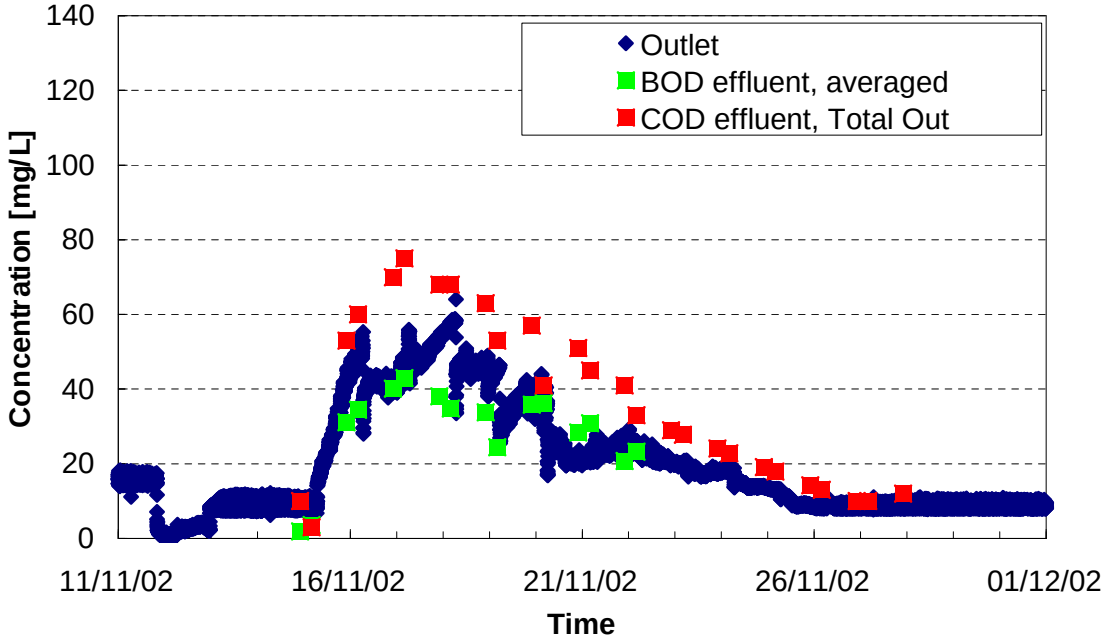

Figure 6.71. Temporal observed effluent concentrations: BiOX-meter, BOD_5 and COD

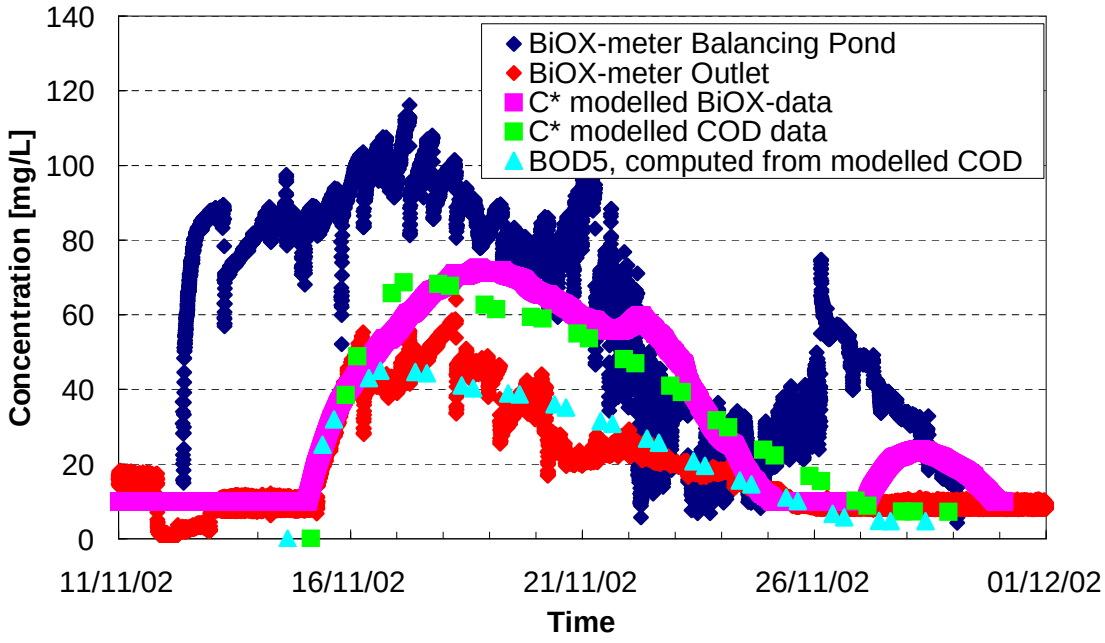

Figure 6.72. *C** modelled effluent concentrations for BiOX-meter readings and COD

6.4.2 Summary of modelling glycol removal in subsurface wetlands

The reduction in glycol measured in COD for the temporal observations and in BiOX-BOD for the BiOX-meter observations was quite accurately modelled with removal levels that are not fixed but related to the influent concentrations. The parameters for the model were taken from the results of the evaluation of the temporal and spatial COD observations. The model is therefore consistent with the previous knowledge.

Chapter 7

CONCLUSIONS

7.1 INTRODUCTION

Due to discharge consent standards and an increase in the public awareness of environmental pollution, many airports are now facing the dual challenge of maintaining public safety and protecting the environment. Very few airports have recovery systems for aircraft de-icer and thus most runoff-based pollutants enter surface waters. Airfield runoff, containing glycol based de-icing agents, has the potential to impose enormous oxygen demands on receiving waters, leading to degradation of the resource. Surface water discharges containing glycol frequently have a BOD in excess of 200 mg/l. This is pressuring airport operators to examine alternative methods for managing de-icing fluid wastewater.

A novel way of treating the airport runoff was introduced with the implementation of a gravel type subsurface flow reed system by British Airport Authorities (BAA) at Heathrow Airport. The use of constructed wetlands has become relatively widespread and covers a large number of applications. Constructed wetlands act as an efficient water purification system and nutrient sink. They efficiently remove BOD, COD, suspended solids, nitrogen, phosphorus metals, hydrocarbons and pathogens. Due to the movement towards sustainable, environmental engineering relying on natural ecologic processes, such artificial systems are being increasingly used rather than traditional energy and chemical intensive treatment processes.

Therefore the assessment of the performance of the subsurface reed beds at Heathrow Airport has a significant importance for further designs of treatment applications. To date no data of real scale applications of subsurface reed beds has been published. Several tests were undertaken to study the removal of glycol within a full-scale constructed wetland. In addition, the hydraulics of the beds were examined by means of fluorescent tracer studies to gain insights into the residence time distribution of pollutants entering the constructed wetland.

7.2 CONCLUCIONS

- Two approaches to modelling the transport of a solute have been evaluated, namely the Aggregated Dead Zone (ADZ) model and the Advective Dispersive Equation (ADE) model. A framework for the application of the models was developed and the ADZ model was extended to the general SRIV modelling technique. Two models were considered for further evaluation, the SRIV model (a multi order ADZ model) and a combined CSTR/ADE model (combining a single ADZ cell and the ADE equation). In addition to the model building process and the estimation of parameters, parametric studies were undertaken because the guidance available for using these models to predict the transport of a solute in subsurface flow wetlands is limited. This modelling study is believed to be one of the most comprehensive undertaken to date in the context of transport of solutes in full-scale subsurface flow wetlands.

    - ***SRIV model.*** The SRIV identified models describe the observed residence time distributions well. For all observed residence time distributions identical model structures were identified. The model structure is a physically very reasonable explanation for the pollutant transport between the inlet and outlet of a subsurface flow wetland.

    - ***CSTR/ADE model.*** The CSTR/ADE model could fit the observed residence time distributions as good as the SRIV-model. The deterministic ADE-module describes the flow through the gravel cells and the stochastic CSTR-module summarises the mixing effects of the open water sections. The estimated parameters for the ADE module of the model compare well to observed values and literature. Since the ADE is used to model groundwater flow, the combined modelling technique is physically very reasonable to explain the mixing between the inlet and outlet of the subsurface wetland and to describe the movement of solutes within the gravel matrix.

- Temporal and spatial observations were undertaken to access the removal of glycol in subsurface flow wetlands. Data was collected for the temporal observations over a period of 14 days from six different beds. Spatial observations were undertaken in two consecutive years on two different beds. This study is believed to be the most comprehensive undertaken to date in the context of a full-scale operative subsurface flow wetland for the treatment of airport runoff.

- The assessment of the data showed consistency between the temporal and spatial observations.

- BOD_5 and COD did show a linear relationship with a BOD_5/COD ratio of 0.66 and indicate that the magnitude of removed glycol can be measured in terms of either BOD_5 or COD.

- Treatment efficiencies were observed in the range of 30% to 70 %.

- Absolute removal of COD was measured up to 45 mg COD/L. The absolute reduction is therefore smaller than the design worst case of 103 mg COD/L.

- The absolute removal of glycol or COD is dependent on the magnitude of influent concentrations into the wetland system and is increasing with a higher influent concentration.

- The removal of COD within the subsurface flow wetland was described best by first order kinetics.

- The removal of COD per area and flow rate was observed of being best for the smallest bed with the highest flow rate. This is consistent with the observation that the main removal of COD takes place within the first half of the beds.

- The overall observed reduction in glycol measured as COD for the temporal observations and in BiOX-BOD for the BiOX-meter observations were accurately modelled using parameters gained from the glycol removal tests and using the previously built transport models. The model is consistent with the knowledge gained from the assessment of the subsurface wetlands hydraulics and the assessment of the removal of glycol within the subsurface flow wetlands. This model is believed to be a unique contribution towards general design of wetlands for treating airport runoff.

Chapter 8

RECOMMENDATIONS FOR FURTHER WORK

In the author's opinion there a two key direction for further work. The first would be an extension of the current study in terms of temporal development of the beds and the change in treatment efficiency with time. The second would be to investigate options that could be added, changed or exchanged to improve the treatment efficiency of glycol removal.

8.1 EXTENSION OF THE CURRENT STUDY

- Repeating of the test with temporal observations of glycol removal at the beginning and ending of the de-icing season in consecutive years.

- Assessment of the removal ability of different glycol types and mixtures of glycol.

- Investigations into the effect of air-temperature on the treatment efficiency of the subsurface flow reed-beds.

- Assessment of the storage pond aeration system in the wintertime. Will the treatment performance of the wetlands be sufficiently different without the aeration of the water in the storage ponds and does the aeration of the water at low air temperatures affect the water temperature and therefore decrease the treatment performance?

- Measurements of the oxygen content at different depth within the bed. Do defined vertical oxygen profiles exist and how do they develop throughout the bed?

- Assessment of the development of preferential flow paths with time and bed maturation.

- More detailed investigations into the effect of the first open channel section on the mixing.

8.2 OTHER POINTS OF INTEREST

- Evaluation of a vertical flow reed bed for the treatment of airport runoff. A vertical flow reed bed could show higher removal rates and treatment efficiencies for glycol since the degradation processes are rather aerobic than anaerobic.

- Assessment of different substrate media to find an optimum substrate for the removal of glycol in subsurface flow wetlands.

- Investigations into the effect of re-aerating the water within the wetland, e.g. installation of aeration pipes in the open channel sections of the wetlands.

- Utilisation of the balancing pond for additional treatment. Since the balancing pond is a fully aerated basin with a relatively long retention time, the option of adding structures with a high surface area in the water body, e.g. artificial elements of trickling filters, might improve the treatment performance drastically. The wetland system might then act as a tertiary treatment system.

REFERENCES

Aris, R., 1956. On the dispersion of a solute in a fluid flowing through a tube. Proceedings of the Royal Society, London, Series A, 235: 67-77.

Armstrong, W., Armstrong, J. and Beckett, P.M., 1990. measurement and modelling of oxygen release from roots of *Phragmites australis.* In: P.F. Cooper and B.C. Findlater (Editors), Constructed Wetlands in Water Pollution Control. Pergamon Press, Oxford, U.K., pp. 41-51.

Bausmith, D.S. and Neufeld, R.D., 1999. Soil biodegradation of propylene glycol based aircraft de-icing fluids. Wat. Env. Res., 71(4): 459-464.

Bear, J., 1972. Dynamics of fluids in porous media. Environmental science series. American Elsevier Pub. Co., New York, 764 pp.

Bear, J. and Corapcioglu, M.Y., 1991. Transport processes in porous media. NATO ASI series. Series E, Applied sciences ; vol. 202. Kluwer Academic Publishers, Dordrecht ; Boston, xii, 825 pp.

Beer, T. and Young, P.C., 1983. Longitudinal dispersion in natural streams. Journal of Environmental Engineering, 109: 769-776.

Betts, K.S., 1999. Airport pollution prevention takes off. Environ. Sci. Technol., 33: 210A-212A.

Beven, K.J., 2000. Rainfall-Runoff Modelling: the primer. John Wilery & Sons, Chichester.

Bielefeldt, A.R., Illangasekare, T., Uttecht, M. and LaPlante, R., 2002. Biodegradation of propylene glycol and assocoated hydrodynamic effects in sand. Water Res., 36: 1707-1714.

Börner, T., von Felde, K., Gschlössl, T., Gschlössl, E., Kunst, S. and Wissing, F.W., 1998. Germany. In: J. Vymazal, H. Brix, P.F. Cooper, M.B. Green and R. Haberl (Editors), Constructed wetlands for wastewater treatment in Europe. Backhuys, Leiden, pp. 17-66.

Briedie, A.L., Wolff, C.J.M. and Winter, M., 1979. BOD and COD of some petrochemicals. Water Res., 13: 627-630.

Brix, H., 1990. Gas exchange through the soil-atmosphere intrface and through dead culmps of *Phragmites australis* in a constructed wetland receiving domestic sewage. Water Res., 24: 259-266.

Brix, H., 1993. Wastewater treatment in constructed wetlands: system design, removal processes and treatment performance. In: G.A. Moshiri (Editor), Constructed Wetlands for Water Quality Improvement. CRC Press, Boca Raton, Florida, pp. 9-22.

Brix, H., 1993a. Macrophyte-mediated oxygen transfer in wetlands: transport mechanisms and rates. In: G.A. Moshiri (Editor), Constructed Wetlands for Water Quality Improvement. CRC Press, Boca Raton, Florida, pp. 391-398.

Brix, H., 1997. Do macrophytes play a role in constructed treatment wetlands? Water Science and Technology, 35(5): 11-17.

Brix, H., 1998. Denmark. In: J. Vymazal, H. Brix, P.F. Cooper, M.B. Green and R. Haberl (Editors), Constructed wetlands for wastewater treatment in Europe. Backhuys, Leiden, pp. 17-66.

Cancilla, D.A., Holtkamp, A., Matassa, L. and Fang, X., 1997. Isolation and charaterization of microtox-active components from aircraft deicing/anti-icing fluids. Environ. Toxicol. Chem., 16: 430-434.

Carleton, J.N., 2002. Damköhler number distribution and constituent removal in treatment wetlands. Ecological Engineering, 19: 233-248.

Chadwick, A.J. and Morfett, J.C., 1993. Hydraulics in civil and environmental engineering. Spon.

Chapra, S.C., 1997. Surface water-quality modelling. McGraw-Hill, New-York.

Charbeneau, R.J., 2000. Groundwater hydraulics and pollutant transport. Prentice Hall, Upper Saddle River, NJ.

Chong, S., Garelick, H., Revitt, D.M., Shutes, R.B.E., Worrall, P. and Brewer, D., 1999. The Microbiology Associated with Glycol Removal in Constructed Wetlands. Water Science and Technology, 40(3): 99-107.

Cooper, P., 1999. A review of the design and performance of vertical-flow and hybrid reed bed treatment systems. Water Science and Technology, 40(3): 1-9.

Cooper, P. and Green, B., 1998. United Kingdom. In: J. Vymazal, H. Brix, P.F. Cooper, M.B. Green and R. Haberl (Editors), Constructed wetlands for wastewater treatment in Europe. Backhuys, Leiden, pp. 17-66.

Cooper, P.F., Job, G.D., Green, M.B. and Shutes, R.B.E., 1996. Reed beds and constructed wetlands for wastewater treatment. WRc plc, Medmenham, U.K.

Cox, D.P., 1978. The biodegradation of polyethylene glycols. Adv. Appl. Microbiol., 23: 173-194.

Cyrotech, 2002. Health and safety data sheet; Kilfrost DF Plus 88 Type I Aircraft Deicing Fluid.

Cyrotech, 2002a. Health and safety data sheet; Kilfrost ABC-S Type IV Aircraft Deicing Fluid.

Etherington, J.R., 1983. Wetland Ecology. Studies in Ecology, 154. Edward Arnold, London.

Evans, W.H. and David, E.J., 1974. Biodegradation of mono, di- and triethylene glycols in river waters under controlled laboratory conditions. Water Res., 8: 97-100.

Fischer, H.B., 1966. A note on the one-dimensional dispersion model. Air & Wat. Pollut. Int. Jour., 10: 443-452.

Fischer, H.B., 1979. Mixing in inland and coastal waters. Academic Press, New York.

Fisher, D.J., Knott, M.H., Turley, S.D., Turley, B.S., Yonkos, L.T. and Ziegler, G.P., 1995. The acute whole effluent toxicity of stormwater from an international airport. Environmental Toxicology and Chemistry, 14(6): 1103-1111.

Flughafen Direktion Zürich, 1999. Reinigung der Enteiserabwässer am Flughafen Zürich, Flughafendirektion Zürich, Zürich.

Flygt, 2003. Pump data sheet. Flygt Pumps, Sweden/U.K.

Freeze, R.A. and Cherry, J.A., 1979. Groundwater. Prentice-Hall, Englewood Cliffs, N.J.

Gopal, B., 1999. Natural and constructed wetlands for wastewater treatment: potentials and problems. Water Science and Technology, 40(3): 27-35.

Gries, C., Kappen, L. and Lösch, R., 1990. Mechanisms of flood tolerance in reed, Phragmites australis (Cav.) Trin. ex Steudel. New Phytol., 114: 589-593.

Guymer, I., 1999. A national database of travel time, dispersion and methologies for the protection of river abstractions; Agency R&D technical report P346, Environment Agency R&D Dissemination Centre, Swindon.

Hammer, M.J., 1986. Water and wastewater technology. Prentice Hall, Englewood Cliffs, New Jersey.

Hartwell, S.I., Jordahl, D.M., Evans, J.E. and May, E.B., 1995. Toxicity of aircraft de-icer and anti-icer solutions to aquatic organisms. Environmental Toxicology and Chemistry, 14(8): 1375-1386.

IWA, 2000. Constructed wetlands for pollution control: Processes, performance, design and operation. IWA Specialist Group on Use of Macrophytes in Water Pollution Control. IWA Publishing, London, UK.

Jank, B.E., Guo, H.M. and Cairns, V.W., 1974. Activated sludge treatment of airport wastewater containing aircraft deicing fluids. Water Res., 8: 875-880.

Kadlec, R.H. and Knight, R.L., 1996. Treatment wetlands. CRC Press, Inc., Boca Raton, Florida.

Kaplan, D.L., Walsh, J.T. and Kaplan, A.M., 1982. Gas Chromatographic Analysis of Glycols To Determine Biodegradability. Environ. Sci. Technol., 16(10): 723-725.

Karrh, J.D., Moriarty, J., Kornuc, J.J. and Knight, R.L., 2002. Sustainable management of aircraft anti/de-icing process effluents using a subsurface-flow treatment wetland, Wetlands for Wastewater Treatment; Wetlands and Remediation II.

Kaul, F. and Stewart, J., 1986. Hydrological and pollution aspects of airport drainage. Public Health Engineer, 14(3): 25-32.

Klecka, G.M., Carpenter, C.L. and Landenberger, B.D., 1993. Biodegradation of aircraft deicing fluids in soil at low temperatures. Ecotoxicology and Environmental Safety, 25: 280-295.

Knight, R.L., Ruble, R.W., Kadlec, R.H. and Reed, S., 1993. Wetlands for wastewater treatment performance database. In: G.A. Moshiri (Editor), Constructed Wetlands for Water Quality Improvement. CRC Press, Boca Raton, Florida, pp. 391-398.

Knopman, D.S. and Voss, C.I., 1987. Behaviour of sensitivities in the one-dimensional advection-dispersion equation: Implications for parameter estimation and sampling design. Water Resources Research, 23(2): 253-272.

Laber, J., Haberl, R. and Shrestha, R., 1999. Two-stage constructed wetland for treating hospital wastewater in Nepal. Wat. Sci. Tech., 40(3): 317-324.

Lagarias, J.C., Reeds, J.A., Wright, M.H. and Wright, P.E., 1998. Convergence Properties of the Nelder-Mead Simplex Method in Low Dimensions. SIAM Journal of Optimization, 9(1): 112-147.

Lamb, C.B. and Jenkins, G.F., 1952. BOD of synthetic organic chemicals. Proc. Ind. Waste Conf., 7th 1952, 79: 326-339.

Litchfield, D.K., 1993. Constructed wetlands for wastewater treatment at Amoco Oil Company's Mandan, North Dakota refinery. In: G.A. Moshiri (Editor), Constructed wetlands for water quality improvement. CRC Press, pp. 485-488.

Ljung, L., 1999. System Identification. Prentice Hall, New Jersey.

Maehlum, T. and Jenssen, P.D., 1998. Norway. In: J. Vymazal, H. Brix, P.F. Cooper, M.B. Green and R. Haberl (Editors), Constructed wetlands for wastewater treatment in Europe. Backhuys, Leiden, pp. 17-66.

Mericas, B. and Wagoner, B., 2000. The challenge of winter weather. Ground Handling International, 1.

Metcalf & Eddy Inc., 1997. Wastewater Engineering: Treatment, Disposal, Reuse. McGraw-Hill, New York.

Nitschke, L., Wagner, H., Metzner, G., Wilk, A. and Huber, L., 1996. Biological treatment of waste water containing glycols from de-icing agents. Water Research, 30(3): 644-648.

Patten, B.C., 1990. Introduction and overview. In: B.C. Patten (Editor), Wetlands and Shallow Continental Water Bodies. SPB Academic Publishing, The Hague, pp. 3-8.

Perfler, R., Laber, J., Langergraber, G. and Haberl, R., 1999. Constructed wetlands for rehabilitation and reuse of surface waters in tropical and subtropical areas - first results from small-scale plots using vertical flow beds. Wat. Sci. Tech., 40(3): 155-162.

Pillard, D.A., 1995. Comparative toxicity of formulated glycol deicers and pure ehtylene and propylene glycol to *Ceriodaphnia dubia* and *Pimephales promelas*. Environ. Toxicol. Chem., 14: 311-315.

Price, K.S., Waggy, G.T. and Conway, R.A., 1974. Brine shrimp bioassay and seawater BOD of petrochemicals. J. Water Pollut. Cont. Fed., 46: 63-77.

Raisin, G.W. and Mitchell, D.S., 1995. The use of wetlands for the control of non point source pollution. Wat. Sci. Tech., 32(3): 177-186.

Reddy, K.R. and D'Angelo, E.M., 1997. Biogeochemical indicators to evaluate pollutant removal efficiency in constructed wetlands. Water Science and Technology, 35(5): 1-10.

Reed, S.C., Middlebrooks, E.J. and Crites, R.W. (Editors), 1995. Natural systems for waste management and treatment. McGraw-Hill, New York.

Revitt, D.M., Shutes, R.B.E., Llewellyn, N.R. and Worrall, P., 1997. Experimental reedbed systems for the treatment of airport runoff. Water Science and Technology, 36(8-9): 385-390.

Richardson, C.J., 1985. Mechanisms controlling phosphorus retention capacity in freshwater wetlands. Science, 228: 1424-1427.

Richter, K.M., Margetts, J.R., Saul, A.J., Guymer, I. and Worrall, P., 2002. Baseline Hydraulic Performance of the Heathrow Constructed Wetlands Subsurface Flow System. In: IWA (Editor), International World Water Conference, Melbourne, Australia.

Rutherford, J.C., 1994. River mixing. John Wiley & Sons, Chichester, England.

Saffermann, S.I., Siruvalure, G.S. and Foppe, L.E., 1998. Deicing fluid treatment in batch-loaded aerobic fluidize bed reactor. Journal of Environmental Engineering, 124(1): 11-15.

Saltelli, A., Chan, K. and Scott, E.M. (Editors), 2000. Mathematical and statistical methods: Sensitivity analysis. John Wiley & Sons, Chichester, England.

Schoenberg, T., Veltman, S. and Switzenbaum, M., 2001. Kinetics of anaerobic degradation of glycol-based Type I aircraft deicing fluids. Biodegradation, 12: 59-68.

Scholes, L.N.L., Shutes, R.B.E., Revitt, D.M., Purchase, D. and Forshaw, M., 1999. The removal of urban pollutants by constructed wetlands during wet weather. Wat. Sci. Tech., 40(3): 333-340.

Shutes, R.B.E., Revitt, D.M., Mungur, A.S. and Scholes, L.N.L., 1997. Design of wetlands for the treatment of urban runoff. Wat. Sci. Tech., 35(5): 19-25.

Sikora, F.J., Thong, Z., Behrends, L.L., Steinberg, S.L. and Coonrod, H.S., 1995. Ammonium removal in constructed wetlands with recirculating subsurface flow: removal rates and mechanisms. Water Science and Technology, 32(3): 193-202.

Söderström, T. and Stoica, P., 1989. System identification. Series in system and control engineering. Prentice Hall International.

Sorrel, B.K. and Armstrong, W., 1994. On the diffculties of measurring oxygen release by root systems of wetland plants. J.Ecol., 82: 177-183.

Sorrel, B.K., Mendelssohn, I.A., McKee, K.L. and Woods, R.A., 2000. Ecophysiology of wetland plant roots, a modelling comparison of aeration in relation to species distribution. Ann.Bot., 86: 675-685.

Switzenbaum, M.S., Veltman, S., Mericas, D., Wagoner, B. and Schoenberg, T., 2001. Best management practices for airport deicing stormwater. Chemosphere, 43(8): 1051-1062.

Tanner, C.C., 2000. Plants as ecosystem engineers in subsurface-flow treatment wetlands. Water Science and Technology, 44(11/12): 9-17.

Tanner, C.C., Sukias, J.P.S. and Upsdell, M.P., 1998. Relationship between loading rate and pollutant removal during maturation of gravel bed constructed wetlands. J. Environ. Qual., 27: 448-458.

Turner-Designs, 2003. Application note: a practical guide to flow measurement. Turner Designs, Sunnyvale.

Unbehauen, H. and Rao, G.P., 1987. Identification of continuous systems. North-Holland systems and control series, 10. Elsevier Science Publisher.

USEPA, 1995. Emerging technology assessment: Preliminary status of airplany fluid recovery system. Report # EPA/832-R-95-005, Office of Waste Management.

Vymazal, J., 1998. Introduction. In: J. Vymazal, H. Brix, P.F. Cooper, M.B. Green and R. Haberl (Editors), Constructed wetlands for wastewater treatment in Europe. Backhuys, Leiden, pp. 1-16.

Vymazal, J., 2002. The use of sub-surface constructed wetlands for wastewater treatment in the Czech Republic: 10 years experience. Ecological Engineering, 18: 633-646.

Vymazal, J., Brix, H., Cooper, P.F., Haberl, R., Perfler, R. and Laber, J., 1998. Removal mechanisms and types of constructed wetlands. In: J. Vymazal, H. Brix, P.F. Cooper, M.B. Green and R. Haberl (Editors), Constructed wetlands for wastewater treatment in Europe. Backhuys, Leiden, pp. 17-66.

Wagner, B.J. and Harvey, J.W., 1997. Experimental design for estimating parameters of rate-limited mass transfer: Analysis of stream tracer studies. Water Resources Research, 33(7): 1731-1741.

Watson, J.T., Reed, S.C., Kadlec, R.H., Knight, R.L. and Whitehouse, A.E., 1989. Performance expectations and loading rates for constructed wetlands. In: D.A. Hammer (Editor), Constructed wetlands for wastewater treatment: municipal, industrial and agricultural. Lewis Publishers, Chelsea, MI, USA, pp. 319-351.

Wetzel, R.G., 2000. Fundamental processes within natural and constructed wetland ecosystems: short-term versus long term objectives. Water Science and Technology, 44(11/12): 1-8.

Wittgren, H.B. and Tobiason, S., 1995. Nitrogen removal from pretreated wastewater in surface flow wetlands. Water Science and Technology, 32(3): 69-78.

Worrall, P., 1995. Reed beds for glycol treatment. IAWQ Specialist Group: The Use of Macrophytes in Water Pollution Control Newsletter, 12: 13-14.

Worrall, P., 2000. Personal Communication; De-icers and anti-icers used at Heathrow airport.

Worrall, P., Revitt, D.M., Pricket, G. and Brewer, D., 2001. Constructed wetlands for airport runoff - the London Heathrow experience. In: K. Nehring and S.E. Brauning (Editors), Wetlands and Remediation II, proceedings of the Second International Conference on Wetlands and Remediation. Batelle Press, Columbus, OH, Burlington, Vermont, September 5-6.

Yang, Y., Zhencheng, X., Kangping, H., Junsan, W. and Guizhi, W., 1995. Removal efficiency of the constructed wetland wastewater treatment system at Bainikeng, Shenzhen. Wat. Sci. Tech., 32(3): 31-40.

Young, P.C., 1984. Recursive estimation and time-series analysis. Communications and control egineering series. Springer-Verlag, Berlin.

Young, P.C., 1985. The instrumental variable method; A practical approach to identification and parameter estimation, 7th IFAC/IFORS Symposium on System Parameter Estimation. Int. Fed. of Autom. Control, York, England.

Young, P.C., 1992. Parallel processes in hydrology and water quality: A unified time-series approach. J. Inst. Water Environ. Manage., 6: 598-612.

Young, P.C., 2001. Data-based mechanistic modelling of environmental systems. International Federation on Automatic Control (IFAC) workshop on environmental systems, Tokyo, Japan.

Young, P.C. and Lees, M., 1993. The active mixing volume: a new concept in modelling environmental systems. In: V. Barnet and K.F. Turkman (Editors), Statistics for the Environment. John Wiley & Sons, New York, pp. 3-43.

Young, P.C. and Wallis, S.G., 1986. The aggregated dead zone (ADZ) model for dispersion in rivers, International Conference on Water Quality Modelling in the Inland Natural Environment. BHRA, Bedford, England, Bournemouth, England: 10-13 June 1986, pp. 421-433.

Zheng, C. and Bennett, G.D., 2002. Applied contaminant transport modelling. John Wiley & Sons, New York.